

Jayangi Dinesha Wagaarachchige

Pushing Technology Boundaries: Monitoring and Optimization of Carbon Capture Solvents

**Dissertation for the
degree of Ph.D**
Process, Energy and
Automation Engineering

Faculty of Technology, Natural
Sciences and Maritime Studies

Jayanghi Dinesha Wagaarachchige

Pushing Technology
Boundaries:
Monitoring and
Optimization of Carbon
Capture Solvents

A PhD dissertation in
Process, Energy and Automation Engineering

© 2024 Jayangi Dinesha Wagaarachchige

Faculty of Technology, Natural Sciences and Maritime Studies
University of South-Eastern Norway
Porsgrunn

Doctoral dissertations at the University of South-Eastern Norway no. 196

ISSN: 2535-5244 (print)
ISSN: 2535-5252 (online)

ISBN: 978-82-7206-862-1 (print)
ISBN: 978-82-7206-863-8 (online)



This publication is licensed with a Creative Commons license. You may copy and redistribute the material in any medium or format. You must give appropriate credit, provide a link to the license, and indicate if changes were made. Complete license terms at <https://creativecommons.org/licenses/by-nc-sa/4.0/deed.en>

Cover image: Jayangi Dinesha Wagaarachchige
Print: University of South-Eastern Norway

Dedicated to my loving parents,

my beloved husband **T**hilina,

and my darling princess Nisali.

Preface

This thesis is submitted to the Department of Electrical Engineering, Information Technology and Cybernetics, Faculty of Technology, Natural Sciences and Maritime Sciences at University of South-Eastern Norway (USN) in partial fulfilment of the degree of Doctor of Philosophy. The research work was funded by the Ministry of Education and Research of the Norwegian Government. This research work was conducted under the supervision of Professor Maths Halstensen (Principal supervisor), Professor Emeritus Klaus-Joachim Jens and Associate Processor Zulkifli Idris from the Faculty of Technology, Natural science, and Maritime studies, USN.

The central idea of this study is to provide insights into options to reducing the cost of amine-based post carbon capture (PCC) technology. The thesis is presented in two parts. The first part is the is the synopsis of the research work. It includes five chapters including the background, literature survey and theory, summary of papers, and conclusions with recommendations. The second part consists of the collection of publications that are published and submitted under this research. Only the initial manuscripts of the submitted articles are attached to the thesis.

Following pages will delve into the nuanced discussions of ‘Pushing Technology Boundaries: Monitoring and Optimization of Carbon Capture Solvents’. I invite you to join me on this intellectual exploration.

Porsgrunn

3rd of January 2024

Acknowledgements

It is with great pleasure I express my sincere gratitude to all who supported me during PhD journey.

First and foremost, I am grateful to my principal supervisor, Professor Maths Halstensen, for his insightful guidance as well as the transfer of knowledge and skills that made this journey both rewarding and enjoyable. I would also like to express my gratitude to my co-supervisor, Professor Emeritus Klaus-Joachim Jens, for his immense endorsement, encouragement, and unwavering support. I wish to express my gratitude to the former Associate Professor Zulkifli Idris for his support and guidance as a co-supervisor.

I would like to express my gratitude to the department team leader, Professor Svein Thore Hagen, for facilitating the necessary support to pursue my work efficiently and enthusiastically. I extend my special thanks to Professor Kim Esbensen, who taught us the importance of the Theory of Sampling in the context of this study. Furthermore, I would like to express my gratitude to the PhD coordinators, Mariken Kjøl-Røsand and Associate Professor Per Morten Hansen for their coordination efforts. Additionally, I would like to thank Professor Lars Erik Øi, Associate Professor Kjell-Arne Solli, Professor Marianne Sørflaten Eikeland, Professor Britt Margrethe Emilie Molde and Associate Professor Ali Ghaderi for their kind assistance. Additionally, I would like to thank Bjørnar Arstad for providing support in conducting NMR analysis at SINTEF Industry. Furthermore, I extend my gratitude to Professor II Emeritus Dag-Arne Eimer at USN, Audun Drageset at TCM, and Jakob Johansson, F. Normann and K. Andersson at Chalmers University for their valuable collaborations.

I extend my heartfelt thanks to Peshalya Kothalawala for being a wonderfully comforting, understanding, and helpful friend. Also, I would like to thank Vafa Ahmadi for being a very nice officemate. Additionally, I would like to say thank you to Lab Engineers, Eirik Rugstad Haugen, Chidapha Deeraksa, Kadja Bless, Fredrik Hansen and Hildegunn Hegna Haugen for being supportive. My special thanks to Sylvi Thorkildsen for her kind support. I extend my gratitude to my friend, Wathsala Jinadasa, and her family for their immense help to start this

PhD journey. Furthermore, I extend my special thanks to my Sri Lankan friends—Hiromi Ariyaratne, Manjula Edirisinghe, Amaranath Sena Kumara, Chameera Jayarathna, Sanoja Jayarathna, Janitha Bandara, Asanthi Jinasena, Sumudu Karunaratne, Gamunu Samarakoon, Vasani Sivalingam, and Viraj Edirisinghe—as well as to all other USN colleagues, school, and university friends for their invaluable friendship and support.

I extend my heartfelt gratitude to Senior Professor Ajith de Alwis, Dean of Postgraduate Studies at the University of Moratuwa, for his guidance and encouragement to my doctoral studies. Additionally, I would like to express my gratitude to all the university professors and schoolteachers in Sri Lanka for the knowledge and guidance provided to me.

I am here today because of my loving mother and father, and I am truly grateful for their love, support, and encouragement to move forward to reach my goals. Additionally, I want to extend my thankfulness to my two sisters, Vidurangi and Yashangi, my brother, Chathuranga, and my sister-in-law, Amila, and their families.

Finally, a huge, warm thank you to my loving husband, Thilina Senaratne, and my darling daughter, Nisali Senaratne, for being the pillars of my emotional strength, providing endless encouragement, and filling my life with love and joy.

Jyangi Dinesha Wagaarachchige

Abstract

The central idea of the dissertation is to provide insight into options to reducing the cost of amine-based PCC technology. Solvent management and high energy demand are two of the challenges that have increased the operational cost of the technology.

To enable effective solvent management in a capture plant, the chemical absorption-desorption process needs to be regularly monitored and controlled. Articles 1 and 2 and Proceeding 2 present a study that offers process analytical technology (PAT) tools for solvent management using Fourier-transform infrared (FTIR) spectroscopic data. This study provides a tool to establish degradation boundaries, initiation, and completion stages of the reclaiming process. Furthermore, these findings provide insight to maintain the accuracy and effectiveness of regression models when CO₂ and amine species in the solvent are monitored over an extended timeframe. Moreover, this study demonstrates the potential use of regression model prediction residuals for the detection and monitoring of degradation species. Furthermore, this work entails the means of providing chemometric assistance for a study aimed at conversion of in-service degradation species of the MEA solvent to MEA (Articles 7 and 8).

Introduction of non-aqueous solvents is a new alternative to current aqueous solvents and is influential in reducing the solvent regeneration-energy demands. Articles 3, 4, 6, and Proceeding 1 report results of a proposed sulfolane-based low viscosity non-aqueous solvent. In Article 3, the proposed solvent produces monomethyl carbonates (MMC) through a reaction with CO₂; MMC can be desorbed at 58°C. Article 4 disclose blend composition optimization and the effect of flue gas humidity on CO₂ up-take including respective solvent speciation. This solvent forms DPAH⁺ carbamate, causing the blend to solidify under certain conditions.

Additionally, this thesis presents an initiative in applying chemometric tools with the goal of understanding the chemistry behind the simultaneous SO_x/ NO_x removal process. Results show that Raman spectroscopy is a practical tool for quantifying species in an aqueous SO_x/ NO_x removal system (Article 5).

Overall, this dissertation presents the prospective application of PAT tools, specifically spectroscopy with chemometrics, in monitoring and optimizing of CO₂ capture solvents.

Key words: Spectroscopy, PLS-R modelling, Solvent Management, CO₂ capture, non-aqueous solvents, Sulfolane, Methanol, Diisopropylamine, Raman, FTIR, Model Residuals, Degradation, Reclaiming

List of Publications

Journal Articles

Article 1

Wagaarachchige, J. D.; Idris, Z.; Khatibzadeh, A.; Drageset, A.; Jens, K.-J.; Halstensen, M., Demonstration of CO₂ Capture Process Monitoring and Solvent Degradation Detection by Chemometrics at the Technology Centre Mongstad CO₂ Capture Plant. *Ind. Eng. Chem. Res.* **2023**, 62, (25), 9747-9754.

<https://doi.org/10.1021/acs.iecr.3c00134>.

Article 2

Wagaarachchige, J.D.; Idris, Z.; Khatibzadeh, A.; Drageset, A.; Jens, K.-J.; Halstensen, M. Demonstration of CO₂ Capture Process Monitoring and Solvent Degradation Detection by Chemometrics at the Technology Centre Mongstad CO₂ Capture Plant. Part II

(submitted on 2nd January 2024 to Industrial Engineering Chemistry Research Journal)

Article 3

Wagaarachchige, J.D.; Idris, Z.; Arstad, B.; Kummamuru, N.B.; Sætre, K.A.S.; Halstensen, M.; Jens, K.-J. Low-Viscosity Nonaqueous Sulfolane–Amine–Methanol Solvent Blend for Reversible CO₂ Capture. *Ind. Eng. Chem. Res.* 2022, 61, 5942-5951

<https://doi.org/10.1021/acs.iecr.1c04946>.

Article 4

Wagaarachchige, J.D.; Idris, Z.; Arstad, B., K.A.S.; Halstensen, M.; Jens, K.-J. Low-Viscosity Non-aqueous Sulfolane-Amine-Methanol Solvent Blend for Reversible CO₂ capture: Part II . Blend Optimization, Water Effect, and Speciation

(submitted on 2nd January 2024 to Industrial Engineering Chemistry Research Journal)

Article 5

Johansson, J.; Wagaarachchige, J.D.; Normann, F.; Idris, Z, Haugen, E. R., Halstensen, M., Jinadasa, W.; Jens, K.-J.; Andersson, K. The Influence of Nitrogen Dioxide Absorption on Sulfite Oxidation Rate in the Presence of Oxygen: On-Line Raman Measurements. *Ind. Eng. Chem. Res.* 2023,62, 21048–2105621055

<https://doi.org/10.1021/acs.iecr.3c01015>

Conference Articles and Proceedings

Article 6

Wagaarachchige, J.D.; Idris, Z.; Halstensen, M.; Jens, K.-J. Fast water-lean solvent screening using FTIR spectroscopy: In-situ (in-line) monitoring using an ATR reaction cell integrated with on-line monitoring attached to a liquid-flowcell. In Proceedings of the TCCS-11 - Trondheim Conference on CO₂ Capture, Transport and Storage, Trondheim, Norway, June 21-23, 2021, 2021; pp. 547-552 <https://hdl.handle.net/11250/2787331>

Article 7

Mereu, F, Wagaarachchige, J.D.; Jens, K.-J; Idris, Z. Application of Multivariate Data Analysis of Raman Spectroscopy Spectra of 2-oxazolidinone The First SIMS EUROSIM Conference on Modelling and Simulation, SIMS EUROSIM 2021, and 62nd International Conference of Scandinavian Simulation Society, SIMS 2021, September 21-23, Virtual Conference, Finland. pp. 16-21. <https://doi.org/10.3384/ecp2118516>

Article 8

Mereu, F, Wagaarachchige, J.D.; Idris, Z.; Halstensen, M.; Jens, K.-J. Response Surface Modelling to Reduce CO₂ Capture Solvent Cost by Conversion of OZD to MEA. In Proceedings of the 64th International Conference of Scandinavian Simulation Society (SIMS), Västerås, Sweden, 2023-10-19, 2023; pp. 14-20. <https://ecp.ep.liu.se/sims>

Proceeding 1

Wagaarachchige, J.D.; Idris, Z.; Arstad, B.; Kummamuru, N.B.; Sætre, K.A.S.; Halstensen, M.; Jens, K.-J. A New Sulfolane based Solvent for CO₂ Capture (April 1, 2021). Proceedings of the 15th Greenhouse Gas Control Technologies Conference 15-18 March 2021, Available at SSRN: <https://ssrn.com/abstract=3817192> or <http://dx.doi.org/10.2139/ssrn.3817192>

Proceeding 2

Wagaarachchige, J.D.; Idris, Z.; Khatibzadeh, A.; Drageset, A.; Jens, K.-J.; Halstensen, M. Demonstration of CO₂ Capture Process Monitoring and Solvent Degradation Detection by Chemometrics – CO₂ Technology Centre Mongstad. Presented in TCCS-12 - Trondheim Conference on CO₂ Capture, Transport and Storage, Trondheim, Norway, June 19-21, 2023

List of Tables

Table 2.1: Commonly using spectral preprocessing methods	10
Table 2.2: Spectroscopy types and their origins ⁴²	15
Table 3.1: The main steps, units and purposes of the TCM amine-based capture plant ⁵¹	24

List of Figures

Figure 1.1: Mind map of the elements of problem-solving approach	2
Figure 1.2: Interconnection of publications with the thesis objectives.....	4
Figure 2.1: Process Analysis Elements.....	5
Figure 2.2: The PAT elements used in the thesis work.	6
Figure 2.3: Classification of data using PCA	8
Figure 2.4: The process of multivariate calibration	9
Figure 2.5: Model prediction error verses number of model components/factors ¹⁷	10
Figure 2.6: Types of electromagnetic waves.....	15
Figure 2.7: Modes of molecular vibrations	17
Figure 2.8: Measurement techniques of FTIR spectroscopy (a) Transmission (b) ATR (c) Reflectance.....	18
Figure 2.9: ATR crystal types (a) single reflection (b) multi-reflection ⁴⁴	19
Figure 2.10: Mechanism of Raman ⁴²	20
Figure 2.11: Three types of scattering by a molecule when excited and the most common transition is marked with red arrows. ⁴²	20
Figure 3.1: Amine-based CO ₂ capture process elements that used in this thesis work.	23
Figure 3.2: Schematic of a chemical absorption process for CO ₂	24
Figure 3.3: Process flow diagram for the reclaiming process at TCM amine plant ^{83, 88}	29
Figure 3.4: Estimated percentages of MEA consumption for different pathways ⁸⁶	30
Figure 4.1: Schematic representation of model residual extraction	32
Figure 4.2: Residual spectra based PLS-R model preparation and prediction.....	33
Figure 4.3: Schematic diagram for ATR-FTIR in-situ monitoring ⁴⁵	34
Figure 4.4: Laboratory Experiment Setup (@USN) for in-situ monitoring using Raman probe. ¹⁰⁰	36
Figure 5.1: Conclusions of proposed chemometric solutions for solvent management.....	39
Figure 5.2: Conclusions of a study on non-aqueous solvent	41
Figure 5.3: Conclusions of Article 5: Simultaneous absorption of SO _x and NO _x system.....	42

Abbreviations

Acronyms

ACRG	The Applied Chemometrics and Research Group
AMP	2- Amino-2-methylpropan-1-ol
ATR	Attenuated Total Reflectance
CCS	CO ₂ Capture and Storage
CESAR 1	a mixture of Piperazine and AMP
CHP	Combined Heat and Power
CO ₂	Carbon Dioxide
CO ₃ ²⁻	Carbonate
CT	Calibration Transfer
DEA	Diethanolamine
DoE	Design of Experiment
DPA	Diisopropylamine
ESR	Electron Spin Resonance
EUROSIM	Federation of European Simulation Societies
FTIR	Fourier Transform Infrared
GHG	Greenhouse Gas
HCl	Hydrogen chloride
HSO ₃ ⁻	Bisulfite
IR	Infrared

MEA	Monoethanolamine
MFC	Mass Flow Controller
MLR	Multiple Linear Regression
MMC	Monomethyl Carbonate
MSC	Multiplicative Scatter Correction
MSPC	Multivariate Statistical Process Control
MUP	Model Updating
MVDA	Multivariate Data Analysis
N ₂	Nitrogen
NaOH	Sodium Hydroxide
NIPALS	Non-linear Iterative Partial Least Squares
NIR	Near Infrared
NMR	Nuclear Magnetic Resonance
NO ₂	Nitrogen Dioxide
NO ₂ ⁻	Nitrite
NO ₃ ⁻	Nitrate
NO _x	Nitrogen Oxides
O ₂	Oxygen
OZD	2-Oxazolidinone
PA	Process Analysis

PACT	The Pilot-scale Advanced CO ₂ Capture Technology
PAT	Process Analytical Technology
PCA	Principal Component Analysis
PCC	Post-combustion Carbon Capture
PCR	Principal Component Regression
PCs	Principal Components
PhD	Doctor of Philosophy
PLS-R	Partial Least Squares regression
PUC	Process Automation and Control
PZ	Piperazine
QbD	Quality by Design
RMSEP	Root Mean Square Error of Prediction
RTM	Real-time Monitoring
S ₂ O ₃ ²⁻	Thiosulfate
SCR	Selective Catalytic Reduction
SIMS	Scandinavian Simulation Society
SNV	Standard Normal Variate
SO ₂	Sulfur dioxide
SO ₃ ²⁻	Sulfite
SO ₄ ²⁻	Sulfate

TA	Total Alkalinity
TCM	Technology Centre Mongstad
TIC	Total Inorganic Carbon
ToS	Theory of sampling
USN	University of South-Eastern Norway
UV	Ultraviolet

Greek Symbols

α	CO ₂ capture capacity (mole CO ₂ /mole amine)
Δ	Delta (difference)
λ	Lambda
ρ	Rho

Other Symbols

E	Energy
h	Plank's constant
Q	Average of spectral residuals
v	Frequency
X	Set of spectra
Y	Reference Data

Table of contents

Preface	III
Acknowledgements	V
Abstract.....	VII
List of Publications.....	IX
List of Tables.....	XI
List of Figures.....	XIII
Abbreviations	XV
Part - I	XXI
1 Introduction.....	1
1.1 Background.....	1
1.1.1 Why Process Analytical Technology (PAT)?	2
1.2 Research Objectives	3
1.3 Research Contributions	3
1.4 Structure of the Thesis	4
2 Process Analytical Technology	5
2.1 Chemometrics	6
2.1.1 Multivariate Data Analysis (MVDA).....	7
2.1.2 Principal Component Analysis (PCA).....	7
2.1.3 Regression Modelling.....	8
2.1.4 Data Preprocessing.....	10
2.1.5 Model Diagnostics and Uses	11
2.1.6 Multivariate Statistical Process Control (MSPC) Principles.....	12
2.1.7 Regression Model Calibration Transfer/Model Maintenance	12
2.1.8 Design of Experiments (DoE).....	13
2.2 Theory of Sampling (ToS)	14
2.3 Spectroscopy	15
2.3.1 Fourier-transform Infrared (FTIR) Spectroscopy.....	16
2.3.2 Raman Spectroscopy	19

3	CO ₂ Capture	23
3.1	Amine Solvent-based CO ₂ Capture Processes.....	24
3.2	CO ₂ Capture Solvents	25
3.3	Solvent Chemistry	27
3.4	Solvent Degradation.....	27
3.5	Solvent Reclaiming	28
3.6	Solvent Management.....	29
4	Summary of Articles	31
5	Conclusions and Recommendations	39
	References.....	45
	Part - II	55
	Article 1	57
	Article 2	67
	Article 3	91
	Article 4	103
	Article 5	141
	Article 6	153
	Article 7	161
	Article 8	169
	Proceeding 1.....	179
	Proceeding 2.....	185
	Appendix A: Supplementary Information of Article 2.....	189
	Appendix B: Supplementary Information of Article 4.....	195

Part - I

1 Introduction

“The challenge of pollution and global warming is no longer the science, or the rate of innovation, but the rate of implementation: We have the clean solutions; now let's bundle them and install them.”

- Jens Martin Skibsted-

This chapter presents a comprehensive background for the study, delineating the research problems and the research objectives, and presenting an outline of the dissertation.

1.1 Background

The primary goal of the Paris Agreement is to limit the global average temperature rise to 1.5°C above pre-industrial levels.^{1,2} The alarming impact of greenhouse gas (GHG) emissions, particularly CO₂ emissions accounting for about 80% of GHG emissions caused by fossil fuels burning and other point sources, is evident in the rapid increase of earth's temperature.³ Post-combustion carbon capture (PCC) is perceived as a practical and a pivotal technology in mitigating global CO₂ emissions from fossil fuel combustion and industrial point sources. Currently, amine technology is among the PCC techniques that are nearly ready for an industry level implementation.^{4, 5} Nonetheless, several critical concerns persist with the amine technology, including high energy demand, higher operation cost, and emissions to the environment.^{6, 7} This thesis aims to provide new insights to improve the amine technology, with a specific focus on the PCC system energy demand and associated operational costs.

The Applied Chemometrics and Research Group (ACRG) at University of South-Eastern Norway (USN) has been conducting studies related to Process Analytical Technology (PAT) for more than 25 years. PAT is an interdisciplinary approach consisting of multivariate methods (i.e., spectroscopy and chemometrics) that enables easy characterization of a process. Recently ACRG started exploring the field of CO₂ capture, particularly with a focus on solutions for real-

time quantitative speciation of CO₂ capture solvents.⁸⁻¹¹ As a member of this team, I used an interdisciplinary approach to address the above mentioned problems of current amine based PCC technologies. Figure 1.1 illustrates a mind map portraying the multidisciplinary elements of competencies that support the problem-solving approach in our study.

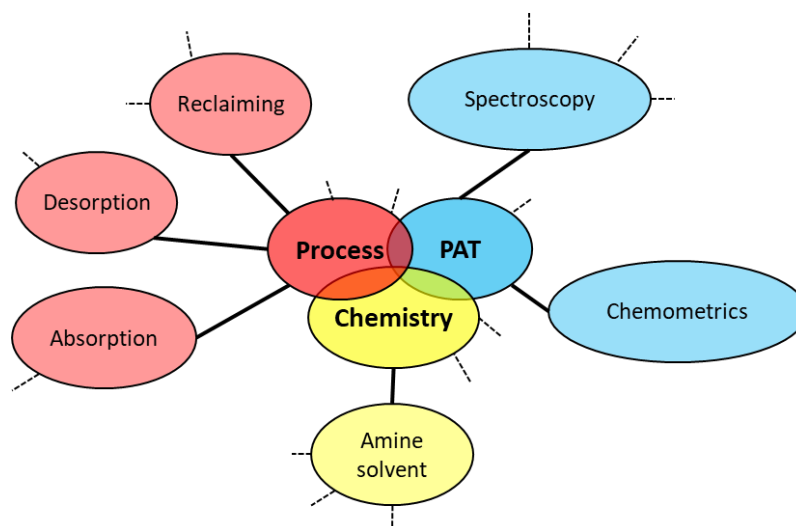


Figure 1.1: Mind map of the elements of problem-solving approach

1.1.1 Why Process Analytical Technology (PAT)?

Amine-based CO₂ capture is a chemical absorption-desorption process that should be carefully monitored to achieve an efficient CO₂ capture performance. Amine solvent is degrading during the operation, consequently reducing the CO₂ capture capacity. For an economical operation, the degraded part of the solvent needs to be cleaned and/or replaced with corresponding fresh amine. Spectroscopy is a useful analytical tool to use in process plant to extract qualitative and quantitative species/chemical information in real-time. The obtained spectrum is complex because it is a combination of individual spectra of all the chemical species presents in the solvent. In order to extract relevant chemical information from the observed spectra, chemometrics offers a useful set of tools that can extract relevant information from the spectroscopic measurements. Furthermore, chemometric tools offer opportunities to detect general changes in a chemical system.

1.2 Research Objectives

Overview of the Research Problem

The central idea of this thesis is to provide insight into reducing the cost of amine-based PCC technology. High energy demand and issues in solvent management are two of the challenges that has heightened the cost of the technology. Water-lean or non-aqueous solvents are emerging as alternatives, particularly targeting to reduce the high regeneration energy required in current aqueous amine-based solvent systems.

An appropriate methodology involves the use of chemometrics and spectroscopy to analyse and to interpret complex chemical systems of the overall study; the solution lies in monitoring and controlling the chemistry behind the amine-based CO₂ capture process.

As a spin-off of this study, we investigated the use of PAT as a methodology to address other similar issues related to flue gas cleaning.

The main objectives of this study are as follows.

1. Propose chemometric solutions for the challenges in solvent management
2. Propose a non-aqueous solvent blend and optimize its composition based on chemometric tools
3. Propose PAT application to address other related gas treating issues

1.3 Research Contributions

In this thesis, the above-mentioned objectives were achieved via work presented in several published papers. Figure 1.2 illustrates how these papers are related to the objectives and to each other.

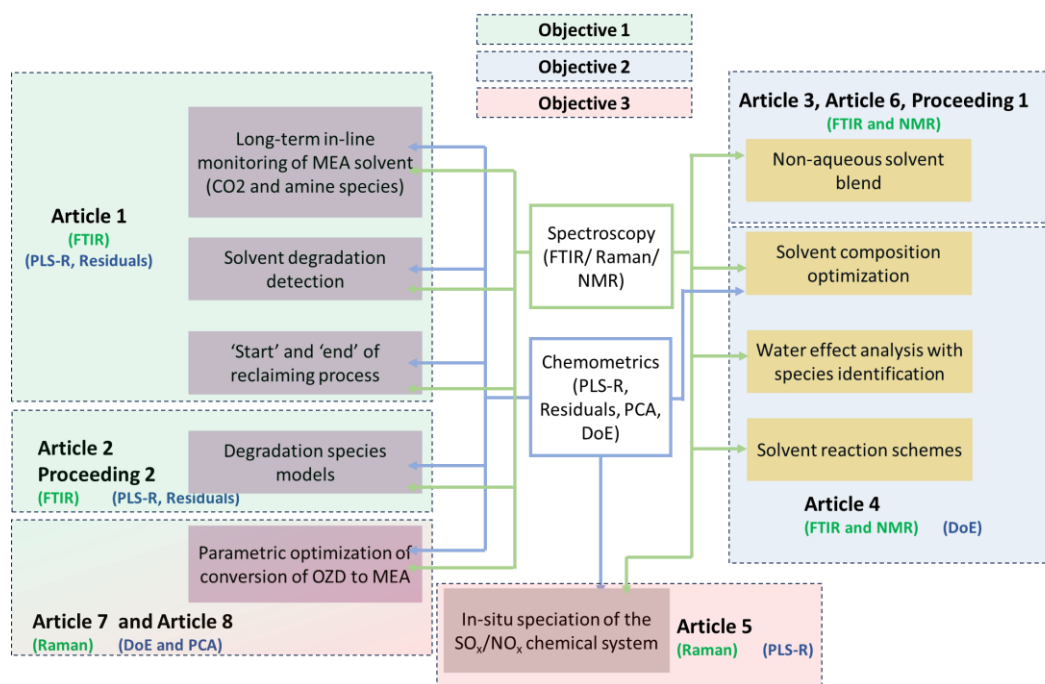


Figure 1.2: Interconnection of publications with the thesis objectives.

1.4 Structure of the Thesis

This PhD thesis consists of two main parts and is presented as a compendium of 6 scientific articles and 2 submitted manuscripts. Part I is the synopsis of the research work and comprises five chapters. Part II is a collection of scientific publications related to the study that are either published or is submitted at the time of writing this narrative.

Chapter 1 comprises the background, research problem, objectives, research contribution and the structure of the thesis. An overview of the Process Analytical Technology (PAT) is presented in Chapter 2. Chapter 3 describes amine-based PCC capture technology, with a brief introduction to CO₂ capture in general. Chapter 4 is a summary of the published articles and the submitted manuscripts.

Conclusions, limitations and recommendations for future investigations are presented in Chapter 5, followed by a list of references.

2 Process Analytical Technology

Process Analytical Technology (PAT) is a comprehensive domain of study that connects a wide range of tools, principles, and expertise; PAT provides process understanding and controlling by digitalization of process industries. This encompasses elements such as process analysis, chemical engineering, chemometrics, process automation and control (PUC), as well as risk management. Chemical processes can get remarkably benefitted by the application of PAT by extracting real-time chemical information for decision making and limiting the need of offline sample analysis and thereby enhancing process efficiencies. Effective PAT solutions are widely established in pharmaceutical and food industries in order to achieve their lean manufacturing and quality by design (QbD) goals.¹²

Process Analysis is one of the essential elements of PAT. Application of real-time analytics and chemometrics for monitoring of chemical or physical attributes or detection of event that cannot be derived from conventional physical measurements (i.e., flow, temperature, pressure, etc.) is called Process Analysis (PA).¹² The basic application of PA is real-time monitoring (RTM) or detection of changes over time in relation to a reference condition using multivariate data sources like process analytical spectroscopy (i.e., FTIR, NIR, Raman). The five elements of PA are shown in Figure 2.1.

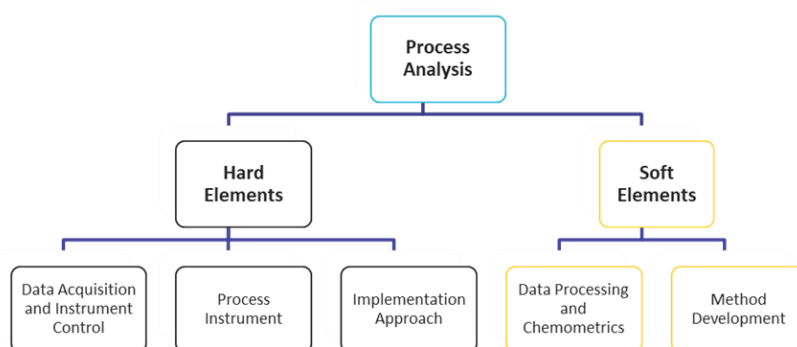


Figure 2.1: Process Analysis Elements

Multivariate data analysis plays a pivotal role in implementing an effective PAT approach into CO₂ capture process systems as the corresponding chemical system is multivariate and complex. Chemometrics provides necessary tools and methods required for multivariate data analysis of chemical data¹³ and this thesis is mainly based on chemometrics approaches. Among the many chemometrics (multivariate data analysis) techniques, appropriate type of methodologies and tools are selected based on the specific process application.

To see the hidden variations of a chemical system, it is crucial to carefully select suitable multivariate data collection instruments. Spectroscopy is one of the chemical data collection techniques that is capable of providing the chemical fingerprint of a chemical system.

Theory of sampling (ToS) is important in PAT applications to derive representative information.

Figure 2.2 illustrates a map of PAT tools that are used in this study, indicating three main categories, i.e., Spectroscopy, chemometrics and ToS.

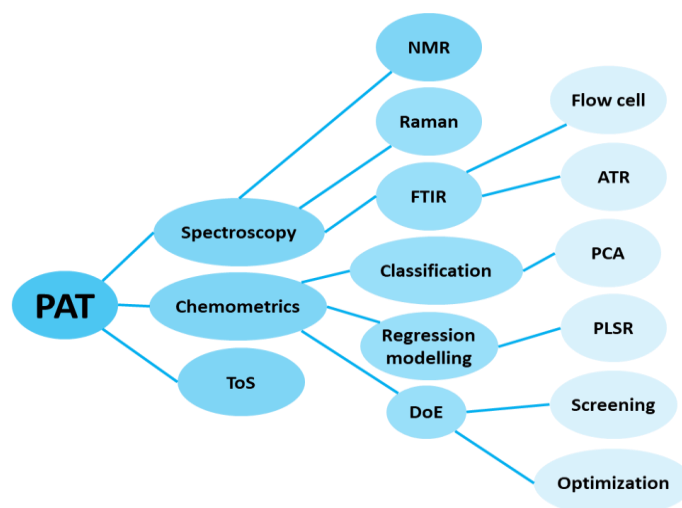


Figure 2.2: The PAT elements used in the thesis work.

2.1 Chemometrics

Chemometric is the art of extracting chemically relevant information from the data produced from chemical analyses, such as spectroscopic and chromatographic data.¹⁴ Mathematical and

statistical analyses play a vital role in extracting these information, patterns, and relationships from complex chemical systems.

Principle Component Analysis (PCA), regression modelling, Multivariate Statistical Process Control (MSPC) and Design of Experiments (DoE) are some of the Multivariate Data Analysis (MVDA) methods that are widely used in chemometrics. Primary uses of chemometrics include data decomposition, pattern recognition, and the preparation of models to understand and interpret chemical information of industries such as manufacturing processes, environmental monitoring, pharmaceutical analysis, and food science.

In this study, these chemometric concepts are applied in order to propose methodologies that can be supportive in monitoring and controlling the chemistry in PCC technology. The MVDA methods employed in this study are explained in the following section.

2.1.1 Multivariate Data Analysis (MVDA)

Global issues are inherently multidimensional. In contrast to univariate methods, which focus on one variable at a time, MVDA enables a comprehensive exploration of correlations among variables and facilitates dimensionality reduction. This capability provides deep insights into the inherent structures and trends within complex datasets. Furthermore, application of these methods not only reduces the dimensionality of data to be handled but also aids informed decision-making and contributes significantly to the advancement of knowledge.

2.1.2 Principal Component Analysis (PCA)

Principal component analysis (PCA) is a prevalent dimensional reduction statistical technique in MVDA and it has been extensively used in food and several other industries.^{15, 16} PCA can decompose the multivariate data matrix (X) into 'structure' and 'noise' (Eq. 2.1); this enables an easy visualization of hidden data structure, referred to as the 'latent structure', while simultaneously removing noise.¹⁷

$$\textit{Observation} = \textit{Data structure} + \textit{Noise (residual)} \qquad 2.1$$

The concept of PCA is to condense the high number of variables of a dataset into a fewer number of compressed variables, called Principal Components (PCs), which describe the important variations and structure of the data.

In predictive modelling such as Partial least squares regression (PLS-R), PCA can be used to select appropriate variables and to eliminate unsuitable data (outliers), thereby improving the model performance and mitigating overfitting of the models. Furthermore, this technique can be used as a visual tool in clustering and classification of complex datasets as shown in Figure 2.3.

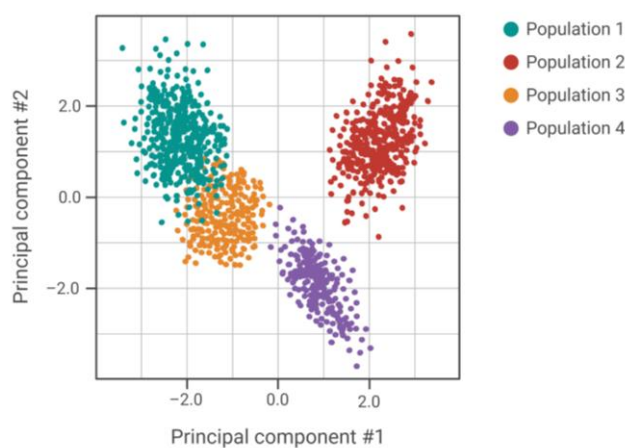


Figure 2.3: Classification of data using PCA

2.1.3 Regression Modelling

Regression modelling has several stages. The first stage is multivariate calibration, and it involves relating two sets of data (X and Y) by regression. In this study, spectroscopic data (X data) and the corresponding species concentration (Y data) are regressed to obtain a calibration model as depicted in Figure 2.4

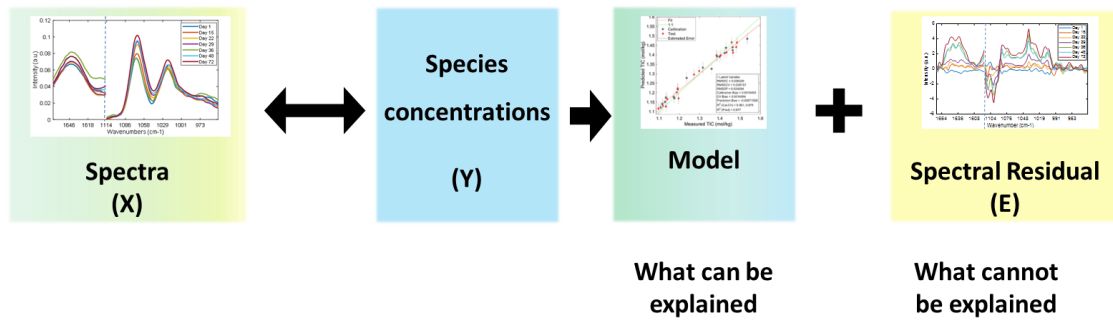


Figure 2.4: The process of multivariate calibration

Regression modelling such as Multiple Linear Regression (MLR), Principal Component Regression (PCR), Partial Least Squares Regression (PLS-R) are used to extract quantitative chemical information from spectroscopic data. PLS-R is considered as a basic tool of chemometrics and is a recently developed generalization of MLR.¹⁸ PLS-R models are developed using the NIPALS algorithm (non-linear iterative partial least squares).¹⁷

Prior to using this calibrated model for the prediction of unknown spectra, it needs to be validated in the second step using a training data set, consisting of known set of X and Y data. This validation method is known as test set validation, and it is the most preferred among the other methods, such as cross-validation or leverage correction.¹⁷

The optimum number of components/factors for the model can then be chosen. The number of factors should be selected such that the model's average prediction error is minimized as shown in Figure 2.5. The average prediction error is often expressed as the residual Y variance, depending on the particular validation method. For test set validation, Root Mean Square Error of Prediction (RMSEP) values (Eq. 2.2) can be employed, representing measures of the total deviation of prediction.^{17, 19}

$$RMSEP = \sqrt{\frac{\sum_{i=1}^I (y_{predicted} - y_{reference})^2}{I}} \quad 2.2$$

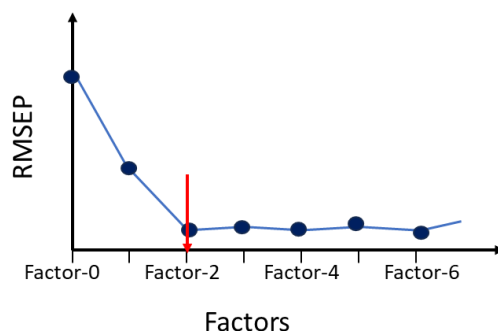


Figure 2.5: Model prediction error versus number of model components/factors¹⁷

2.1.4 Data Preprocessing

In MVDA, data preprocessing is vital and is chosen based on the requirement. Data preprocessing is primarily done to improve robustness and precision of a model. When discrete data are used, mean centering and autoscaling are commonly used as preprocessing methods. However, autoscaling is not commonly applied with spectral data as X.

When spectral data are used as X, there are several preprocessing steps that can be applied. Table 2.1 summarizes such commonly applied spectral preprocessing methods.

Table 2.1: Commonly using spectral preprocessing methods

Preprocessing Method	When the method is applied	Other comments
Baseline correction using Whittaker filter ²⁰	To remove baseline error To separate overlapping vibrational bands	Model robustness is improved by reducing the number of components/factors of the model.
Normalization ¹⁷	To keep all the samples (rows) of the data set on a common ground around a selected reference band	This method was useful when PLS-R models were developed using Raman spectra. By adding normalization around 751 cm^{-1} (considered as an instrument peak) to Raman spectra, the predictability was improved

		for a measured spectrum of any different experimental setup.
Standard Normal Variate (SNV) ²¹	To center the spectral data at the overall average level of the spectrum and to scale the data to a unit variance To de-trend or to correct multiplicative errors ²²	This method calculates a global mean and standard deviation for entire spectral range selected. This method is not used in this study.
Multiplicative Scatter Correction (MSC) ^{23, 24}	A spectral transformation method that can also be used to compensate for both multiplicative and additive effects.	This method is not used in this study.
Derivatives (1 st and 2 nd) ^{17, 22}	1 st derivative: Removes baseline and slope effects 2 nd derivative: Corrects quadratic baseline effects	In definition, derivatives measure the rate of change of data. Savitzky–Golay is the most common derivative method. These are not used in this thesis work.

2.1.5 Model Diagnostics and Uses

There are several diagnostic parameters that are available to analyze predictions of a model and model residuals are one of them. Residuals can either be Y residuals or X residuals. In this thesis, two types of X residuals are used: X residual spectra and average X residuals, also referred to as Q residuals.¹⁷ Another significant measure is Hotelling's T^2 statistics²⁵, which measures the distance from the center of a multivariate model. This measure is useful in various areas of data analysis.

In this study, Hotelling's T^2 versus Q residuals are used as a measure to detect undesirable changes in the solvent of amine-based CO_2 capture process.^{17, 26} Additionally, Q residuals are used as a quantifier for solvent change (degradation) as they are directly proportional to each other.

The parameter known as Leverage is also a measure of the effect of a sample on a calculated model, expressed on a scale of 0 to 1. Samples with leverage close to 1 are considered extremely influential, while typical samples tend to have a leverage close to 0. Leverages of samples are useful when selecting new calibration samples to update models, enabling them to adopt to dynamic changes.²⁷

2.1.6 Multivariate Statistical Process Control (MSPC) Principles

In contrast to monitoring trends of a dynamic chemical process system through wet chemistry or any other specific chemical analysis, MSPC considers the overall projection of the chemical process data by using an existing model such as PLS-R. This projection indicates how well the process is controlled. The two model diagnostics, Q residuals and Hotelling's T^2 can be used for this purpose, withing the model validated confidence intervals. Article 1 discusses a demonstration of how MSPC can be used in amine solvent management.¹¹

2.1.7 Regression Model Calibration Transfer/Model Maintenance

Calibration transfer (CT) involves a series of chemometric methods and/or analytical approaches used to convert an existing model from the primary domain to secondary domains while retaining accuracy and precision.²⁸ Model calibration transfer includes two main scenarios. It is applied when the same model needs to be used in different secondary instruments or when any accessory modifications took place in the primary instrument. Alternatively, CT is done to adopt the model (model maintenance) to any changes of the measuring domain.

Application of preprocessing techniques and various chemometric standardization techniques are necessary to amend spectral changes.²⁹⁻³² Nevertheless, some studies successfully used a

simple method called slope/bias correction on reference (Y) data, for global spectral differences.³³⁻³⁶

Proper planning for model updating and maintenances procedures is essential to ensure stable online monitoring of PLS models. Model updating (MUP) is a successful approach to update models for real-time monitoring of degrading amine solvent.^{11, 27} Wise et al. proposed a flow chart for the model maintenance roadmap.³⁷

2.1.8 Design of Experiments (DoE)

The traditional way to conduct experiments is by varying one variable at a time while keeping the other variables a constant. In Design of Experiments (DoE), several variables are simultaneously varied in a systematic way using the concept of factorial design. In this approach, researchers obtain more information from a fewer number of experiments by focusing on collecting the relevant information that are aligned with the design objectives.

DoE has following advantages: (i) number of experiments is known, (ii) individual effects of each variable and the way they interact can be studied independently, (iii) result of DoE is a model which enables prediction within the design space, and (iv) statistical significance can be assigned to the observed effects. DoE strategies used in this work are described in Manuscript 4 and Article 8 in detail.³⁸

2.2 Theory of Sampling (ToS)

In Theory of Sampling (ToS), there are four defined critical success factors before analysis.³⁹ Representative sampling aimed at unwanted error in data, is one of the important aspects of a successful PAT application.^{12, 40, 41}

In general, all instruments used for spectral and reference method analysis need to be properly maintained and calibrated before data gathering. Furthermore, if we are preparing gravimetric samples, it is important to use a suitable analytical balance with appropriate sensitivity for the weighing measurements to reduce the gravimetric sampling uncertainties. Additionally, CO₂ loaded amine solution has tendency to settle during long-term storage. Therefore, it is essential that the samples bottle is adequately mixed to reduce sample heterogeneity to acquire a representative spectrum from the sample.

A comprehensive understanding of all aspects of data quality is vital in a chemometric study of actual pilot plant data, such as in the TCM 2015 campaign data that were used in Articles 1 and 2.¹¹ In order to construct a good quality multivariate models using FTIR spectroscopic data, it is important that the data acquisition is done with a proper background analysis, at a suitable resolution and a number of scans per spectrum. Raman spectroscopy analysis is slightly different from FTIR analysis as Raman data acquisition does not need a background analysis. However, it is necessary to provide a suitable exposure time to enable photon scattering and the respective exposure time varies according to the sample composition.

In this study, an in-situ monitoring setup with an ATR crystal was used to monitor the CO₂ loading reactions. It is important to note that ATR FTIR measurements are characterized by a few-micron penetrations of a sample. Article 6 discusses in detail a comparison of ATR cell results with bulk flow cell for the same reaction system to ensure the representativeness of the ATR-FTIR in-situ monitoring cell for further analysis work.

Moreover, knowledge of ToS is helpful in eliminating possible sampling errors during experimental work, as such errors cannot be corrected by any data preprocessing methods.

2.3 Spectroscopy

Spectroscopy is an analytical technique that offers valuable insights into an analyte by perceiving the interaction between matter and electromagnetic radiation. Figure 2.3 depicts several types of electromagnetic waves included in the electromagnetic spectrum.

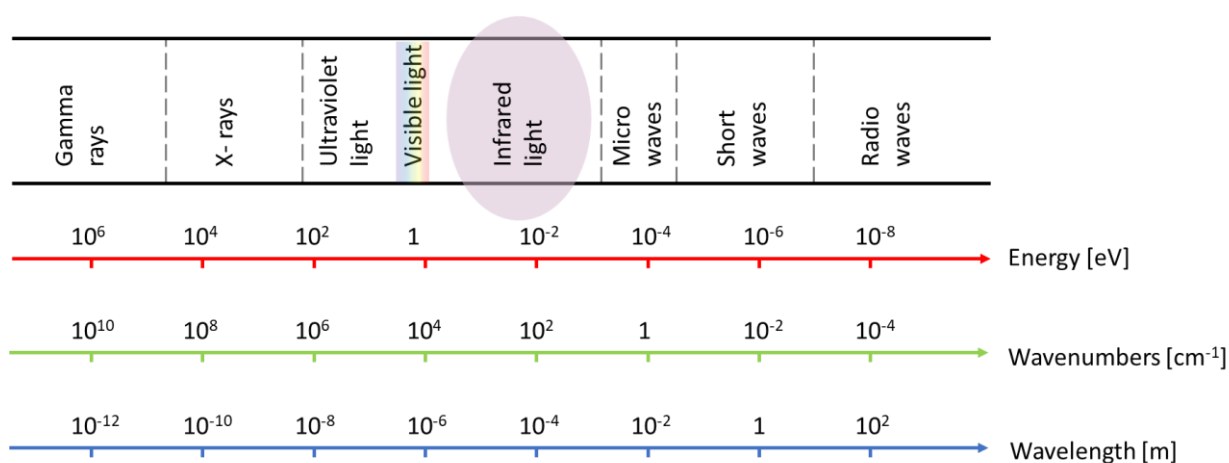


Figure 2.6: Types of electromagnetic waves

The spectral ranges and origins of different types of spectroscopies are tabulated Table 2.2; the transition between vibrational levels of chemical species⁴² can be observed through Raman and Infrared (IR) spectroscopies.

Table 2.2: Spectroscopy types and their origins⁴²

Spectroscopy	Origin
Gamma	Rearrangement of elementary particles in the nucleus
X-ray	Transitions between energy levels of inner electrons of atoms and molecules
UV-visible	Transitions between energy levels of valence electrons of atoms and molecules
Raman and Infrared	Transitions between vibrational levels (change of configuration)
Microwave	Transitions between rotational levels (change orientation)
Electron spin resonance (ESR)	Transitions between electron spin levels in magnetic field.
Nuclear magnetic resonance (NMR)	Transitions between nuclear spin levels in magnetic fields

Spectroscopic measurement (spectrum) includes qualitative and quantitative information about the chemical species in the measured chemical sample. Additionally, spectroscopic measurements encompass information about the physical changes of the system such as density and viscosity.¹¹

In this study, Fourier-transform Infrared (FTIR), Raman, and Nuclear Magnetic Resonance (NMR) spectroscopy were used. FTIR and Raman spectroscopy were used to extract both qualitative and quantitative chemical information from solvent systems, while NMR spectroscopy was utilized in confirming the presence of specific species.

NMR analyses was conducted in collaboration with SINTEF Industry, Oslo. In the subsequent sections, analysis of FTIR and Raman spectroscopy are comprehensively detailed. Methods and procedures for NMR analysis are described in Articles 3 and 4.

2.3.1 Fourier-transform Infrared (FTIR) Spectroscopy

FTIR spectroscopy is the technique used to identify chemical compounds based on how the infrared radiation (IR) is absorbed by the molecules. Molecules absorb, transmit, and reflect light according to the available chemical bonds. The absorbed light is read by the FTIR detector and in this study, IR absorption was used. This technique provides information about the functional groups present in molecules. When infrared absorption occurs, the molecular shapes are changing due to the changes in modes of molecular vibrations. Figure 2.7 depicts the five different models of molecular vibrations that are experienced in IR excitation.

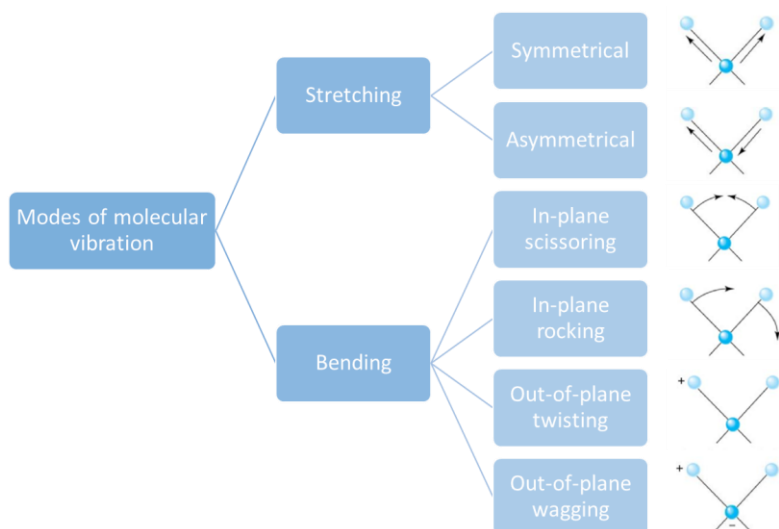


Figure 2.7: Modes of molecular vibrations

All molecules are not IR active. Molecules need a permanent dipole moment to be active, i.e., N_2 is inactive but HCl is an IR active molecule. Vibrations can induce changes in either bond length (stretching) or bond angle (bending). Some bonds can undergo symmetric stretching within the plane or asymmetric stretching outside the plane. Bending vibrations encompass in-plane variations like scissoring and rocking, as well as out-of-plane movements such as wagging and twisting.

There are different types of FTIR measurement techniques such as transmission, attenuated total reflectance (ATR), reflectance, etc. The transmission technique was originally used in this study. The IR beam passes through the samples completely as shown in Figure 2.8 (a). Here, samples are often prepared differently. In this study, a liquid flow cell is used to monitor CO_2 loading reactions of a nonaqueous solvent. The methodology is described in Article 6.⁴³

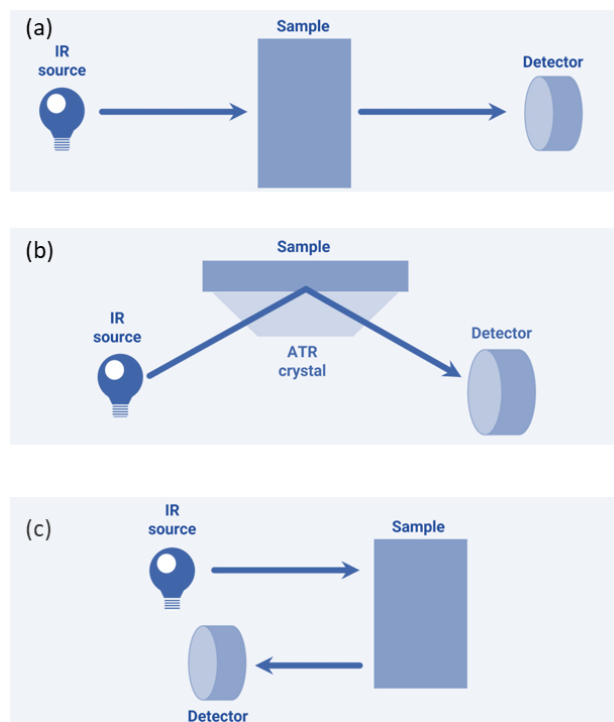


Figure 2.8: Measurement techniques of FTIR spectroscopy (a) Transmission (b) ATR (c) Reflectance

Advancements in infrared spectroscopy during the last 20 years have transformed ATR-FTIR spectroscopy as an easy, versatile, and an essential tool in chemistry, physics, materials, and biology.⁴⁴ An ATR crystal, typically made of diamond or zinc selenide, is commonly used in spectroscopic studies. Figure 2.8 (b) presents a schematic of ATR-FTIR acquisition method. During its measurement, light interacts only with a few microns' depth in the sample. Different types of ATR sampling accessories are available including single reflection or multi-reflection crystals (Figure 2.9); these are chosen based on the required measurement sensitivity.

The final measurement technique is reflection, where IR light is reflected off the surface of the sample as shown in Figure 2.8 (c). This method is useful for examining solid samples that are difficult or impossible to analyse using the other two techniques.

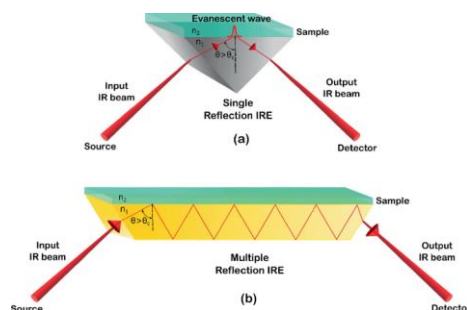


Figure 2.9: ATR crystal types (a) single reflection (b) multi-reflection⁴⁴

ATR-FTIR is a valuable tool for observing the formation and breaking of molecular bonds when coupled with a reaction cell. It provides means to monitor the reactions in-situ, enabling real-time measurements via ATR-FTIR. It makes it possible to determine key reaction characteristics in-real time, including initiation, reaction intermediate, end points, kinetics, and mechanistic information. ATR-FTIR in-situ monitoring was conducted during the characterization of non-aqueous solvents, and the experimental procedures and setup are described in Article 3.⁴⁵

When regression models are prepared using FTIR spectra, the instrument can effectively provide real-time quantitative information. Article 1 and 2 provide more insight into the use of FTIR spectroscopy for qualitative measures.¹¹ Furthermore, a FTIR instrument when paired with chemometric tools, is successful in detecting changes in chemical processes, as demonstrated in Article 1.¹¹

2.3.2 Raman Spectroscopy

In 1928, the Indian physicist Chandrasekhara Venkata Raman first reported Raman scattering, together with his research partner K. S. Krishnan.⁴⁶ In Raman spectroscopy, Raman scattering from the sample is extracted after an application of incident light as illustrated in Figure 2.10.

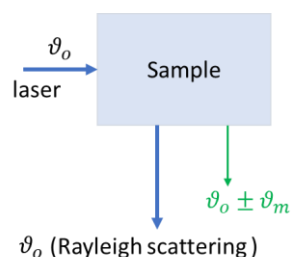


Figure 2.10: Mechanism of Raman ⁴²

There are two types of scattering in spectroscopy, named Rayleigh and Raman. The frequency of Rayleigh scattering equals the frequency of the excitation laser, and it does not provide insightful particulars about the molecular speciation. However, Raman scattering is an inelastic photon scattering process that is uniquely and highly informative for chemical analysis. The Raman scattering process involves two steps: (i) the introduced laser excites the molecule to a virtual energy stage (ii) the molecules relax through release of scattering photons to ground state. Therefore, samples need to be subjected to a suitable exposure time to complete both steps during the measurements. This scattering can either be Stokes Raman scattering, where scattered photons have a longer frequency than the incident laser, or anti-Stokes scattering, where the frequency is shorter than the incident laser frequency (Figure 2.11).

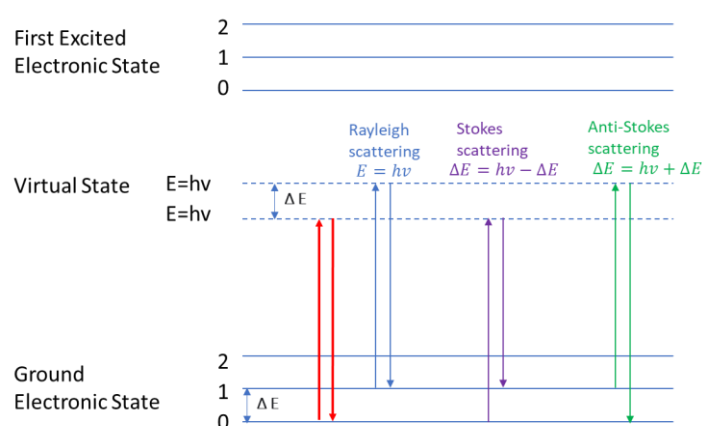


Figure 2.11: Three types of scattering by a molecule when excited and the most common transition is marked with red arrows.⁴²

Raman spectroscopy is susceptible to fluorescence effects, and acquiring spectra from dark samples is challenging. Nonetheless, after the introduction of FT-Raman technology, which could reduce the fluorescence effect, Raman scattering is increasingly used in various industries.⁴² The main advantage of Raman spectroscopy is that interference from solutes in aqueous systems does not occur because water is a weak Raman scatterer. Therefore, Raman spectroscopy is ideal for aqueous systems, including applications in biochemical, medical systems. In-line monitoring of a pilot scale 30 wt% aqueous MEA-based CO₂ capture solvent was successfully conducted using Raman spectroscopy at the PACT plant in Sheffield, UK and at USN in Porsgrunn.^{8,9}

Raman spectroscopy is employed in the work presented in Articles 5, 7, and 8. For detailed information, the articles can be found in Part II.

3 CO₂ Capture

CO₂ capture and storage (CCS) is an essential component of the widespread efforts in mitigating CO₂ emissions from energy production and industrial point sources. There are three main types of CO₂ capture processes: pre-combustion capture, oxy-fuel combustion capture, and post combustion carbon capture (PCC).^{4, 47} Each process has its own advantages and challenges; selection of a technology is often done based on the specific characteristics of the industrial process or the power plant.⁴⁷ Among the PCC technologies, amine-based chemical absorption is considered a well-established method that can be used to capture CO₂ from fossil fuel burnings^{5, 48}, particularly at relatively low CO₂ concentrations (i.e., 7-14% for coal-fired and as low as 4% for gas-fired⁴⁷). Nonetheless, the cost of PCC remains a significant concern; the U.S. National Energy Technology Laboratory estimated that the cost of electricity production could increase by 70% with a PCC system installation.⁴⁹

The primary focus of this study is the application of PAT to the development of an amine-based PCC technology. Amine based capture technology is a chemical assisted CO₂ absorption-desorption process, and the process should be controlled in accordance with the chemical changes within the system. PAT plays a vital role in digitalization of such chemical process control. Key elements of CO₂ capture technology that are considered in this study are mapped in Figure 3.1. and are discussed in detailed in the following sub sections.

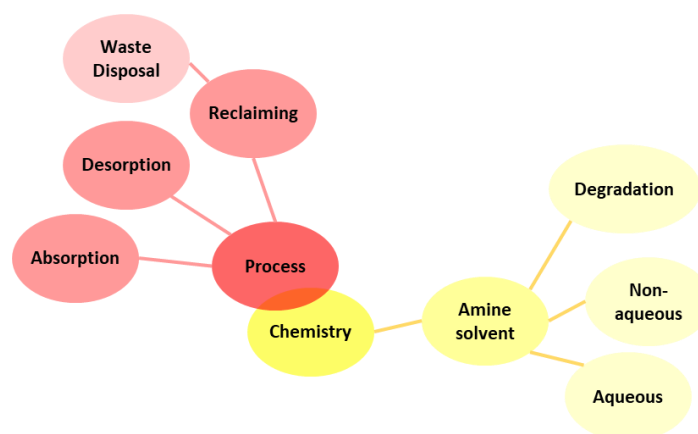


Figure 3.1: Amine-based CO₂ capture process elements that used in this thesis work.

3.1 Amine Solvent-based CO₂ Capture Processes

Amine-based CO₂ capture process is the most mature technology for CO₂ separation from fossil fuel combustion.⁵⁰ In general, it includes two main process steps: absorption (scrubbing) and desorption (stripping) as depicted in the simplified schematic in Figure 3.2.

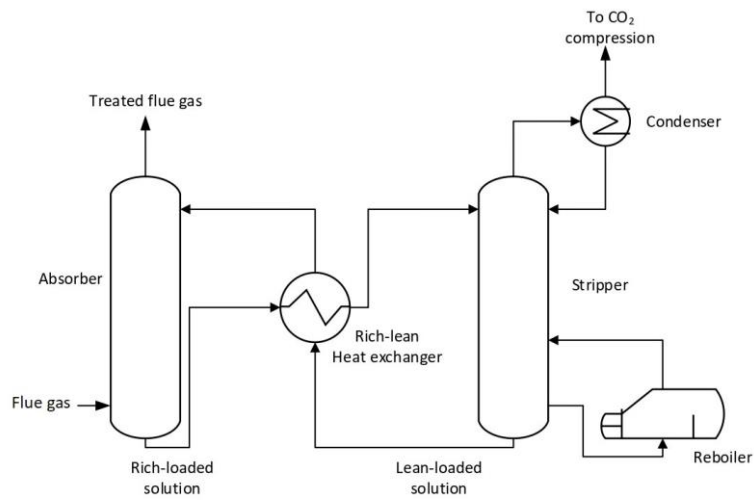


Figure 3.2: Schematic of a chemical absorption process for CO₂

Bui et al. published a detailed process flow diagram of the amine-based CO₂ capture process at TCM, Mongstad, which is configured to treat flue gas from a combined heat and power (CHP) plant.⁵¹ The main units and purposes of the TCM amine-based capture plant are detailed in Table 3.1.

Table 3.1: The main steps, units and purposes of the TCM amine-based capture plant⁵¹

Steps	Unit	Purpose
1	Direct contact cooler (counter-current contact flue gas and water)	Flue gas is quenched, cooled and pre-scrubbed before the scrubber.
2	Absorber (flue gas enters from the base of the column, lean)	Chemical absorption of CO ₂ from the flue gas.

	solvent flows counter-currently from the top)	
3	Water washers (placed on the upper section of the absorber)	Processed flue gas is scrubbed and is released from the top of the absorber column. The two main purposes of water washers are to maintain a closed water balance in the solvent and to reduce the concentration of volatile organic compounds in the depleted flue gas.
4	Cross heat exchanger (Rich–Lean Heat Exchanger)	Rich solvent exits the bottom of the absorber column and is heated by a counter current stream of hot lean solvent. The rich solvent is directed to the stripper column.
5	Stripper (Heat is supplied by steam at 140–160 °C)	As rich solvent flows down the stripper column, CO ₂ is desorbed from the solvent. The lean solvent stream then exits the bottom of the stripper column while CO ₂ is released from the top of the column.
7	Cross heat exchanger (Rich lean heat exchange)	The lean solvent is cooled by the low temperature rich amine stream. The lean solvent is then further cooled by the lean amine cooler at the absorber inlet.
8	Condenser and Reflux Drum	Entrained droplets in the CO ₂ stream are removed prior to being sent to the CO ₂ stack.

3.2 CO₂ Capture Solvents

Chemical absorption of CO₂ using solvents provides better selectivity for CO₂ capture, facilitates easy regeneration and promote solvent recycling. Amines, potassium/sodium carbonates, ammonia, and ionic liquids are the typical solvents applied in industrial scale chemical absorption of CO₂. Amines are widely used for CO₂ capture owing to their favourable chemical reactivities, selectivity, and commercial availabilities and is a proven and a successful technology implemented in various industries.

Amines can be classified as primary, secondary or tertiary based on the number of hydrogen atoms attached to the nitrogen: 2 for primary, 1 for secondary and 0 for tertiary. Within primary and secondary amines, certain compounds are categorized as 'sterically hindered', based on the location of the carbon atom to which the amino group is attached.⁴ These amine groups exhibit distinctive characteristics in CO₂ absorption chemistry.

Aqueous monoethanolamine (MEA) of 30 wt% is a first generation CO₂ capture solvent, and has a high reactivity.^{5, 52} MEA is an efficient solvent for CO₂ absorption, with a capture efficiency over 90% compared to other aqueous alkanolamines (i.e., DEA).⁵³ Numerous studies regards MEA as the typical benchmark solvent for chemical absorption of CO₂.^{5, 54, 55} Major challenges of this solvent are the high energy penalty that is estimated to be around 4 GJ per ton of CO₂ captured⁵⁶ and in-service solvent losses due to solvent degradation.⁵⁷ Furthermore, MEA is a chemical species that can cause metal corrosion and has proven to deteriorate pipelines and column walls.^{58, 59}

Numerous research studies are being conducted to explore capture solvents with a lower energy penalty. Second generation aqueous capture solvents like piperazine (PZ) or its derivatives are found to lower the operational energy by enhancing the theoretical capture capacity and reducing the regeneration energy.^{60, 61} CESAR 1, a blend of piperazine (PZ) and amino-methyl-propanol (AMP) (13 wt% PZ, 27 wt% AMP, 60 wt% H₂O),^{62, 63} is currently considered as the new benchmark solvent for CO₂ capture solvent development and has recorded high oxidative and thermal stability compared to 30 wt% aqueous MEA.²⁵ Fluor's advanced Econamine and Mitsubishi's KS-1 are second generation proprietary solvents.^{60, 64} Nonetheless, new solvent formulas are still in need to attain a low cost capture performances.⁶⁵

Non-aqueous/water-lean amine blends are currently being considered for CO₂ capture, owing to their potential advantages, including reduced energy requirements and lower corrosivity.⁵⁴ A recent review by Heldebrant et al. discuss fundamentals, uncertainties, and opportunities of water-lean solvents.⁶⁶ Typically, these water-lean solvents are similar to conventional aqueous solvents wherein organics, often alcohols are used instead of water.⁶⁶⁻⁶⁸

3.3 Solvent Chemistry

A general reaction scheme for 30% aqueous MEA is reported by McCann et al.⁶⁹ Key CO₂ capture species of 30% MEA solvent are carbamate, carbonate/bicarbonates, and protonate amines. In general, CO₂ loaded solvents ought to be heated to 110-120°C to reverse the CO₂ capture reactions—one of the main reasons for rapid solvent degradation during in-service.

In amine-based PCC, different types of amines are used such as primary, secondary, or tertiary amines. Furthermore, some amines are considered sterically hindered. Sterically hindered amines could provide high theoretical capture capacity and lower regeneration temperature because they form bicarbonate during CO₂ absorption. Unfortunately, the kinetics of these amines are much slower than MEA. Furthermore, CO₂ absorption chemistry varies according to the functional group arrangement of these amines and their diluent solvent properties. Kortunov et al. reports CO₂ reaction schemes of different solvent blends generated from NMR based in-situ monitoring studies.⁷⁰⁻⁷³

The formation of alkyl carbonate species in non-aqueous/water-lean solvent systems during their CO₂ absorption enables low-temperature solvent regeneration due to their lower heat stabilities.^{64, 74, 75} Nucleophilic alcoholysis of the hydroxyl functional group of alkanolamine and alcoholic diluents on the unstable carbamate intermediate direct the formation of alkyl carbonate species.⁷⁴⁻⁷⁹ Monomethyl carbonate (MMC) is the smallest specie of alkyl carbonate group and it can be regenerated at around 60°C.⁴⁵ Additional deliberation about the solvent chemistries related to this study are mentioned in Articles 3 and 4. However, solvents that form alkyl carbonate are still not ready for industrial development.

3.4 Solvent Degradation

In amine-based PCC, the solvent recycles through the absorption-desorption processes for an extended run time. During this cycle, the fresh solvent gradually degrades, and impurities gets accumulated in the degraded solvent. Solvent degradation is driven by several conditions such as the oxygen content and other impurities in the flue gas and the higher working temperature

gradient. Solvent degradation is typically classified into two main reaction pathways – oxidative and thermal degradation.

Solvent degradation can lead to several issues including reduced solvent absorption capacity, equipment corrosion, and emission of toxic volatile substances.^{80, 81} Morken et al. reported several potential degradation species that can be encountered in 30% aqueous MEA solvent degradation.⁸² In 2022, TCM investigated solvent degradation and solvent losses of the non-proprietary solvent CESAR-1, and reported an overview of thermal and oxidative degradation, as well as the potential degradation species for the PZ and AMP.⁸³

3.5 Solvent Reclaiming

Prolonged use of degraded solvents leads to a reduction in CO₂ capture performance and simultaneously accelerates solvent degradation and corrosion of equipment/piping. Nonetheless, complete replacement of used and degraded solvent with fresh solvent is costly. Reusing the degraded/dirty solvent can be accomplished through a purification technique, thus ensuring a sustainable solvent performance. Among the potential solvent treatment techniques are ion exchange, electrodialysis, and thermal reclaiming.⁸⁴

Thermal Reclaiming: Degradation products of amines with a higher boiling point and accumulated suspended solids can be removed from amine solutions through the distillation process.⁴ Thermal reclaimers are used to eliminate accumulated degradation products and to improve the solvent performance, particularly with MEA or MEA blends.⁸⁵⁻⁸⁷ In thermal reclaiming, a small sidestream (usually 0.5 to 2% of the main flow⁴) of the solvent is distilled to remove the degraded products; nevertheless, the process remains energy-intensive.⁸⁴ Figure 3.3 depicts the process flow diagram of the thermal reclaiming process unit at the TCM plant in Mongstad.^{83, 88} Campbell et al. outlined the operational procedure and the corresponding outcomes of the reclaimer relevant to the CESAR 1 test campaign (2019-2020).⁸³

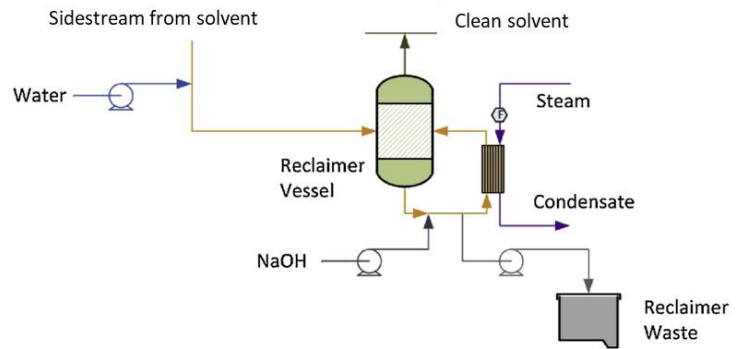


Figure 3.3: Process flow diagram for the reclaiming process at TCM amine plant^{83, 88}

In this study, a chemometric tool is proposed to follow-up the thermal reclaiming process, allowing for its application without the need for individual chemical analysis of solvent degradation species.⁸⁹

3.6 Solvent Management

Amine-based PCC technology is in the stage of commercialization. Nonetheless, the deployment of commercial scale amine-based PCC systems may need further emphasis in effective solvent management and emission control procedures to minimize of potential technical issues and environmental impact.^{88, 90, 91}

In MEA-based PCC solvent management, the key segments to be considered are solvent reclaiming, corrosion control, foaming control, and management of solid and aqueous waste.⁹² Figure 3.4 illustrates the estimated relative solvent loss patterns when MEA is used in a natural gas power station.^{90, 93} Solvent evaporation instigates the largest solvent loss, and the lost solvent can generally be collected in the water wash.

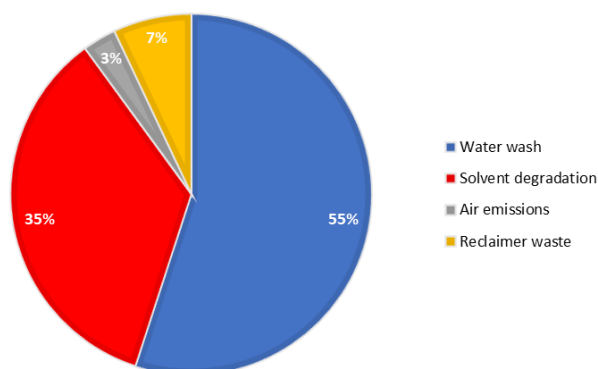


Figure 3.4: Estimated percentages of MEA consumption for different pathways⁸⁶

The second-highest solvent loss (MEA) is attributed to solvent degradation; this emphasizes the importance of reclamation to ensure long-term stability of the solvent.

All solvents degrade during operation, thereby increasing solvent disposal costs and solvent make-up costs.⁹⁴ The solvent make-up cost is approximately 10% of the total operating cost when MEA is used as a solvent.⁹¹

In general, solvent losses range from about 0.01 - 0.8 kg per tonne of CO₂ captured.⁹⁵ In Norway, it is estimated that the establishment of a full scale CCS system at the 420 MW gas power plant in Kårstø, may lead to an annual amine emissions of 40–160 tonne.⁹⁶

Overall, an extended waste management of liquid, gaseous, and solid waste is crucial and necessary for the PCC technology to deliver a net positive impact on both cost and the environment.

4 Summary of Articles

This dissertation comprises 6 published articles and 2 submitted manuscripts that cover the three main objectives, to propose: (i) chemometric solutions for the challenges in solvent management, (ii) a non-aqueous solvent blend and optimized composition based on chemometric tools, (iii) PAT application to address other related gas treating issues. This chapter presents the highlights of each publication, along with a brief overview of the respective studies.

Article 1: Demonstration of CO₂ Capture Process Monitoring and Solvent Degradation Detection by Chemometrics at the Technology Centre Mongstad CO₂ Capture Plant

Authors: Wagaarachchige, J. D.; Idris, Z.; Khatibzadeh, A.; Drageset, A.; Jens, K.-J.; Halstensen, M.

Published in Industrial & Engineering Chemistry Research. 2023, 62, (25), 9747-9754.

<https://doi.org/10.1021/acs.iecr.3c00134>.

This article proposes a set of chemometric tools for the solvent management of MEA based PCC technology. A combination of multivariate methods (PLS-R, MSPC) and process analytical spectroscopy (FT-IR) is established as a tool to monitor and control PCC process performances. A large-scale 1960 h test campaign data (Technology Centre Mongstad, Norway, 2015 MEA Test) is used in this study.

Highlights:

- Two MEA solvent monitoring PLS-R models were prepared for total inorganic carbon (TIC) content and total alkalinity (TA).
- A specific model update methodology was demonstrated to keep the models updated, resulting in good long-term monitoring ability of the TIC and TA models.
- Quantification of solvent degradation/changes, with reference to the clean solvent, can be achieved using model Q residuals.

- A multivariate statistical process control (MSPC) strategy was demonstrated for solvent degradation detection and to follow-up the thermal reclaiming.

Article 2: Demonstration of CO₂ Capture Process Monitoring and Solvent Degradation Detection by Chemometrics at the Technology Centre Mongstad CO₂ Capture Plant. Part II

Authors: Wagaarachchige, J. D.; Idris, Z.; Khatibzadeh, A.; Drageset, A.; Jens, K.-J.; Halstensen, M.

Submitted to Industrial & Engineering Chemistry Research.

This work constitutes Part II of Article 1. In this submitted manuscript, we demonstrated a PLS-R model preparation approach based on FTIR residual spectra for the quantification a of group of degradation species. Schematic representation of model residual extraction is shown in Figure 4.1.

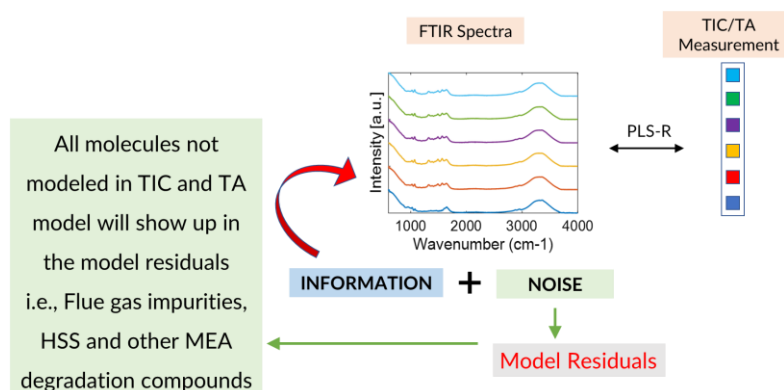


Figure 4.1: Schematic representation of model residual extraction

Highlights:

- Residual spectra were extracted from TIC and TA model during the model prediction stage.
- The vibrational band at 1581 cm⁻¹ of the formate species was identified in the residual spectra which is extracted from the TIC model.

- PLS-R prediction models were presented for two groups of species: (i) HSS and (ii) Total amine degradation products. Schematics of HSS model preparation and obtaining predictions are shown in Figure 4.2.

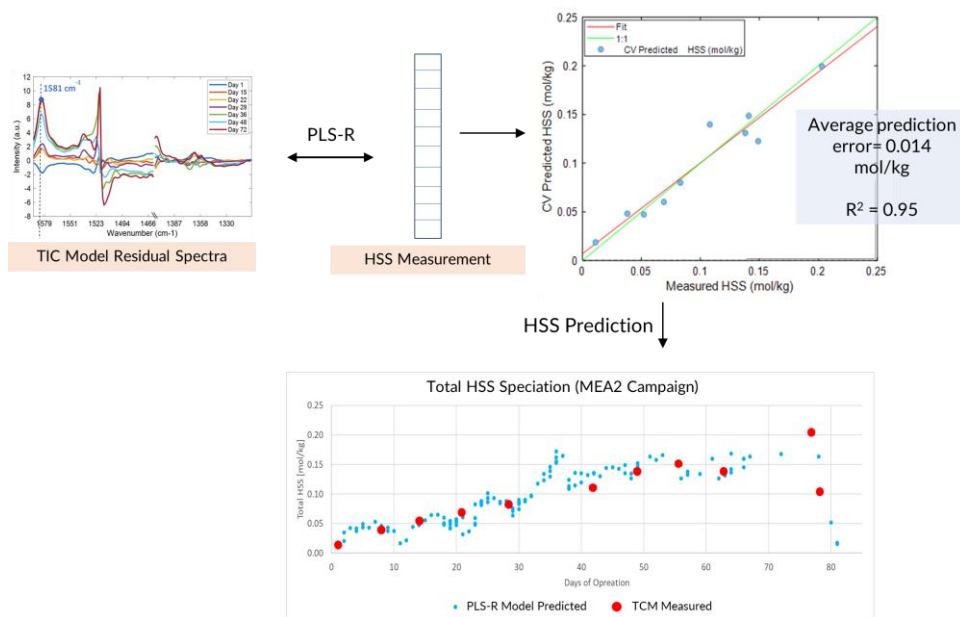


Figure 4.2: Residual spectra based PLS-R model preparation and prediction

Article 3: Low-Viscosity Nonaqueous Sulfolane – Amine –Methanol Solvent Blend for Reversible CO₂ Capture.

Authors: Wagaarachchige, J.D.; Idris, Z.; Arstad, B.; Kummamuru, N.B.; Sætre, K.A.S.; Halstensen, M.; Jens, K.-J.

Published in *Industrial & Engineering Chemistry Research*. 2022, 61, 5942-5951,

<https://doi.org/10.1021/acs.iecr.1c04946>.

This article presents the first set of results generated from the proposal for a non-aqueous solvent for PCC (Objective 2). The absorption–desorption performance of CO₂ in solvent blends is monitored using ATR-FTIR spectroscopy (Figure 4.3) to select a suitable amine.

Highlights:

- Diisopropylamine (DPA) was selected to blend with sulfolane and methanol.
- The DPA-based non-aqueous solvent formed monomethyl carbonate (MMC) entirely with a capture capacity of 0.88 molCO₂/mol amine, a cyclic capacity of 0.48 molCO₂/mol amine, and a CO₂-loaded solvent viscosity of 3.28 mPa·s.
- This solvent can be regenerated at around 60°C.

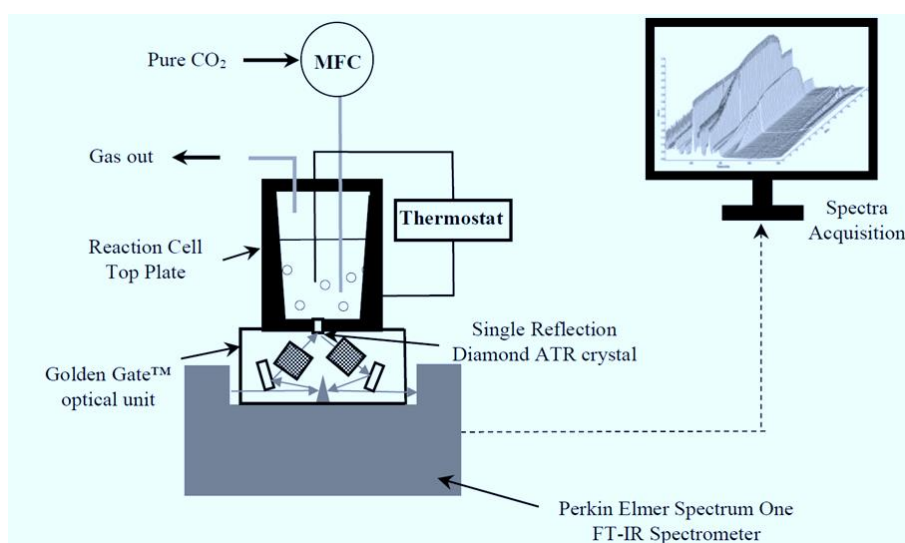


Figure 4.3: Schematic diagram for ATR-FTIR in-situ monitoring ⁴⁵

Article 4: Low-Viscosity Non-aqueous Sulfolane-Amine-Methanol Solvent Blend for Reversible CO₂ capture: Part II. Blend Optimization, Water Effect, and Speciation

*Authors: Wagaarachchige, J.D.; Idris, Z.; Arstad, B., K.A.S.; Halstensen, M.; Jens, K.-J.
Submitted to Industrial & Engineering Chemistry Research.*

The second part of the proposal for a non-aqueous solvent blend is presented in this manuscript which is submitted to the journal of Industrial & Engineering Chemistry Research (IECR). This work presents the optimization of solvent blend composition, an analysis of the effect of water, and solvent speciation.

Highlights:

- The solvent blend was optimized for CO₂ capture using a Design of Experiment (DoE) strategy.
- DPA and methanol distinctly indicate a positive interaction effect on CO₂ absorption via MMC.
- An optimized non-aqueous blending region for CO₂ capture was proposed.
- In non-aqueous conditions, solvent blends tend to form a solid/slurry during CO₂ absorption when the wt% of DPA is equal to or larger than the wt% of methanol. Moreover, a similar solidification is observed with water availability
- The solvent solidification is initiated by the formation of carbamate.
- A working window of CO₂ capture capacity was proposed to prevent solidification in the presence of water.

Article 5: The Influence of Nitrogen Dioxide Absorption on Sulfite Oxidation Rate in the Presence of Oxygen: On-Line Raman Measurements.

Authors: Johansson, J.; Wagaarachchige, J.D.; Normann, F.; Idris, Z, Haugen, E. R., Halstensen, M., Jinadasa, W.; Jens, K.-J.; Andersson, K.

Published in Industrial & Engineering Chemistry Research. 2023,62, 21048–21056 <https://doi.org/10.1021/acs.iecr.3c01015>

This article covers the third objective of this study and is a collaborative effort to integrate PAT into an ongoing project with a research team from Chalmers university on simultaneous absorption of sulphur dioxide (SO₂) and nitrogen oxide (NO_x)⁹⁷⁻⁹⁹ using Raman spectroscopy. We conducted series of experiments with on-line monitoring using Raman spectroscopy, using the experimental setup illustrated in Figure 4.4. My contribution in this article involved planning, preparation, and validation of PLS-R models to quantify SO₃²⁻, HSO₃⁻, S₂O₃²⁻, SO₄²⁻, NO₂⁻, NO₃⁻, and CO₃²⁻ species in the reaction setup. All model information and quantification results are reported in Article 5. The article is included in Part II of this dissertation.

Relevant highlights from my contribution:

- PLS-R models to quantify SO_3^{2-} , HSO_3^- , $\text{S}_2\text{O}_3^{2-}$, SO_4^{2-} , NO_2^- , NO_3^- and CO_3^{2-} species in the reaction setup were developed.
- Liquid composition is measured in situ using Raman spectroscopy equipped with immersion probes.
- On-line Raman spectroscopy can speciate and quantify SO_3^{2-} , HSO_3^- , $\text{S}_2\text{O}_3^{2-}$ and SO_4^{2-} even in a mixture with NO_2^- , NO_3^- and CO_3^{2-} .
- Speciation is successful within the limits of the experiment for most of the molecules.
- The measured reaction rates of sulfite (SO_3^{2-}) and bisulfite (HSO_3^-) oxidation with O_2 are in agreement with the reviewed literature.

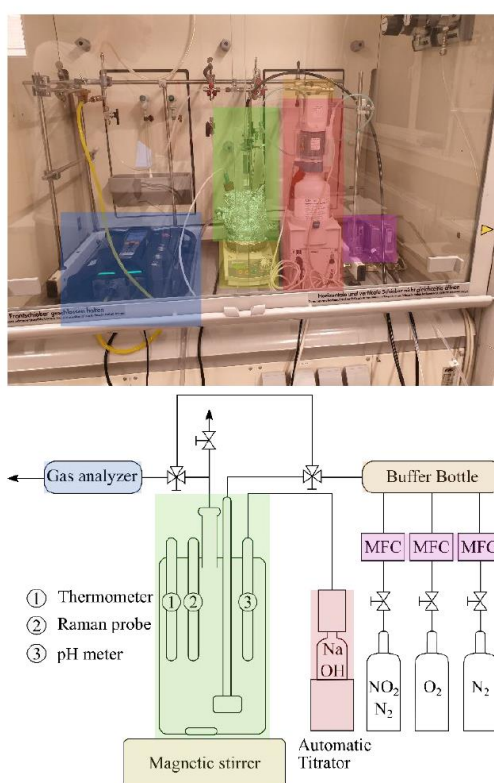


Figure 4.4: Laboratory Experiment Setup (@USN) for in-situ monitoring using Raman probe.¹⁰⁰

Article 6: Fast water-lean solvent screening using FTIR spectroscopy: In-situ (in-line) monitoring using an ATR reaction cell integrated with on-line monitoring attached to a liquid-flowcell.

Authors: Wagaarachchige, J.D.; Idris, Z.; Halstensen, M.; Jens, K.-J.

Published in Proceedings of the TCCS-11 - Trondheim Conference on CO₂ Capture, Transport and Storage, Trondheim, Norway, June 21-23, 2021, 2021; pp. 547-552

<https://hdl.handle.net/11250/2787331>

This is a conference article published in the proceedings of TCCS11 conference. Article 6 presents a fast and precise spectroscopic method that can be used for solvents characterization and to facilitate screening of novel CO₂ capture systems.

Highlights:

- Time-base Attenuated Total Reflectance-Fourier Transform Infrared (ATR-FTIR) spectroscopy was employed for the in-situ monitoring of CO₂ absorption and desorption processes in non-aqueous amine systems.
- The method enables the identification of the reaction mechanism, along with comprehensive speciation.
- To confirm repeatability and representativeness of the screening test, a replication experiment is conducted using liquid-flow cell FTIR analysis.

Article 7 and 8: Conversion of OZD to MEA

Article 7: *Application of Multivariate Data Analysis of Raman Spectroscopy Spectra of 2-oxazolidinone*

Authors: Mereu, F, Wagaarachchige, J.D.; Jens, K.-J; Idris, Z.

Published in SIMS EUROSIM 2021, and 62nd International Conference of Scandinavian Simulation Society, SIMS 2021, September 21-23, Virtual Conference, Finland. pp. 16-

21. <https://doi.org/10.3384/ecp2118516>

Article 8: *Response Surface Modelling to Reduce CO₂ Capture Solvent Cost by Conversion of OZD to MEA*

Authors: Mereu, F, Wagaarachchige, J.D.; Idris, Z.; Halstensen, M.; Jens, K.-J.

Published in Proceedings of the 64th International Conference of Scandinavian Simulation Society (SIMS), Västerås, Sweden, 2023-10-19, 2023; pp. 14-20.

<https://ecp.ep.liu.se/sims>

Articles 7 and 8 are published in the conference proceedings of SIMS EUROSIM 2021 and SIMS 2023 conferences, respectively. These articles address objectives 2 and 3 of this thesis. Both articles present findings from a chemometric investigation of the transformation of degradation species within the MEA solvent during service, focusing on 2-oxazolidinone (OZD), a heterocyclic five-membered organic ring compound, and its conversion back to MEA. My contribution in these articles includes multivariate data analysis, planning the design of experiments (DoE), and partial involvement in writing the article.

5 Conclusions and Recommendations

This chapter presents the conclusions of the study, followed by recommendations and future work.

Aligned with the first two main objectives of the work, this study employs a two-fold approach to provide insights into options to reduce the cost of amine-based PCC technology. The third objective offers directives to apply PAT in other gas treating technologies.

Figure 5.1 outlines the proposed set of chemometric approaches relevant to solvent management challenges in amine-based PCC technology.

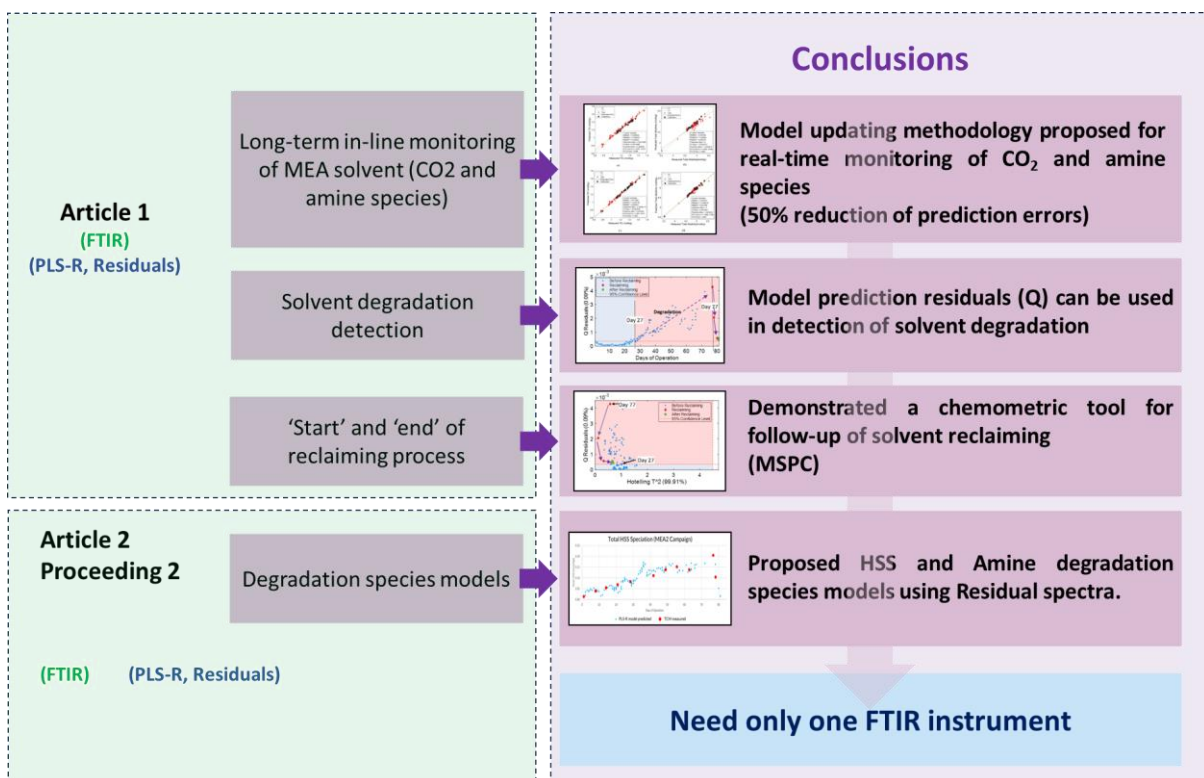


Figure 5.1: Conclusions of proposed chemometric solutions for solvent management

The four main conclusions that are given in Figure 5.1 are described below. All these four chemometric approaches can be applied using a single FTIR instrument.

- (i) FTIR spectroscopy can be successfully used for the chemical quantification of CO₂ and amine species in a 30 wt% aqueous MEA solvent using PLS-R models. Implementing a specific model updating plan enhances the ability of these models to cope with ongoing solvent degradation or changes during the plant operation, subsequently reducing initial model prediction errors by 50%.
- (ii) PLS-R model residuals of any species (either CO₂ or MEA) are instrumental in detecting solvent degradation. Average prediction residuals (Q values) can be used as a measure to quantify the extent of solvent degradation. This approach eliminates the need for specific degradation species analysis that are otherwise used in determining the extent of solvent degradation.
- (iii) Q residual values of PLS-R model predictions can be used to identify the 'start' and 'end' of solvent reclamation process. These results suggest that the application of PLS-R model based multivariate statistical process control (MSPC) is a reliable decision-making tool that can be used in solvent management practices.
- (iv) Prediction residual spectra of PLS-R models demonstrate a potential to be used in model preparation for degradation species quantification i.e., HSS and amine degradation products.

Figure 5.2 displays the main conclusions derived from the studies on the proposed non-aqueous solvent.

In-situ monitoring with an ATR-FTIR reaction cell was used and DPA is selected as the suitable amine to blend with methanol and sulfolane among the six other amines. The solvent blend composition, 30 wt% DPA, 35 wt% methanol, and 35 wt% sulfolane produces only MMC as the CO₂ capture product. Around 60°C, MMC is easily decomposed into CO₂. At 40°C, solvent viscosity changes from 1.02 mPa.s to 3.28 mPa.s, as the solvent condition transforms from unloaded to a fully CO₂-loaded ($\alpha = 0.88$) solvent. These viscosity changes closely align with the solvent viscosity changes of 30 wt% aqueous MEA.

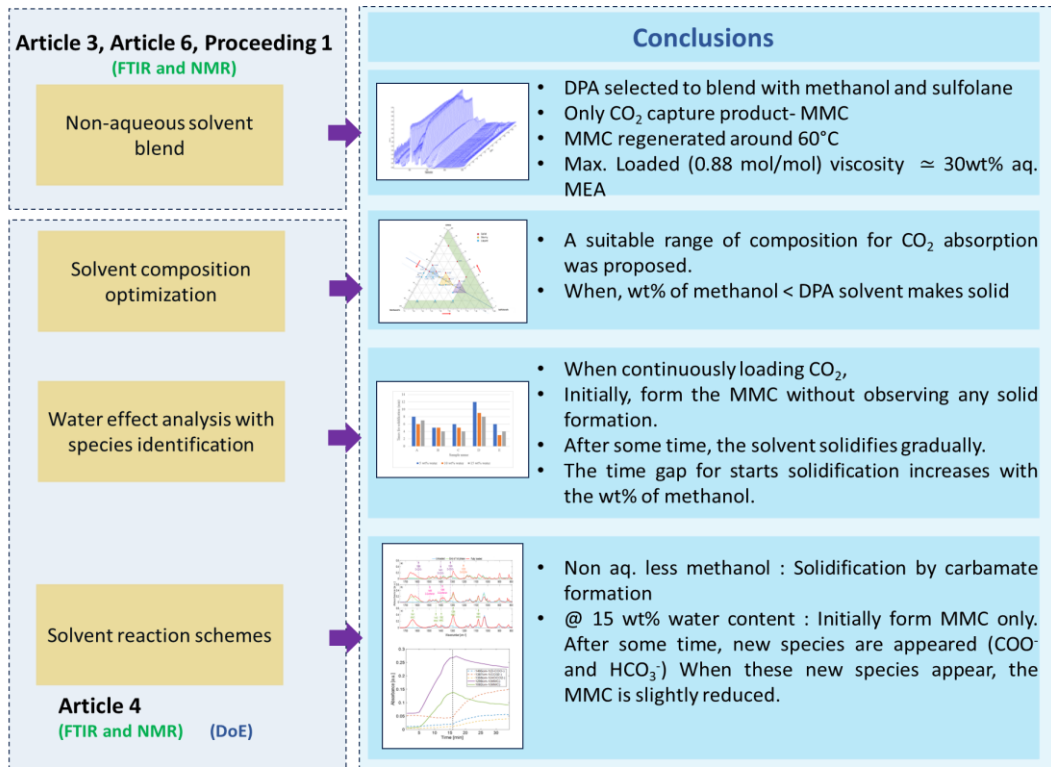


Figure 5.2: Conclusions of a study on non-aqueous solvent

Next step of the solvent investigation is to optimize the solvent composition and to evaluate the effect of water on solvent's CO₂ capture reactions. Results of the compositional optimization study is presented in a triangular plot in Article 4. Accordingly, it is found that, this solvent tends to solidify during the CO₂ absorption when the wt% of DPA is higher than or equal to wt% of methanol. Furthermore, maintaining the wt% of methanol higher than the wt% of DPA is crucial for preventing solvent solidification under non-aqueous conditions.

Despite containing 15 wt% of water, solvent initiates the formation of MMC with CO₂, as the first phase. However, after a while, the solvent starts to form carbamates and bicarbonates, leading to a reduction in the MMC formed during the first phase. To effectively prevent solidification in the presence of water, it is necessary to maintain a higher wt% of methanol than the wt% of DPA in the solvent and to control CO₂ absorption capacity only within a specific operational window.

Possible reaction schemes for these two conditions are proposed with the aid of species identification based on the FTIR and NMR analysis results.

A similar PAT approach is suggested to address other related flue gas testing issues as outlined below. Article 5 and Articles 7, 8 present the results of such two separate projects, in which I primarily contributed to the application of chemometrics.

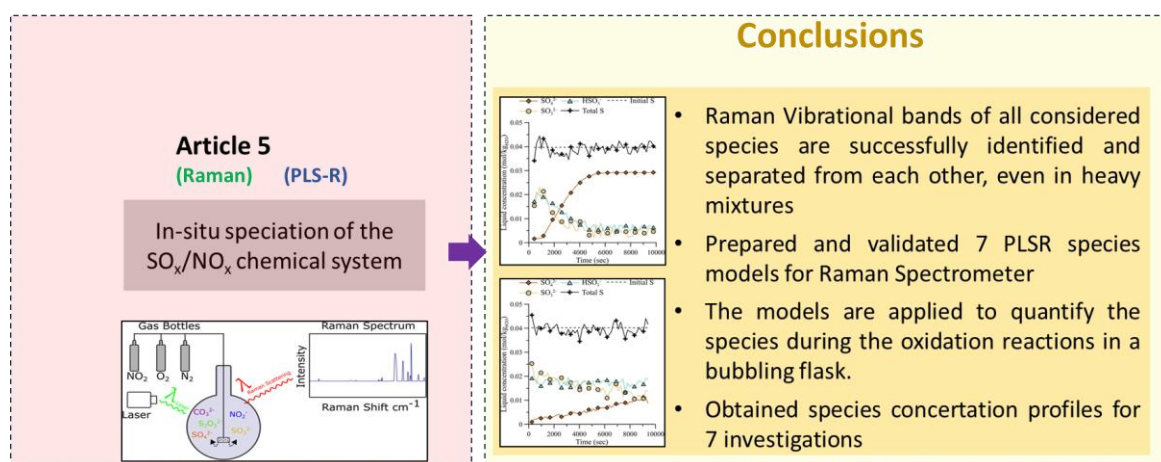


Figure 5.3: Conclusions of Article 5: Simultaneous absorption of SO_x and NO_x system

Figure 5.3 summarizes the main conclusions of Article 5 and its contribution to in-situ speciation of the SO_x and NO_x chemical system. Seven PLS-R models for SO_3^{2-} , HSO_3^- , $S_2O_3^{2-}$, SO_4^{2-} , NO_2^- , NO_3^- , and CO_3^{2-} were calibrated and subsequently validated using an independent test set. Raman vibrational bands of all considered species are successfully identified and separated from each other, even in mixtures, by using baseline correction with a Whitaker filter at $\lambda = 1$, $\rho = 1000$. Utilizing these models, we obtained seven concentration profiles for seven distinct experimental recipes through in-situ monitoring of the reaction flask using a Raman immersion probe. Accordingly, it is suggested that Raman spectroscopy could be a suitable method for liquid analysis of a combined NO_x/SO_x removal system.

Furthermore, this work influenced another project that was designed to obtain parametric optimization of a lab scale conversion of OZD back to MEA. Raman spectra of 40 OZD samples were collected, and PCA was applied to study these samples. The reaction parameters were optimized using design of experiments.

Recommendations and Future Work

For PAT application of acid gas absorption: In a previous study of our team, speciation models were developed and validated in the laboratory and were transferred to pilot scale application.⁸ This thesis demonstrates that PAT is useful for MEA solvent speciation for long-term solvent monitoring and solvent degradation follow-up, using TCM pilot plant analysis data; and in particular

1. Speciation models developed and validated using pilot scale analysis data-Useful for process monitoring of TIC & TA.
2. Development of self-adapting models to process and solvent changes, i.e., degradation.
3. Monitoring of the reclaiming process for follow-up and optimization by utilization of model residuals.

Relevant to the above three conclusions, following future work can be proposed.

- Item 1 above: In-line real-time long-term demonstration.
- Item 2 above: Investigation of effect of flue-gas composition and flow-rate variation in combination with USN's solvent degradation rig.
- Item 2 above: Application for degradation follow up of mixed amine solvent i.e., CESAR 1.
- Item 3 above: Optimization of MEA reclaiming: residence time, temperature, chemical composition in lab scale (reclaiming strategy 'fixed process' optimization)

For non-aqueous solvent study: Considering the tendency of the proposed non-aqueous solvent to form solids with water, it would be vital to develop a conceptual process design using Aspen Plus and evaluate the process design attributes for this type of a solvent.

For the study of simultaneous absorption of SO_x and NO_x system: Quantification of NO₂⁻ and NO₃⁻ is difficult in the present system with the chosen method. Addition of necessary species interactions to the PLS-R species model using DoE for calibration sample preparation will be more suitable for in-line monitoring of heavily mixed species systems.

References

1. IPCC, *Global Warming of 1.5°C: IPCC Special Report on Impacts of Global Warming of 1.5°C above Pre-industrial Levels in Context of Strengthening Response to Climate Change, Sustainable Development, and Efforts to Eradicate Poverty*. Cambridge University Press: Cambridge, 2022.
2. Cuff, M., Beyond 1.5°C: The hell years. *New Scientist* **2023**, 258, (3442), 32-35.
3. Pachauri, R. K.; Allen, M. R.; Barros, V. R.; Broome, J.; Cramer, W.; Christ, R.; Church, J. A.; Clarke, L.; Dahe, Q.; Dasgupta, P., *Climate change 2014: synthesis report. Contribution of Working Groups I, II and III to the fifth assessment report of the Intergovernmental Panel on Climate Change*. Ippc: 2014.
4. Kohl, A. L.; Nielsen, R. B., *Gas Purification*. Gulf Professional Publishing: Houston, 1997.
5. Rochelle, G. T., Amine Scrubbing for CO₂ Capture. *Science* **2009**, 325, (5948), 1652-1654.
6. Wang, M.; Lawal, A.; Stephenson, P.; Sidders, J.; Ramshaw, C., Post-combustion CO₂ capture with chemical absorption: A state-of-the-art review. *Chem. Eng. Res. Des.* **2011**, 89, (9), 1609-1624.
7. Rubin, E. S.; Davison, J. E.; Herzog, H. J., The cost of CO₂ capture and storage. *Int. J. Greenhouse Gas Control* **2015**, 40, 378-400.
8. Akram, M.; Jinadasa, M. H. W. N.; Tait, P.; Lucquiaud, M.; Milkowski, K.; Szuhanszki, J.; Jens, K.-J.; Halstensen, M.; Pourkashanian, M., Application of Raman spectroscopy to real-time monitoring of CO₂ capture at PACT pilot plant; Part 1: Plant operational data. *Int. J. Greenhouse Gas Control* **2020**, 95, 102969.
9. Jinadasa, M. H. W. N.; Jens, K.-J.; Øi, L. E.; Halstensen, M., Raman Spectroscopy as an Online Monitoring Tool for CO₂ Capture Process: Demonstration Using a Laboratory Rig. *Energy Procedia* **2017**, 114, 1179-1194.
10. Halstensen, M.; Jilvero, H.; Jinadasa, W. N.; Jens, K.-J., Equilibrium Measurements of the NH₃-CO₂-H₂O System: Speciation Based on Raman Spectroscopy and Multivariate Modeling. *J. Chem.* **2017**, 2017, 1-13.
11. Wagaarachchige, J. D.; Idris, Z.; Khatibzadeh, A.; Drageset, A.; Jens, K.-J.; Halstensen, M., Demonstration of CO₂ Capture Process Monitoring and Solvent Degradation Detection by Chemometrics at the Technology Centre Mongstad CO₂ Capture Plant. *Ind. Eng. Chem. Res.* **2023**, 62, (25), 9747-9754.

12. Bakeev, K. A., *Process analytical technology: spectroscopic tools and implementation strategies for the chemical and pharmaceutical industries*. John Wiley & Sons: 2010.
13. Oliveri, P.; Malegori, C.; Casale, M., 2 - Chemometrics: multivariate analysis of chemical data. In *Chemical Analysis of Food (Second Edition)*, Pico, Y., Ed. Academic Press: 2020; pp 33-76.
14. Wold, S., Chemometrics; what do we mean with it, and what do we want from it? *Chemometrics and Intelligent Laboratory Systems* **1995**, 30, (1), 109-115.
15. Kallithraka, S.; Arvanitoyannis, I. S.; Kefalas, P.; El-Zajouli, A.; Soufleros, E.; Psarra, E., Instrumental and sensory analysis of Greek wines; implementation of principal component analysis (PCA) for classification according to geographical origin. *Food Chemistry* **2001**, 73, (4), 501-514.
16. Martín-Sanz, J. P.; de Santiago-Martín, A.; Valverde-Asenjo, I.; Quintana-Nieto, J. R.; González-Huecas, C.; López-Lafuente, A. L., Comparison of soil quality indexes calculated by network and principal component analysis for carbonated soils under different uses. *Ecological Indicators* **2022**, 143, 109374.
17. Esbensen, K. H.; Swarbrick, B., *Multivariate Data Analysis: An introduction to Multivariate Analysis, Process Analytical Technology and Quality by Design* 6th ed.; CAMO software AS: 2017; p 452.
18. Wold, S.; Sjöström, M.; Eriksson, L., PLS-regression: a basic tool of chemometrics. *Chemometrics and Intelligent Laboratory Systems* **2001**, 58, (2), 109-130.
19. Sjöblom, J.; Svensson, O.; Josefson, M.; Kullberg, H.; Wold, S., An evaluation of orthogonal signal correction applied to calibration transfer of near infrared spectra. *Chemometrics and Intelligent Laboratory Systems* **1998**, 44, (1), 229-244.
20. Eilers, P. H. C., A Perfect Smoother. *Anal. Chem.* **2003**, 75, (14), 3631-3636.
21. Barnes, R. J.; Dhanoa, M. S.; Lister, S. J., Standard Normal Variate Transformation and De-Trending of Near-Infrared Diffuse Reflectance Spectra. *Appl. Spectrosc.* **1989**, 43, (5), 772-777.
22. Esquerre, C.; Gowen, A. A.; Burger, J.; Downey, G.; O'Donnell, C. P., Suppressing sample morphology effects in near infrared spectral imaging using chemometric data pre-treatments. *Chemometrics and Intelligent Laboratory Systems* **2012**, 117, 129-137.
23. Martens, H.; Nielsen, J. P.; Engelsen, S. B., Light Scattering and Light Absorbance Separated by Extended Multiplicative Signal Correction. Application to Near-Infrared Transmission Analysis of Powder Mixtures. *Anal. Chem.* **2003**, 75, (3), 394-404.

24. Stark, E. W.; Martens, H.; Vegen, G.; G., M.; Hieftje; Hirschfeld, T.; Åge, S. H.; Jensen In *Multivariate Linearity Transformations for Near-Infrared Reflectance Spectrometry*, 2017; 2017.
25. Hotelling, H., Analysis of a complex of statistical variables into principal components. *J. Educ. Psychol.* **1933**, 24, 417-441.
26. Cook, R. D.; Weisberg, S., *Residuals and Influence in Regression*. New York: Chapman and Hall: 1982.
27. Ni, W.; Brown, S. D.; Man, R., Data fusion in multivariate calibration transfer. *Anal. Chim. Acta* **2010**, 661, (2), 133-142.
28. Workman, J. J., A Review of Calibration Transfer Practices and Instrument Differences in Spectroscopy. *Appl. Spectrosc.* **2018**, 72, (3), 340-365.
29. Workman, J. J., The Essential Aspects of Multivariate Calibration Transfer. In *40 Years of Chemometrics – From Bruce Kowalski to the Future*, American Chemical Society: 2015; Vol. 1199, pp 257-282.
30. Fearn, T., Standardisation and Calibration Transfer for near Infrared Instruments: A Review. *J. Near Infrared Spectrosc.* **2001**, 9, (4), 229-244.
31. Bouveresse, E.; Massart, D. L., Standardisation of near-infrared spectrometric instruments: A review. *Vib. Spectrosc.* **1996**, 11, (1), 3-15.
32. Feudale, R. N.; Woody, N. A.; Tan, H.; Myles, A. J.; Brown, S. D.; Ferré, J., Transfer of multivariate calibration models: a review. *Chemometrics and Intelligent Laboratory Systems* **2002**, 64, (2), 181-192.
33. Bergman, E.-L.; Brage, H.; Josefson, M.; Svensson, O.; Sparén, A., Transfer of NIR calibrations for pharmaceutical formulations between different instruments. *Journal of Pharmaceutical and Biomedical Analysis* **2006**, 41, (1), 89-98.
34. Bouveresse, E.; Hartmann, C.; Massart, D. L.; Last, I. R.; Prebble, K. A., Standardization of Near-Infrared Spectrometric Instruments. *Anal. Chem.* **1996**, 68, (6), 982-990.
35. Walczak, B.; Bouveresse, E.; Massart, D. L., Standardization of near-infrared spectra in the wavelet domain. *Chemometrics and Intelligent Laboratory Systems* **1997**, 36, (1), 41-51.
36. Osborne, B. G.; Fearn, T., Collaborative evaluation of universal calibrations for the measurement of protein and moisture in flour by near infrared reflectance. *International Journal of Food Science & Technology* **1983**, 18, (4), 453-460.
37. Wise, B. M.; Roginski, R. T., A Calibration Model Maintenance Roadmap. *IFAC-PapersOnLine* **2015**, 48, (8), 260-265.

38. Montgomery, D. C., *Design and Analysis of experiments* John Wiley & Sons, Inc New York Wiley, 2001.
39. Wagner, C.; Esbensen, K. H., Theory of Sampling: Four Critical Success Factors Before Analysis. *Journal of AOAC INTERNATIONAL* **2019**, 98, (2), 275-281.
40. Esbensen, K., *Introduction to the Theory and Practice of Sampling*. IM Publication Open, 2020; Vol. 2020.
41. Esbensen, K.; Sivalingam, V., The sampling interface—A critical Theory of Sampling success factor in process sampling and PAT. **2022**, 11, (1), 115-129.
42. Ferraro, J. R.; Nakamoto, K., *Introductory Raman Spectroscopy*. Elsevier Science: 2012.
43. Wagaarachchige, J. D.; Idris, Z.; Halstensen, M.; Jens, K.-J., Fast water-lean solvent screening using FTIR spectroscopy: In-situ (in-line) monitoring using an ATR reaction cell integrated with on-line monitoring attached to a liquid-flowcell. In *TCCS-11 - Trondheim Conference on CO₂ Capture, Transport and Storage*, SINTEF proceedings no 7: Trondheim, Norway, 2021; pp 547-552.
44. Kaur, H.; Rana, B.; Tomar, D.; Kaur, S.; Jena, K. C., Fundamentals of ATR-FTIR Spectroscopy and Its Role for Probing In-Situ Molecular-Level Interactions. In *Modern Techniques of Spectroscopy: Basics, Instrumentation, and Applications*, Singh, D. K.; Pradhan, M.; Materny, A., Eds. Springer Singapore: Singapore, 2021; pp 3-37.
45. Wagaarachchige, J. D.; Idris, Z.; Arstad, B.; Kummamuru, N. B.; Sætre, K. A. S.; Halstensen, M.; Jens, K.-J., Low-Viscosity Nonaqueous Sulfolane–Amine–Methanol Solvent Blend for Reversible CO₂ Capture. *Ind. Eng. Chem. Res.* **2022**, 61, (17), 5942-5951.
46. Raman, C. V.; Krishnan, K. S., A New Type of Secondary Radiation. *Nature* **1928**, 121, (3048), 501-502.
47. Leung, D. Y. C.; Caramanna, G.; Maroto-Valer, M. M., An overview of current status of carbon dioxide capture and storage technologies. *Renewable and Sustainable Energy Reviews* **2014**, 39, 426-443.
48. Rezazadeh, F.; Gale, W. F.; Rochelle, G. T.; Sachde, D., Effectiveness of absorber intercooling for CO₂ absorption from natural gas fired flue gases using monoethanolamine solvent. *Int. J. Greenhouse Gas Control* **2017**, 58, 246-255.
49. Elwell, L. C.; Grant, W. S., Technology options for capturing CO₂. *Power (New York)* **2006**, 149, Medium: X; Size: page(s) 60,62-65 2010-06-03.
50. Bhowan, A. S.; Freeman, B. C., Analysis and Status of Post-Combustion Carbon Dioxide Capture Technologies. *Environ. Sci. Technol.* **2011**, 45, (20), 8624-8632.

51. Bui, M.; Flø, N. E.; de Cazenove, T.; Mac Dowell, N., Demonstrating flexible operation of the Technology Centre Mongstad (TCM) CO₂ capture plant. *Int. J. Greenhouse Gas Control* **2020**, 93, 102879.
52. Roberts, R. B. Process for Separating Acidic Gases. U. S. Patent No. 1,783,901
1930.
53. Veawab, A.; Aroonwilas, A.; Tontiwachwuthikul, P., CO₂ absorption performance of aqueous alkanolamines in packed columns. *Fuel Chemistry Division Preprints* **2002**, 47, (1), 49-50.
54. Barzagli, F.; Lai, S.; Mani, F., Novel non-aqueous amine solvents for reversible CO₂ capture. *Energy Procedia* **2014**, 63, 1795-1804.
55. van der Spek, M.; Bonalumi, D.; Manzolini, G.; Ramirez, A.; Faaij, A., Techno-economic Comparison of Combined Cycle Gas Turbines with Advanced Membrane Configuration and Monoethanolamine Solvent at Part Load Conditions. *Energy & Fuels* **2018**, 32, (1), 625-645.
56. Sodiq, A.; Hadri, N. E.; Goetheer, E. L. V.; Abu-Zahra, M. R. M., Chemical reaction kinetics measurements for single and blended amines for CO₂ postcombustion capture applications. *Int. J. Chem. Kinet.* **2018**, 50, (9), 615-632.
57. Yang, D.; Lv, M.; Chen, J., Efficient non-aqueous solvent formed by 2-piperidineethanol and ethylene glycol for CO₂ absorption. *Chem. Commun.* **2019**, 55, (83), 12483-12486.
58. Song, J.-H.; Yoon, J.-H.; Lee, H.; Lee, K.-H., Solubility of Carbon Dioxide in Monoethanolamine + Ethylene Glycol + Water and Monoethanolamine + Poly (ethylene glycol) + Water. *J. Chem. Eng. Data* **1996**, 41, (3), 497-499.
59. DuPart, M. S.; Bacon, T. R.; Edwards, D. J., Understanding corrosion in alkanolamine gas treating plants: Part 1. *Hydrocarbon Processing; (United States)* **1993**, Medium: X; Size: Pages: 75-80.
60. Rochelle, G.; Chen, E.; Freeman, S.; Van Wagener, D.; Xu, Q.; Voice, A., Aqueous piperazine as the new standard for CO₂ capture technology. *Chem. Eng. J.* **2011**, 171, (3), 725-733.
61. Chen, X.; Rochelle, G. T., Aqueous piperazine derivatives for CO₂ capture: Accurate screening by a wetted wall column. *Chem. Eng. Res. Des.* **2011**, 89, (9), 1693-1710.
62. Mangalapally, H. P.; Hasse, H., Pilot plant study of two new solvents for post combustion carbon dioxide capture by reactive absorption and comparison to monoethanolamine. *Chem. Eng. Sci.* **2011**, 66, (22), 5512-5522.

63. Knudsen, J. N.; Andersen, J.; Jensen, J. N.; Biede, O., Evaluation of process upgrades and novel solvents for the post combustion CO₂ capture process in pilot-scale. *Energy Procedia* **2011**, 4, 1558-1565.
64. Heldebrant, D. J.; Koech, P. K.; Glezakou, V.-A.; Rousseau, R.; Malhotra, D.; Cantu, D. C., Water-Lean Solvents for Post-Combustion CO₂ Capture: Fundamentals, Uncertainties, Opportunities, and Outlook. *Chem. Rev.* **2017**, 117, (14), 9594-9624.
65. *Accelerating Breakthrough Innovation in Carbon Capture, Utilization, and Storage ; Mission Innovation workshop, September 2017*; U.S. Department of Energy, Houston, Texas, USA: 2017.
66. Heldebrant, D. J.; Koech, P. K.; Rousseau, R.; Glezakou, V.-A.; Cantu, D.; Malhotra, D.; Zheng, F.; Whyatt, G.; Freeman, C. J.; Bearden, M. D., Are Water-lean Solvent Systems Viable for Post-Combustion CO₂ Capture? *Energy Procedia* **2017**, 114, 756-763.
67. Lail, M.; Tanthana, J.; Coleman, L., Non-Aqueous Solvent (NAS) CO₂ Capture Process. *Energy Procedia* **2014**, 63, 580-594.
68. Bougie, F.; Pokras, D.; Fan, X., Novel non-aqueous MEA solutions for CO₂ capture. *Int. J. Greenhouse Gas Control* **2019**, 86, 34-42.
69. McCann, N.; Phan, D.; Wang, X.; Conway, W.; Burns, R.; Attalla, M.; Puxty, G.; Maeder, M., Kinetics and Mechanism of Carbamate Formation from CO₂(aq), Carbonate Species, and Monoethanolamine in Aqueous Solution. *The Journal of Physical Chemistry A* **2009**, 113, (17), 5022-5029.
70. Kortunov, P. V.; Baugh, L. S.; Siskin, M.; Calabro, D. C., In Situ Nuclear Magnetic Resonance Mechanistic Studies of Carbon Dioxide Reactions with Liquid Amines in Mixed Base Systems: The Interplay of Lewis and Brønsted Basicities. *Energy & Fuels* **2015**, 29, (9), 5967-5989.
71. Kortunov, P. V.; Siskin, M.; Baugh, L. S.; Calabro, D. C., In Situ Nuclear Magnetic Resonance Mechanistic Studies of Carbon Dioxide Reactions with Liquid Amines in Non-aqueous Systems: Evidence for the Formation of Carbamic Acids and Zwitterionic Species. *Energy & Fuels* **2015**, 29, (9), 5940-5966.
72. Kortunov, P. V.; Siskin, M.; Baugh, L. S.; Calabro, D. C., In Situ Nuclear Magnetic Resonance Mechanistic Studies of Carbon Dioxide Reactions with Liquid Amines in Aqueous Systems: New Insights on Carbon Capture Reaction Pathways. *Energy & Fuels* **2015**, 29, (9), 5919-5939.
73. Kortunov, P. V.; Siskin, M.; Paccagnini, M.; Thomann, H., CO₂ Reaction Mechanisms with Hindered Alkanolamines: Control and Promotion of Reaction Pathways. *Energy & Fuels* **2016**, 30, (2), 1223-1236.

74. Wanderley, R. R.; Høisæter, K. K.; Knuutila, H. K., Signs of alkylcarbonate formation in water-lean solvents: VLE-based understanding of pKa and pKs effects. *Int. J. Greenhouse Gas Control* **2021**, 109, 103398.
75. Wanderley, R. R.; Pinto, D. D. D.; Knuutila, H. K., From hybrid solvents to water-lean solvents – A critical and historical review. *Sep. Purif. Technol.* **2021**, 260, 118193.
76. Barzagli, F.; Mani, F.; Peruzzini, M., Efficient CO₂ absorption and low temperature desorption with non-aqueous solvents based on 2-amino-2-methyl-1-propanol (AMP). *Int. J. Greenhouse Gas Control* **2013**, 16, 217-223.
77. Behrens, R.; Kessler, E.; Münnemann, K.; Hasse, H.; von Harbou, E., Monoalkylcarbonate formation in the system monoethanolamine–water–carbon dioxide. *Fluid Phase Equilib.* **2019**, 486, 98-105.
78. Cieslarova, Z.; dos Santos, V. B.; do Lago, C. L., Both carbamates and monoalkyl carbonates are involved in carbon dioxide capture by alkanolamines. *Int. J. Greenhouse Gas Control* **2018**, 76, 142-149.
79. Heldebrant, D. J.; Yonker, C. R.; Jessop, P. G.; Phan, L., CO₂-binding organic liquids (CO₂ BOLs) for post-combustion CO₂ capture. *Energy Procedia* **2009**, 1, (1), 1187-1195.
80. Rochelle, G. T., Thermal degradation of amines for CO₂ capture. *Current Opinion in Chemical Engineering* **2012**, 1, (2), 183-190.
81. Fredriksen, S. B.; Jens, K.-J., Oxidative Degradation of Aqueous Amine Solutions of MEA, AMP, MDEA, Pz: A Review. *Energy Procedia* **2013**, 37, 1770-1777.
82. Morken, A. K.; Pedersen, S.; Kleppe, E. R.; Wisthaler, A.; Vernstad, K.; Ullestad, Ø.; Flø, N. E.; Faramarzi, L.; Hamborg, E. S., Degradation and Emission Results of Amine Plant Operations from MEA Testing at the CO₂ Technology Centre Mongstad. *Energy Procedia* **2017**, 114, 1245-1262.
83. Campbell, M.; Akhter, S.; Knarvik, A.; Muhammad, Z.; Wakaa, A., CESAR1 Solvent Degradation and Thermal Reclaiming Results from TCM Testing. In *16th Greenhouse Gas Control Technologies Conference (GHGT-16)* SSRN: <https://ssrn.com/abstract=4286150> or <http://dx.doi.org/10.2139/ssrn.4286150>: Lyon, France, 2022.
84. Wang, T.; Hovland, J.; Jens, K. J., Amine reclaiming technologies in post-combustion carbon dioxide capture. *J. Environ. Sci.* **2015**, 27, 276-289.
85. Idem, R.; Wilson, M.; Tontiwachwuthikul, P.; Chakma, A.; Veawab, A.; Aroonwilas, A.; Gelowitz, D., Pilot Plant Studies of the CO₂ Capture Performance of Aqueous MEA and Mixed MEA/MDEA Solvents at the University of Regina CO₂ Capture Technology Development Plant

and the Boundary Dam CO₂ Capture Demonstration Plant. *Ind. Eng. Chem. Res.* **2006**, 45, (8), 2414-2420.

86. Strazisar, B. R.; Anderson, R. R.; White, C. M., Degradation Pathways for Monoethanolamine in a CO₂ Capture Facility. *Energy & Fuels* **2003**, 17, (4), 1034-1039.

87. Flø, N. E.; Faramarzi, L.; de Cazenove, T.; Hvidsten, O. A.; Morken, A. K.; Hamborg, E. S.; Vernstad, K.; Watson, G.; Pedersen, S.; Cents, T.; Fostås, B. F.; Shah, M. I.; Lombardo, G.; Gjernes, E., Results from MEA Degradation and Reclaiming Processes at the CO₂ Technology Centre Mongstad. *Energy Procedia* **2017**, 114, 1307-1324.

88. Morken, A. K.; Pedersen, S.; Nesse, S. O.; Flø, N. E.; Johnsen, K.; Feste, J. K.; de Cazenove, T.; Faramarzi, L.; Vernstad, K., CO₂ capture with monoethanolamine: Solvent management and environmental impacts during long term operation at the Technology Centre Mongstad (TCM). *Int. J. Greenhouse Gas Control* **2019**, 82, 175-183.

89. Wagaarachchige, J. D.; Idris, Z.; Khatibzadeh, A.; Drageset, A.; Jens, K.-J.; Halstensen, M., Demonstration of CO₂ Capture Process Monitoring and Solvent Degradation Detection by Chemometrics at the Technology Centre Mongstad CO₂ Capture Plant. *Ind. Eng. Chem. Res.* **2023**.

90. Reynolds, A. J.; Verheyen, T. V.; Adeloju, S. B.; Meuleman, E.; Feron, P., Towards Commercial Scale Postcombustion Capture of CO₂ with Monoethanolamine Solvent: Key Considerations for Solvent Management and Environmental Impacts. *Environ. Sci. Technol.* **2012**, 46, (7), 3643-3654.

91. Mazari, S. A.; Si Ali, B.; Jan, B. M.; Saeed, I. M.; Nizamuddin, S., An overview of solvent management and emissions of amine-based CO₂ capture technology. *Int. J. Greenhouse Gas Control* **2015**, 34, 129-140.

92. Kohl, A.; Richard, N., *Gas Purification*. 1997.

93. Veltman, K.; Singh, B.; Hertwich, E. G., Human and Environmental Impact Assessment of Postcombustion CO₂ Capture Focusing on Emissions from Amine-Based Scrubbing Solvents to Air. *Environ. Sci. Technol.* **2010**, 44, (4), 1496-1502.

94. Supap, T.; Saiwan, C.; Idem, R.; Tontiwachwuthikul, P. P. T., Part 2: Solvent management: solvent stability and amine degradation in CO₂ capture processes. *Carbon Management* **2011**, 2, (5), 551-566.

95. Karl, M.; Wright, R. F.; Berglen, T. F.; Denby, B., Worst case scenario study to assess the environmental impact of amine emissions from a CO₂ capture plant. *Int. J. Greenhouse Gas Control* **2011**, 5, (3), 439-447.

96. Shao, R.; Stangeland, A., Amines Used in CO₂ Capture. *The Bellona Foundation Technical Report, Oslo, Norway* **2009**.

97. Johansson, J.; Heijnesson Hultén, A.; Normann, F.; Andersson, K., Simultaneous Removal of NO_x and SO_x from Flue Gases Using ClO₂: Process Scaling and Modeling Simulations. *Ind. Eng. Chem. Res.* **2021**, 60, (4), 1774-1783.

98. Johansson, J.; Normann, F.; Sarajlic, N.; Andersson, K., Technical-Scale Evaluation of Scrubber-Based, Co-Removal of NO_x and SO_x Species from Flue Gases via Gas-Phase Oxidation. *Ind. Eng. Chem. Res.* **2019**, 58, (48), 21904-21912.

99. Asghar, U.; Rafiq, S.; Anwar, A.; Iqbal, T.; Ahmed, A.; Jamil, F.; Khurram, M. S.; Akbar, M. M.; Farooq, A.; Shah, N. S.; Park, Y.-K., Review on the progress in emission control technologies for the abatement of CO₂, SO_x and NO_x from fuel combustion. *Journal of Environmental Chemical Engineering* **2021**, 9, (5), 106064.

100. Johansson, J.; Wagaarachchige, J. D.; Normann, F.; Idris, Z.; Haugen, E. R.; Halstensen, M.; Jinadasa, W.; Jens, K. J.; Andersson, K., Influence of Nitrogen Dioxide Absorption on the Sulfite Oxidation Rate in the Presence of Oxygen: Online Raman Measurements. *Ind. Eng. Chem. Res.* **2023**.

Part - II

Article 1

Demonstration of CO₂ Capture Process Monitoring and Solvent Degradation Detection by Chemometrics at the Technology Centre Mongstad CO₂ Capture Plant

Jayangi D. Wagaarachchige¹, Zulkifli Idris², Ayandeh Khatibzadeh¹, Audun Drageset³, Klaus-J.
Jens², and Maths Halstensen^{1*}

¹Department of Electrical, IT and Cybernetics, University of South-Eastern Norway,
Porsgrunn, Norway

²Department of Process, Energy and Environmental Technology, University of South-Eastern
Norway, Porsgrunn, Norway

³Technology Center Mongstad (TCM-DA), Mongstad, Norway

Published in Industrial & Engineering Chemistry Research Journal, ACS Publications

<https://doi.org/10.1021/acs.iecr.3c00134>

Demonstration of CO₂ Capture Process Monitoring and Solvent Degradation Detection by Chemometrics at the Technology Centre Mongstad CO₂ Capture Plant

Jayangi D. Wagaarachchige, Zulkifli Idris, Ayandeh Khatibzadeh, Audun Drageset, Klaus-J. Jens, and Maths Halstensen*

Cite This: *Ind. Eng. Chem. Res.* 2023, 62, 9747–9754

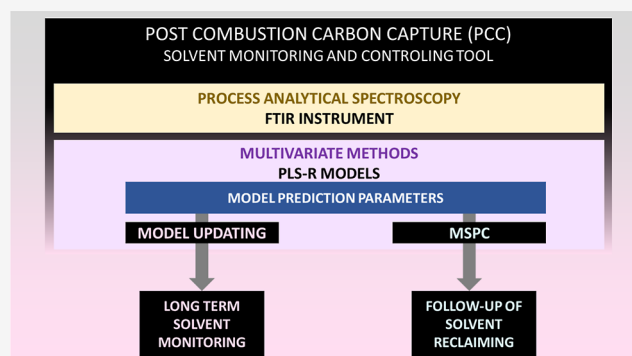
Read Online

ACCESS |

Metrics & More

Article Recommendations

ABSTRACT: Solvent management is one of the important current challenges in post combustion carbon capture (PCC) technology development. Using large-scale 1960 h test campaign data (Technology Centre Mongstad, Norway, 2015 MEA Test), we demonstrate a combination of multivariate methods (PLS-R, MSPC) and process analytical spectroscopy (FT-IR) as a tool to monitor and control PCC process performance. Two MEA solvent monitoring models, total inorganic carbon (TIC) content and total alkalinity (TA), were prepared. In long-term solvent monitoring, PLS-R model prediction uncertainty increased due to gradual solvent changes, e.g., solvent degradation and impurity accumulation. Hence, we show a specific model update methodology to keep the models updated, leading to good long-term monitoring ability of the TIC and TA models. In addition to reliable long-term solvent monitoring ability, a new principle for follow-up of thermal solvent reclaiming was demonstrated. This shows that the need for solvent reclaiming can be quantified. Furthermore, this methodology is an indicator to see the actual solvent deviation from the fresh solvent. This quantification may provide an input for “start” and “end of reclaiming operation” identification. Hence, we demonstrate that it is possible to extract information for process performance follow-up, solvent monitoring, and solvent reclaiming from a single spectroscopic instrument.



1. INTRODUCTION

The devastating environmental impacts of climate change are the biggest challenges of the 21st century. Post-combustion carbon capture (PCC) is an essential effort to eliminate the anthropogenic CO₂ emissions from burning of fossil fuels. The gas–liquid absorption–desorption process is the most prevailing abatement technology available in the industry. The 30 wt % aqueous monoethanolamine (MEA) solution is considered a typical benchmark solvent for CO₂ capture.¹ High energy penalty for solvent regeneration² corrosivity of the solvent,^{3,4} high solvent losses due to oxidative and thermal degradations,^{5–9} and environmental concerns due to possible emissions¹⁰ are major issues that still need to be addressed for an effective operation of PCC.

In order to maintain optimal performance of the CO₂ capture process, it needs to be monitored and controlled. The application of process analytical technology (PAT) using spectroscopy is an important approach for enhanced control of CO₂ capture operations. Spectroscopy is a powerful non-invasive analytical technique for chemical analyses giving direct speciation measurements at molecular level. Partial least squares regression (PLS-R) is a valuable statistical method to extract

quantitative chemical information from spectroscopic data. PLS-R models have been successfully used by us for online monitoring/speciation of MEA solvent-based CO₂ capture.^{11,12} Furthermore, preparation of Fourier-transform infrared (FTIR) spectroscopy-based PLS-R models for MEA solvent is published.^{13–15} This contribution demonstrates application of PAT and spectroscopy for solvent degradation follow up exemplified by the use of available test campaign data of the TCM MEA2 campaign.

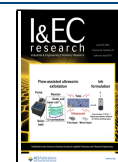
In terms of solvent management, spectroscopy is useful since it is sensitive to molecular change of the chemical system. PLS-R models are useful for extraction of specific chemical information of interest, for instance total solvent alkalinity, total inorganic carbon, etc. from spectroscopic data. These data are useful to

Received: January 13, 2023

Revised: June 6, 2023

Accepted: June 6, 2023

Published: June 16, 2023



give an early warning of upcoming chemical solvent change. As the solvent composition changes in service (i.e., solvent degradation and accumulation of flue gas impurities contents), the PLS-R model of the monitoring loop must be updated to stay representative for the state of the process. A deviation of the PLS-R model prediction parameters [i.e., Q -residual (Q) and Hotelling's T^2 (T^2)] is an indication of a deviation between actual solvent state and fresh solvent. Multivariate statistical process control (MSPC) is a method that can be used in process control with the use of, e.g., PLS-R models diagnostic measures such as Q and T^2 .^{16,17} Hence, suitable process control decisions for solvent management can be taken accordingly.

The Technology Centre Mongstad (TCM) is one of the largest global post-combustion CO₂ capture test centers which holds the most advanced test arena for CO₂ capture. Until now, several test campaigns using aqueous 30 wt % MEA solvent have been demonstrated and the outcomes from these campaigns have been published.^{10,18–22} The University of South-Eastern Norway (USN) received a comprehensive data set of TCM's 2015 campaign (MEA2) for chemometric evaluation.

This paper presents a FTIR-based PAT approach using PLS-R models for continuous process monitoring and solvent degradation detection in an amine-based CO₂ capture plant using data from the TCM plant.

2. MATERIALS AND METHODS

2.1. Materials. In this study, TCM-MEA2 campaign FTIR spectra and corresponding analytical data were utilized. All data used are off-line sample measurements that were obtained from the same sampling point (Lean stream) of the TCM Amine Plant located at Mongstad, Norway.

FTIR spectra of 125 samples were measured during the total campaign period using a Bruker ALPHA ATR-FTIR spectrometer with a diamond crystal and were used as input data to the PLS-R models. Furthermore, TCM provided the total inorganic carbon (TIC) and total alkalinity (TA) analysis data (reference data) that were recorded during the actual campaign period corresponding to the given spectra. The reference data were used as the response output variables of the PLS-R models that were prepared in this work. The details are shown in Table 1.

Table 1. Details of the Reference Data Used for the Preparation of Models (MEA2 Campaign)

reference analysis method ¹⁰	species group	reference analysis unit	number of reference data
total alkalinity	amine species	mol/kg	103
total inorganic carbon	CO ₂ species	mol/kg	120

2.1.1. Origin of Data: The 2015 TCM-DA MEA2 Campaign. MEA2 is a 1960 h operation which started on 6th of July 2015 and lasted until 17th October, 2015.¹⁰ The base case testing was performed on 7th September, 2015 in the steady state condition after approximately 8 weeks since startup.¹⁸ Morken et al. illustrated the overall campaign operational hours,¹⁰ whereas Gjernes et al. tabulated the overall test activities.²⁰ This operation was mainly conducted using a combined-cycle gas turbine-based combined-heat-and-power (CHP) plant flue gas that contains about 3.5% CO₂.²⁰ Furthermore, a mixture of CHP and RFCC (residual fluidized catalytic cracker)/RFCC flue gas

alone was used for a few days.²⁰ This work contributed to several TCM authored publications on aqueous MEA-based CO₂ capture by covering solvent emissions and degradation,¹⁰ corrosion,²¹ and reclaiming.¹⁹ Thermal reclaiming was performed for 92 h after 1830 (day 77) h of campaign operation. After the reclaiming process was completed, the operation continued for another 28 h. Hence, the MEA2 campaign mainly comprises of the primary stages of an amine-based CO₂ capture plant operation.

2.2. Methods. Figure 1 lists the three key stages of the data analysis hierarchy employed in this work. Figure 2 illustrates the main chemometric activities in each stage which are listed in Figure 1—using PLS-R model of CO₂ (TIC-1). The same approach was followed in the analysis work on the total alkalinity model (TA-1). All the abbreviations/statistical parameters used in this work are tabulated in Table 2.

2.2.1. Stage 1: Preparation of the Initial Models (TIC-1 and TA-1). As shown in Figure 1, Stage 1, PLS-R models for CO₂ (TIC-1) and total alkalinity (TA-1) species groups were initially prepared. The PLS-R algorithm known as NIPALS (nonlinear iterative partial least squares) was used in the model preparation.^{23,24} Campaign data gathered up to 15th August 2015 (approximately initial 600 h of operation) were selected for calibration and validation processes of the TIC-1 and TA-1 models.¹⁰ This was done to select the samples representing the non-degraded/fresh solvent. The infrared (IR) vibration band assignment of the chemical species was used to ensure only relevant variable ranges were used in the modeling. The FTIR spectra were preprocessed using the baseline correction method called Whittaker filter to remove unwanted baseline variation.²⁵ The models were validated using an independent test data sets which were obtained from the same initial 600 h MEA2 operation. Average model prediction errors were calculated as residual Y-variance of prediction which are denoted as root mean square error of prediction (RMSEP) (eq 1).²³ The optimal number of latent variables (LVs)²³ in the models were selected to attain the lowest values of RMSEP. Then, the models (TIC-1 and TA-1) were used for the prediction of the complete set of spectra of the MEA2 campaign.

$$\text{RMSEP} = \sqrt{\frac{\sum_{i=1}^I (y_{\text{predicted}} - y_{\text{reference}})^2}{I}} \quad (1)$$

where i —no of samples; $y_{\text{predicted}}$ —predicted value; and $y_{\text{reference}}$ —measured value.

2.2.2. Stage 2: Refining PLS-R Models to Handle a Degraded Solvent. During the second stage, important statistical parameters²³ of TIC-1 and TA-1 predictions, such as Q residuals (Q), Hotelling's T^2 (T^2), and leverages were recorded to adopt the models to the degraded solvent. All the spectral samples of the MEA2 campaign were mapped in the plot of T^2 versus Q which is an important tool in fault detection. Recorded prediction leverages were used to select new samples for the model updating step which is described in Section 2.2.3.2.

2.2.3. Stage 3: Applications of PLS-R Model's Prediction Statistics for Degrading Solvent Monitoring and Management. In the third stage, three different chemometric approaches were explored to demonstrate how the PLS-R model statistical parameters can be used to update the model to stabilize predictions during the whole operation, and how the model residuals are useful for solvent management.

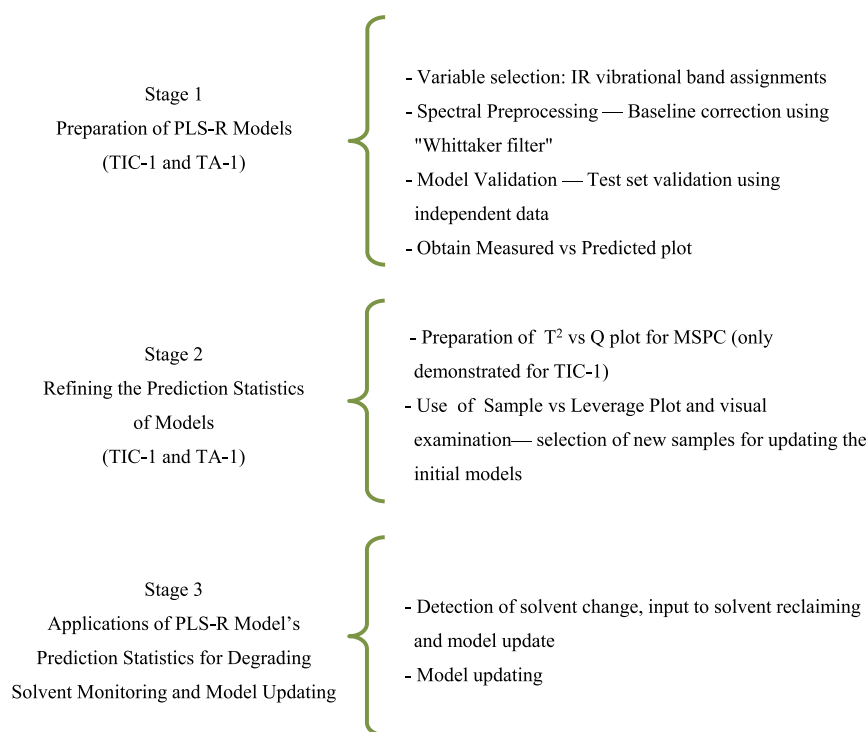


Figure 1. Main stages of chemometric analysis.

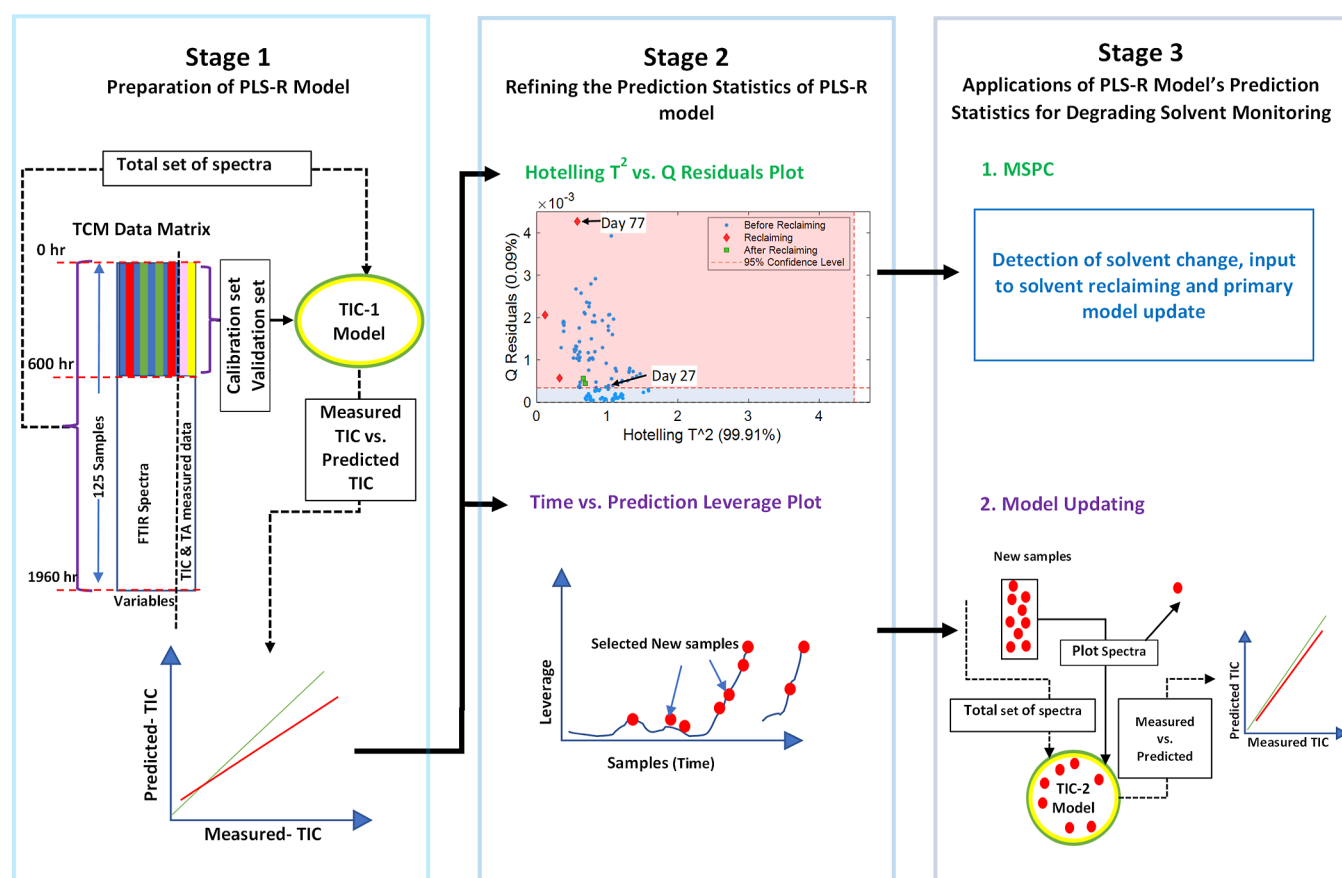


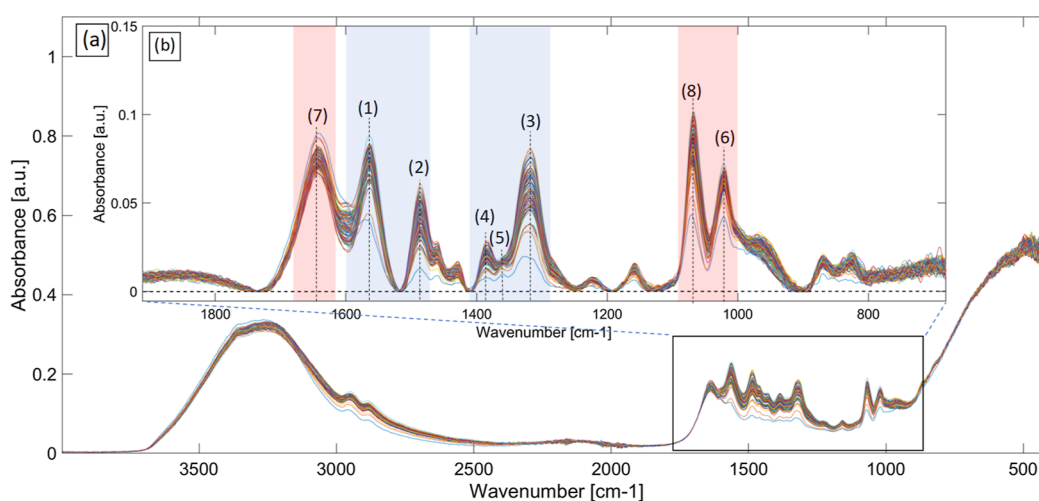
Figure 2. Illustration of the main chemometric stages using the model—TIC-1.

2.2.3.1. *MSPC Demonstration.* The plot of T^2 versus Q of TIC-1 model is used for MSPC demonstration. Moreover, calculated Q were used to check the lack-of-fit of the models for

the entire campaign period. All the results are discussed in Section 3.2.

Table 2. Abbreviations/Statistical Parameters Used in the Chemometric Study

abbreviation/statistical parameter	standfor	description
PLS-R models	partial least regression models	prediction models prepared using NIPALS algorithm; input variable is a part of a FTIR spectrum; output variables are total inorganic content (TIC) and total alkalinity values (TA)
TIC-1	initial model of TIC	initial prediction model prepared for TIC
TA-1	initial model of TA	initial prediction model prepared for TA
TIC-2	updated model of TIC	updated prediction model for TIC
TA-2	updated model of TA	updated prediction model for TA
RMSEP	average model prediction error	used to compare the model predictability and to select optimum latent variables (LVs)
LVs	latent variables	indicate number of components of PLS-R models
Q residual (Q)	quantification of the spectral information which not utilized in the PLS-R model prediction	indicate unusual spectral changes. Increase of Q indicate the more altered solvent condition than the fresh solvent state
leverage	measure of the effect of a sample on a PLS-R model/distance of a sample from PLS-R model centre	used to find suitable samples to use in model updating
Hotelling's T^2 (T^2)	measure of the distance of sample from the centre of PLS-R model	in principle leverage and Hotelling's T^2 indicate same meaning; Hotelling's T^2 (T^2) values are the standard for MSPC statistics (stage 2)

**Figure 3.** FTIR spectra of the MEA2 Campaign (a) raw spectra (full spectral range), (b) preprocessed spectra ($1900\text{--}650\text{ cm}^{-1}$), (1–8) are IR bands assignments according to Table 3, red shade—total alkalinity, and blue shade—TIC.

2.2.3.2. Model Updating. TIC-1 and TA-1 models were improved for reliable long-term predictions. Here, TIC-1 and TA-1 models were converted to upgraded models (TIC-2 and TA-2) for a better predictions of in the degraded/changed solvent conditions using a calibration transfer method²⁶ called model updating (MUP).^{27,28} In order to convert the models, a few new calibration samples were selected to describe the solvent degradation/change of the total campaign. These samples were selected using prediction leverage versus samples (time) plot, as shown in Figure 2 stage 2. These selected samples were formerly studied by visualization of spectra to identify the spectral quality of the samples, prior to incorporating them in the available models. The model updating approach comprises several iterations to arrive at properly updated prediction models (TIC-2 and TA-2). Section 3.3 discusses the results of model updating approach of TIC and TA models.

All data analysis were performed on the MATLAB platform using PLS Toolbox 8.6.2 software.

3. RESULTS AND DISCUSSION

3.1. Preparation of Initial PLS-R Models. The use of authentic industrial data will make the PLS-R models more tolerant to the actual process variations by the assimilation of realistic dynamic process variations. In this work, initial PLS-R

models (TIC-1 and TA-1) were prepared for the demonstration of the and solvent change detection and PLS-R model updating during long-term operation.

Spectral preprocessing is a significant step of PLS-R model calibration using spectroscopic data. To extract chemical species variation, specific IR bands (Figure 3) are selected to improve the ratio of signal-to-noise. Initially, all spectra were baseline-corrected using the Whittaker filter with Lambda and Rho at 1000 and 0.001, respectively.²⁵ The raw spectra and preprocessed spectra of the MEA2 campaign are shown in Figure 3a,b. Additionally, Figure 3b indicates the variable ranges used in the TIC (blue shade) and total alkalinity (red shade) models.

The preferred method for preparing a robust model is selection of the specific IR vibrational bands of the specific species/group to be investigated. Table 3 summarizes the main selected species, the corresponding IR bands selected for models, model variable ranges, and reference literature.

Two models (TIC-1 and TA-1) were calibrated with test set validation. The used number of samples are presented in Table 4. Figure 4a,b depict the measured versus predicted plots of TIC-1 and TA-1 models, respectively. These figures indicate that the regression line of the models (fit line: red color) sets very close to the targeted line (1:1 line: green color). Model

Table 3. PLS-R Model Species, Identified IR Bands, Corresponding Literature IR Bands, and Variable Ranges of the Models

models	species	identified IR bands (cm ⁻¹)	corresponding literature IR bands (cm ⁻¹)	variable ranges of models (cm ⁻¹)
TIC	MEACOO ⁻	1562 (1)	1568, ^{14,29} 1564 ³⁰	[1590–1467], [1407–1301]
		1486 (2)	1486 ^{14,29}	
		1320 (3)	1322 ¹⁴	
	CO ₃ ²⁻	1387 (4)	1388, ^{14,30} 1386 ²⁹	
total alkalinity	HCO ₃ ⁻	1362 (5)	1360, ^{14,30}	
	MEA	1020 (6)	1024 ¹⁴	[1670–1590], [1113–944]
	MEA ⁺	1638 (7)	1634 ¹⁴	
		1067 (8)	1069, ¹⁴ 1064, ³⁰ 1066 ²⁹	

Table 4. Calibration and Validation Details of the Models (TIC-1 and TA-1)

model	number of samples		model range mol/kg	RMSEP mol/kg	LVs	R ² (pred)
	calibration set	validation set				
TIC-1	17	16	1.1–1.5	0.024264	1	0.977
TA-1	13	13	4.5–5.2	0.039841	2	0.948

performance indicators—model range, RMSEP, number of LVs used, and R² predicted—are tabulated in Table 4.

3.2. Follow-Up and Control of Solvent Reclaiming.

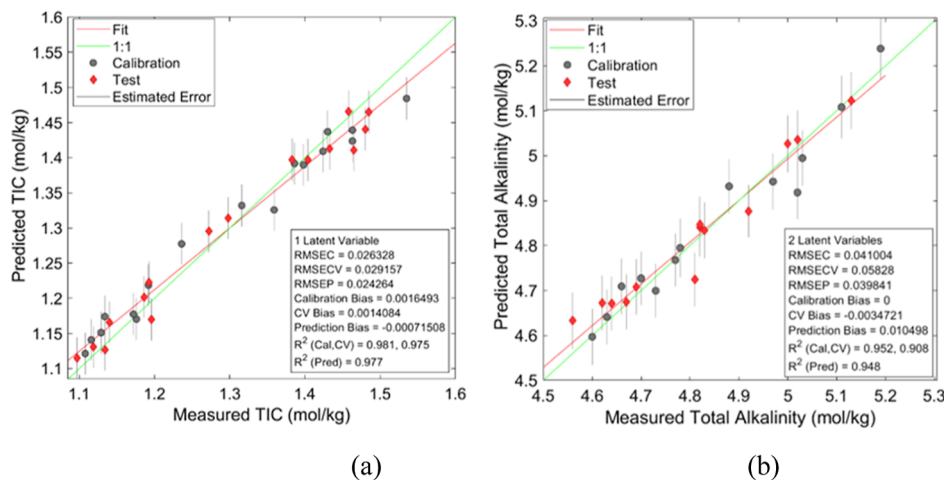
Reclaiming is an important part of CO₂ capture solvent management. Thermal solvent reclaiming has been practiced in the gas sweetening industry for a long time³¹ and recommendations vary on the maximum allowable amount of degraded solvent/contaminants.³² The end point of thermal reclaiming has also been connected to the reclaimer temperature.³³ In conclusion, a more detailed method for thermal reclaimer follow-up seems desirable. We assess MSPC as a potential concept for thermal reclaimer follow-up and control. MSPC is an effective concept to follow-up and control of solvent reclaiming. One of the pillars of MSPC is PLS-R models which

contribute by effective extraction of the information about the solvent changes from spectroscopic data (i.e., FTIR).²³

In this work, the T^2 and Q statistics is made by mapping all T^2 versus MEA2 campaign samples' Q values of TIC-1 model predictions (Figure 5a). Furthermore, Q values of MEA2 samples were plotted versus the days of operation (Figure 5b). Figure 5a shows the process variations in the MEA2 operation. The blue shaded area holds the campaign samples which agree with solvent composition at the start of operation. The samples in the red shaded area indicate the samples deviating from the average of model population (fresh solvent condition). Increased Q values indicates increased deviation. In addition, the red dashed lines separate the 95% confidence level of Q and T^2 .

Figure 5a is a plot showing solvent degradation during the CO₂ capture process. Figure 5b depicts that the deviation of the Q residual is drastically increasing after day 27. (Date: 23 August 2015; @around 800 h of operation).¹⁰ This deviation of the Q residuals indicates the difference between the current solvent state and the fresh solvent. According to Morken et al., the day 27 sample consists of about 0.5 wt % of heat stable salts (HSS) based on MEA weight, 3000 mg/L of anionic IC species, and 30,000 mg/L of main amine degradation products.¹⁰ The observations in the T^2 and Q statistics (Figure 5a) agree hence with the campaign sample analytics result. Furthermore, the plot indicates that Q s of the sample recorded on the day 77 and onward decrease and finally closely resemble the calibration samples. Solvent reclaiming started on day 77 of the campaign corresponding to samples collected on 12th October 2015 at around 1852 operation hours. Furthermore, this implies that the T^2 and Q statistics have the ability to detect/indicate sufficient time/extent of reclaiming of the degraded solvent.

According to Figure 5b, Q show an increasing trend in three different stages starting from mid of August 2015 until solvent reclaiming initiation on 12th October 2015. A similar trend was observed by Flø et al. by solvent viscosity measurements at two different temperatures (30 °C and 60 °C).¹⁹ This observation demonstrates that physical solvent changes influence the solvent spectra and correlate with prediction residual spectra (Q residual). In addition, the variation of HSS concentrations displays a similar tendency.¹⁰ Therefore, Q s are mimicking both the physical and chemical variations observed during the MEA2 campaign operation.

**Figure 4.** Measured vs Predicted plots of (a) TIC-1 and (b) TA-1.

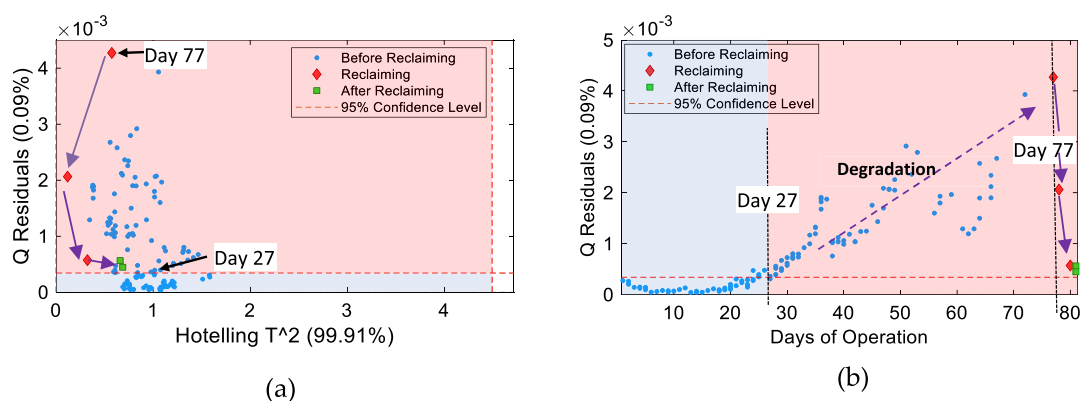


Figure 5. TIC-1 model (a) T^2 vs Q (b) days of operation; shaded areas: blue: gives the samples complementary with the model calibration samples, red: indicate the sample difference from the average of sample population.

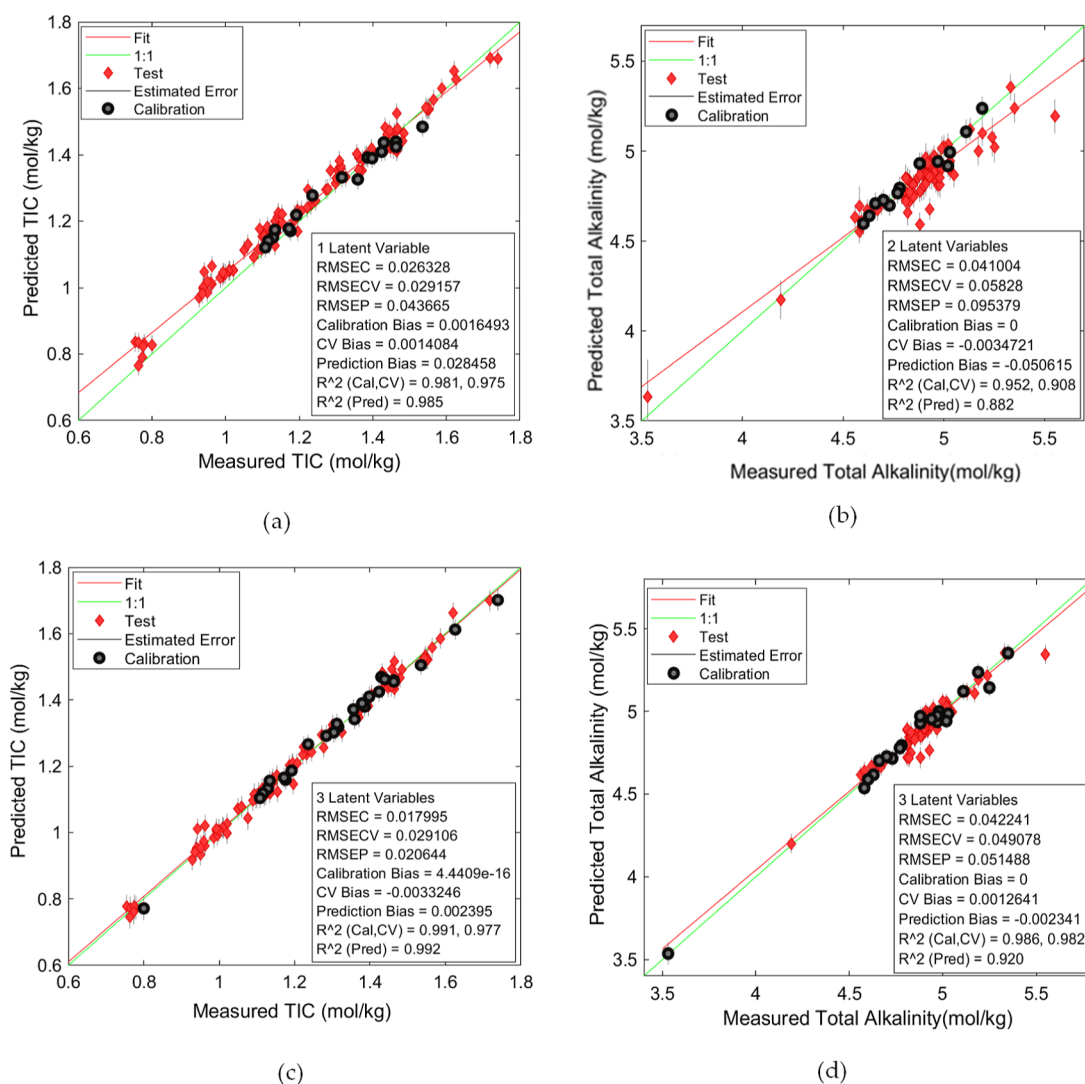


Figure 6. Total campaign predictions using (a) TIC-1 model, (b) TA-1 model, (c) TIC-2 model [improved: prediction error (RMSEP) reduced around 50%], and (d) TA-2 model [improved: prediction error (RMSEP) reduced around 50%].

Although the initial PLS-R models are useful for MSPC, they must be updated during the time of operation for reliable online monitoring. In this case, the T^2 and Q statistics are useful for detection of the time to update the corresponding model. The adaptation of PLS-R models for prediction of the degraded solvent system is described in the following section.

3.3. Preparation of Updated (TIC-2 and TA-2) Models.

Industrial PAT applications will fail if not model adaptation is carried out during the long-term use. PLS-R model calibration transfer methods are selected consequently based on the nature of the changes in the measuring environment, i.e., chemical changes, physical changes, instrument changes, etc. An

applicable model updating method for CO₂ capture solvent degradation is discussed below.

Figure 6a,b illustrates the total campaign prediction models of TIC-1 and TA-1, respectively. These plots indicate that the prediction error (RMSEP) of the TIC-1 and TA-1 models are increased by 70 and 123%, respectively, as time passes. Increase of the RMSEPs suggest that these model predictions develop a higher uncertainty over time in operation. In this context, the initial calibration data set needs to be expanded to obtain stable predictions during the total campaign. In order to expand the calibration data set of the models, a sufficient number of new samples need to be integrated. This is an iterative trial-and-error method across the total run time. In selecting new samples for a model renewal, leverage or T^2 values are helpful statistical parameters.

Proper sampling techniques are essential to minimize sampling uncertainties/errors. Furthermore, identification of new samples needs to be done carefully since the selected sample may have a higher tendency for being an outlier. Visual observation of raw spectra of the samples is commonly used in identifying erroneous spectra. In addition, corresponding reference values (e.g., species concentration) of the selected samples should be acquired.

TIC-1 and TA-1 models were improved by adding 9 and 8 new data, respectively. Prediction parameters of the initial models (TIC-1 and TA-1) and updated models (TIC-2 and TA-2) are tabulated in Table 5, which indicates that the RMSEPs of

Table 5. Initial Models and Updated Models' Performance Statistics

model parameters	TIC models		total alkalinity models	
	TIC-1	TIC-2	TA-1	TA-2
RMSEP (mol/kg)	0.0415	0.0206	0.0953	0.0514
R ² (predicted)	0.985	0.992	0.882	0.920
LVs	1	3	2	3

the updated models were reduced by about 50% compared to the initial models. In agreement with Figure 6c,d, the prediction slopes of the TIC-2 and TA-2 models are improved—0.992 and 0.957, respectively. The number of latent variables of the updated models are also limited to three components, implying that the models are more robust in the predictive nature.

4. CONCLUSIONS

MEA speciation models from the Technology Centre Mongstad 2015 MEA 2 Test campaign were developed. On this basis, two MEA solvent monitoring models, total inorganic carbon (TIC) content and total alkalinity (TA), were prepared. In addition, the ability of the models to cope with ongoing solvent change during the test campaign was demonstrated by application of a specific model update methodology.

Finally, to the best of our knowledge, a new method for solvent monitoring and management has been discovered and demonstrated. The need for solvent reclaiming can be quantified by the combination of statistical TIC or TA prediction model residuals. This methodology also provides “start” and “end of reclaiming operation” identification.

Hence, we demonstrate using large scale test campaign data that it is possible to monitor and follow-up process performance including solvent reclaiming operation and solvent monitoring using a single spectroscopic instrument.

Further development work is in progress on the issue of reclaiming monitoring and optimization.

■ AUTHOR INFORMATION

Corresponding Author

Maths Halstensen — Department of Electrical, IT and Cybernetics, University of South-Eastern Norway, 3918 Porsgrunn, Norway; Phone: +4735575187; Email: Maths.Halstensen@usn.no

Authors

Jayangi D. Wagaarachchige — Department of Electrical, IT and Cybernetics, University of South-Eastern Norway, 3918 Porsgrunn, Norway; orcid.org/0000-0002-1544-7169

Zulkifli Idris — Department of Process, Energy and Environmental Technology, University of South-Eastern Norway, 3918 Porsgrunn, Norway; orcid.org/0000-0001-7905-9686

Ayandeh Khatibzadeh — Department of Electrical, IT and Cybernetics, University of South-Eastern Norway, 3918 Porsgrunn, Norway

Audun Drageset — Technology Center Mongstad (TCM-DA), 5954 Mongstad, Norway

Klaus-J. Jens — Department of Process, Energy and Environmental Technology, University of South-Eastern Norway, 3918 Porsgrunn, Norway; orcid.org/0000-0002-9022-5603

Complete contact information is available at: <https://pubs.acs.org/10.1021/acs.iecr.3c00134>

Author Contributions

The manuscript was written through contributions of all authors. All authors have given approval to the final version of the manuscript.

Funding

This work was funded by the Ministry of Education and Research of the Norwegian Government.

Notes

The authors declare no competing financial interest.

■ ACKNOWLEDGMENTS

The authors gratefully acknowledge the staff of TCM DA, Gassnova, Equinor, Shell, and TotalEnergies for their interest in this work and particularly for access to data from the TCM DA facility. The authors also gratefully acknowledge Gassnova, Equinor, Shell, and TotalEnergies as the owners of TCM DA for their financial support and contributions. One of the authors (K.-J.J.) would like to thank Arne Henriksen for an inspiring discussion on the use of spectral residuals.

■ ABBREVIATIONS

TCM-DA	CO ₂ Technology Center Mongstad
CO ₂	carbon dioxide
PLS-R	partial least squares regression
MSPC	multivariate statistical process control
Q	Q-Residual
T^2	Hotelling's T^2
HSS	heat stable salts
MEA	monoethanolamine
USN	University of South-Eastern Norway
PACT	pilot-scale advanced capture technology

ATR-FTIR	attenuated total reflectance-Fourier transform infrared spectroscopy
CHP	combined heat and power
RFCC	residual fluidized catalytic cracker
TIC	total inorganic content
TA	total alkalinity
IR	infrared
L	leverage
NIPALS	nonlinear iterative partial least squares
LVs	latent variables
RMSEP	root mean square error of prediction
MUP	model updating
PAT	process analytical technology

REFERENCES

- (1) Rochelle, G. T. Amine Scrubbing for CO₂ Capture. *Science* **2009**, *325*, 1652–1654.
- (2) Sodiq, A.; Hadri, N. E.; Goetheer, E. L. V.; Abu-Zahra, M. R. M. Chemical reaction kinetics measurements for single and blended amines for CO₂ postcombustion capture applications. *Int. J. Chem. Kinet.* **2018**, *50*, 615–632.
- (3) Song, J.-H.; Yoon, J.-H.; Lee, H.; Lee, K.-H. Solubility of Carbon Dioxide in Monoethanolamine + Ethylene Glycol + Water and Monoethanolamine + Poly (ethylene glycol) + Water. *J. Chem. Eng. Data* **1996**, *41*, 497–499.
- (4) DuPart, M. S.; Bacon, T. R.; Edwards, D. J. Understanding corrosion in alkanolamine gas treating plants: Part 1. *Hydrocarbon Process.* **1993**, *72*.
- (5) Vevelstad, S. J.; Buvik, V.; Knuutila, H. K.; Grimstvedt, A.; da Silva, E. F. Important Aspects Regarding the Chemical Stability of Aqueous Amine Solvents for CO₂ Capture. *Ind. Eng. Chem. Res.* **2022**, *61*, 15737–15753.
- (6) Chahen, L.; Huard, T.; Cuccia, L.; Cuzuel, V.; Dugay, J.; Pichon, V.; Vial, J.; Gouedard, C.; Bonnard, L.; Cellier, N.; Carrette, P.-L. Comprehensive monitoring of MEA degradation in a post-combustion CO₂ capture pilot plant with identification of novel degradation products in gaseous effluents. *Int. J. Greenhouse Gas Control* **2016**, *51*, 305–316.
- (7) Einbu, A.; DaSilva, E.; Haugen, G.; Grimstvedt, A.; Lauritsen, K. G.; Zahlsen, K.; Vassbotn, T. A new test rig for studies of degradation of CO₂ absorption solvents at process conditions; comparison of test rig results and pilot plant data for degradation of MEA. *Energy Procedia* **2013**, *37*, 717–726.
- (8) da Silva, E. F.; Lepaumier, H.; Grimstvedt, A.; Vevelstad, S. J.; Einbu, A.; Vernstad, K.; Svendsen, H. F.; Zahlsen, K. Understanding 2-Ethanolamine Degradation in Postcombustion CO₂ Capture. *Ind. Eng. Chem. Res.* **2012**, *51*, 13329–13338.
- (9) Supap, T.; Saiwan, C.; Idem, R.; Tontiwachwuthikul, P. P. T. Part 2: Solvent management: solvent stability and amine degradation in CO₂ capture processes. *Carbon Manage.* **2011**, *2*, 551–566.
- (10) Morken, A. K.; Pedersen, S.; Kleppe, E. R.; Wisthaler, A.; Vernstad, K.; Ullestad, Ø.; Flø, N. E.; Faramarzi, L.; Hamborg, E. S. Degradation and Emission Results of Amine Plant Operations from MEA Testing at the CO₂ Technology Centre Mongstad. *Energy Procedia* **2017**, *114*, 1245–1262.
- (11) Akram, M.; Jinadasa, M. W. N.; Tait, P.; Lucquiaud, M.; Milkowski, K.; Szuhanzski, J.; Jens, K.-J.; Halstensen, M.; Pourkashanian, M. Application of Raman spectroscopy to real-time monitoring of CO₂ capture at PACT pilot plant; Part 1: Plant operational data. *Int. J. Greenhouse Gas Control* **2020**, *95*, 102969.
- (12) Jinadasa, M. W. N.; Jens, K.-J.; Øi, L. E.; Halstensen, M. Raman Spectroscopy as an Online Monitoring Tool for CO₂ Capture Process: Demonstration Using a Laboratory Rig. *Energy Procedia* **2017**, *114*, 1179–1194.
- (13) Grimstvedt, A.; Wiig, M.; Einbu, A.; Vevelstad, S. J. Multi-component analysis of monoethanolamine solvent samples by FTIR. *Int. J. Greenhouse Gas Control* **2019**, *83*, 293–307.
- (14) Richner, G.; Puxty, G. Assessing the Chemical Speciation during CO₂ Absorption by Aqueous Amines Using in Situ FTIR. *Ind. Eng. Chem. Res.* **2012**, *51*, 14317–14324.
- (15) Kachko, A.; van der Ham, L. V.; Bardow, A.; Vlugt, T. J. H.; Goetheer, E. L. V. Comparison of Raman, NIR, and ATR FTIR spectroscopy as analytical tools for in-line monitoring of CO₂ concentration in an amine gas treating process. *Int. J. Greenhouse Gas Control* **2016**, *47*, 17–24.
- (16) Kourti, T.; MacGregor, J. F. Multivariate SPC Methods for Process and Product Monitoring. *J. Qual. Technol.* **1996**, *28*, 409–428.
- (17) Wise, B. M.; Gallagher, N. B. The process chemometrics approach to process monitoring and fault detection. *J. Process Control* **1996**, *6*, 329–348.
- (18) Faramarzi, L.; Thimsen, D.; Hume, S.; Maxon, A.; Watson, G.; Pedersen, S.; Gjernes, E.; Fostås, B. F.; Lombardo, G.; Cents, T.; Morken, A. K.; Shah, M. I.; de Cazenove, T.; Hamborg, E. S. Results from MEA Testing at the CO₂ Technology Centre Mongstad: Verification of Baseline Results in 2015. *Energy Procedia* **2017**, *114*, 1128–1145.
- (19) Flø, N. E.; Faramarzi, L.; de Cazenove, T.; Hvidsten, O. A.; Morken, A. K.; Hamborg, E. S.; Vernstad, K.; Watson, G.; Pedersen, S.; Cents, T.; Fostås, B. F.; Shah, M. I.; Lombardo, G.; Gjernes, E. Results from MEA Degradation and Reclaiming Processes at the CO₂ Technology Centre Mongstad. *Energy Procedia* **2017**, *114*, 1307–1324.
- (20) Gjernes, E.; Pedersen, S.; Cents, T.; Watson, G.; Fostås, B. F.; Shah, M. I.; Lombardo, G.; Desvignes, C.; Flø, N. E.; Morken, A. K.; de Cazenove, T.; Faramarzi, L.; Hamborg, E. S. Results from 30 wt% MEA Performance Testing at the CO₂ Technology Centre Mongstad. *Energy Procedia* **2017**, *114*, 1146–1157.
- (21) Hjelmaas, S.; Storheim, E.; Flø, N. E.; Thorjussen, E. S.; Morken, A. K.; Faramarzi, L.; de Cazenove, T.; Hamborg, E. S. Results from MEA Amine Plant Corrosion Processes at the CO₂ Technology Centre Mongstad. *Energy Procedia* **2017**, *114*, 1166–1178.
- (22) Bui, M.; Flø, N. E.; de Cazenove, T.; Mac Dowell, N. Demonstrating flexible operation of the Technology Centre Mongstad (TCM) CO₂ capture plant. *Int. J. Greenhouse Gas Control* **2020**, *93*, 102879.
- (23) Esbensen, K. H.; Swarbrick, B., *Multivariate Data Analysis: An Introduction to Multivariate Analysis, Process Analytical Technology and Quality by Design*. 6th ed.; CAMO software AS: 2018.
- (24) Wold, H. Soft Modelling by Latent Variables: The Non-Linear Iterative Partial Least Squares (NIPALS) Approach. *J. Appl. Probab.* **1975**, *12*, 117–142.
- (25) Eilers, P. H. C. A Perfect Smoother. *Anal. Chem.* **2003**, *75*, 3631–3636.
- (26) Workman, J. J. The Essential Aspects of Multivariate Calibration Transfer. *40 Years of Chemometrics – From Bruce Kowalski to the Future*; American Chemical Society, 2015; Vol. 1199, pp 257–282.
- (27) Wise, B. M.; Roginski, R. T. A Calibration Model Maintenance Roadmap. *IFAC-PapersOnLine* **2015**, *48*, 260–265.
- (28) Tan, H.; Sum, S. T.; Brown, S. D. Improvement of a Standard-Free Method for Near-Infrared Calibration Transfer. *Appl. Spectrosc.* **2002**, *56*, 1098–1106.
- (29) Sun, C.; Dutta, P. K. Infrared Spectroscopic Study of Reaction of Carbon Dioxide with Aqueous Monoethanolamine Solutions. *Ind. Eng. Chem. Res.* **2016**, *55*, 6276–6283.
- (30) du Preez, L. J.; Motang, N.; Callanan, L. H.; Burger, A. J. Determining the Liquid Phase Equilibrium Speciation of the CO₂–MEA–H₂O System Using a Simplified in Situ Fourier Transform Infrared Method. *Ind. Eng. Chem. Res.* **2019**, *58*, 469–478.
- (31) Kohl, A. L.; Nielsen, R. B. *Gas Purification*; Gulf Professional Publishing: Houston, 1997.
- (32) Dumée, L.; Scholes, C.; Stevens, G.; Kentish, S. Purification of aqueous amine solvents used in post combustion CO₂ capture: A review. *Int. J. Greenhouse Gas Control* **2012**, *10*, 443–455.
- (33) ElMoudir, W.; Supap, T.; Saiwan, C.; Idem, R.; Tontiwachwuthikul, P. Part 6: Solvent recycling and reclaiming issues. *Carbon Manage.* **2012**, *3*, 485–509.

Article 2

Demonstration of CO₂ Capture Process Monitoring and Solvent Degradation Detection by Chemometrics at the Technology Centre Mongstad CO₂ Capture Plant. Part II

Jayangi D. Wagaarachchige¹, Zulkifli Idris², Ayandeh Khatibzadeh¹, Audun Drageset³, Klaus-J.
Jens², and Maths Halstensen^{1*}

¹Department of Electrical, IT and Cybernetics, University of South-Eastern Norway,
Porsgrunn, Norway

²Department of Process, Energy and Environmental Technology, University of South-Eastern
Norway, Porsgrunn, Norway

³Technology Center Mongstad (TCM-DA), Mongstad, Norway

Submitted to Industrial & Engineering Chemistry Research Journal, ACS Publications

*Demonstration of CO₂ Capture Process Monitoring and Solvent
Degradation Detection by Chemometrics at the Technology
Centre Mongstad CO₂ Capture Plant: Part II*

*Jayangi D. Wagaarachchige¹, Zulkifli Idris², Ayandeh Khatibzadeh¹, Audun Drageset³, Klaus-J.
Jens², Maths Halstensen^{1*}*

¹Department of Electrical, IT and Cybernetics, University of South – Eastern Norway, Kjølnes
ring 56, 3918 Porsgrunn, Norway

²Department of Process, Energy and Environmental Technology, University of South – Eastern
Norway, Kjølnes ring 56, 3918 Porsgrunn, Norway

³Technology Center Mongstad (TCM-DA), 5954 Mongstad, Norway

Part I: Demonstration of CO₂ Capture Process Monitoring and Solvent Degradation Detection by
Chemometrics at the Technology Centre Mongstad CO₂ Capture Plant

<https://doi.org/10.1021/acs.iecr.3c00134>

KEYWORDS

Process Analytical Spectroscopy, Partial Least Squares Regression, Fourier Transform Infrared
Spectroscopy, Residual Spectra, Online Monitoring, Solvent Management Tool

ABSTRACT

This paper presents Part II of a study of the Demonstration of CO₂ Capture Process Monitoring and Solvent Degradation Detection by Chemometrics at the Technology Centre Mongstad CO₂ Capture Plant. This study is based on a 1960-hour test campaign conducted at the Technology Centre Mongstad, Norway, in 2015 using 30 wt% aqueous MEA solvent. This contribution demonstrates a tool for degradation monitoring and solvent management follow-up based on the residuals of solvent speciation models (TIC, TA) reported in Part I, which presents chemometric models to predict CO₂ and amine content in the solvent. In this Part II, residual spectra were extracted and used to formulate prediction models for in-line follow up of degradation species groups: i) Total HSS species and ii) Total Amine Degradation Products (ADP). This new tool for continuous solvent degradation quantification can supplement the current practice of indirect estimation of when to start and/or stop solvent reclaiming.

1. Introduction

The global temperature rise is rapidly approaching the IPCC defined critical threshold of 1.5 degrees Celsius¹ in just a few years, and 2024 could be the first year to experience it.² The deployment of post-combustion carbon capture is one of the urgently needed actions to limit carbon dioxide (CO₂) emissions from fossil fuel burning. Gas-liquid absorption is the most applied method, and 30 wt% MEA (monoethanolamine) is widely used as solvent due to its high reactivity with CO₂, non-volatility, and low cost. Until now, the utilization of amine solvents in post-combustion capture (PCC) technology has been widely recognized as an established method for CO₂ capture. However, the PCC technology still faces several challenges, including process energy requirements, operational costs, in terms of solvent degradation, etc.,

Several studies have been published on MEA solvent degradation, providing an in-depth understanding of the identity and mechanisms of degradation species as well as the complexity of their chemical identification.³⁻⁵ HSS can be produced by reaction of amine solvent with CO₂ and/or flue gas impurities.. Both the former and latter molecular class have been identified as early stage solvent degradation species which participate subsequently in further solvent degradation⁶ and plant corrosion.^{7, 8} Solvent degradation is a continuous process starting slowly but typically following an exponential curve pattern⁹ Analysis of degradation species using various off-line analytical methods, such as Liquid Chromatography–Mass Spectrometry (LC-MS QQQ) and Anion Chromatography (IC-ECD) can give detailed molecular information, but also become tedious, time consuming, and often require specialized subcontractors.^{3, 10} However, this approach is necessary in the research and evaluation phase of solvent development.

In real world service, detection and degradation compound removal (e.g., by ion exchange or solvent reclaiming methodology) is important;⁸ the reclaimer solvent waste generation is reported to vary in the range of 0.1-14.9 kg reclaimer waste per ton of CO₂ captured.¹¹ Solvent degradation thus generates both solvent replenishing and solvent waste disposal cost. Hence, solvent management is important for PCC process/cost optimization.

Process optimization requires performance monitoring vs desired target(s); often, in-line spectroscopy is useful because it provides real-time solvent monitoring data. In Part I of this work, we reported FTIR spectroscopic PLSR-models for monitoring of TIC (Total Inorganic Carbon i.e., solvent CO₂ capture capacity) and TA (Total Alkalinity i.e., solvent capture ‘strength’) of continuous degrading MEA solvent. At the same time, these models provided qualitative detection of solvent degradation and solvent reclaiming. Despite ongoing solvent composition change (degradation) the uncertainty of these models was satisfactory due to continuous model update. In

this Part II we used the extracted residual Fourier-transformed infrared (FTIR) spectra from the PLS-R models developed in Part I¹² for quantitative solvent degradation and solvent reclaiming monitoring.

The TCM database for Part I and Part II of this work contains 17 manual samples of the 1960-hour MEA test campaign analyzed off-line as described above.³ In this case, FTIR real-time monitoring would provide a more complete database for identification of a solvent management strategy as well as optimal solvent management action points (e.g., initiation and end point of solvent reclaiming). Furthermore, instead of taking many samples and perform the respective off-line analyses, including using specialized instruments including the analytical logistics, the necessary monitoring data is provided by one in-line FTIR spectrometer.

Previously, Grimstvedt et. al suggested that CO₂ model residuals might be useful to determine the concentration of HSS species in a degraded aqueous solution of MEA.¹³

In this contribution, for the first time, we present a novel tool for development and follow-up of PCC solvent management actions.

To improve the MEA-based process and develop better solvent systems, it is essential to detect solvent degradation. Furthermore, an understanding of solvent degradation is significant for emission monitoring and emission control.¹⁰ Online monitoring of a group of degradation species using process analytical spectroscopy can be less time-consuming and provide time dependent solvent deterioration information.

Previously, we demonstrated a chemometric approach for process monitoring and solvent degradation detection using the MEA test campaign of TCM, which was conducted in 2015.¹² This demonstration included the preparation of two Partial Least Squares regression (PLS-R) models

for monitoring CO₂ species and amine species in the solvent. Furthermore, that study indicated a methodological hierarchy for updating the models during their use throughout the entire campaign period. Moreover, the follow-up on solvent reclaiming using these models was also discussed. This paper represents the second part (Part II) of the above work ¹² and presents an approach to quantify the accumulation of degradation species in the solvent.

2 Materials and Methods

2.1 Materials

This work (Part II) employs the same real plant data gathered during the TCM MEA2 campaign (30 wt% aqueous MEA) as in Part I.¹²

MEA2 campaign, a 1960-hour operation, commenced on July 6th, 2015, and concluded on October 17th, 2015.³ The base case testing took place on September 7th, 2015, under steady state conditions, around 8 weeks after the startup.¹⁴ Morken et. al illustrated the overall campaign operational hours³ wherein Gjernes et. al tabulated the overall test activities¹⁵ of MEA2 campaign. The MEA2 campaign mainly comprises of the primary stages of an amine-based CO₂ capture plant operation. Statistical parameters/abbreviations of this work are given in Table 1.

Table 1: Abbreviations/ statistical parameters

Abbreviations/ parameter	statistical	Stand for	Note
PLS-R models		Partial squares regression models	least NIPALS algorithm used. Input variable is Raw FTIR or residual spectra, output variables are Total inorganic content (TIC), Total Alkalinity (TA), Total Heat Stable Salts (HSS) and Amine degradation products (ADP)
TIC Model		PLS-R model of Total Inorganic Content	More details are published in Wagaarachchige et. al ¹²

TA model	PLS-R model of Total Alkalinity	More details are published in Wagaarachchige et. al ¹²
RMSECV	Average model error of cross validation	To select optimum latent variables and compare the model performance
RMSEP	Average model error of prediction	To select optimum latent variables and compare the model performance.
LVs	Latent variables	No of component of a PLS-R model
Q- residuals	Quantification of the spectral part which not used in the PLS-R model	Unusual spectral changes are evident, and an increase in Q residuals indicates a more altered solvent condition compared to the fresh solvent state.

2.2 Methods

In Part I of this work¹², two PLS-R models were calibrated and validated for predicting CO₂ (TIC model) and MEA (TA model) species of the TCM MEA2 campaign. We used one-third of the campaign data for model preparation and reserved the remaining two-thirds for model updating and validation.

These models were used to demonstrate model updating during operation, resulting in improved predictions of the entire campaign with reduced uncertainty. ¹² Figure 1 illustrates how the models were prepared and updated using TCM data.

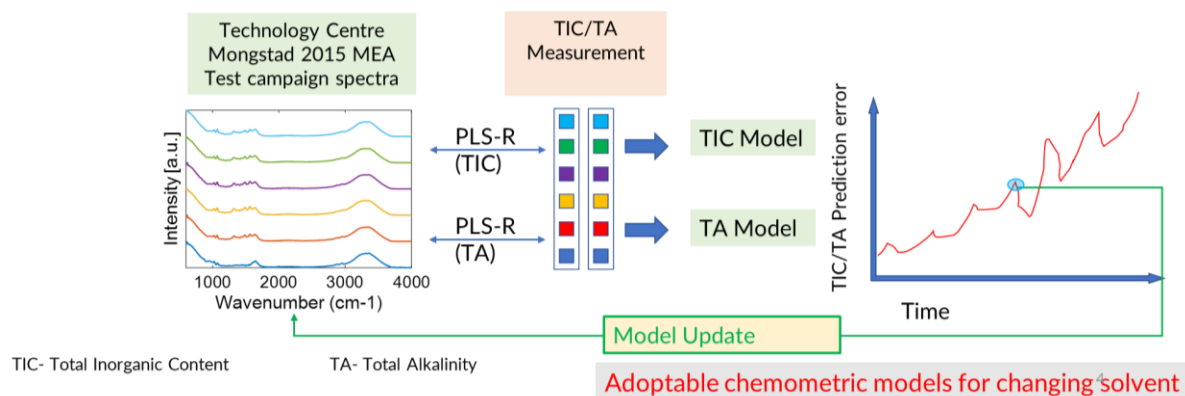


Figure 1: PLS-R model (TIC and TA) calibration and model updating

For the current work (Part II), a set of residual spectra (the portions of the FTIR spectra not used for the models' predictions) was extracted during the TIC and TA modeling process which was reported in Part I.¹² Gathered residual spectra were used to prepare PLS-R models for degradation product groups i.e., total HSS and total Amine Degradation Species. Section 3.1 presents the key findings of Part I. to establish a good foundation for understanding the results presented in the current work (Part II).

Table 2 indicates the details of data used for these degradation species models. Two degradation species group models were prepared to predict total HSS and total amine degradation species of the degrading solvent. Reference values for these models were obtained from offline measurements of the MEA2 campaign, corresponding to specific species groups. Variable selection was done using approximate estimation of common anion IR vibrational bands of degradation products. These models were prepared using only 10-11 samples and validated by using the full cross validation method due the absence of sufficient reference data.¹⁶ Finally, use of residual spectra-based models for the degradation product speciation of total MEA2 campaign was tested. Section 3.2 provides the results of this work.

Table 2: Details of the Data Used for residual model development

modeled species group	species counted	spectral data (X)	reference analysis method (Y)	reference analysis unit	number of samples
Total Heat Stable Salts (HSS)	formate acetate glycolate oxalate sulphate	TIC model prediction residuals	Ion exchange and following titration	mol/kg	11
Total Amine Degradation Products (ADP)	4-(2-hydroxyethyl)piperazin-2-one (HEPO) N-(2-hydroxyethyl)glycine (HeGly) N-(2-hydroxyethyl)imidazole (HEI) N-(2-hydroxyethyl)formamide (HEF) 2-Oxazolidone (OZD) N-(2-hydroxyethyl) acetamide (HEA) NN'-Bis(2-hydroxyethyl)oxamide (BHEOX)	TA model prediction residuals	LC-MS QQQ	mg/L	10

All data analysis were performed on the MATLAB platform using PLS Toolbox 8.6.2 software.

3. Results and Discussion

Section 3.1 outlines the results of Part I¹² to provide a distinct understanding of the complete study.

In Section 3.2, the discussion focuses on the results of this work (Part II).

3.1 TIC and TA Models and Solvent Reclaiming Follow-Up

This section provides details about the initial TIC and TA models, the process of model updating, and the subsequent follow-up on solvent reclaiming.

TIC and TA models were prepared to predict the concentration of CO₂ species and amine species during the total MEA 2 campaign. Variable windows of the TIC model—[1590-1467] and [1407-1301]—were selected to cover the FTIR vibrational bands (1562, 1486, 1320, 1387, 1362 cm⁻¹) of MEACOO⁻, CO₃²⁻, and HCO₃⁻ species.¹² Similarly, the vibrational bands at 1020, 1638, and 1067 cm⁻¹ were accounted for in the selection of variable windows of the TA model—[1670-1590] and [1113-944]—to cover MEA and protonated MEA species.¹² These two PLS-R models were calibrated using NIPALS (nonlinear iterative partial least squares) algorithm and validated using an independent data set of the same campaign.¹⁷ All spectra were baseline corrected using the Whittaker filter¹⁸ to remove baseline noise. The prediction errors of these models for the total campaign predictions were discussed and proposed as a method to update the models accordingly to avoid increasing prediction errors.¹²

Figure 2 and Figure 3 indicate the prediction errors of the TIC and TA models, respectively. The blue columns represent the initial model's prediction errors, showing an increasing trend, whereas the red columns correspond to the predictions of the updated TIC model. As a result of these updates, both models demonstrated an average reduction of approximately 50% in their prediction errors¹²

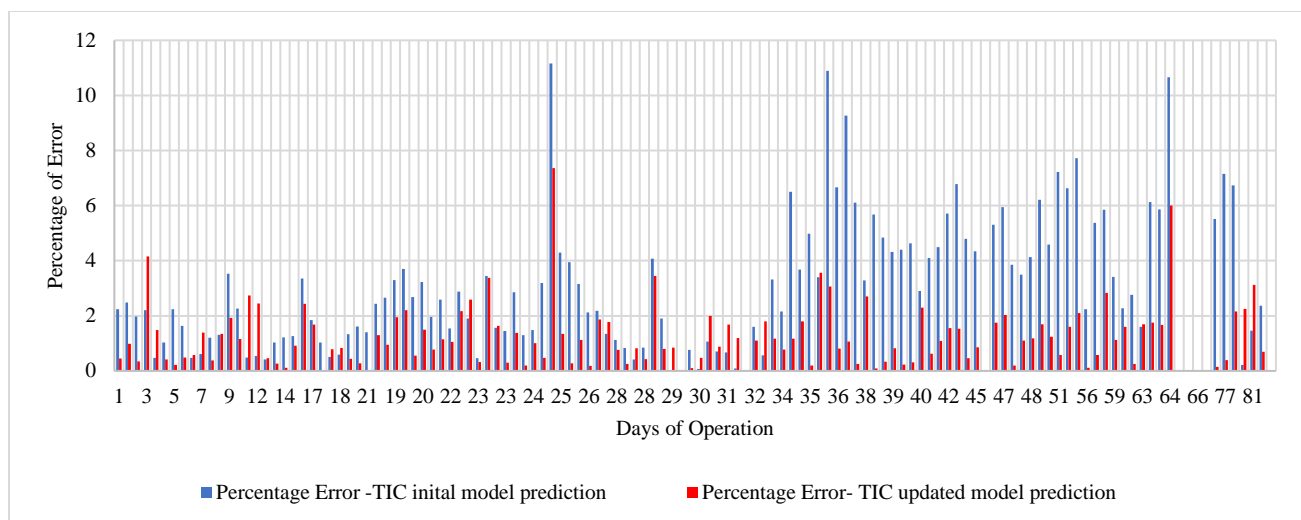


Figure 2: Percentage of errors of TIC model; Blue-Initial model, Red-Updated model

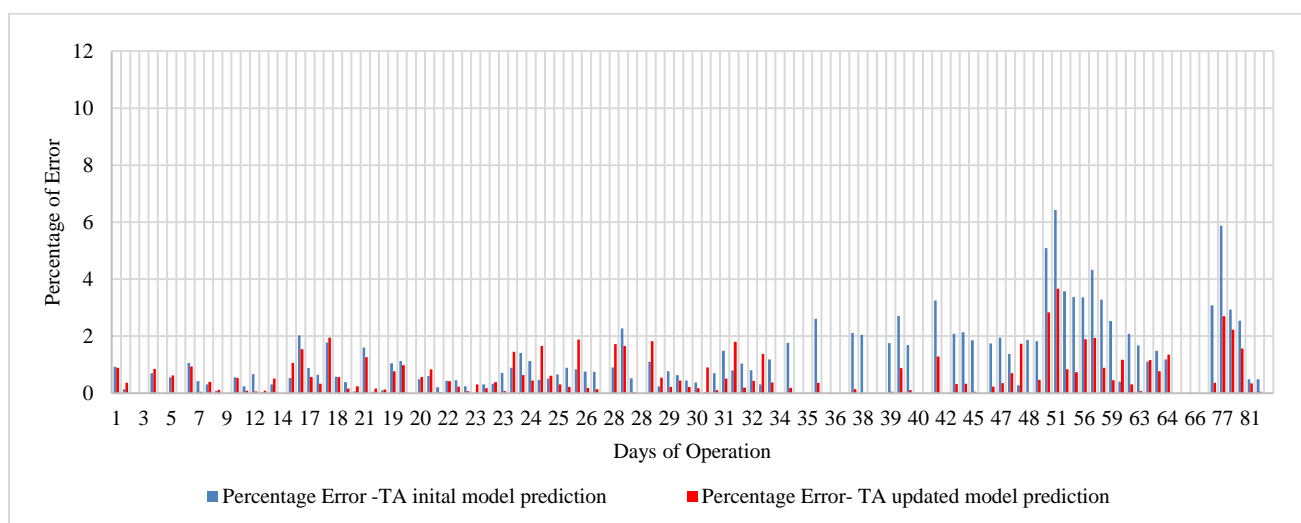


Figure 3: Percentage of errors of TA model; Blue-Initial model, Red-Updated model

Spectroscopic measurement provides a chemical fingerprint of the measured solvent sample, indicating the vibrational bands of all chemical species. When obtaining model predictions using FTIR spectra, these models extract useful information from the spectra, while the unused parts are filtered out as spectral residuals. Figure 4 depicts the schematic representation of model residual extraction.

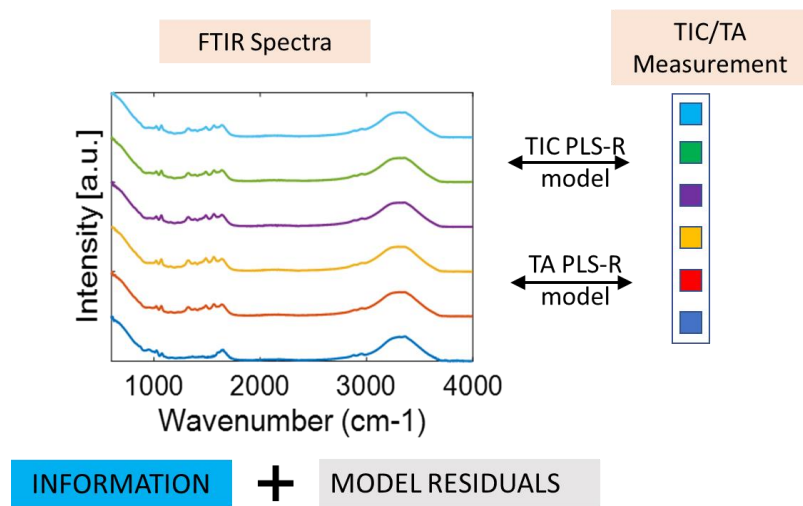


Figure 4: Schematic representation of model residual extraction

These spectral residuals were used to calculate the average residuals of the spectra, which are known as Q-residuals (Qs) ^{.17} In long-term monitoring of the solvent system, these residuals indicate changes in the solvent over time, such as solvent degradation. Figure 5 shows Qs versus the days of operation of the MEA2 campaign. In Figure 5, blue-colored dots indicate Qs calculated before the reclaiming starts, and the red dashed line represents the time when the reclaiming started. These blue dots demonstrate that the TIC model's Q residuals increase with the time of the campaign operations. However, from day 77 onwards (when the reclaiming started on day 77), the Q values of predictions decrease, eventually closely resembling the fresh solvent state (at the 95% confidence level). This observation can also be seen in the variation of the TA model's Q residuals over time, as shown in Figure S1. The possibility of applying multivariate statistical process control (MSPC) for the follow-up and control of solvent reclaiming is discussed in Part I.¹²

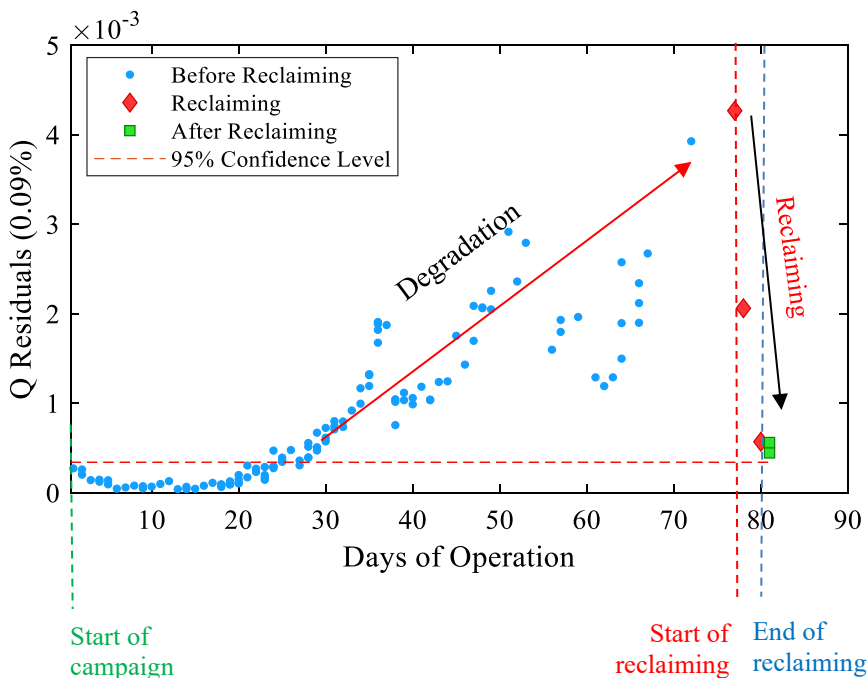


Figure 5. TIC model Qs versus days of MEA2 campaign operation

3.2 PLS-R models for degradation species groups; HSS and total amine degradation products

In an amine-based CO₂ capture plant, the solvent is changing due to several reasons, e.g., amine degradation, flue gas impurity accumulation, piping corrosion products accumulation, solvent emissions etc. Additionally, it is obvious that the concentrations of these degradation species tend to increase in the solvent during long-term operation.

This group of degradation species is a heavy mix of different types of chemical compounds, e.g., HSS, amine degradation products, corrosion products, etc. In 2016, Morken et. al. discussed about such identified and unidentified degradation products of MEA2 operation.³ If these species can quantitatively be identified by using an online monitoring with a spectroscopic method, it will minimize the use of specific offline sample analysis methods like, titration, Ion chromatography (IC), Liquid chromatography–mass spectrometry (LC-MS), etc.

In the following sections, PLS-R model preparation based on residual spectra for two main degradation species groups are discussed.

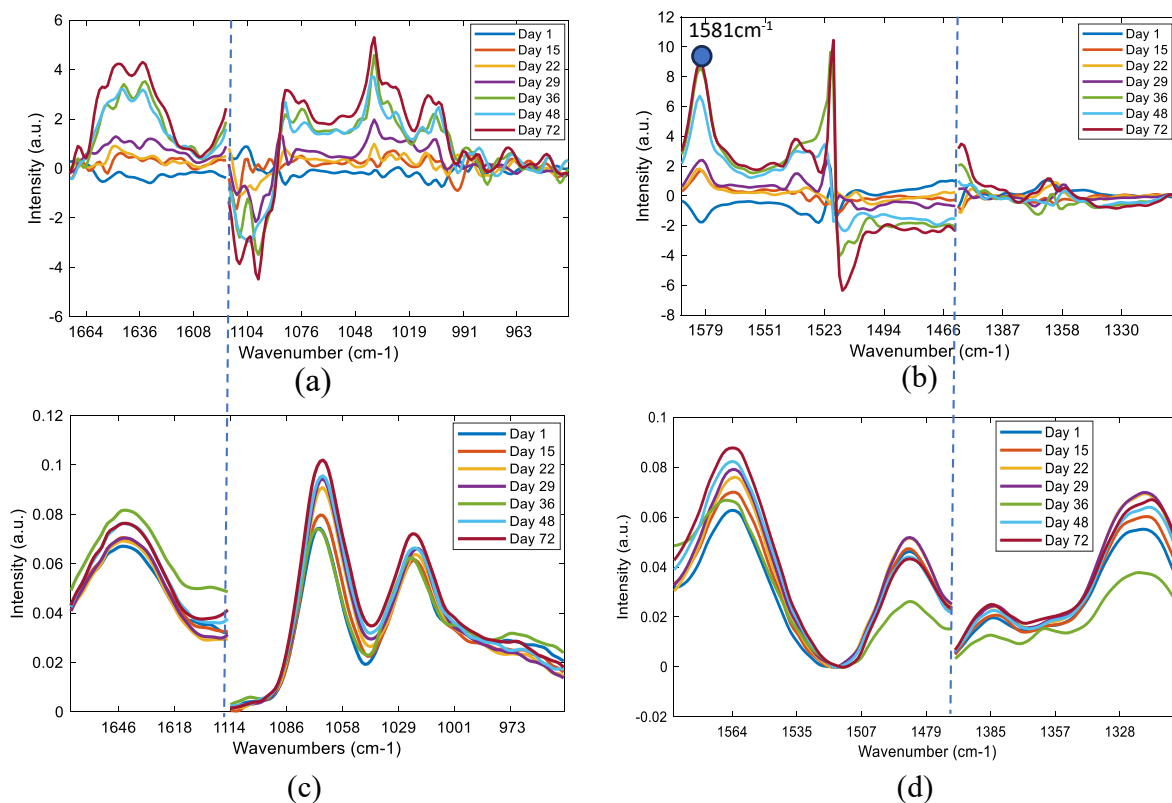


Figure 6: residual spectra from (a) TA model (b) TIC model; corresponding FTIR spectra (c) TA model (d) TIC model

Table 3: HSS species, Identified IR bands and Corresponding literature IR Bands

HSS species	Identified IR bands	IR Bands in literature/observed lab testing
formate	1581	C–O stretching 1585 ¹⁹ , 1581*, 1411,
acetate	-	C–O stretching 1555 ¹⁹ , 1550*
glycolate	1581	1581*, 1411*, 1320*, 1072*
oxalate	1581	1581*, 1303*
nitrate		1350*, 1411*
nitrite		1334*, 1226*

*Confirmed by lab testing in USN lab

Residual spectra from TA and TIC model development are shown in Figure 6 (a) and Figure (b), respectively. Nonetheless, these spectra are a valuable source for monitoring low concentration species. Although the spectra look different from normal FTIR spectra, these figures show something important about the solvent changes. Most distinct observable is the increase of intensity of residual spectra with the operation time; as shown in Fig. 5. The anion analysis of this campaign shows that the formate anion has the highest concentration with the acetate anion in the second position among all the HSS species.³ Ito et. al. published the IR vibrational band for C–O stretching of formate and anions at 1585 cm^{-1} and 1555 cm^{-1} , respectively.¹⁹ As shown in Figure S2 ATR-FTIR analysis results of specific species indicate distinctive peaks for formate and acetate at 1581 and 1550 cm^{-1} , respectively. Interestingly, Figure 6 (b) depicts a distinctive residual peak variation at 1581 cm^{-1} and it might indicate formate or the presence of a formate-glycolate-oxalate mix (see Table 3). This identification supports that the residual spectra show the vibrational bands of HSS species which are not clearly visible (Figure 6 (d)). Consequently, identification of degradation species by FTIR analysis, can be a suitable preprocessing approach.

Among the identified degradation species of the MEA2 campaign, HSS is a major group. At the starting point of solvent reclaiming, HSS concentration is recorded as 1 wt% MEA.³ HSS represent salts formed by reaction of acid with amine base forming anionic species like formate, acetate, oxalate, glycolate, nitrate, sulfate, etc. Consequently, the HSS species group is very complex to assign exact IR band assignments. Reference to Figure 6 (b), TIC model's residual spectra may indicate the presence of formate/ Glycolate/Oxalate anions or mix of all anions by the peak at 1581 cm^{-1} . Additionally, based on the chemical structures of all identified anionic species,³ HSS group might be presented in the TIC variable range due to their vibrational bands i. e. C-O_{str}, -CO₂⁽⁻⁾_{asy},

-CH₃ asy , -SO₂ asy, and C-H asy.²⁰ Therefore, the total variable range of TIC model’s residual spectra was selected for the PLS-R model calibration of HSS group.

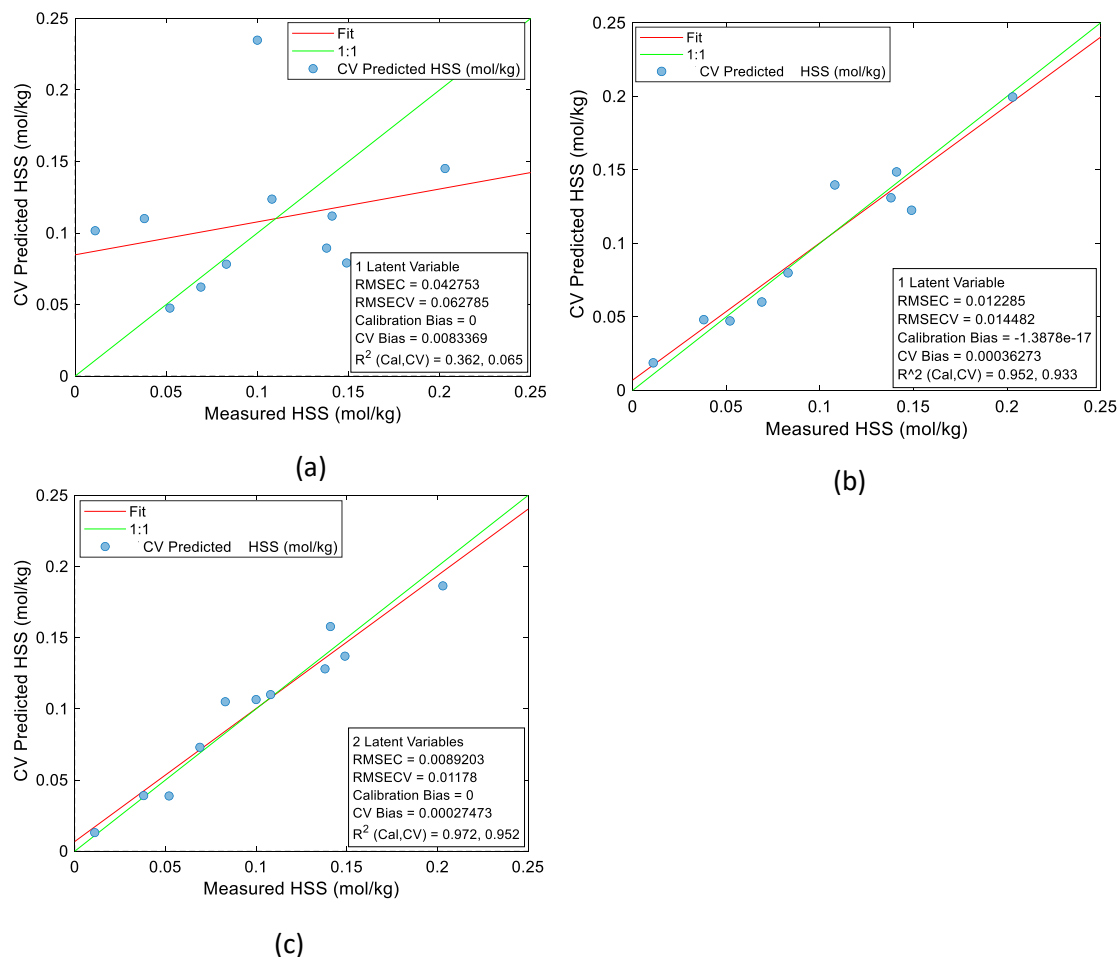


Figure 7: PLS-R model for HSS raw FTIR spectra (a) with one LV (b) using residual spectra of TIC model (c) with two LVs (variable range of the TIC model is used)

To test the suitability of using raw FTIR spectra for degradation product speciation, the raw FTIR spectra were subjected to the PLS-R algorithm and the model plots generated for one and two latent variables (LVs) are shown in Figure 7 (a) and 7(c), respectively. The plot depicts the raw FTIR spectral correlation with the HSS concentrations using two LVs — $R^2(CV)= 0.952$ and

RMSECV=0.0117 mol/Kg. The calibrated PLS-R model using TIC model's residual spectra in Figure 7 (b) has a clear correlation with $R^2(\text{CV})=0.933$ and RMSECV=0.0144 mol/Kg only using one LV. Hence, HSS species concentration calibration is possible either using raw FTIR spectra or residual spectra from the TIC modelling. However, for identification of degradation species the residual extraction approach is superior to models based on raw FTIR spectra. Furthermore, model based on residual spectra are less complex than the raw FTIR spectra approach. Figure 8 shows the total HSS concentration mapping of measured and residual spectra (TIC) based model predicted values of MEA2 campaign.

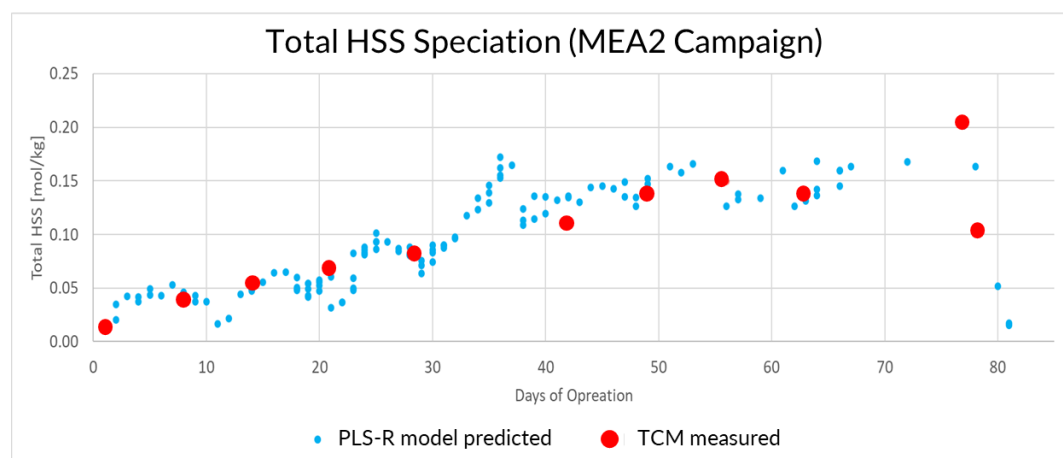


Figure 8. HSS quantification of the MEA2 campaign; red-TCM measured, residual based model prediction.

HSS species (e.g., organic acids) react with MEA and CO_2 generating new amine degradation compounds. A simplified scheme of these given by Morken et. al.³ In the present work, we attempt to calibrate a speciation model for the sum of amine degradation products (ADP) which were identified during the MEA2 campaign. Hence, HEPO (CAS No: 23936-04-1), HEGly (CAS No: 5835-28-9), HEF (CAS No: 693-06-1), HEA (CAS No: 142-26-7), HEI (CAS No: 1615-14-1) and OZD (CAS No: 497-25-6) were used in the PLS-R calibration. Since these species show up in the

same spectral range as used in the Total Alkalinity (TA) model, the model was calibrated using the residual spectra of the TA model. The prediction plot of the total ADP model is shown in Figure S3. The R^2 (CV) and RMSECV of the model are 0.916 and 4621 mg/L respectively.

However, these HSS and ADP models are prepared by using a very limited number of samples and validated with cross-validation only. Therefore, before use in a PAT application, proper validation by use of more and independent data is required.

4. Conclusion

Following the approach suggested by Grimstvedt et al. we have demonstrated a tool for degradation monitoring and solvent management follow-up based on the residuals of solvent speciation models (TIC, TA) of the 2015 TCM MEA2 test campaign.

This contribution (Part II) presents the continuation work of the endeavor by Wagaarachchige et al. (Part I) demonstrating application of Process Analytical Spectroscopy and chemometric modeling as a tool for real-time follow-up of solvent change in a CO₂ capture unit.¹² Our new tool for continuous solvent degradation quantification can supplement the current practice¹⁵ of indirect estimation of when to start and/or stop solvent reclaiming.

ASSOCIATED CONTENT

Supporting Information

Figure S1: Initial TA model's prediction Qs with Days of operation of MEA2 campaign

Figure S2: ATR-FTIR lab analysis spectra of formate and acetate anions

Figure S3: PLS-R model calibration for Amine Degradation Products (ADP) using residual spectra of TA model

AUTHOR INFORMATION

Corresponding Author

Maths Halstensen- Department of Electrical, IT and Cybernetics, University of South – Eastern Norway, Kjølnes ring 56, 3918 Porsgrunn, Norway

E-mail: Maths.Halstensen@usn.no Tel: +4735575187

Authors

Jayangi D. Wagaarachchige - Department of Electrical, IT and Cybernetics, University of South – Eastern Norway, Kjølnes ring 56, 3918 Porsgrunn, Norway

Zulkifli Idris - Department of Process, Energy and Environmental Technology, University of South – Eastern Norway, Kjølnes ring 56, 3918 Porsgrunn, Norway

Ayandeh Khatibzadeh –Department of Process, Energy and Environmental Technology, University of South – Eastern Norway, Kjølnes ring 56, 3918 Porsgrunn, Norway,

Audun Drageset -CO₂ technology Center Mongstad (TCM-DA), 5954 Mongstad, Norway

Klaus-J. Jens- Department of Process, Energy and Environmental Technology,

University of South – Eastern Norway, Kjølnes ring 56, 3918 Porsgrunn, Norway

Present Addresses

Author Contributions

The manuscript was written through contributions of all authors. All authors have given approval to the final version of the manuscript.

Funding Sources

This work was funded by the Ministry of Education and Research of the Norwegian Government.

Notes

The authors declare no competing financial interest.

ACKNOWLEDGMENT

The authors gratefully acknowledge the staff of TCM DA, Gassnova, Equinor, Shell and TotalEnergies for their interest in this work and particularly for access to data from the TCM DA facility. The authors also gratefully acknowledge Gassnova, Equinor, Shell, and TotalEnergies as the owners of TCM DA for their financial support and contributions.

We would like to thank Arne Henriksen for an inspiring discussion on the use of residual spectra.

ABBREVIATIONS

TCM-DA, CO₂ Technology Center Mongstad

CO₂, Carbon dioxide

PLS-R, Partial least squares regression

MSPC, Multivariate statistical process control

Q, Q-residual

HSS, Heat stable salts

MEA, monoethanolamine

MEA2, TCM 2015 MEA campaign

USN, University of South-Eastern Norway

FTIR, Fourier transform infrared spectroscopy

ADP- Amine Degradation Products

TIC, Total Inorganic Content

TA, Total Alkalinity

LC-MS QQQ, Triple Quad Liquid chromatography–mass spectrometry

IR, Infrared

LVs, latent variables

RMSECV ,Root Mean Square Error of Cross Validation

CV, Cross Validation

RMSEP, Root Mean Square Error of Prediction

PAT, Process Analytical Technology

IC, Ion chromatography

HEGly, N-(2-hydroxyethyl)glycine (CAS No: 5835-28-9)

HEPO, 4-(2-hydroxyethyl) piperazin-2-one (CAS No: 23936-04-1)

HEF, N-(2-hydroxyethyl)formamide (CAS No: 693-06-1)

HEA, N-(2-hydroxyethyl) acetamide (CAS No: 142-26-7)

HEI , N-(2-hydroxyethyl)imidazole (CAS No: 1615-14-1)

OZD, 2-Oxazolidone (CAS No: 497-25-6)

HEPO (CAS No: 23936-04-1), HEGly (CAS No: 5835-28-9)

HEF (CAS No: 693-06-1), HEA (CAS No: 142-26-7)

HEI (CAS No: 1615-14-1) and, OZD (CAS No: 497-25-6)

REFERENCES

1. IPCC, *Global Warming of 1.5°C: IPCC Special Report on Impacts of Global Warming of 1.5°C above Pre-industrial Levels in Context of Strengthening Response to Climate Change, Sustainable Development, and Efforts to Eradicate Poverty*. Cambridge University Press: Cambridge, 2022.
2. Cuff, M., Beyond 1.5°C: The hell years. *New Scientist* **2023**, 258, (3442), 32-35.
3. Morken, A. K.; Pedersen, S.; Kleppe, E. R.; Wisthaler, A.; Vernstad, K.; Ullestad, Ø.; Flø, N. E.; Faramarzi, L.; Hamborg, E. S., Degradation and Emission Results of Amine Plant Operations from MEA Testing at the CO₂ Technology Centre Mongstad. *Energy Procedia* **2017**, 114, 1245-1262.
4. Flø, N. E.; Faramarzi, L.; de Cazenove, T.; Hvidsten, O. A.; Morken, A. K.; Hamborg, E. S.; Vernstad, K.; Watson, G.; Pedersen, S.; Cents, T.; Fostås, B. F.; Shah, M. I.; Lombardo, G.; Gjernes, E., Results from MEA Degradation and Reclaiming Processes at the CO₂ Technology Centre Mongstad. *Energy Procedia* **2017**, 114, 1307-1324.
5. Strazisar, B. R.; Anderson, R. R.; White, C. M., Degradation Pathways for Monoethanolamine in a CO₂ Capture Facility. *Energy & Fuels* **2003**, 17, (4), 1034-1039.
6. Supap, T.; Idem, R.; Tontiwachwuthikul, P., Mechanism of formation of heat stable salts (HSSs) and their roles in further degradation of monoethanolamine during CO₂ capture from flue gas streams. *Energy Procedia* **2011**, 4, 591-598.
7. Tanthapanichakoon, W.; Veawab, A.; McGarvey, B., Electrochemical Investigation on the Effect of Heat-stable Salts on Corrosion in CO₂ Capture Plants Using Aqueous Solution of MEA. *Ind. Eng. Chem. Res.* **2006**, 45, (8), 2586-2593.
8. Thompson, J. G.; Frimpong, R.; Remias, J. E.; Neathery, J. K.; Liu, K., Heat Stable Salt Accumulation and Solvent Degradation in a Pilot-Scale CO₂ Capture Process Using Coal Combustion Flue Gas. *Aerosol and Air Quality Research* **2014**, 14, (2), 550-558.
9. Moser, P.; Wiechers, G.; Schmidt, S.; Garcia Moretz-Sohn Monteiro, J.; Charalambous, C.; Garcia, S.; Sanchez Fernandez, E., Results of the 18-month test with MEA at the post-combustion capture pilot plant at Niederaussem – new impetus to solvent management, emissions and dynamic behaviour. *Int. J. Greenhouse Gas Control* **2020**, 95, 102945.

10.da Silva, E. F.; Lepaumier, H.; Grimstvedt, A.; Vevelstad, S. J.; Einbu, A.; Vernstad, K.; Svendsen, H. F.; Zahlse, K., Understanding 2-Ethanolamine Degradation in Postcombustion CO₂ Capture. *Ind. Eng. Chem. Res.* **2012**, 51, (41), 13329-13338.

11.IEAGHG *Evaluation of Reclaimer Sludge Disposal from Post-Combustion CO₂ capture*; 2014.

12.Wagaarachchige, J. D.; Idris, Z.; Khatibzadeh, A.; Drageset, A.; Jens, K.-J.; Halstensen, M., Demonstration of CO₂ Capture Process Monitoring and Solvent Degradation Detection by Chemometrics at the Technology Centre Mongstad CO₂ Capture Plant. *Ind. Eng. Chem. Res.* **2023**, 62, (25), 9747-9754.

13.Grimstvedt, A.; Wiig, M.; Einbu, A.; Vevelstad, S. J., Multi-component analysis of monethanolamine solvent samples by FTIR. *Int. J. Greenhouse Gas Control* **2019**, 83, 293-307.

14.Faramarzi, L.; Thimsen, D.; Hume, S.; Maxon, A.; Watson, G.; Pedersen, S.; Gjernes, E.; Fostås, B. F.; Lombardo, G.; Cents, T.; Morken, A. K.; Shah, M. I.; de Cazenove, T.; Hamborg, E. S., Results from MEA Testing at the CO₂ Technology Centre Mongstad: Verification of Baseline Results in 2015. *Energy Procedia* **2017**, 114, 1128-1145.

15.Gjernes, E.; Pedersen, S.; Cents, T.; Watson, G.; Fostås, B. F.; Shah, M. I.; Lombardo, G.; Desvignes, C.; Flø, N. E.; Morken, A. K.; de Cazenove, T.; Faramarzi, L.; Hamborg, E. S., Results from 30 wt% MEA Performance Testing at the CO₂ Technology Centre Mongstad. *Energy Procedia* **2017**, 114, 1146-1157.

16.Roberts, D. R.; Bahn, V.; Ciuti, S.; Boyce, M. S.; Elith, J.; Guillera-Aroita, G.; Hauenstein, S.; Lahoz-Monfort, J. J.; Schröder, B.; Thuiller, W.; Warton, D. I.; Wintle, B. A.; Hartig, F.; Dormann, C. F., Cross-validation strategies for data with temporal, spatial, hierarchical, or phylogenetic structure. *Ecography* **2017**, 40, (8), 913-929.

17.Esbensen, K. H.; Swarbrick, B., *Multivariate Data Analysis: An introduction to Multivariate Analysis, Process Analytical Technology and Quality by Design* 6th ed.; CAMO software AS: 2017; p 452.

18.Eilers, P. H. C., A Perfect Smoother. *Anal. Chem.* **2003**, 75, (14), 3631-3636.

19.Ito, K.; Bernstein, H. J., THE VIBRATIONAL SPECTRA OF THE FORMATE, ACETATE, AND OXALATE IONS. *Can. J. Chem.* **1956**, 34, (2), 170-178.

20.Socrates, G., *Infrared and Raman characteristic group frequencies : tables and charts*. Wiley: Chichester; New York, 2000.

Article 3

Low-Viscosity Nonaqueous Sulfolane–Amine–Methanol Solvent

Blend for Reversible CO₂ Capture

Jayangi D. Wagaarachchige¹, Zulkifli Idris², Bjørnar Arstad³, Nithin B. Kummamuru², Kai A. S. Sætre², Klaus-J. Jens², and Maths Halstensen^{1*}

¹Department of Electrical, IT and Cybernetics, University of South-Eastern Norway,
Porsgrunn, Norway

²Department of Process, Energy and Environmental Technology, University of South-Eastern
Norway, Porsgrunn, Norway

³ SINTEF Materials and Chemistry, 0314 Oslo, Norway

Published in Industrial & Engineering Chemistry Research Journal, ACS Publications

<https://doi.org/10.1021/acs.iecr.1c04946>

Low-Viscosity Nonaqueous Sulfolane–Amine–Methanol Solvent Blend for Reversible CO₂ Capture

Jayangi D. Wagaarachchige, Zulkifli Idris, Bjørnar Arstad, Nithin B. Kummamuru, Kai A. S. Sætre, Maths Halstensen, and Klaus-J. Jens*



Cite This: *Ind. Eng. Chem. Res.* 2022, 61, 5942–5951



Read Online

ACCESS |



Metrics & More

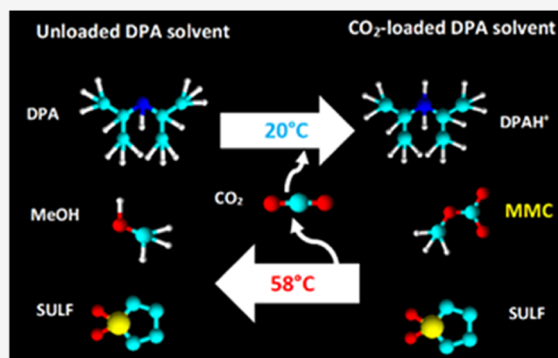


Article Recommendations



Supporting Information

ABSTRACT: In this work, the absorption–desorption performance of CO₂ in six new solvent blends of amine (diisopropylamine (DPA), 2-amino-2-methyl-1-propanol (AMP), methyldiethanolamine (MDEA), diethanolamine (DEA), diisopropanolamine (DIPA), and ethanolamine (MEA)), sulfolane, and methanol has been monitored using ATR-FTIR spectroscopy. Additionally, NMR-based species confirmation and solvent viscosity analysis were done for DPA solvent samples. The identified CO₂ capture products are monomethyl carbonate (MMC), carbamate, carbonate, and bicarbonate anions in different ratios. The DPA solvent formed MMC entirely with 0.88 mol_{CO₂}/mol_{amine} capture capacity, 0.48 mol_{CO₂}/mol_{amine} cyclic capacity, and 3.28 mPa·s CO₂-loaded solvent viscosity. MEA, DEA, DIPA, and MDEA were shown to produce a low or a negligible amount of MMC while AMP occupied an intermediate position.



1. INTRODUCTION

Mitigation of global warming and its potential adverse effects is the greatest environmental challenge associated with the rapid increase of greenhouse gas (GHG) emissions. Anthropogenic CO₂ emissions from fossil fuel burning and other activity account for about 78% of the total GHG emissions in the last four decades.¹ Efforts from governments and industries around the world are needed to reduce greenhouse gas emissions. A major portion of the world's net CO₂ discharge originates from fossil fuel combustion in industrial processes and power generation. Postcombustion CO₂ capture (PCCC) is seen as a viable pivotal attempt to reduce global CO₂ emissions from fossil fuel combustion. The benchmark CO₂ capture technology is the gas–liquid absorption–desorption process using an aqueous 30 wt % monoethanolamine (MEA) solution. The first-generation MEA CO₂ capture solvent is known for its high reactivity and low cost.^{2–4} However, the major challenge is still the high energy penalty for solvent regeneration, which is estimated to be around 4 GJ per ton of CO₂ capture.⁵ Furthermore, MEA is corrosive and is shown to deteriorate pipelines and column walls^{6,7} with high solvent losses due to oxidative and thermal degradations.⁸

Much research has been focused on finding CO₂ capture solvents with a lower energy penalty. Second-generation aqueous CO₂ capture solvents such as piperazine and piperazine derivatives were found to reduce operational energy expenditure by providing higher capture capacity and lowering the regeneration energy.^{9,10} Other examples of these second-

generation solvents include proprietary Mitsubishi's KS-1 and Fluor's advanced Econamine.^{9,11} However, there is still a need for new solvent chemistries that reduce cost, e.g., mitigating energy needs.¹²

K₂Sol is a third-generation proprietary water-lean solvent system, which demonstrated reduced solvent regeneration energy of around 35% in comparison to MEA.¹³ Water-lean solvents are summarized in a recent review in terms of fundamentals, uncertainties, and opportunities.¹¹ In these systems, typically, the solvent water portion is substituted by organics, often alcohols.^{8,11,14,15} In comparison to aqueous solvents, this modifies solvent physical properties and the chemical CO₂ binding mechanism providing novel solvent chemistry but also requiring process technology adaption for potential application.

This study introduces nonaqueous sulfolane-based solvents for carbon capture that can regenerate at low temperatures. Sulfolane, methanol, and amine are the three components of these solvents. Sulfolane (SULF) is a well-known industrial chemical that can be used as a low-volatile organic diluent. It is a polar aprotic solvent with a strong affinity for acid gases.^{16,17}

Received: December 22, 2021

Revised: April 13, 2022

Accepted: April 14, 2022

Published: April 25, 2022



Table 1. Information of Chemicals Used in This Work^{a,b,c,d,e}

Chemical name	CAS number	Chemical structure	Purity ^a (%)	pKa	Supplier
2-amino-2-methyl-1-propanol (AMP)	124-68-5		≥0.99	9.73 ^b	Sigma-Aldrich
diisopropylamine (DPA)	108-18-9		≥0.99	11 ^c	Sigma-Aldrich
methyldiethanolamine (MDEA),	105-59-9		≥0.99	8.56 ^d	Sigma-Aldrich
diisopropanolamine (DIPA)	110-97-4		≥0.98	8.88 ^d	Sigma-Aldrich
diethanolamine (DEA)	111-42-2		≥0.99	8.88 ^d	Sigma-Aldrich
ethanolamine (MEA)	141-43-5		≥0.99	9.45 ^c	Sigma-Aldrich
Sulfolane (SULF)	126-33-0		≥0.99	n.a.	Sigma-Aldrich
Methanol (MeOH)	67-56-1		≥0.99	n.a.	VWR
Carbon dioxide (CO ₂)	124-38-9		0.99999	n.a.	AGA Norge AS

^aAs given by the supplier. ^bKim et al.³⁰ ^cZeng et al.³¹ ^dKim et al.³² ^en.a.: not applicable.

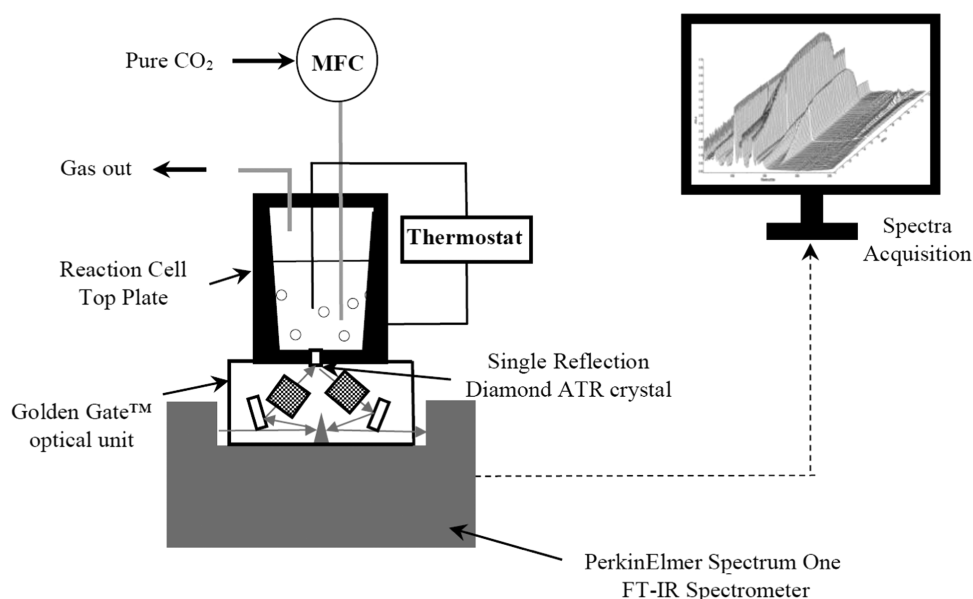


Figure 1. Schematic diagram for ATR-FTIR in situ monitoring.

Sulfolane enhances CO₂ absorption rate and solubility during the chemical absorption without participating in the chemical reaction.¹⁸ In a recent article by Zou et al.,¹⁹ it was shown that the addition of sulfolane enables higher absorption and desorption rates and higher cyclic capacity in CO₂ capture in comparison to the aqueous MEA. A study on the sulfolane-based semiaqueous piperazine (PZ) system concluded that addition of sulfolane increased the equilibrium constant at medium CO₂ loadings and slightly increased the CO₂ cyclic capacity.²⁰ Lidong and co-workers suggested that addition of sulfolane to make a semiaqueous system of diethylenetriamine (DETA) resulted in a higher CO₂ removal rate and energy-saving than the respective aqueous solvent.^{21,22} However, there

is also a claim that sulfolane affects corrosion in the presence of water, oxygen, or oxidizing agents.²³

The second component in our reported solvents is methanol. It has the ability to reduce the heat capacity of solvent blends.²⁴ In addition, it was investigated as a component for hybrid solvents to reduce regeneration cost due to its low boiling point, low viscosity, and lower corrosivity than water.^{25,26} Sulfolane and methanol are commercially available organic chemicals that are used in Sulfinol^{16,27} and Aminol²⁸ processes, respectively. The third solvent component is commercially available amines MEA, 2-amino-2-methyl-1-propanol (AMP), diisopropylamine (DPA), methyldiethanol-

amine (MDEA), diethanolamine (DEA), and diisopropanolamine (DIPA).

The most promising solvent blend was characterized using nuclear magnetic resonance (NMR) spectroscopy to confirm monomethyl carbonate (MMC) formation. MMC is the simplest species of monoalkyl carbonic acid ester compounds that can easily be decomposed at a mild temperature.²⁹ In addition, viscosity measurements were also performed on the most promising solvent type.

2. MATERIALS AND METHODS

2.1. Solvent/Sample Preparation. Details of chemicals used in this study are listed in Table 1. These chemicals were used as received without further purification.

As part of our interest in sulfolane-based nonaqueous CO₂ capture solvents, the reported solvent composition was found by serendipity. The DPA solvent was prepared by mixing 30% DPA, 35% methanol, and 35% sulfolane, resulting in a molar ratio of 1.000, 3.6846, and 0.9824 for DPA, methanol, and sulfolane, respectively. All other solvent amine (AMP, MDEA, DIPA, MEA, and DEA) mixtures are prepared in a manner that achieves the same molar ratios. All of the samples contain 14.8 mmol of amine, 54.6 mmol of methanol, and 14.5 mmol of sulfolane. A PB-303S analytical weighing balance from Mettler Toledo with an accuracy of ±0.01 g was used to weigh the required amount of chemicals.

2.2. Solvent Screening with In Situ ATR-FTIR Analysis. The schematic diagram of the ATR-FTIR spectroscopy setup is shown in Figure 1.

To evaluate the effectiveness of the solvents, CO₂ absorption and desorption tests were performed in a reaction cell top plate (P/N GS10507) connected to a Golden Gate single reflection diamond ATR system (GS10500 Series). The reaction cell is a stainless steel double-jacketed conical-cylindrical chamber with a stainless steel top plate, a type-K thermocouple, and stainless steel tubing for the gas inlet and outlet. The empty cell was first flushed with high-purity nitrogen gas (N₂) for several minutes, and then an ATR-FTIR background scan was collected. Prior to the absorption experiment, a known amount of solvent was placed inside the reaction cell according to Table 2, and the top plate was tightened properly. Absorption

Table 2. Solvent Sample Weights Used in ATR-FTIR In Situ Monitoring

solvent amine type	mass of sample (g)
DPA	5.00
AMP	4.82
MDEA	5.27
DIPA	5.47
MEA	4.40
DEA	5.05

and desorption experiments were conducted at two different temperatures of 20 and 58 °C continuously for around 2 h. In situ reaction monitoring was performed using a PerkinElmer Spectrum One FTIR spectrometer. IR spectra were recorded every minute using PerkinElmer's TimeBase software. Each IR spectrum was an average of 16 scans in the wavenumber range of 400–4000 cm⁻¹ at a resolution of 4.0 cm⁻¹. Before CO₂ was introduced into the reaction cell, several ATR-FTIR scans of the fresh solvent were taken. During these scans, only peaks corresponding to the amine, MeOH, and SULF blend were

observed. CO₂ gas was introduced into the reaction cell at a flow rate of 0.02 L/min using a mass flow controller (MFC) from Sierra Instruments. After reaching the maximum height of increasing CO₂-related peaks, the CO₂ flow was set to zero and the temperature of the ATR-FTIR reaction cell was increased to 58 °C. A typical desorption experiment lasted around 40 min until the minimum decreasing peak intensity was reached. For quantification of the liquid sample CO₂-loading at the end of the experiments, the BaCl₂ titration method was used.³³

2.3. ¹³C and ¹H NMR Spectroscopy Analysis. ¹³C and ¹H NMR experiments were performed for the unloaded and CO₂-loaded DPA solvent samples. The NMR measurements were performed for qualitative molecular structure identification and confirmation of FTIR band assignment. Analysis was conducted using a Bruker Avance III 400 MHz spectrometer with a BBFO Plus double-resonance probe head at 298 K. After acquisition, the spectra were processed using MestreNova software v 10.0.2. The ¹³C NMR spectra were processed by proper signal phasing and baseline correction. A line broadening factor of 1.5 Hz was applied to enhance the signal-to-noise ratio.

2.4. Viscosity Determination. For viscosity analysis of the DPA solvent, predetermined CO₂-loaded samples were prepared by bubbling pure CO₂ gas into an unloaded solvent. The actual CO₂ content was confirmed by the BaCl₂ titration method.³³ Regeneration of the CO₂-loaded solvents was performed at 60 °C in a laboratory-scale CO₂ desorption apparatus as shown in Figure 2. The solvent was heated at 60 °C with stirring for 2 h to ensure complete regeneration.

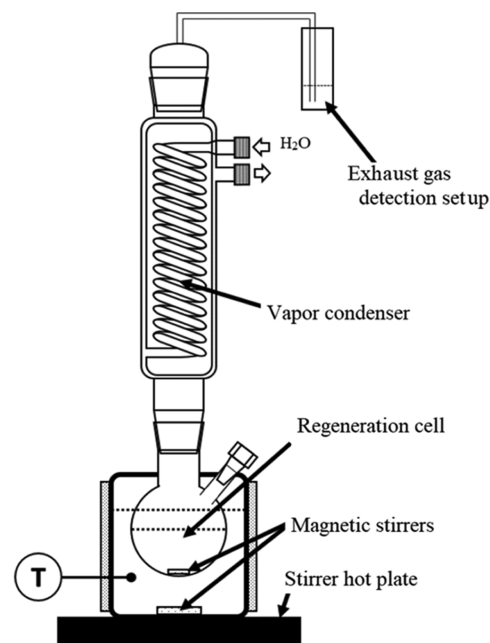


Figure 2. Schematic diagram of the laboratory-scale CO₂ desorption apparatus.

An Anton Paar Physica MCR 101 rheometer with a doubled-gap pressure cell XL was used to measure the dynamic viscosity of the unloaded, CO₂-loaded, and regenerated DPA solvent. The measurements in this work were taken at 40 °C using the procedure described in our previous publication.³⁴ The rheometer used for the viscosity

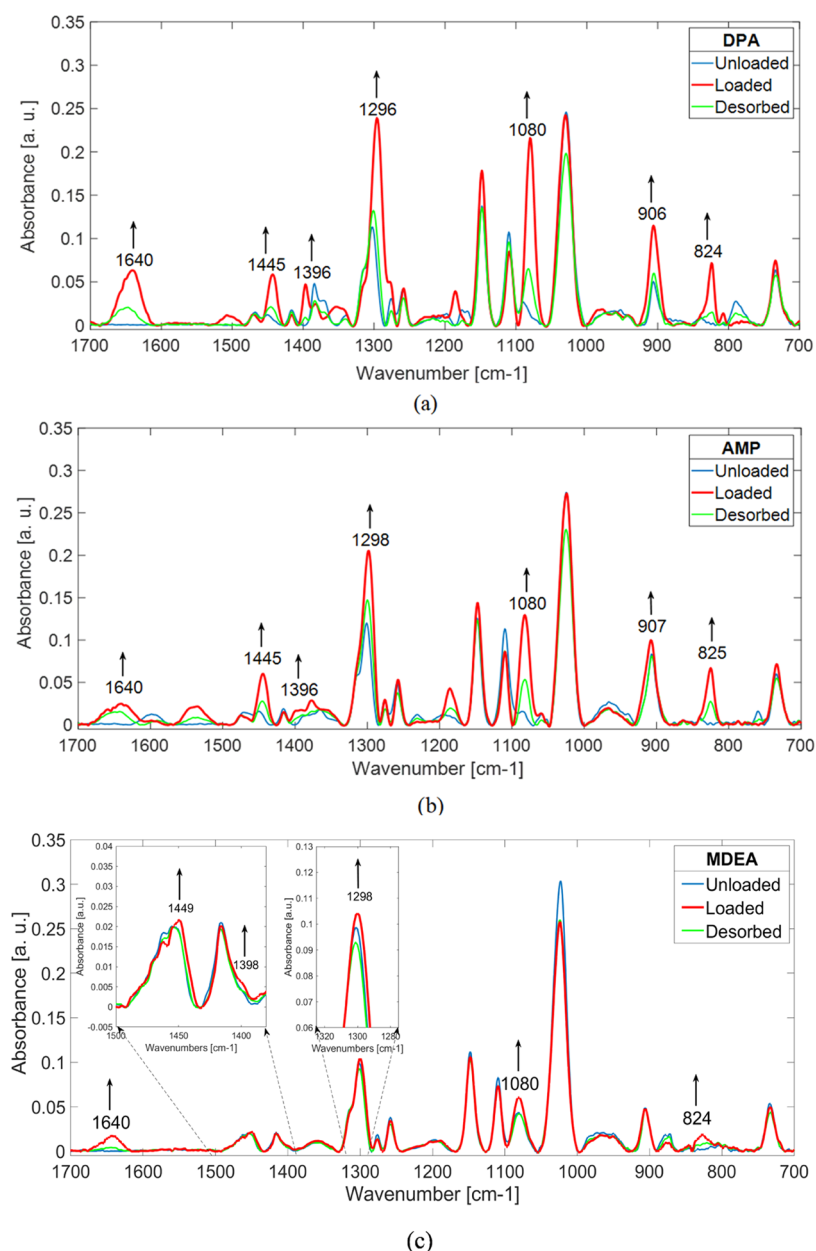


Figure 3. Baseline-corrected ATR-FTIR spectra of unloaded (blue line), CO₂-loaded (red line), and desorbed (green line) DPA (a)-, AMP (b)-, and MDEA (c)-based solvents.

measurements has a standard uncertainty for temperature and torque of 0.03 K and 0.0002 Nm, respectively.

3. RESULTS AND DISCUSSION

The results of the solvent screening experiments are discussed in this section. MMC and carbamate formation during CO₂ absorption are discussed based on FTIR vibrational band assignments. Confirmation of MMC formation for the best-performing solvent (DPA) is discussed using ¹³C and ¹H NMR spectroscopy results. This is then followed by a discussion of solvent viscosity.

3.1. ATR-FTIR In Situ Monitoring: CO₂ Absorption and Desorption. As explained in Section 2.2, CO₂ absorption and desorption experiments of six sulfolane-based solvents were monitored using ATR-FTIR.

To identify the reaction products, the IR spectra were baseline-corrected and the vibrational modes of possible CO₂

capture products were assigned according to the corresponding wavenumbers. The baseline-corrected spectra of unloaded, CO₂-loaded, and regenerated DPA-, AMP-, and MDEA-based solvents are shown in Figure 3a–c, respectively.

New species are formed when CO₂ reacts with the solvent, and these are indicated by formation of new FTIR peaks. In Figure 3a, new peaks at 1640, 1443, 1396, 1298, 1080, 906, and 824 cm⁻¹ were observed for the DPA-based solvent. These peaks decreased during desorption, suggesting a mild temperature regeneration ability of the DPA-based solvent. Table 3 summarizes these peaks and their respective IR vibrational modes. Earlier work by Behrendt and co-workers show these new peaks observed in the DPA solvent to be indicative of MMC formation.³⁵ Furthermore, IR peaks at 1636 and 1290 cm⁻¹ assigned to an alkylcarbonate species were also observed by Yang et al.⁸ in the CO₂-loaded nonaqueous solvent of 2-piperidineethanol (2-PE) and ethylene glycol (EG). IR

Table 3. FTIR Peak Identification of DPA-, AMP-, and MDEA-Based Solvents^a

characteristic IR vibrational bands, ν_{\max} (cm ⁻¹)			IR peak assignment
DPA	AMP	MDEA	
1640	1640	1640	C=O stretching vibration ^{8,35,38}
1445	1445	1449	CH ₃ asymmetric deformation ^{35,38}
1396	1396	1398	CH ₃ symmetric deformation ^{35,38}
1296	1298	1298	O–C–O asymmetric stretching vibration ^{8,35,38}
1080	1082	1080	O–C–O symmetric stretching vibration ^{35,38}
906	907	n.o.	CH ₃ –O stretching ^{35,38}
824	824	824	CO ₃ deformation ^{35,38}

^an. o.: not observed.

carbamate peaks are normally observed^{8,36,37} in the wavenumber range of 1550–1450 cm⁻¹. Interestingly, no carbamate peaks were visible, indicating no carbamate end-product formation for the CO₂-loaded solvent. IR peaks of the DPA-, AMP-, and MDEA-based solvents are assigned to the respective IR vibrational modes in Table 3. Interestingly, MDEA exhibits only a negligible amount of MMC.

Figure 4 shows the baseline-corrected unloaded, CO₂-loaded, and regenerated spectra of the MEA sulfolane solvent. The peak development pattern during CO₂ absorption was slightly different from those of the aforementioned DPA and AMP-based solvents. The newly increased peaks included MMC vibrational wavenumbers, but the maximum peak height was considerably lower than those of DPA- and AMP-based solvents. During mild temperature desorption, these peaks were reduced. Three additional peaks at 1574, 1486, and 1382 cm⁻¹ were also observed during CO₂ absorption. These peaks represent the asymmetric and symmetric stretching bands of MEA-carbamate^{8,36,37,39} and C–O stretching bands of the carbonate^{37,39} (CO₃²⁻) anion. Similar behavior with strong carbamate formation with few alkylcarbonate species was observed by Chen and co-workers for the MEA/EG non-aqueous solvent.⁸ The former peaks did not change during desorption, suggesting that a higher temperature was required for a complete regeneration for the MEA-based solvent. It is well known that carbamate requires a high temperature for regeneration. Similar behavior as that of the MEA-based solvent was seen for the DEA- and DIPA-based solvents;

reaction with CO₂ for these solvents produced a mixture of carbamate and MMC species, and the carbamate needed a higher temperature for complete regeneration. FTIR spectra for DEA- and DIPA-based solvents are provided in Figure S1.

In FTIR spectroscopy, the chemical species concentration is directly proportional to the corresponding peak area or, as an approximation, the peak height. The distinctive MMC peak at 1080 cm⁻¹ is used for qualitative comparison of MMC formation between these solvents. Based on Figure 5, it can be seen that DPA produces most MMC, followed by AMP, MEA, DEA, and DIPA. MDEA is not included in this and other comparisons below due to its negligible formation of MMC.

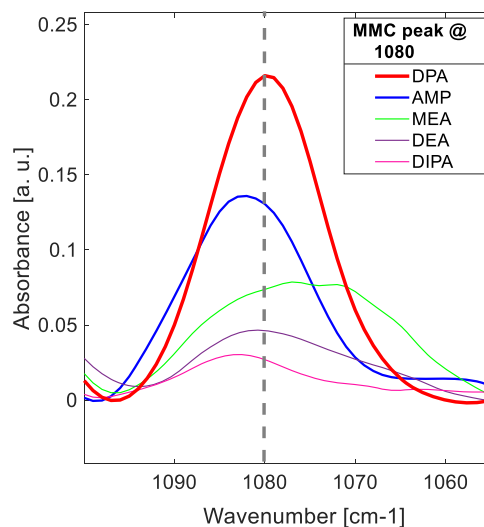


Figure 5. FTIR-based comparison of MMC formation of five solvents tested in this work.

CO₂ cyclic capacity, the difference between rich loading and lean loading, is an important solvent feature.⁴⁰ This property is of special interest for process design in terms of solvent flow rates, size of the absorber and stripper, etc. In this work, results from continuous CO₂ absorption and desorption experiments on five solvents were used to evaluate their CO₂ capture and cyclic capacities. A typical example of time-based ATR-FTIR spectra obtained for the DPA solvent is shown in Figure 6. Formation of peaks corresponding to MMC can be seen

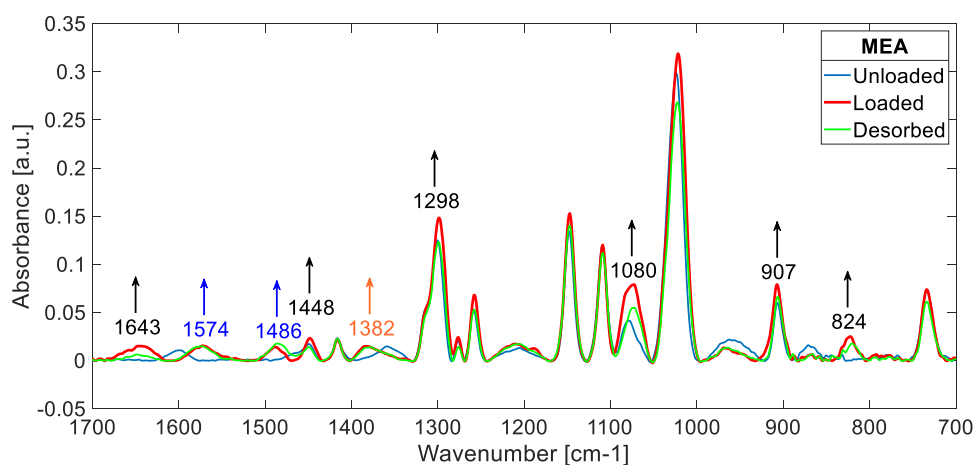


Figure 4. Baseline-corrected ATR-FTIR spectra of unloaded (blue line), CO₂-loaded (red line), and desorbed (green line) MEA solvent.

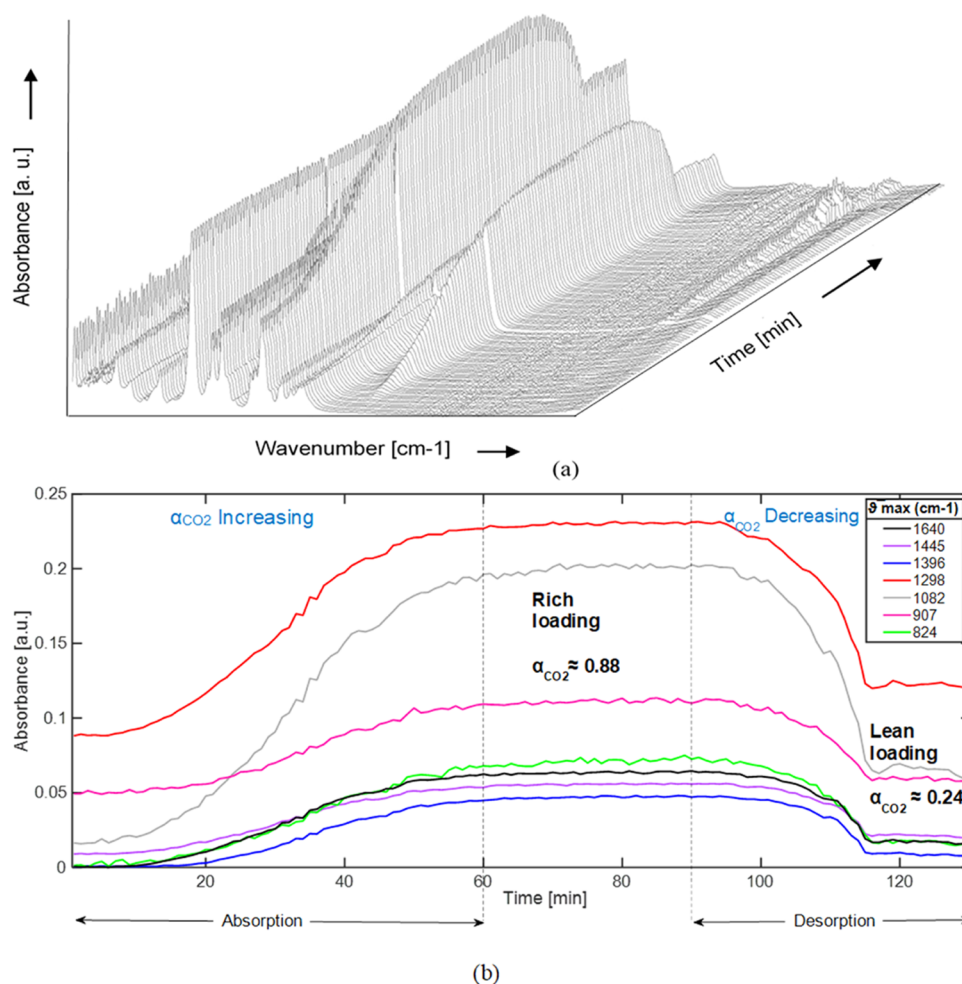


Figure 6. CO₂ absorption–desorption cycle of the DPA solvent over time. ATR-FTIR scans (a) and MMC IR vibrational band variation (b).

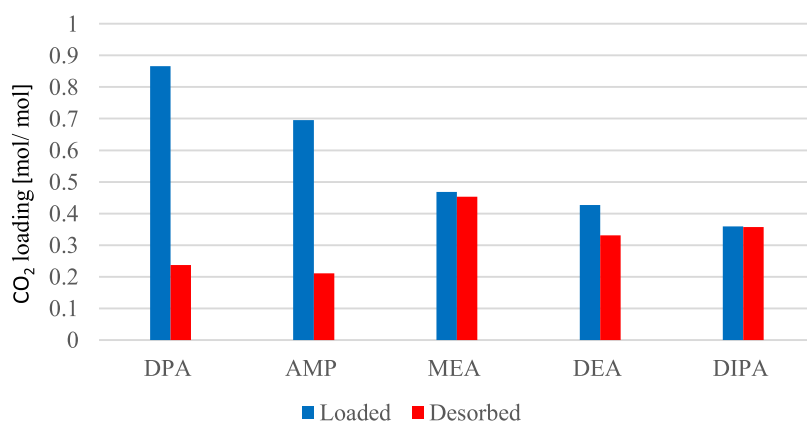


Figure 7. CO₂-rich and -lean loading of five investigated solvents.

clearly; these peaks decreased during the desorption step. At the end of absorption and desorption experiments, liquid samples were collected and titrated using the BaCl₂ method to determine the CO₂ loadings (α). The results obtained are depicted in the bar chart as shown in Figure 7. At an absorption temperature of 20 °C, the DPA solvent has the highest CO₂ capture capacity with α of 0.88 mol_{CO₂}/mol_{amine}, followed by the AMP solvent with an α of 0.695 mol_{CO₂}/mol_{amine}. On the other hand, MEA, DEA, and DIPA solvents showed lower α of 0.467, 0.426, and 0.358 mol_{CO₂}/mol_{amine}

respectively. Overall, the maximum α of the DPA solvent is close to 1, which corresponds to the stoichiometry of MMC formation in the nonaqueous solvent. The low CO₂ capture capacity seen in the case of MEA, DEA, and DIPA solvents may be attributed to the reaction stoichiometry based on the carbamate formation. During desorption experiments at a temperature of 58 °C, α of the regenerated samples of DPA and AMP solvents was reduced by around 70% suggesting that the capture products are reversible at a low temperature. No noticeable change in α was observed during desorption for

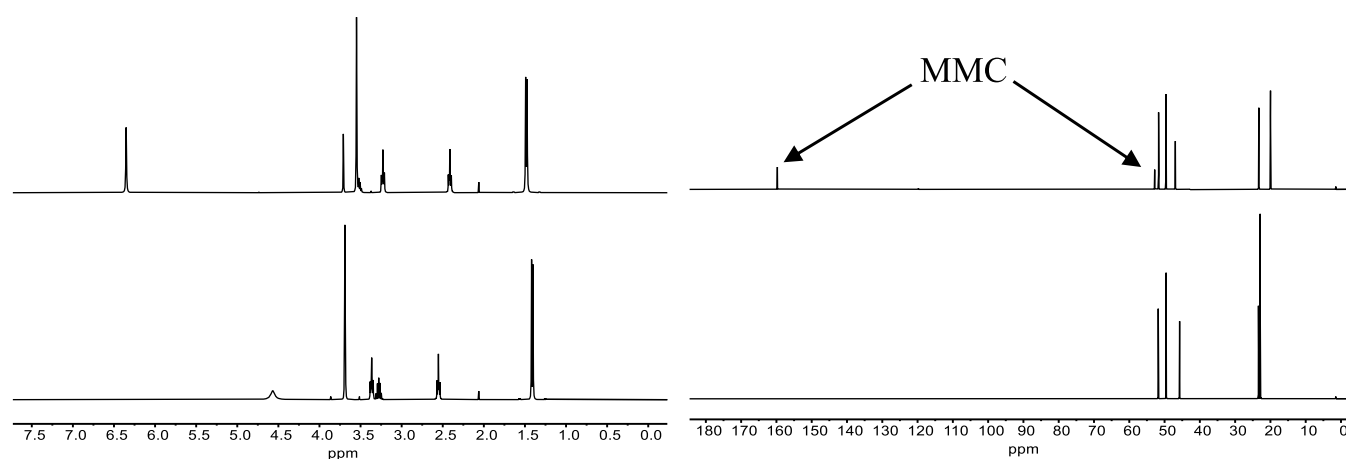


Figure 8. ^1H (left) and ^{13}C (right) NMR spectra of CO_2 -loaded (top) and unloaded (bottom) DPA nonaqueous solvent.

MEA, DEA, and DIPA solvents, which can be attributed to the stable carbamate formation in these solvents.

Based on Figure 7, the cyclic capacity for CO_2 absorption for each of the solvents tested in this work can be calculated by subtracting the lean loading at 58°C from the rich loading at 20°C . The DPA solvent has the highest cyclic capacity of $0.629\text{ mol}_{\text{CO}_2}/\text{mol}_{\text{amine}}$. This is followed by AMP, DEA, MEA, and DIPA with cyclic capacities of 0.484, 0.096, 0.015, and $0.002\text{ mol}_{\text{CO}_2}/\text{mol}_{\text{amine}}$, respectively. As a comparison, aqueous 30 wt % MEA cyclic capacity is reported to reach between 0.34 and $0.1\text{ mol}_{\text{CO}_2}/\text{mol}_{\text{amine}}$.^{14,41} Cyclic capacities of RTI's NAS solvents have been reported to be between 0.2 and $0.4\text{ mol}_{\text{CO}_2}/\text{mol}_{\text{amine}}$.¹⁴ The cyclic capacity of the proposed nonaqueous solvent by Chen and co-workers was around $1\text{ mol}_{\text{CO}_2}/\text{mol}_{\text{amine}}$.⁸ The relatively high cyclic capacity of our DPA solvent is beneficial for the design of absorption and desorption columns. Since it is superior in terms of cyclic capacity to the other tested solvent examples, it was selected for further characterization as discussed below.

3.2. NMR Results of DPA Solvent and the Mechanism of Reaction. Typical ^{13}C and ^1H NMR spectra of unloaded and CO_2 -loaded DPA solvent are shown in Figure 8, whereas the ^{13}C and ^1H chemical shift values of the species are tabulated in Table 4.

Two new peaks at 53.1 and 160.1 ppm can be observed in the ^{13}C NMR spectrum of the CO_2 -loaded DPA solvent, and

Table 4. ^1H and ^{13}C Chemical Shift Values of Unloaded and Loaded Samples of DPA Solvent

sample	species	chemical shift values [ppm]	
		^1H	^{13}C
unloaded	DPA	1.3 and 3.2	20.3 and 47.3
	methanol	3.6	49.9
	sulfolane	2.5 and 3.3	23.6 and 52.1
	exchange peak ^a	4.5	
CO_2 -loaded	DPA	1.4 and 3.4	23.2 and 46.1
	methanol	3.6 (unreacted)	49.9
	sulfolane	2.3 and 3.1	23.7 and 52.0
	MMC	3.4 (methyl) and 6.3 (carbonate)	53.1 and 160.1

^aExchange peak denotes fast exchanging amine/protonated amine protons.

two new peaks appeared at 6.3 and 3.4 ppm in the ^1H NMR spectrum. The peak at 160.1 ppm has been identified earlier as the ^{13}C NMR signal of the carbon atom of the $-\text{OCO}_2-$ moiety in the MMC group.^{8,42} The resonance at 53.1 ppm corresponds to the methyl carbon of MMC derived from MeOH.⁸ In the ^1H NMR spectrum of the CO_2 -loaded solvent, the peak at 6.3 ppm is attributed to the methylcarbonate group and the peak at 3.4 ppm represents the signal of the methyl group of MMC and DPA. There was no sign of carbamate formation in the ^1H NMR spectra: however, carbamate has a distinctive ^{13}C NMR signal at 164 ppm^{8,42–44} which was not observed either. Hence, the sample does not contain carbamate anions. Overall, the NMR results confirm that both DPA and MeOH take part in the CO_2 absorption reaction by forming MMC as the sole CO_2 -containing product.

For alcohol-containing nonaqueous AMP solution, alkylcarbonate formation is suggested to occur by nucleophilic alcoholysis of the unstable AMP carbamate intermediate.^{45,46} In analogy to this proposed mechanism, Figure 9 shows the proposal for the DPA solvent. Alkylcarbonate formation in the anhydrous alcoholic condition is thought not to occur through the reaction of tertiary amine and CO_2 since tertiary amines do not form carbamate species.⁴⁵

In contrast, the reaction of CO_2 with alcohol or alcohol derivatives and tertiary amines in the neat state^{47,48} or in a nonaqueous solution of primary or secondary amine⁴⁹ leads to alkylcarbonate formation. It is proposed that in the latter case, the hydroxyl group functions as a nucleophile toward CO_2 ; the amine stabilizes both the nucleophilic hydroxyl group and the alkylcarbonic acid ester product as shown in Figure 10.⁴⁹

Both DPA and AMP are steric-hindered amines,⁵⁰ which should form intermediate carbamate species. Our data does not provide indications to which and what extent the two above-proposed alkylcarbonate mechanisms would apply for the amines of this work; however, concurrent operation of both mechanisms in analogy^{49,53} to CO_2 absorption into aqueous alkanolamine solution seems possible for all alkanolamine solvents of this work. Elucidation of what governs the amount of formed MMC including the high reactivity of the DPA solvent requires further work.

3.3. DPA Solvent Viscosity. Solvent viscosity is a critical parameter of the CO_2 capture solvent since it affects column design. Viscous solvents cause lower CO_2 capture efficiency due to reduced mass transfer. Additionally, larger heat exchangers are needed for highly viscous solvents due to

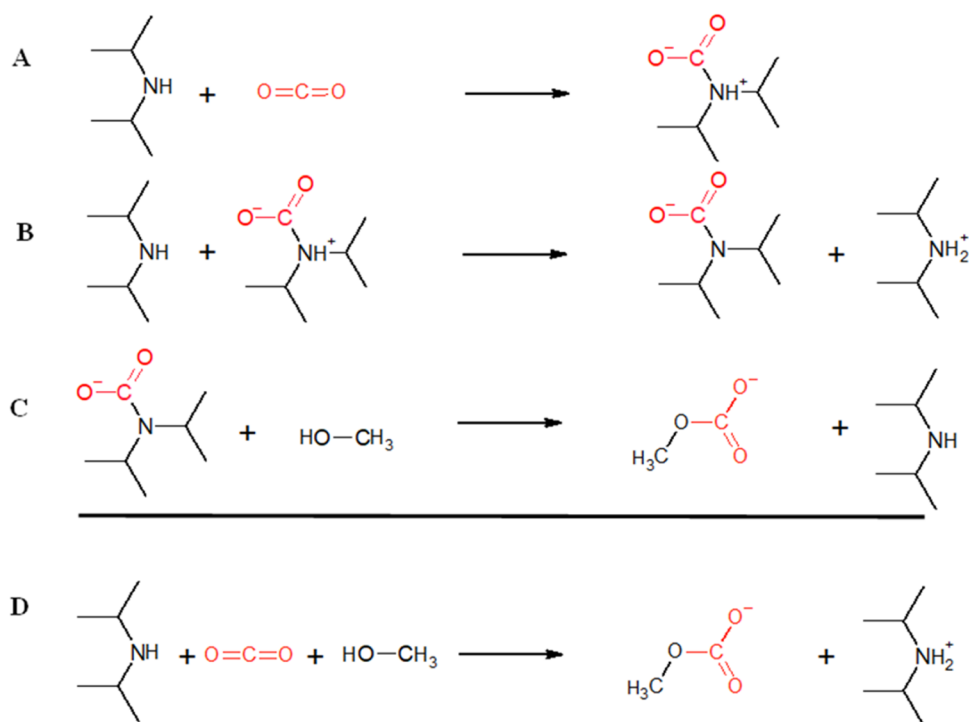


Figure 9. Possible reaction mechanism for monomethyl carbonate formation by the nucleophilic attack of methanol on intermediate DPA carbamate proposed in analogy to the literature.^{45,46}

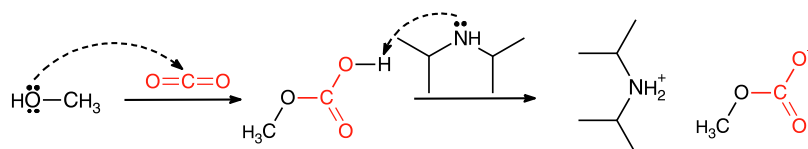


Figure 10. Possible alkylcarbonate formation through deprotonation of methylcarbonic acid proposed in analogy to the literature.⁴⁹

their lower heat transfer, which leads to extra capital costs. One of the main concerns with nonaqueous solvent is the high viscosity of the solution upon exposure to CO_2 .¹¹

Viscosity results for the DPA solvent are compared to the reported viscosity of 30 wt % MEA¹² and are shown in Figure 11. At 40 °C, the viscosity of the DPA solvent only minimally increased from 1.02 mPa·s for unloaded to 3.28 mPa·s at a loading of 0.88 mol CO_2 /mol amine . This is comparable to the

benchmark 30 wt % MEA solvent in which the viscosity changes from 1.7 to 2.7 mPa·s at 40 °C from lean to rich streams.^{14,51} Other nonaqueous solvents tend to have high viscosity. For example, the RTI's NAS2 and Gen2 NAS both have a viscosity of 27.1 and 9.34 mPa·s upon CO_2 uptake.¹⁴ The CO_2 -binding organic solvents CO_2 BOLs on the other hand show viscosities in the range of 200 mPa·s upon CO_2 absorption.^{14,52} The comparable viscosity of the DPA solvent studied in this work with that of MEA is beneficial.

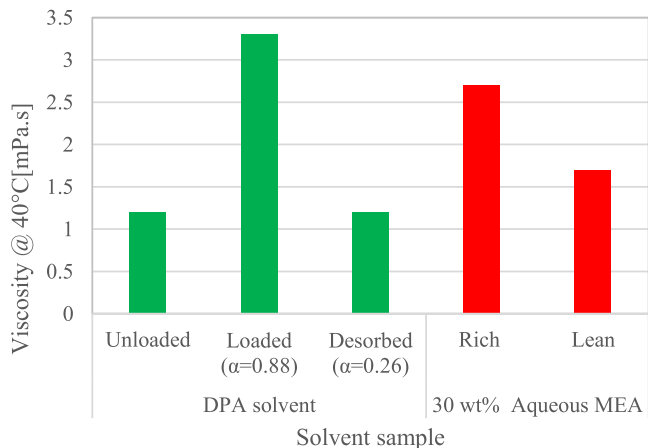


Figure 11. Viscosity comparison: DPA (green columns) solvent with 30% aqueous MEA (red columns) at 40 °C.

4. CONCLUSIONS

Six new CO_2 capture solvent blends, each composed of amine (DPA, AMP, MDEA, DEA, DIPA, MEA), sulfolane, and methanol, were prepared and screened for CO_2 absorption and desorption capability, which was monitored by ATR-FTIR spectroscopy. CO_2 was captured through formation of monomethyl carbonate (MMC) and carbamate anion. The ratio of these species toward each other was different for the various amines; DPA formed exclusively MMC, while MDEA, MEA, DEA, and DIPA did not or rarely formed it. AMP occupies an intermediate position in this group of amines. The solvent speciation is confirmed by IR literature reference and NMR analysis of the DPA solvent. MMC can be readily decomposed to amine and CO_2 at a temperature of around 60 °C. The solvent viscosity ($T = 40$ °C) changes from 1.02 to 3.28 mPa·s for unloaded to fully CO_2 -loaded ($\alpha = 0.88$) solvents. This viscosity data is comparable to that of aq. 30 wt

% MEA solvent. Further work must consider an optimal solvent blend composition and the effect of water on solvent CO₂ capture performance.

■ ASSOCIATED CONTENT

SI Supporting Information

The Supporting Information is available free of charge at <https://pubs.acs.org/doi/10.1021/acs.iecr.1c04946>.

Baseline-corrected ATR-FTIR spectra of unloaded, CO₂-loaded, and desorbed DEA and DIPA solvents and viscosities at 40 °C of DPA (PDF)

■ AUTHOR INFORMATION

Corresponding Author

Klaus-J. Jens – Department of Process, Energy and Environmental Technology, University of South – Eastern Norway, 3918 Porsgrunn, Norway; orcid.org/0000-0002-9022-5603; Phone: +4735575193; Email: Klaus.J.Jens@usn.no

Authors

Jayangi D. Wagaarachchige – Department of Electrical, IT and Cybernetics, University of South – Eastern Norway, 3918 Porsgrunn, Norway

Zulkifli Idris – Department of Process, Energy and Environmental Technology, University of South – Eastern Norway, 3918 Porsgrunn, Norway; orcid.org/0000-0001-7905-9686

Bjørnar Arstad – SINTEF Materials and Chemistry, 0314 Oslo, Norway

Nithin B. Kummamuru – Department of Process, Energy and Environmental Technology, University of South – Eastern Norway, 3918 Porsgrunn, Norway

Kai A. S. Sætre – Department of Process, Energy and Environmental Technology, University of South – Eastern Norway, 3918 Porsgrunn, Norway

Maths Halstensen – Department of Electrical, IT and Cybernetics, University of South – Eastern Norway, 3918 Porsgrunn, Norway

Complete contact information is available at: <https://pubs.acs.org/doi/10.1021/acs.iecr.1c04946>

Author Contributions

The manuscript was written through the contributions of all authors. All authors have given approval to the final version of the manuscript.

Funding

This work was funded by the Ministry of Education and Research of the Norwegian Government.

Notes

The authors declare no competing financial interest.

■ ABBREVIATIONS USED

ATR-FTIR	attenuated total reflectance fourier transform infrared
MMC	monomethyl carbonate
CO ₂	carbon dioxide
DPA	diisopropylamine
AMP	2-amino-2-methyl-1-propanol
MEA	monoethanolamine
DEA	diethanolamine
DIPA	diisopropanolamine

MDEA	methyldiethanolamine
MAC	monoalkyl carbonate
MeOH	methanol
α	CO ₂ loading
NMR	nuclear magnetic resonance
NAS	nonaqueous solvent
2-PE	2-piperidineethanol
EG	ethylene glycol

■ REFERENCES

- (1) Pachauri, R. K.; Allen, M. R.; Barros, V. R.; Broome, J.; Cramer, W.; Christ, R.; Church, J. A.; Clarke, L.; Dahe, Q.; Dasgupta, P. *Climate Change 2014: Synthesis Report. Contribution of Working Groups I, II and III to the Fifth Assessment Report of the Intergovernmental Panel on Climate Change*; IPCC, 2014.
- (2) Rochelle, G. T. Amine Scrubbing for CO₂ Capture. *Science* **2009**, *325*, 1652–1654.
- (3) Lepaumier, H.; Picq, D.; Carrette, P.-L. New Amines for CO₂ Capture. I. Mechanisms of Amine Degradation in the Presence of CO₂. *Ind. Eng. Chem. Res.* **2009**, *48*, 9061–9067.
- (4) Roberts, R. B. Process for Separating Acidic Gases. U.S. Patent US1,783,9011930.
- (5) Sodiq, A.; Hadri, N. E.; Goetheer, E. L. V.; Abu-Zahra, M. R. M. Chemical reaction kinetics measurements for single and blended amines for CO₂ postcombustion capture applications. *Int. J. Chem. Kinet.* **2018**, *50*, 615–632.
- (6) Song, J.-H.; Yoon, J.-H.; Lee, H.; Lee, K.-H. Solubility of Carbon Dioxide in Monoethanolamine + Ethylene Glycol + Water and Monoethanolamine + Poly (ethylene glycol) + Water. *J. Chem. Eng. Data* **1996**, *41*, 497–499.
- (7) DuPart, M. S.; Bacon, T. R.; Edwards, D. J. Understanding corrosion in alkanolamine gas treating plants: Part I. *Hydrocarbon Processing; (United States)* **1993**, *72*, 75–80.
- (8) Yang, M. L.; Lv, M.; Chen, J. Efficient non-aqueous solvent formed by 2-piperidineethanol and ethylene glycol for CO₂ absorption. *Chem. Commun.* **2019**, *55*, 12483–12486.
- (9) Rochelle, G.; Chen, E.; Freeman, S.; Van Wagener, D.; Xu, Q.; Voice, A. Aqueous piperazine as the new standard for CO₂ capture technology. *Chem. Eng. J.* **2011**, *171*, 725–733.
- (10) Chen, X.; Rochelle, G. T. Aqueous piperazine derivatives for CO₂ capture: Accurate screening by a wetted wall column. *Chem. Eng. Res. Des.* **2011**, *89*, 1693–1710.
- (11) Heldebrant, D. J.; Koech, P. K.; Glezakou, V.-A.; Rousseau, R.; Malhotra, D.; Cantu, D. C. Water-Lean Solvents for Post-Combustion CO₂ Capture: Fundamentals, Uncertainties, Opportunities, and Outlook. *Chem. Rev.* **2017**, *117*, 9594–9624.
- (12) *Accelerating Breakthrough Innovation in Carbon Capture, Utilization, and Storage; Mission Innovation Workshop, September 2017*, U.S. Department of Energy: Houston, Texas, USA, 2017.
- (13) Hwang, J.; Kim, J.; Lee, H. W.; Na, J.; Ahn, B. S.; Lee, S. D.; Kim, H. S.; Lee, H.; Lee, U. An experimental based optimization of a novel water lean amine solvent for post combustion CO₂ capture process. *Appl. Energy* **2019**, *248*, 174–184.
- (14) Lail, M.; Tanthana, J.; Coleman, L. Non-Aqueous Solvent (NAS) CO₂ Capture Process. *Energy Procedia* **2014**, *63*, 580–594.
- (15) Bougie, F.; Pokras, D.; Fan, X. Novel non-aqueous MEA solutions for CO₂ capture. *Int. J. Greenhouse Gas Control* **2019**, *86*, 34–42.
- (16) Nikolic, D.; Wijntje, R.; Patil Hanamant Rao, P.; Van Der Zwet, G. *Sulfinol-X: Second-generation Solvent for Contaminated Gas Treating*, International Petroleum Technology Conference, 2009.
- (17) Roberts, B. E.; Mather, A. E. Solubility of H₂S and CO₂ in sulfolane. *The Canadian Journal of Chemical Engineering* **1988**, *66*, 519–520.
- (18) Kohl, A. L.; Nielsen, R. B. Alkanolamines for Hydrogen Sulfide and Carbon Dioxide Removal. In *Gas Purification*, 5th ed.; Kohl, A. L.; Nielsen, R. B., Eds.; Gulf Professional Publishing: Houston, 1997; pp. 40–186.

- (19) Zou, L.; Gao, H.; Wu, Z.; Liang, Z. Fast screening of amine/physical solvent systems and mass transfer studies on efficient aqueous hybrid MEA/Sulfolane solution for postcombustion CO₂ capture. *J. Chem. Technol. Biotechnol.* **2019**, *95*, 649–664.
- (20) Yuan, Y.; Rochelle, G. T. CO₂ absorption rate and capacity of semi-aqueous piperazine for CO₂ capture. *Int. J. Greenhouse Gas Control* **2019**, *85*, 182–186.
- (21) Wang, L.; Yu, S.; Li, Q.; Zhang, Y.; An, S.; Zhang, S. Performance of sulfolane/DETA hybrids for CO₂ absorption: Phase splitting behavior, kinetics and thermodynamics. *Appl. Energy* **2018**, *228*, 568–576.
- (22) Wang, L.; Zhang, Y.; Wang, R.; Li, Q.; Zhang, S.; Li, M.; Liu, J.; Chen, B. Advanced Monoethanolamine Absorption Using Sulfolane as a Phase Splitter for CO₂ Capture. *Environ. Sci. Technol.* **2018**, *52*, 14556–14563.
- (23) Kubiszal, J.; Łosiewicz, B.; Dybal, P.; Kozik, V.; Bak, A. Temperature-Related Corrosion Resistance of AISI 1010 Carbon Steel in Sulfolane. *Materials* **2020**, *13*, 2563–2575.
- (24) Carlson, H. G.; E, F. W., Jr. Methanol: Heat Capacity, Enthalpies of Transition and Melting, and Thermodynamic Properties from 5–300°K. *J. Chem. Phys.* **1971**, *54*, 1464–1471.
- (25) Pakzad, P.; Mofarahi, M.; Izadpanah, A. A.; Afkhamipour, M. Experimental data, thermodynamic and neural network modeling of CO₂ absorption capacity for 2-amino-2-methyl-1-propanol (AMP) + Methanol (MeOH) + H₂O system. *J. Nat. Gas Sci. Eng.* **2020**, *73*, No. 103060.
- (26) Kadiwala, S.; Rayer, A. V.; Henni, A. Kinetics of carbon dioxide (CO₂) with ethylenediamine, 3-amino-1-propanol in methanol and ethanol, and with 1-dimethylamino-2-propanol and 3-dimethylamino-1-propanol in water using stopped-flow technique. *Chem. Eng. J.* **2012**, *179*, 262–271.
- (27) Zarker, H. D. Sulfinol—A New Process for Gas Purification. In *6th World Petroleum Congress*, World Petroleum Congress: Frankfurt am Main, Germany, 1963; p. 12.
- (28) Rufford, T. E.; Smart, S.; Watson, G. C. Y.; Graham, B. F.; Boxall, J.; Diniz da Costa, J. C.; May, E. F. The removal of CO₂ and N₂ from natural gas: A review of conventional and emerging process technologies. *J. Pet. Sci. Eng.* **2012**, *94*–95, 123–154.
- (29) Cieslarova, Z.; dos Santos, V. B.; do Lago, C. L. Both carbamates and monoalkyl carbonates are involved in carbon dioxide capture by alkanolamines. *Int. J. Greenhouse Gas Control* **2018**, *76*, 142–149.
- (30) Kim, I.; Jens, C. M.; Grimstvedt, A.; Svendsen, H. F. Thermodynamics of protonation of amines in aqueous solutions at elevated temperatures. *J. Chem. Thermodyn.* **2011**, *43*, 1754–1762.
- (31) Zeng, Y.; Chen, X.; Zhao, D.; Li, H.; Zhang, Y.; Xiao, X. Estimation of pKa values for carboxylic acids, alcohols, phenols and amines using changes in the relative Gibbs free energy. *Fluid Phase Equilib.* **2012**, *313*, 148–155.
- (32) Kim, J.-H.; Dobrogowska, C.; Hepler, L. G. Thermodynamics of ionization of aqueous alkanolamines. *Can. J. Chem.* **1987**, *65*, 1726–1728.
- (33) Weiland, R. H.; Trass, O. Titrimetric determination of acid gases in alkali hydroxides and amines. *Anal. Chem.* **1969**, *41*, 1709–1710.
- (34) Idris, Z.; Kummamuru, N. B.; Eimer, D. A. Viscosity measurement of unloaded and CO₂-loaded aqueous monoethanolamine at higher concentrations. *J. Mol. Liq.* **2017**, *243*, 638–645.
- (35) Behrendt, W.; Gattow, G.; Dräger, M. Über Chalkogenolate. LXI. Untersuchungen über Halbester der Kohlensäure. I. Darstellung und Eigenschaften von MonomethylCE und Monoäthylcarbonaten. *Z. Anorg. Allg. Chem.* **1973**, *397*, 237–246.
- (36) du Preez, L. J.; Motang, N.; Callanan, L. H.; Burger, A. J. Determining the Liquid Phase Equilibrium Speciation of the CO₂–MEA–H₂O System Using a Simplified in Situ Fourier Transform Infrared Method. *Ind. Eng. Chem. Res.* **2019**, *58*, 469–478.
- (37) Sun, C.; Dutta, P. K. Infrared Spectroscopic Study of Reaction of Carbon Dioxide with Aqueous Monoethanolamine Solutions. *Ind. Eng. Chem. Res.* **2016**, *55*, 6276–6283.
- (38) Socrates, G., *Infrared and Raman Characteristic Group Frequencies: Tables and Charts*. Wiley: Chichester; New York, 2000.
- (39) Richner, G.; Puxty, G. Assessing the Chemical Speciation during CO₂ Absorption by Aqueous Amines Using in Situ FTIR. *Ind. Eng. Chem. Res.* **2012**, *51*, 14317–14324.
- (40) Chowdhury, F. A.; Yamada, H.; Higashii, T.; Goto, K.; Onoda, M. CO₂ Capture by Tertiary Amine Absorbents: A Performance Comparison Study. *Ind. Eng. Chem. Res.* **2013**, *52*, 8323–8331.
- (41) Schäffer, A.; Brechtel, K.; Scheffknecht, G. Comparative study on differently concentrated aqueous solutions of MEA and TETA for CO₂ capture from flue gases. *Fuel* **2012**, *101*, 148–153.
- (42) Barzagli, F.; Lai, S.; Mani, F. Novel non-aqueous amine solvents for reversible CO₂ capture. *Energy Procedia* **2014**, *63*, 1795–1804.
- (43) Chen, S.; Chen, S.; Zhang, Y.; Qin, L.; Guo, C.; Chen, J. Species distribution of CO₂ absorption/desorption in aqueous and non-aqueous N-ethylmonoethanolamine solutions. *Int. J. Greenhouse Gas Control* **2016**, *47*, 151–158.
- (44) Yamada, H.; Matsuzaki, Y.; Goto, K. Quantitative Spectroscopic Study of Equilibrium in CO₂-Loaded Aqueous 2-(Ethylamino)ethanol Solutions. *Ind. Eng. Chem. Res.* **2014**, *53*, 1617–1623.
- (45) Barzagli, F.; Mani, F.; Peruzzini, M. Efficient CO₂ absorption and low temperature desorption with non-aqueous solvents based on 2-amino-2-methyl-1-propanol (AMP). *Int. J. Greenhouse Gas Control* **2013**, *16*, 217–223.
- (46) Kortunov, P. V.; Siskin, M.; Paccagnini, M.; Thomann, H. CO₂ Reaction Mechanisms with Hindered Alkanolamines: Control and Promotion of Reaction Pathways. *Energy Fuels* **2016**, *30*, 1223–1236.
- (47) Rainbolt, J. E.; Koech, P. K.; Yonker, C. R.; Zheng, F.; Main, D.; Weaver, M. L.; Linehan, J. C.; Heldebrant, D. J. Anhydrous tertiary alkanolamines as hybrid chemical and physical CO₂ capture reagents with pressure-swing regeneration. *Energy Environ. Sci.* **2011**, *4*, 480–484.
- (48) Heldebrant, D. J.; Koech, P. K.; Rainbolt, J. E.; Zheng, F. CO₂-binding organic liquids, an integrated acid gas capture system. *Energy Procedia* **2011**, *4*, 216–223.
- (49) Kortunov, P. V.; Baugh, L. S.; Siskin, M.; Calabro, D. C. In Situ Nuclear Magnetic Resonance Mechanistic Studies of Carbon Dioxide Reactions with Liquid Amines in Mixed Base Systems: The Interplay of Lewis and Brønsted Basicities. *Energy Fuels* **2015**, *29*, 5967–5989.
- (50) Sartori, G.; Savage, D. W. Sterically hindered amines for carbon dioxide removal from gases. *Ind. Eng. Chem. Fundam.* **1983**, *22*, 239–249.
- (51) Amundsen, T. G.; Øi, L. E.; Eimer, D. A. Density and Viscosity of Monoethanolamine + Water + Carbon Dioxide from (25 to 80) °C. *J. Chem. Eng. Data* **2009**, *54*, 3096–3100.
- (52) Heldebrant, D. J.; Yonker, C. R.; Jessop, P. G.; Phan, L. CO₂-binding organic liquids (CO₂ BOLs) for post-combustion CO₂ capture. *Energy Procedia* **2009**, *1*, 1187–1195.
- (53) Cieslarova, Z.; dos Santos, V. B.; do Lago, C. L. Both carbamates and monoalkyl carbonates are involved in carbon dioxide capture by alkanolamines. *Int. J. Greenhouse Gas Control* **2018**, *76*, 142–149.

Article 4

Low-Viscosity Non-aqueous Sulfolane-Amine-Methanol Solvent Blend for Reversible CO₂ capture: Part II. Blend Optimization, Water Effect, and Speciation.

Jayangi D. Wagaarachchige¹, Zulkifli Idris², Bjørnar Arstad³, Klaus-J. Jens², and Maths
Halstensen^{1*}

¹Department of Electrical, IT and Cybernetics, University of South-Eastern Norway,
Porsgrunn, Norway

²Department of Process, Energy and Environmental Technology, University of South-Eastern
Norway, Porsgrunn, Norway

³ SINTEF Materials and Chemistry, 0314 Oslo, Norway

Submitted to Industrial & Engineering Chemistry Research Journal, ACS Publications

Low-Viscosity Non-aqueous Sulfolane-Amine- Methanol Solvent Blend for Reversible CO₂ Capture: Part II. Blend Optimization, Water Effect, and Speciation.

Jayangi D. Wagaarachchige¹, Zulkifli Idris², Bjørnar Arstad³, Maths Halstensen¹, Klaus-J. Jens^{2}*

¹Department of Electrical, IT and Cybernetics, University of South – Eastern Norway, Kjølnes ring 56, 3918 Porsgrunn, Norway

²Department of Process, Energy and Environmental Technology, University of South – Eastern Norway, Kjølnes ring 56, 3918 Porsgrunn, Norway

³SINTEF Materials and Chemistry, Forskningveien 1, 0314 Oslo, Norway

KEYWORDS

Diisopropylamine; Water Tolerance; Monomethyl Carbonate; Nuclear Magnetic Resonance; Design of Experiments; Fourier Transform Infrared Spectroscopy

ABSTRACT

This work is Part II of the investigation of a low viscosity, low regeneration energy non-aqueous CO₂ capture solvent blend consisting of readily available chemicals: diisopropylamine (DPA) – methanol – sulfolane. We show that CO₂ absorption species are monomethyl carbonate anion

(MMC), carbamic acid and carbamate anion. The MMC specie is responsible for low temperature solvent regeneration and high CO₂ capacity due to a 1:1 mol CO₂/mol amine molecular structure. The region of practical solvent composition, high CO₂ capacity, low regeneration energy and avoidance of solvent solidification at CO₂ capture condition, is identified by design of experiment methodology combined with solvent ATR-FTIR and NMR monitoring and speciation analysis. Flue gas contains water vapor, hence solvent water stability is important. The limit of solvent blend water content to 15 wt% because of MMC decomposition to DPA-bicarbonate and -carbamate.

1 Introduction

The current state of climate gas emissions from fossil fuel combustion and industrial point sources makes CO₂ capture imperative with the Gas-Liquid absorption process being one of the immediate options for post-combustion carbon capture (PCC). However, important PCC technology challenges remain to be solved such as high energy penalty of the process. Targeted solutions include the development of non-aqueous/water-lean solvents that reduce CO₂ stripping energy consumption by replacing water with organic diluents.¹ Since flue gas carries some percentage (approximately 10%) of water vapor, water tolerance is needed for these non-aqueous PCC systems; control of water content is also important to keep the stripper reboiler duty even.^{2, 3} A recent review by Heldebrant et al.³ summarizes opportunities and uncertainties of these water-lean solvents.

The reaction pathways of non-aqueous amine solvents are different, complex, and still in the emerging stage as compared to the typical benchmark solvent—30 wt% aqueous monoethanolamine (MEA).⁴⁻⁸ Nuclear magnetic resonance (NMR) studies demonstrate that for non-aqueous CO₂ absorption systems different reaction pathways are available as compared to aqueous solutions.^{4, 5} Non-aqueous CO₂ solvents may form alkyl carbonates as CO₂ capturing

species, which enable energy ‘lean’ solvent regeneration at low stripping temperatures.^{9, 10} Eimer postulated in 1994 formation of alkyl carbonates for the reactive absorption of CO₂ into non-aqueous tertiary amines;¹¹ which was later verified by several NMR- and experimental studies.¹²⁻¹⁴ In general, alkyl carbonates may be formed from solvent components^{8, 12, 14} or from alkanolamine itself such as methyl diethanolamine (MDEA)¹⁵ and triethanolamine (TEA).¹⁶

In 2022 (Part I of this study), we reported a low-viscosity solvent blend consisting of industrial readily available chemicals i.e., 35 wt% sulfolane, 30 wt% diisopropylamine (DPA), and 35 wt% methanol, for reversible CO₂ capture, as studied by ATR-FTIR spectroscopic analysis.⁸ This blend yields a single CO₂ capture product—monomethyl carbonate (MMC)—with the ability to desorb CO₂ at a mild temperature of 58°C.⁸ This study was an early stage of solvent investigation, hence, the effect of solvent composition, the interplay of reaction species on a broader scope and the impact of water was not in focus.

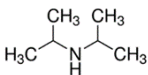
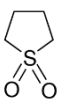
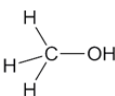
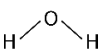
Therefore, in this Part II of the solvent exploration, we put focus on solvent blend composition optimization, the effect of water-lean conditions on the CO₂ capture reaction and reaction speciation. The objectives of this contribution are hence: (i) to find the optimum non-aqueous solvent blend composition; (ii) to test the effect of water on the solvent’s CO₂ capture performance; and (iii) to propose reaction schemes corresponding to the different investigated conditions.

2 Materials and Methods

2.1 Materials

All chemicals (Table 1) were used as received without further purification.

Table 1. Chemicals used for solvent preparation in this work.

Chemical name	CAS number	Chemical structure	Supplier	Description
Diisopropylamine (DPA)	108-18-9		Sigma-Aldrich	$pK_b = 3.43$ (in water) Brønsted/weak Lewis base
Sulfolane (SULF)	126-33-0		Sigma-Aldrich	Non-protic Polar = 4.35D
Methanol (MeOH)	67-56-1		VWR	$pK_a = 15.5$ (in water) Weak Brønsted acid and base Weak Lewis base
Carbon dioxide (CO ₂)	124-38-9	O=C=O	AGA Norge AS	Lewis acid Not Brønsted acid/base Non-polar
Water (H ₂ O)			Double distilled water	$pK_a = 15.7$ Weak Brønsted acid and base Weak Lewis base

2.2 Experimental strategy and study execution

Figure 1 gives an overview of the employed two stage experimental strategy.

Stage 1- Solvent blend composition optimization: CO₂ absorption of the solvent⁸ was investigated at four solvent parameters (i.e., DPA wt%, methanol wt%, sulfolane wt% and absorption temperature (T_{ab}) (Table 2). As explained in Figure 1, Stage 1, a suitable CO₂ absorption temperature and the optimum solvent blend region for CO₂ capture was determined through experimental design methodology.

All solvent mixtures (Tables S1, S2, 3) were prepared gravimetrically. A Mettler Toledo analytical balance type NewClassic MF (MS105DU) (± 0.01 mg) was used for weighing of chemicals.

CO₂ absorption of samples was analyzed by in-situ ATR-FTIR monitoring using a Perkin-Elmer Spectrum 1 spectrometer.⁸ The preprocessed FTIR spectra were used for both quantitative CO₂ absorption comparison and qualitative molecular specie identification.

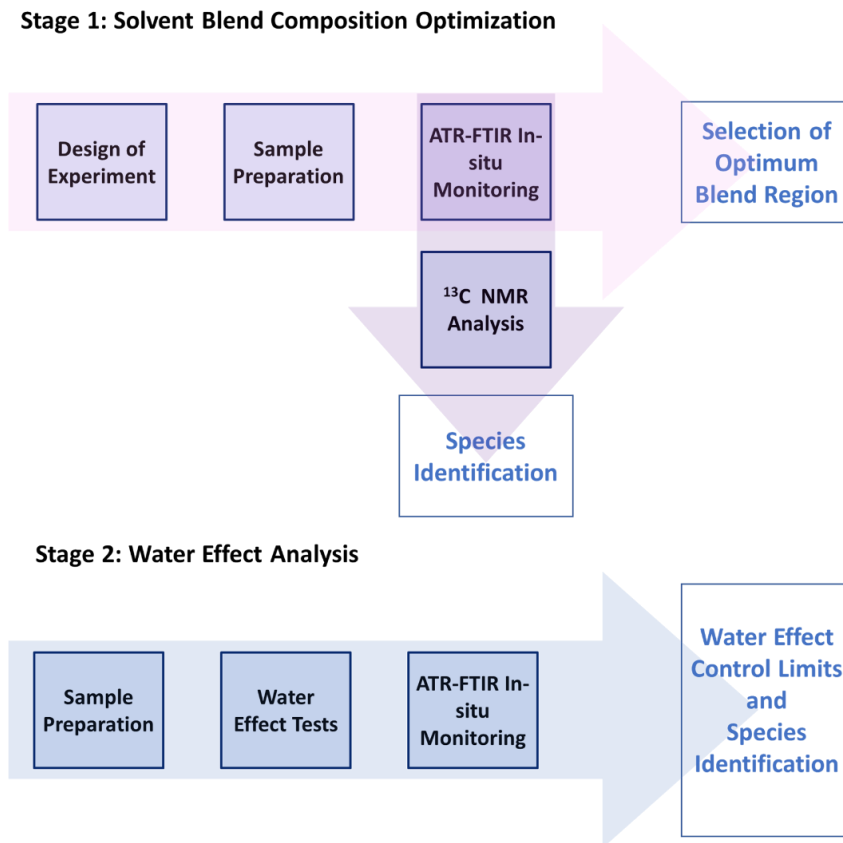


Figure 1: Overview of the experimental strategy

Stage 2 - Solvent performance at water lean conditions: Five non-aqueous solvent blends were selected from the optimized solvent blend region, and CO₂ absorption was tested in the presence of three water weight percentages: 5%, 10%, and 15%. One composition of the optimized blend region (composition F, Table 3), 35 wt% DPA, 50 wt% methanol and 15 wt% sulfolane, was subjected to in-situ ATR-FTIR monitoring at 1, 2, and 15 wt% water content. All infrared (IR) spectra were analyzed for identification of reaction/specie changes during CO₂ loading.

2.3 Methods

Design of Experiments (DoE):¹⁷ Four parameters (factors) were selected for the design; T_{ab} and three weight percentages of the mixture components. A D-optimal factorial design was chosen as

the first design method since the parameters consist of weight percentages of mixture components as well as physical parameters.¹⁷ The geometrical representation (Figure 2 (a)) and Table 2 present the levels of each parameter of the D-optimal experimental design. In Figure 2 (a), four trapezoids are shaded in red, yellow, green, and blue, representing the temperature levels of 25°C, 30°C, 35°C, and 45°C, respectively. Colored circles located on the same-colored trapezoids represent the sample compositions analyzed at each corresponding temperature. The black circle on the green layer represents the center-point (CP)—30 wt% sulfolane, 35 wt% DPA, 35 wt% methanol, 35°C—of the D-optimal design. The center-point experiment was conducted three times, and all other experiments were replicated twice. Altogether, the D-optimal design comprises forty-five (45) in-situ ATR-FTIR monitoring experiments. The details are tabulated in Table S1.

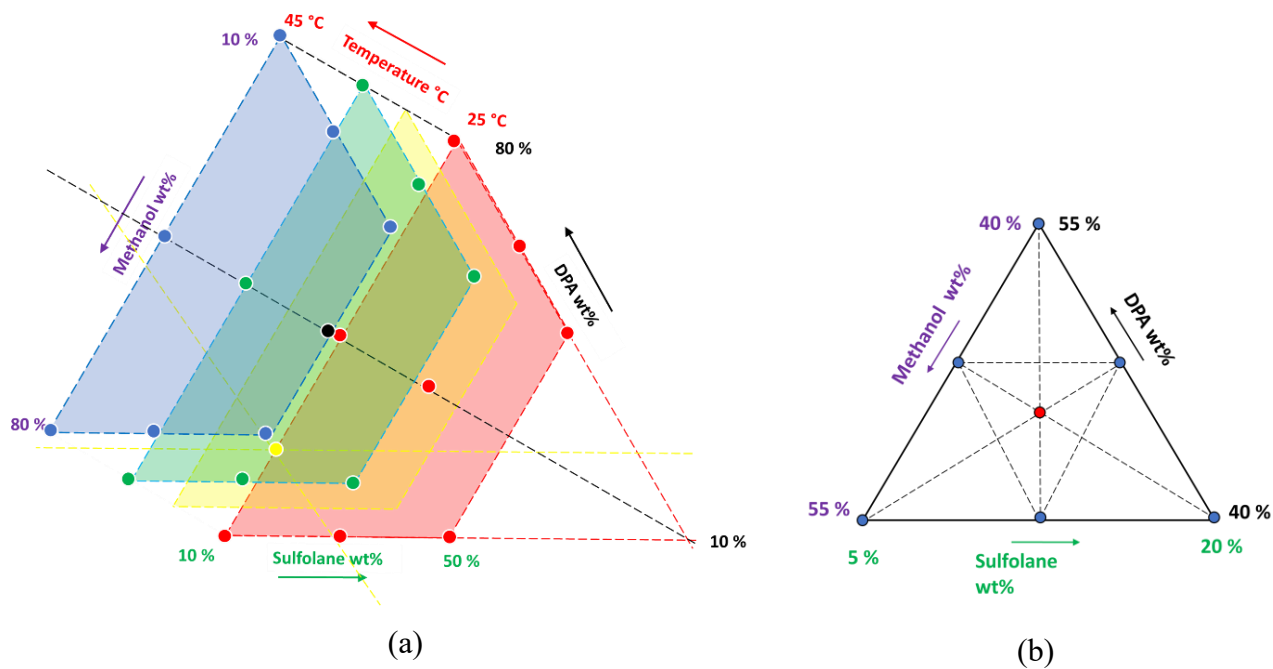


Figure 2: (a) Geometrical representation of the D-optimal design (b) a simplex-shaped mixture design

Table 2. D-optimization design parameters (factors), values (levels), and variable ranges

Parameters /Factors (unit)	Values (level)	No of levels	Range
DPA (wt%)	10, 22.5, 35, 40, 45, 60, 80	7	10-80
Methanol (wt%)	10, 35, 40, 45, 57.5, 60, 80	7	10-80
Sulfolane (wt%)	10, 20, 30, 50	4	10-50
T _{ab} (°C)	25, 30, 35, 45	4	25-45

After completion of the D-optimal experimental protocol, twenty (20) supplementary experiments were conducted to find the optimum blend region for the non-aqueous blend for CO₂ absorption at 25°C. For these experiments, solvent blend compositions were obtained using a simplex-shaped mixture design ¹⁷, while the other three mixtures points were selected arbitrarily. Figure 2 (b) illustrates a simplex-shaped blend design; the red circle represents the design CP: 45 wt% DPA: 45 wt% methanol: 10 wt% sulfolane. All solvent blend design details are tabulated in Table S2.

Lean-water solvent investigation: 5, 10 and 15 wt% water amounts were added to a solvent blend sample (Table 3). 5g of each sample was loaded with CO₂ at a flow rate of 0.04 L/min using the apparatus shown in Figure 3.

Table 3: Solvent blends employed for the lean water content investigation.

Sample name	Non-aqueous solvent blend information (wt%)		
	DPA	methanol	sulfolane
A	30	50	20
B	35	45	20
C	30	40	30
D	30	60	10
E	40	50	10
F	35	50	15

The time until solidification was recorded using a stopwatch.



Figure 3: Experimental setup for CO₂ loading and determination of onset of solid formation. (a) Schematic Diagram, (b) Laboratory setup at the onset of solidification.

Figure 4 shows the apparatus for determination of CO₂ loading including a gas wash bottle for methanol saturation of the CO₂ gas. Two solvent blends (Table 3, D and E which containing 15 wt% water) were tested for determination of CO₂ capacity before onset of solidification.

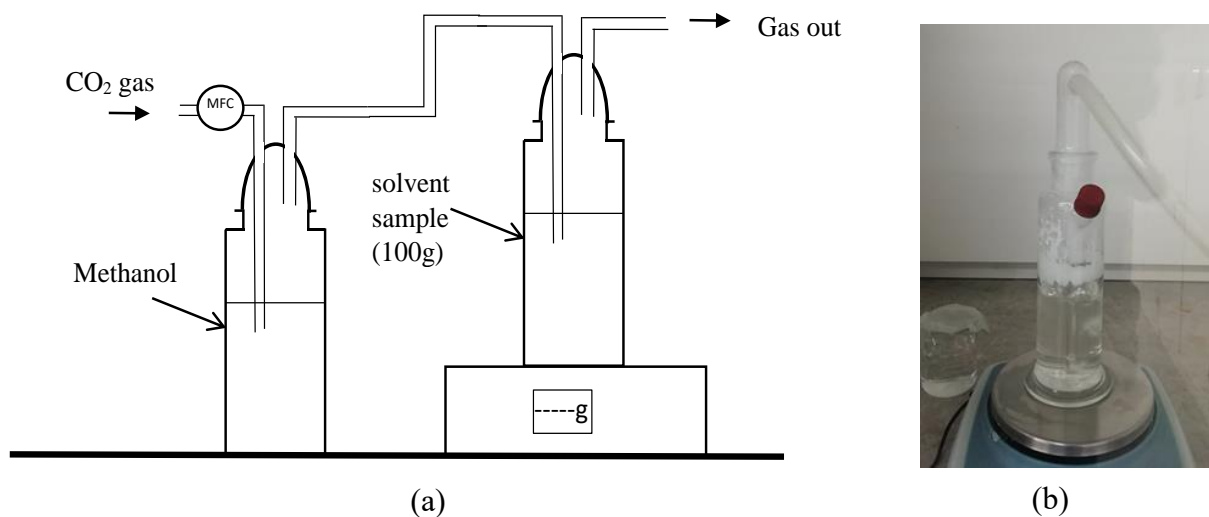


Figure 4: (a) Schematic diagram of the Weight-based CO₂ Loading Apparatus, (b) CO₂-loaded sample of solvent blend E

ATR-FTIR Spectroscopy: A schematic diagram of the experimental set-up is reported in Part I of this work.⁸ In short, 5g solutions were prepared and monitored during CO₂ absorption at a flow rate of 0.04 L/min of pure CO₂.

¹³C and ¹H NMR Spectroscopy: Selected samples of this study were qualitatively analyzed using NMR spectroscopy. Liquid sample measurements were carried out using a Bruker AVANCE III spectrometer operating at a magnetic field of 9.4T. ¹H and ¹³C spectra were acquired using a standard single pulse sequence and a power gated decoupling sequence, respectively. For the ¹H spectra 16 transients/ free induction decays (FIDs) were accumulated with a recycle delay of 5 s. For the ¹³C spectra the corresponding numbers were 512 and 10s. For solid samples ¹³C (1H) MAS cross polarization experiments were carried out using a Bruker AVANCE III spectrometer operating at a magnetic field of 11.7 T. The MAS rate was 10 kHz for all experiments except one (sample A). For each spectrum, 200 transients were accumulated with a recycle delay of 5s. The

contact time for all experiments was 2 milliseconds. Before Fourier transformation of the accumulated free induction decays, the spectra were zero filled. Apodization and baseline corrections were applied for improved spectrum quality.

3. Results and Discussion

In part I of this work we reported a non-aqueous solvent blend composed of i) an amine to extract CO₂ from flue gas, ii) methanol for conversion of CO₂ loaded amine into MMC for low temperature CO₂ regeneration, and iii) sulfolane as the blend base component.⁸ In this part II, we present solvent blend composition optimization and the effect of water on CO₂ absorption. An overall reaction scheme reflecting this optimization work is proposed at the end of this section.

3.1 Solvent Blend Composition Optimization

The target of this section is to identify the optimal solvent blend composition region for CO₂ absorption.

Initially, a sequence of in-situ ATR-FTIR monitoring experiments was undertaken to assess solvent performance in terms of CO₂ absorption temperatures (T_{ab}) and different DPA-methanol-sulfolane blend ratios (Table S1 and Table S2). Figure 5 shows a typical example of ATR-FTIR time-based, in-situ monitoring. The intensity of the MMC vibrational band at 1640 cm⁻¹ ^{8, 18} (H) was used to estimate the amount of CO₂ absorbed (MMC formation) for each experimental run. Hence, H was taken as the response variable (Y) in the optimization study. Before determining the H value, all the spectra were baseline-corrected using the Whittaker filter.¹⁹

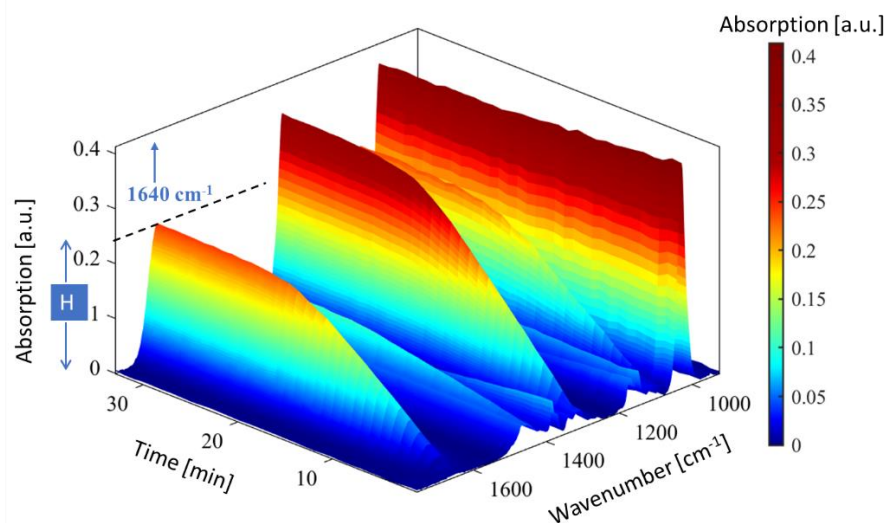


Figure 5: A typical diagram of ATR-FTIR time-based, in-situ monitoring.

The D-optimal design matrix (X), as provided in Table S1, was initially analyzed with H values as the response variable (Y) to find the relation between solvent compositions versus CO₂ absorption temperature (T_{ab}). Figure 6 shows the reduction in H with increase of T_{ab} for six non-aqueous mixtures (Table 4). The blend K and M both containing equal amounts of DPA and methanol distinctly indicate a clear positive interaction effect on CO₂ absorption. Obviously, this interaction effect is determining CO₂ absorption. Furthermore, all blends show an expected negative correlation of H with T_{ab}.

Table 4: Solvent compositions used in Figure 6.

Name	solvent composition (wt%)		
	DPA	methanol	sulfolane
I	10	80	10
J	10	60	30
K	45	45	10
L	10	40	30
M	35	35	30
N	60	10	30

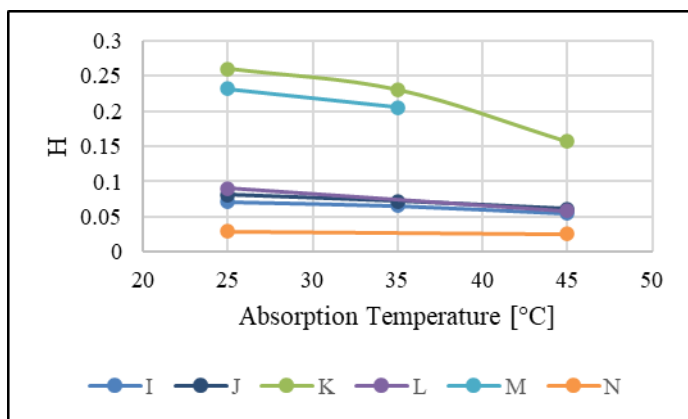


Figure 6: CO₂ absorption temperature (Tab) vs. H (maximum 1640 cm⁻¹ band intensity)

Composition optimization for CO₂ loading and maximum MMC formation (H) were performed at 25°C. Figure 7 summarizes the results of the composition optimization of the non-aqueous solvent.

In this diagram, the white area represents the investigated blend region, while the green shaded area represents the omitted blend region. The diagram provides two main indications: (i) the state of the sample at the end of the experiment; blue, yellow and red dots indicate a liquid, slurry or solid, respectively, and (ii) the H value (the number indicating the maximum relative amount of MMC formed) of the respective solvent blends. The blue line in Figure 7 indicates the 1:1 line of DPA to methanol weight ratio which corresponds to maximum CO₂ capture (see discussion on Figure 6); all the samples lying on it, result in slurries or solids after full CO₂ loading. Furthermore, all samples positioned in the region above the line formed solids at the end of the experiment, while all samples below the line did remain in the liquid state at their respective maximum CO₂ loading. Blend solidification is mainly determined by the DPA to methanol ratio; however, it is also influenced to a minor degree by sulfolane as shown by the colored dots on the blue line.

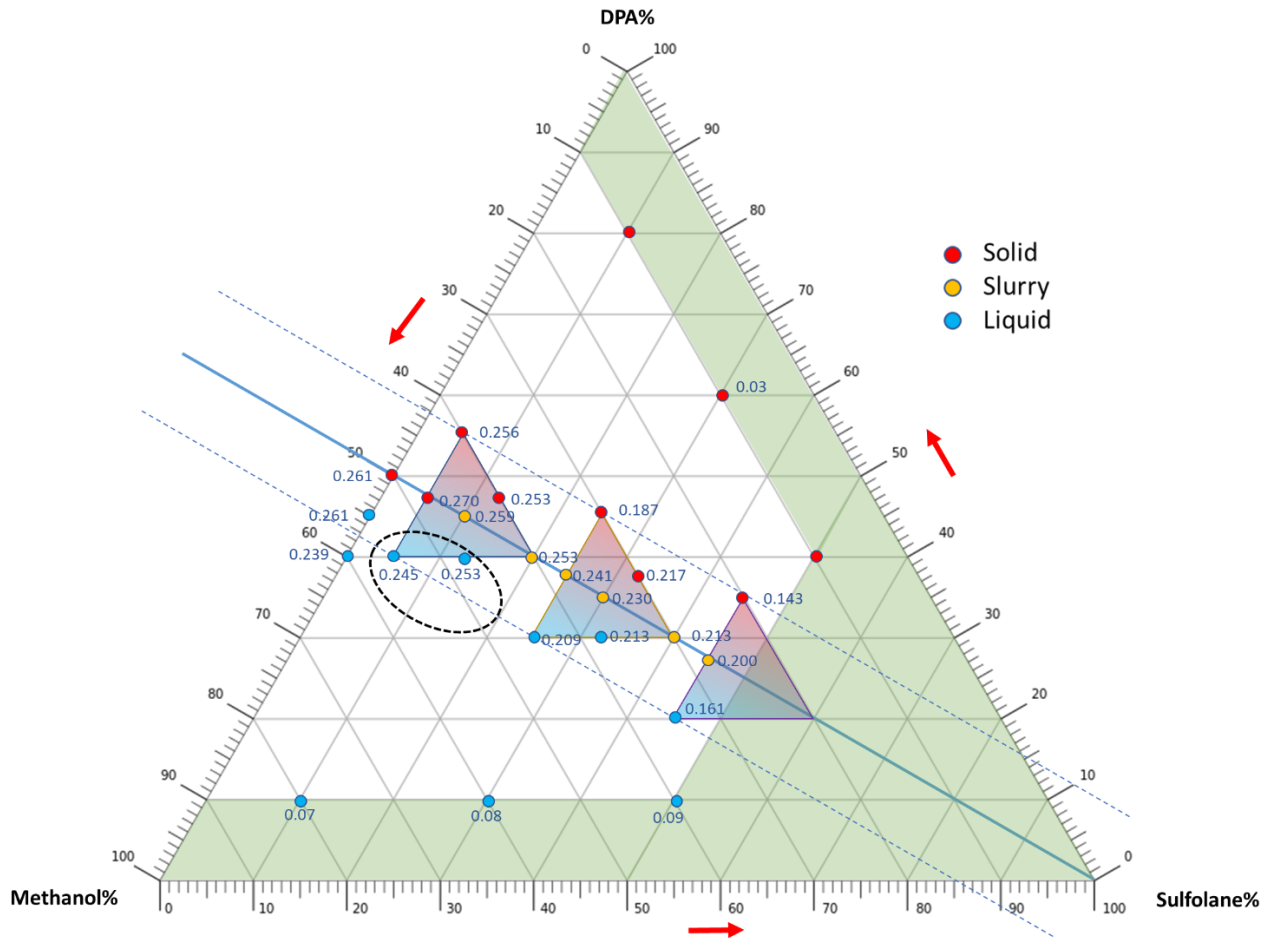


Figure 7: Solvent composition optimization results at 25°C; Dots: Red-solid, Yellow-slurry, Blue-liquid; the numbers indicate relative H values for each experiment.

In conclusion, the solvent blends tend to form a solid/slurry during CO₂ absorption when the DPA wt% is larger or equal to methanol wt%. In contrast, the region below the blue line in Figure 7 shows no solid/slurry formation during CO₂ absorption. Hence, controlling the DPA to methanol wt ratio is a critical factor avoiding solvent solidification at non-aqueous solvent conditions. Furthermore, the region for practical solvent blend operation is indicated by the dashed oval in Figure 7.

3.1.1. CO₂ speciation of loaded solvent blends at high and low DPA to methanol weight ratio

Since in-situ ATR-FTIR monitoring of the CO₂ absorption process also provides information on molecular change, spectra of three solvent samples (three points of Figure 7) involving solidification were analyzed for speciation. Table 5 summarizes solvent compositions details.

Table 5: Solvent compositions of the chosen blends for ATR-FTIR analysis.

Name	solvent composition (wt%)			Comment
	DPA	methanol	sulfolane	
Case (i)	80	10	10	Solidified at the end of experiment
Case (ii)	55	40	5	
Base case	40	47.5	12.5	Fully loaded without solidification

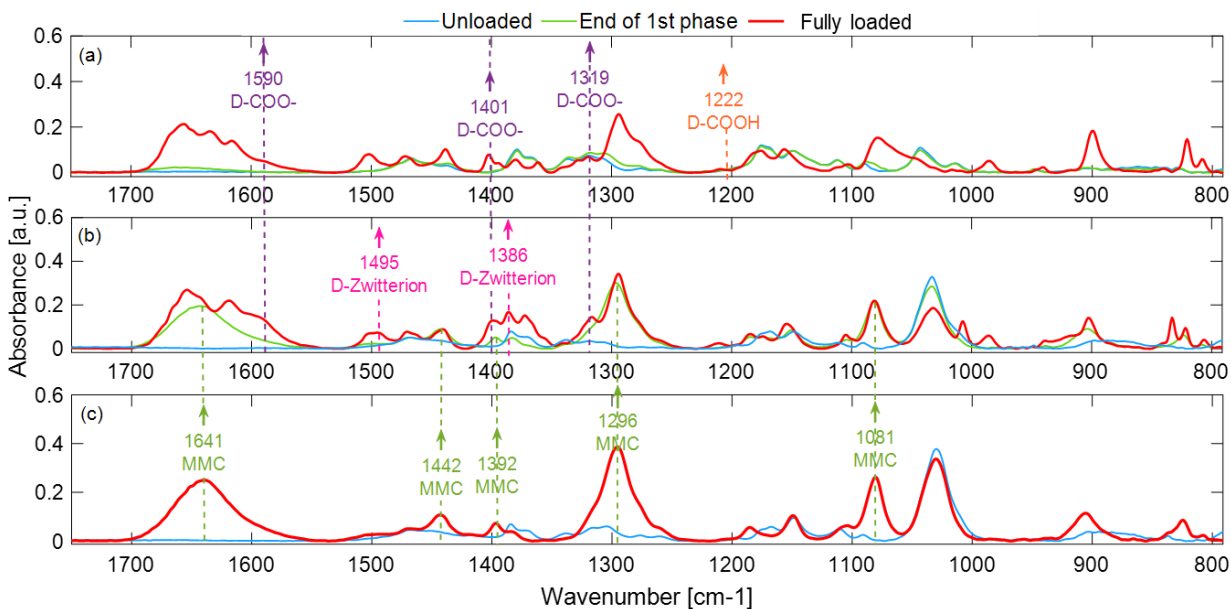


Figure 8: Baseline corrected ATR-FTIR spectra (a) case (i) (b) case (ii) and (c) base-case

Two cases were analyzed: (i) a solvent composition with significantly higher DPA than methanol wt% and (ii) a solvent composition with a moderately higher percentage of DPA than methanol wt%. Figure 8 (a) and (b) show the baseline corrected FTIR spectra of case (i) and (ii), respectively.

For comparison, the baseline corrected spectrum of a non-solidifying solvent blend (Figure 7, optimized region) is included in Figure 8 (c) as the base-case.

In the base case IR spectrum (Fig 8 (c), bands at 1641, 1442, 1392, 1296 and 1081 cm^{-1} can be attributed to MMC formation upon CO_2 loading.⁸ In the two solidification cases (Figure 8 (a) and (b)), the appearing vibrational bands differ from those of the base case and indicate CO_2 absorption to pass through two phases. The green spectra of Figure 8(a) and (b) correspond to the first CO_2 absorption step while the blue and red spectra of Figure 8 (a)-(c) correspond to unloaded and fully loaded solvent, respectively. The IR band assignments for case (i) and (ii) are listed in Table 6.

Table 6: IR band assignments for CO_2 loaded samples for case (i) and case (ii); see also Table 5.

Species	IR peak vibrational assignment	Characteristic IR vibrational bands (ν_{\max}) (cm^{-1})			
		case (i)		case (ii)	
		1 st Phase	2 nd Phase	1 st Phase	2 nd Phase
MMC	C=O stretching ^{8, 18}	n.o.	n.o.	1641	O.
	CH_3 asymmetric deformation ^{8, 18}	n.o.	n.o.	1442	1442
	CH_3 symmetric deformation ^{8, 18}	n.o.	n.o.	1392	O.
	O-C-O asymmetric stretching ^{8, 18}	n.o.	n.o.	1296	1296
	O-C-O symmetric stretching ^{8, 18}	n.o.	n.o.	1081	1081
DPA-COO ⁻ / Zwitterion	COO ⁻ asymmetric stretching ²⁰⁻²³	n.o.	1590	n.o.	1590
	COO ⁻ symmetric stretching ^{20, 21, 23}	n.o.	1402	n.o.	1400
	N-COO ⁻ Skeletal vibration ^{21, 23}	n.o.	1319	n.o.	1319
	N ⁺ -H asymmetric stretching ²⁰	n.o.	n.o.	n.o.	1495
	C-O stretching ^{23, 24}	n.o.	n.o.	n.o.	1386
DPACOOH	COOH stretching ^{23, 25, 26}	1222	n.o.	n.o.	n.o.

n.o.: not observed, O.: overlapping with other IR band(s)

Case (i): Figure 8 (a) show several slightly increased IR bands at 1662, 1437, 1318, 1308, 1277, and 1222 cm^{-1} (green spectrum), which develop during the first phase of CO_2 absorption (0-13 min). The characteristic peak at 1222 cm^{-1} can be assigned to the CO–OH stretch band of carbamic acid.^{25, 26} The red spectrum of Figure 8 (a) shows several other new IR bands with the disappearance of the 1222 cm^{-1} carbamic acid band. The new IR bands at 1590 and 1402 cm^{-1} can be assigned to the asymmetric and symmetric stretching vibrations of the carbonyl (COO^-) group, respectively.^{20, 21, 23} Furthermore, the band at 1319 cm^{-1} can be attributed to the N-COO- skeletal vibration of the carbamate specie.^{21, 23} Absence of an IR band at about 1360 cm^{-1} implies that the solvent does not produce any bicarbonate at non-aqueous condition. Moreover, there is no clear indication of MMC formation during the complete CO_2 absorption period in this borderline case in Figure 7.

Case (ii): Figure 8 (b) shows the spectra of unloaded, intermediate and fully CO_2 loaded solvent samples composed of 55 wt% DPA and 40 wt% methanol. As observed for case (i), CO_2 absorption proceeds in two phases. The green spectrum of Figure 8 (b) represents the end of phase 1 after 23 mins of CO_2 absorption. Increasing IR bands of the 1st phase at 1641, 1442, 1392 and 1296 cm^{-1} document formation of MMC.⁸ There is no indication of any other CO_2 related specie formation during this 1st phase. However, after 23 minutes of CO_2 absorption, new IR bands appeared while the MMC bands remained almost stable as shown in the red spectrum of Figure 8 (b). These three IR bands at 1590, 1400 and 1319 cm^{-1} are assigned to the bands of a DPA-carbamate specie.^{20, 21, 23} Furthermore, two other new bands at 1495 and 1386 cm^{-1} could be the IR stretching vibrations of the $\text{N}^+\text{-H}$ and C-O^- group of a DPA Zwitterion.^{20, 23, 24}

In conclusion, at solvent composition of DPA (80 wt%) \gg than methanol, two phases were observed during CO_2 loading. A first short phase (13 min), involving the formation of DPA

carbamic acid. Thereafter, formation of DPA-carbamate, which continues until the end of CO₂ absorption. At slightly higher DPA than methanol wt% MMC forms as the sole CO₂ capture product during the first phase of CO₂ absorption. However, after 23min of CO₂ absorption, this solvent begins to produce carbamate species as secondary products start to solidify. Hence, formation of carbamate leads solvent solidification. Furthermore, based on the band intensities of these species, it seems that the MMC quantity is considerably higher than the amount of carbamate species.

3.1.2 Solvent blend NMR speciation

Table 7: Solvent compositions for species analysis by NMR.

Name	solvent composition (wt%)			Comment
	DPA	methanol	sulfolane	
Case (i)	100	0	0	Solidified at the end of experiment
Case (ii)	55	40	5	
Base case	30	50	20	Fully loaded without solidification

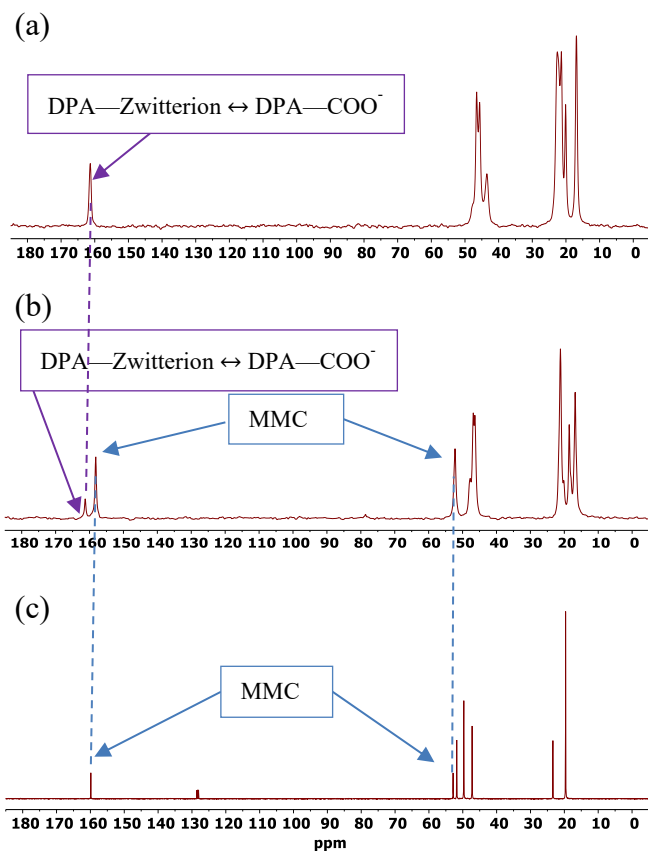


Figure 9 ^{13}C NMR spectra (a) DPA only (b) moderately higher methanol content than DPA (c) Base case (see Table 7).

Table 7 gives the solvent composition of the solvent blends analyzed by ^{13}C NMR. Figure 9 (a) and (b) show the spectra obtained for two solvent compositions which solidified after CO_2 loading. Figure 9 (c) confirms that the base case solvent (Table 7) only produces MMC as the sole CO_2 capture product. The CO_2 loaded solvent is in the liquid homogeneous state. The ^{13}C NMR chemical shifts at 52.9 and 159.9 ppm in Figure 9 (c) can be assigned to MMC species.⁸

The solid-state MAS ^{13}C NMR spectra in Figure 9 (a) and (b) were obtained from the solid samples of CO_2 -loaded neat DPA and a CO_2 -loaded blend with moderately higher wt% DPA than methanol, respectively. In the solid sample obtained after bubbling CO_2 into DPA only, the

chemical shift at 161.3 ppm signifies the DPA-carbamate species (Figure 9 (a)) as the CO₂ capture product.⁵ In this samples no indication of MMC formation is observed.

Figure 9 (b), exhibiting the spectrum of a sample with moderately higher wt% of DPA than methanol, the spectrum shows a chemical shift at 161.3 ppm, attributed to carbamates species⁵, while the chemical shifts at 52.9 and 158.1 ppm correspond to the MMC species.^{8, 27} These findings are consistent with the FTIR speciation of Case (ii).

In conclusion, the NMR data confirm the speciation obtained by ATR-FTIR spectral analysis.

3.2 Analysis of selected water lean solvent compositions

Since flue gas contains water, we also investigated the interaction of water with five CO₂ loaded non-aqueous solvent compositions (Table 3 – A to E compositions) by using the experimental setup shown in Figure 3. These introductory experiments showed solvent solidification to occur upon exposure of loaded solvent blend to water. The experimental setup depicted in Figure 3 (a) was hence used to identify the time to onset of solidification (TTOS) in blends at 5, 10, and 15 wt% water percentage. The results are shown in Figure 10 (a). Figure 10 (b) shows how the solvent composition influences the TTOS in response to solvent water content.

For the same DPA to methanol to solvent weight ratio (C-B-E in Figure 10 (b)) the TTOS remains the same. However, for lower DPA to methanol weight ratios the TTOS will increase. Therefore, the DPA to methanol weight ratio is important to avoid solidification with respect to water content.

Similar TTOS are observed in the presence of water. Moreover, when comparing blends C, A, and D all containing 30 wt% DPA, an increase in methanol wt% results in larger TTOS. This suggests that methanol wt% of the solvent blend is important in terms of solidification control at wet flue

gas conditions. Among the five investigated solvents, sample D, which has the highest methanol to DPA mole ratio, exhibits the longest TTOS.

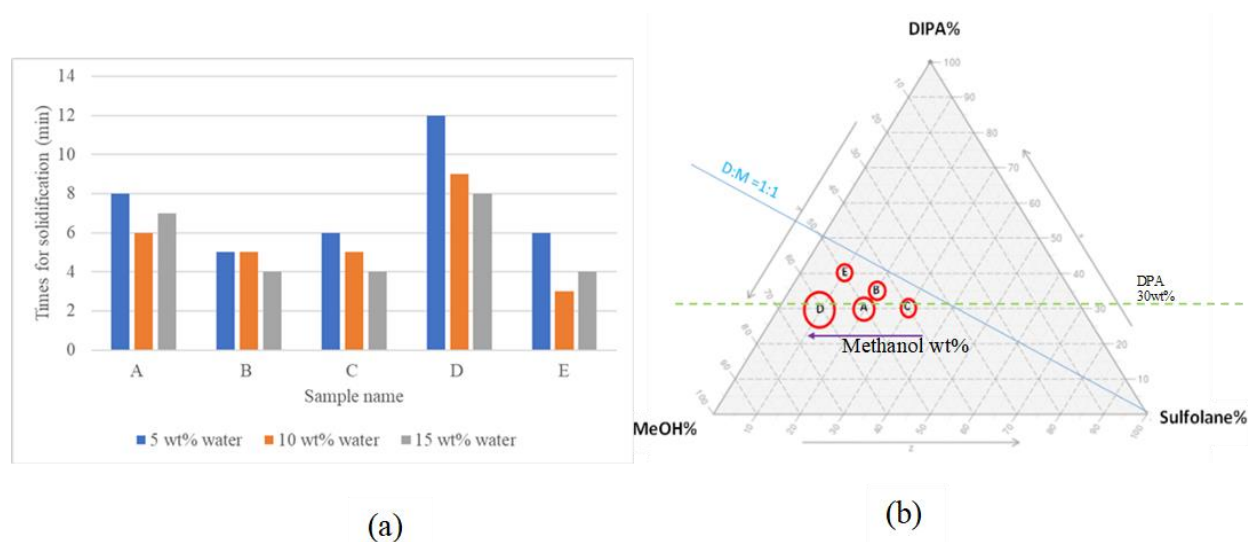


Figure 10: Time intervals to onset of solidification of five solvent blends (A, B, C, D, and E) at 5, 10 and 15 wt% water content. (a) bar chart (b) triangular plot — the size of the red circles indicates the different time intervals to onset of solidification.

As step two of this study, we selected two solvent blends to quantify CO_2 loading before TTOS using the Weight-based CO_2 loading apparatus (Figure 4). Solvent blends E and D (Table 3) containing 15 wt% water each showed a slight reduction in transparency (start of solidification) at CO_2 loading of 0.95 mol CO_2 /mol DPA (2.38 mol CO_2 /kg water-lean solvent) and 0.78 mol CO_2 /mol DPA (2.63 mol CO_2 /kg water-lean solvent), respectively (For information about CO_2 lading values, see Table S3). Blend E contains a larger DPA wt% than blend D, suggesting that CO_2 loading before solidification decreases with an increase in DPA wt%. For instance, for the non-aqueous solvent blend D mixed with 15 wt% water, the CO_2 absorption process can proceed without solidification if CO_2 loading is limited to below 0.90 mol CO_2 / mol DPA.

Therefore, this solvent has an effective window for CO₂ loading which prevents solvent solidification.

3.2.1 Speciation of the CO₂ loaded water lean solvent blend by in situ ATR-FTIR monitoring

CO₂ loading of a non-aqueous solvent composition (Table 3, F) was investigated for 0, 1, 2 and 15% water content by in situ ATR-FTIR spectroscopy. The purpose of this work section was to understand the chemical effect of water on the CO₂ absorption reaction.

Figures S1, S2, S3 and 11 display the obtained ATR-FTIR spectra from monitoring of CO₂ loading into above solvent F containing 0, 1, 2 and 15 wt% water, respectively. The identified IR bands of the obtained spectra are tabulated in Table 8.

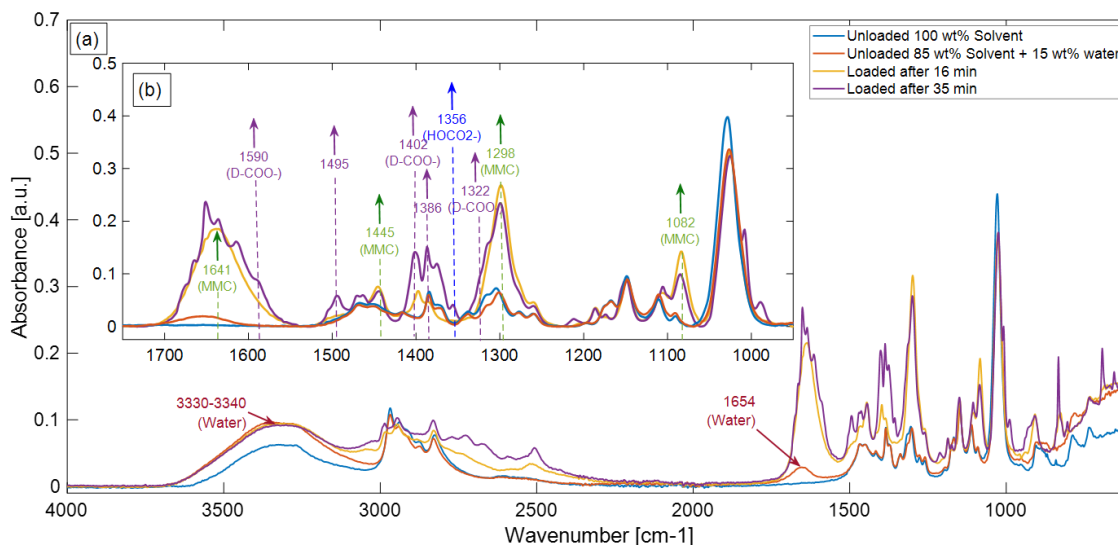


Figure 11: ATR-FTIR spectra of CO₂ absorption into solvent F containing 15 wt% water (a) raw spectra (variable range: 4000-600 cm⁻¹) (b) baseline corrected spectra (variable range: 1750-950 cm⁻¹)

Table 8: IR band assignments for CO₂ loaded solvent F (Table 3) containing 15 wt% water.

Species	IR peak vibrational assignment	Characteristic IR vibrational bands (ν_{\max})(cm^{-1})	
		Solvent with 15% water	Solvent with no water
MMC	C=O stretching ^{8, 18}	1639	1641
	CH ₃ asymmetric deformation ^{8, 18}	1444	1445
	CH ₃ symmetric deformation ^{8, 18}	O.	1398
	O-C-O asymmetric stretching ^{8, 18}	1296	1298
	O-C-O symmetric stretching ^{8, 18}	1082	1082
DPA-COO ⁻ /Zwitterion	COO ⁻ asymmetric stretching ²⁰⁻²³	1590	n.o.
	COO ⁻ symmetric stretching ^{20, 21, 23}	1402	n.o.
	N-COO ⁻ skeletal vibration ^{21, 23}	1322	n.o.
	N ⁺ -H asymmetric stretching ²⁰	1495	n.o.
	C-O stretching ^{23, 24}	1387	n.o.
HCO ₃ ²⁻	C-O stretching ^{21, 24}	1356	n.o.
Physically absorbed CO ₂	C=O asymmetric stretching ²⁸	n.o.	2341
H ₂ O	OH stretching ²⁹	3330-3340	n.o.
	H ₂ O scissor ²⁹	1654	n.o.

n.o.: not observed, O.: overlapping with CO₃²⁻ IR band.

Figure 11 (a) shows the raw spectra of CO₂ loaded solvent F containing 15 wt% water. The blue spectrum represents the non-aqueous unloaded solvent before addition of water; the red spectrum depicts the solvent after addition of water, exhibiting an IR band at 1654 cm⁻¹, which can be assigned to the scissor vibration of H₂O.

Figure 11 (b) shows the baseline corrected spectrum, clearly showing new IR bands emerging during CO₂ loading until maximum CO₂ absorption is reached.

The orange spectrum of Figure 11 (b) depicts the increase in IR bands at 1639, 1445, 1397, 1299 and 1083 cm⁻¹ during the 1st phase of CO₂ absorption which can be attributed to the characteristic IR vibrations of MMC.⁸

The purple spectrum of Figure 11 (b) provides information about new CO₂ species that arise during the 2nd phase of CO₂ lading. Here, bands at 1590 and 1401 cm⁻¹ indicate carbonyl stretching vibrations²⁰⁻²³ while the band at 1322 cm⁻¹ represents the N-COO⁻ skeletal vibration^{21, 23} assigned to DPA-carbamate. Furthermore, the bands at 1495 and 1387 cm⁻¹ could indicate the presence of a zwitterion.^{20, 23, 24} Finally, the IR band at 1356 cm⁻¹ can be attributed to the C-O stretching vibration of the bicarbonate ion.^{21, 24}

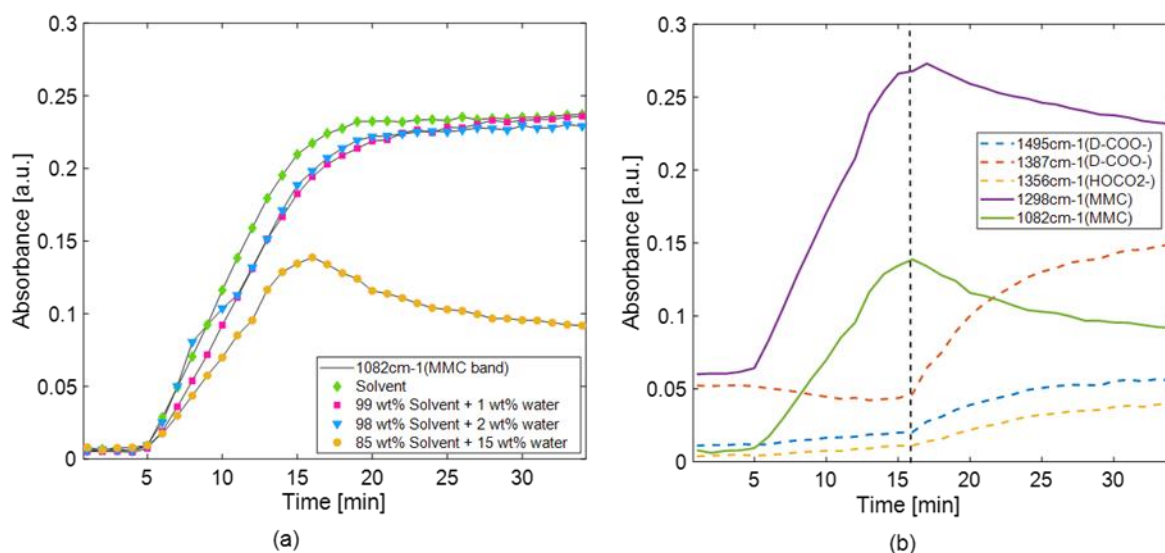


Figure 12: ATR-FTIR bands vs time: analysis of water lean solvent F (a) MMC vibrational band (1082 cm⁻¹) for 0, 1, 2, 15 wt% of water content (b) MMC and other IR bands of CO₂ derived species for 15 wt% water content

Finally, Figure 12 (a) depicts the variation in peak intensity of the IR band at 1081 cm⁻¹ (representing MMC) in solvent samples containing 0, 1, 2, and 15 wt% water. This shows that 15 wt% water significantly influences MMC formation and hence may represent the limit of CO₂ absorption into solvent F. Noticeably, formation of new species such as carbamate and bicarbonate, begin to appear at the same time (after 16 minutes) during CO₂ loading at 15% water

content. Furthermore, Figure 12 (b) also shows the MMC bands (species) decreasing as the new bands (species) evolve.

In conclusion, in spite of 15wt% water content, the solvent initially forms MMC during the first phase of CO₂ loading. However, after some time, carbamate and bicarbonate species appear at the expense of MMC formed during the first phase of CO₂ absorption.

3.3 Molecular effects and reactions for loaded non-aqueous and water-lean solvent.

This section summarizes molecular effects and reaction sequences based on CO₂ related speciation elucidated through ATR-FTIR and NMR spectroscopic analysis of CO₂ loaded solvent blends at non-aqueous and water-lean conditions.

The dashed oval in Figure 7 indicates the region for practical solvent blend operation where the DPA to methanol weight ratio is a critical factor influencing solvent solidification at both non-aqueous and water-lean solvent conditions. In general, a solution is defined to consist of a solvent and a solute whereas the former represents the larger mole fraction than the latter. Furthermore, molecules can be characterized in terms of polarity e.g., a polar or polar and in particular by their specific dielectric constants. The term solvation refers to the surrounding of each dissolved molecule or ion by a shell of solvent molecules. The most important electron pair donors (i.e., hydrogen bond acceptors) are the oxygen atoms in for instance the -OH group in alcohols and the N atoms in e.g., amines.³⁰

For the specific DPA-methanol-sulfolane blend sample D (i.e., 30wt% DPA, 60wt% methanol 10 wt% sulfolane) is part of the optimum blend composition region. We can classify as solvent methanol and sulfolane, the latter since it is not participating in the chemical reaction with CO₂. DPA and CO₂ loaded molecules are defined as solutes. One of the most common examples of

hydrogen bonds are formed in liquid alcohols and/or water³¹ Hence, the above solutes can be assumed to be solvated by methanol through hydrogen bonds. The observed solidification of non-aqueous and water-lean blends of low methanol wt% content therefore likely due to disturbed solvation of polar solutes e.g., carbamic acid, carbamate anion – ammonium cation salts.

The CO₂-amine reaction consists of a nucleophilic addition of the amine to the electrophilic carbon of CO₂. The reaction proceeds through several steps depending on the reaction solvent. Figure 13 shows our proposed reaction step summary for the DPA, methanol and sulfolane solvent blend case updated with results of this Part II contribution.

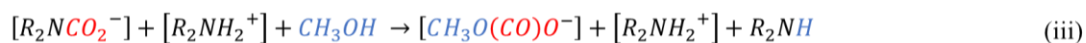


Figure 13: Updated reaction step summary for reaction of CO₂ with the DPA-methanol-sulfolane blend system.

The reaction series of Figure 13 is conducted in homogeneous liquid state; the solvent is methanol and sulfolane. Step (i) proceeds to the reactive carbamic acid³⁰ molecule, through a Zwitterion intermediate.³² Carbamic acid is suggested to be in equilibrium with its analogous Zwitterion⁵ and a portion can be deprotonated by appropriate bases e.g., DPA (step ii). MMC (i.e., [CH₃O(CO)O⁻]+ [R₂NH₂⁺]) may be formed as shown in step (iii) or it may alternatively be produced through an

acid base reaction (methanol addition to CO₂) followed by proton transfer to DPA⁸ (See Figure 13 step (iv)). Figure 14 shows the chemical summary equation of Figure 13.



Figure 14: Chemical summary equation of the DPA, CO₂, methanol and sulfolane reaction.

Figure 14 exhibits the 1:1 relation between DPA and methanol, which is possibly the reason for the distinct DPA-methanol interaction observed in section 3.1. Furthermore, the 1:1 amin CO₂ mole ratio makes MMC a favorable CO₂ capture reagent as compared to primary and secondary amines and last not least also due to the low MMC regeneration temperature.⁸

For non-aqueous solvent blends at low methanol content, we observe carbamic acid formation only which would correspond to Figure 13, step (i). As methanol content is increased, MMC formation increases. The possible mechanistic pathway is unclear, both Figure 13 step (i) to (iii) or step (iv) could be active. However, as CO₂ loading proceeds, DPA carbamate content increases (Figure 12). MMC is the sole CO₂ capture product only at high methanol blend content (see Figure 8 (c)).

Water-lean solvent blends: Section 3.2 and Figure 12 (a) confirm that, at low water concentration, the solvent primarily produces MMC with minimal deviation from the non-aqueous solvent case. Increasing the solvent content to 15 wt% water, the solvent produces MMC during the first phase and during the second phase, as shown in Figure 11 and Table 8, DPAH⁺-carbamate together with bicarbonate as known from aqueous amine CO₂ capture chemistry. Figure 12 (b) shows the initial formation of MMC, passing through a maximum while the DPAH⁺-carbamate and bicarbonate species appear in the solution at this point in time. Hence, we perceive this to be the limit for water lean operation.

Sulfolane is a dipolar aprotic solvent in which water is fully miscible; amines are moderate Brønsted bases that deprotonate water to a small extent to form amine hydroxide.³³ Such mixture can cleave esters (e.g. MMC).³⁴ Hence, we propose an initial hydrolysis of MMC to bicarbonate/carbonate. Bicarbonate is in equilibrium with amine carbamate³⁵ which could produce DPAH⁺ carbamate as observed by ATR-FTIR spectroscopy (Figure 11 and 12 (b)).

4. Conclusions

1. In Part I of this work⁸ we report a non-aqueous low viscosity CO₂ capture solvent blend regenerable at low temperature. In this Part II we now disclose blend composition optimization and the effect of flue gas humidity on CO₂ up-take including respective solvent speciation.
2. The non-aqueous diisopropylamine (DPA)-methanol-sulfolane blend solidifies during CO₂ loading in respect to DPA-methanol weight ratio. At high DPA wt% DPAH⁺ carbamate is formed which solidifies the blend. At high methanol wt% DPAH⁺ monomethyl carbonate (MMC) is formed; the blend stays in the homogeneous liquid state. Through use of experimental design methodology, a blend composition region (see Figure 7) for practical gas-liquid CO₂ capture is identified.
3. High solvent CO₂ capacity (MMC 1:1 vs carbamate 1:2 mol CO₂/mol amine loading) is achieved through avoidance of DPAH⁺ carbamate formation during blend CO₂ loading.
4. The respective water-lean solvent blend forms DPAH⁺ bicarbonate simultaneous with DPAH⁺ MMC. 15 wt% water content is the practical solvent limit (0.9 mol CO₂/mol DPA)

for the solvent blend; decomposition of DPAH⁺ MMC to DPAH+ bicarbonate/carbonate and carbamate is now significant.

ASSOCIATED CONTENT

Supporting Information

AUTHOR INFORMATION

Corresponding Author

Klaus-J. Jens

Department of Process, Energy and Environmental Technology,

University of South – Eastern Norway, Kjølnes ring 56, 3918 Porsgrunn, Norway

E-mail: Klaus.J.Jens@usn.no Tel: +4735575193

Authors

Jayangi D. Wagaarachchige - Department of Electrical, IT and Cybernetics, University of South – Eastern Norway, Kjølnes ring 56, 3918 Porsgrunn, Norway

Zulkifli Idris - Department of Process, Energy and Environmental Technology, University of South – Eastern Norway, Kjølnes ring 56, 3918 Porsgrunn, Norway

Bjørnar Arstad - SINTEF Materials and Chemistry, Forskningveien 1, 0314 Oslo, Norway

Kjell-Arne Solli- Department of Process, Energy and Environmental Technology, University of South – Eastern Norway, Kjølnes ring 56, 3918 Porsgrunn, Norway

Maths Halstensen- Department of Electrical, IT and Cybernetics, University of South – Eastern Norway, Kjølnes ring 56, 3918 Porsgrunn, Norway

Present Addresses

Author Contributions

The manuscript was written through contributions of all authors. All authors have given approval to the final version of the manuscript.

Funding Sources

This work was funded by the Ministry of Education and Research of the Norwegian Government.

Notes

The authors declare no competing financial interest.

ACKNOWLEDGMENT

ABBREVIATIONS

MMC	monomethyl carbonate anion
CO ₂	Carbon dioxide
PCC	post-combustion carbon capture
ATR	Attenuated total reflectance
FTIR	Fourier transform infrared
NMR	Nuclear magnetic resonance
MDEA	methyl diethanolamine

TEA	Triethanolamine
DPA	Diisopropylamine
SULF	Sulfolane
MeOH	Methanol
H ₂ O	Water
IR	Infrared
DoE	Design of Experiments
CP	center-point
FIDs	free induction decays
Y	Response variable
H	intensity of the MMC vibrational band at 1640 cm ⁻¹
X	D-optimal design matrix
DPA-COO ⁻	DPA carbamate anion
DPAH ⁺ COO ⁻	DPA Zwitterion
DPACOOH	DPA carbamic acid
n.o.	not observed
O.	overlapping with other- IR band(s)
TTOS	time to onset of solidification
T _{ab}	Absorption temperature
DPAH ⁺	Protonated DPA

REFERENCES

1. Wanderley, R. R.; Pinto, D. D. D.; Knuutila, H. K., Investigating opportunities for water-lean solvents in CO₂ capture: VLE and heat of absorption in water-lean solvents containing MEA. *Sep. Purif. Technol.* **2020**, 231, 115883.
2. James, I. I. I. R. E.; Keairns, D.; Turner, M.; Woods, M.; Kuehn, N.; Zoelle, A. *Cost and Performance Baseline for Fossil Energy Plants Volume 1: Bituminous Coal and Natural Gas to Electricity*; United States, 2019-09-24, 2019.
3. Heldebrant, D. J.; Koech, P. K.; Glezakou, V.-A.; Rousseau, R.; Malhotra, D.; Cantu, D. C., Water-Lean Solvents for Post-Combustion CO₂ Capture: Fundamentals, Uncertainties, Opportunities, and Outlook. *Chem. Rev.* **2017**, 117, (14), 9594-9624.
4. Kortunov, P. V.; Baugh, L. S.; Siskin, M.; Calabro, D. C., In Situ Nuclear Magnetic Resonance Mechanistic Studies of Carbon Dioxide Reactions with Liquid Amines in Mixed Base Systems: The Interplay of Lewis and Brønsted Basicities. *Energy & Fuels* **2015**, 29, (9), 5967-5989.
5. Kortunov, P. V.; Siskin, M.; Baugh, L. S.; Calabro, D. C., In Situ Nuclear Magnetic Resonance Mechanistic Studies of Carbon Dioxide Reactions with Liquid Amines in Non-aqueous Systems: Evidence for the Formation of Carbamic Acids and Zwitterionic Species. *Energy & Fuels* **2015**, 29, (9), 5940-5966.
6. Kortunov, P. V.; Siskin, M.; Paccagnini, M.; Thomann, H., CO₂ Reaction Mechanisms with Hindered Alkanolamines: Control and Promotion of Reaction Pathways. *Energy & Fuels* **2016**, 30, (2), 1223-1236.
7. Barzagli, F.; Giorgi, C.; Mani, F.; Peruzzini, M., Reversible carbon dioxide capture by aqueous and non-aqueous amine-based absorbents: A comparative analysis carried out by ¹³C NMR spectroscopy. *Appl. Energy* **2018**, 220, 208-219.

8. Wagaarachchige, J. D.; Idris, Z.; Arstad, B.; Kummamuru, N. B.; Sætre, K. A. S.; Halstensen, M.; Jens, K.-J., Low-Viscosity Nonaqueous Sulfolane–Amine–Methanol Solvent Blend for Reversible CO₂ Capture. *Ind. Eng. Chem. Res.* **2022**, 61, (17), 5942-5951.
9. Barbarossa, V.; Barzagli, F.; Mani, F.; Lai, S.; Stoppioni, P.; Vanga, G., Efficient CO₂ capture by non-aqueous 2-amino-2-methyl-1-propanol (AMP) and low temperature solvent regeneration. *RSC Adv.* **2013**, 3, (30), 12349-12355.
10. Dezhong Yang, M. L., Jie Chena Efficient non-aqueous solvent formed by 2-piperidineethanol and ethylene glycol for CO₂ absorption. *Chem. Commun.* **2019**, 55, (83), 12483-12486.
11. Eimer, D. Simultaneous removal of water and hydrogen sulphide from natural gas. Norway, 1994.
12. Barzagli, F.; Giorgi, C.; Mani, F.; Peruzzini, M., Comparative Study of CO₂ Capture by Aqueous and Nonaqueous 2-Amino-2-methyl-1-propanol Based Absorbents Carried Out by ¹³C NMR and Enthalpy Analysis. *Ind. Eng. Chem. Res.* **2019**, 58, (11), 4364-4373.
13. Chowdhury, F. A.; Goto, K.; Yamada, H.; Matsuzaki, Y., A screening study of alcohol solvents for alkanolamine-based CO₂ capture. *Int. J. Greenhouse Gas Control* **2020**, 99, 103081.
14. Chen, S.; Chen, S.; Zhang, Y.; Chai, H.; Qin, L.; Gong, Y., An investigation of the role of N-methyl-diethanolamine in non-aqueous solution for CO₂ capture process using ¹³C NMR spectroscopy. *Int. J. Greenhouse Gas Control* **2015**, 39, 166-173.
15. Behrens, R.; Kessler, E.; Münnemann, K.; Hasse, H.; von Harbou, E., Monoalkylcarbonate formation in the system monoethanolamine–water–carbon dioxide. *Fluid Phase Equilib.* **2019**, 486, 98-105.

16. Cieslarova, Z.; dos Santos, V. B.; do Lago, C. L., Both carbamates and monoalkyl carbonates are involved in carbon dioxide capture by alkanolamines. *Int. J. Greenhouse Gas Control* **2018**, *76*, 142-149.
17. Eriksson, L.; Johansson, E.; Kettaneh-Wold, N.; Wikström, C.; Wold, S., *Design of experiments : principles and applications*. 3 ed.; Umetrics, Umeå: Umetrics Academy, 2008.
18. Behrendt, W.; Gattow, G.; Dräger, M., Über Chalkogenolate. LXI. Untersuchungen über Halbestere der Kohlensäure. 1. Darstellung und Eigenschaften von Monomethyl- und Monoäthylcarbonaten. *Zeitschrift für anorganische und allgemeine Chemie* **1973**, *397*, 237-246.
19. Eilers, P. H. C., A Perfect Smoother. *Anal. Chem.* **2003**, *75*, (14), 3631-3636.
20. Tu, Z.; Han, F.; Liu, C.; Wang, Y.; Wei, J.; Zhou, X., 2-Amino-2-methyl-1-propanol regulated triethylenetetramine-based nonaqueous absorbents for solid-liquid phase-change CO₂ capture: Formation of crystalline powder products and mechanism analysis. *Sep. Purif. Technol.* **2023**, *307*, 122722.
21. Yu, J.; Chuang, S. S. C., The Structure of Adsorbed Species on Immobilized Amines in CO₂ Capture: An in Situ IR Study. *Energy & Fuels* **2016**, *30*, (9), 7579-7587.
22. Kachko, A.; van der Ham, L. V.; Bardow, A.; Vlugt, T. J. H.; Goetheer, E. L. V., Comparison of Raman, NIR, and ATR FTIR spectroscopy as analytical tools for in-line monitoring of CO₂ concentration in an amine gas treating process. *Int. J. Greenhouse Gas Control* **2016**, *47*, 17-24.
23. Kachko, A.; van der Ham, L. V.; Bakker, D. E.; van de Runstraat, A.; Nienoord, M.; Vlugt, T. J. H.; Goetheer, E. L. V., In-Line Monitoring of the CO₂, MDEA, and PZ Concentrations in the Liquid Phase during High Pressure CO₂ Absorption. *Ind. Eng. Chem. Res.* **2016**, *55*, (13), 3804-3812.

24. Richner, G.; Puxty, G., Assessing the Chemical Speciation during CO₂ Absorption by Aqueous Amines Using in Situ FTIR. *Ind. Eng. Chem. Res.* **2012**, 51, (44), 14317-14324.

25. Shen, S.; Shi, X.; Li, C.; Guo, H.; Long, Q.; Wang, S.; Yin, X., Nonaqueous (amine + glycol ether) solvents for energy-efficient CO₂ capture: New insights into phase change behaviors and assessment of capture performance. *Sep. Purif. Technol.* **2022**, 300, 121908.

26. Jackson, P.; Robinson, K.; Puxty, G.; Attalla, M., In situ Fourier Transform-Infrared (FT-IR) analysis of carbon dioxide absorption and desorption in amine solutions. *Energy Procedia* **2009**, 1, (1), 985-994.

27. Barzagli, F.; Mani, F.; Peruzzini, M., Efficient CO₂ absorption and low temperature desorption with non-aqueous solvents based on 2-amino-2-methyl-1-propanol (AMP). *Int. J. Greenhouse Gas Control* **2013**, 16, 217-223.

28. Liu, A.-H.; Li, J.-J.; Ren, B.-H.; Lu, X.-B., Development of High-Capacity and Water-Lean CO₂ Absorbents by a Concise Molecular Design Strategy through Viscosity Control. *ChemSusChem* **2019**, 12, (23), 5164-5171.

29. Schmidt, D. A.; Miki, K., Structural Correlations in Liquid Water: A New Interpretation of IR Spectroscopy. *The Journal of Physical Chemistry A* **2007**, 111, (40), 10119-10122.

30. Hampe, E. M.; Rudkevich, D. M., Exploring reversible reactions between CO₂ and amines. *Tetrahedron* **2003**, 59, (48), 9619-9625.

31. Anslyn, E. V.; Dougherty, D. A., *Modern Physical Organic Chemistry*. illustrated edition ed.; 2005.

32. Caplow, M., Kinetics of carbamate formation and breakdown. *Journal of the American Chemical Society* **1968**, 90, (24), 6795-6803.

33. Tilstam, U., Sulfolane: A Versatile Dipolar Aprotic Solvent. *Organic Process Research & Development* **2012**, 16, (7), 1273-1278.

34. Vollhardt, K. P. C.; Schore, N. E., *Organic Chemistry: Structure and Function*. 8 ed.; W. H. Freeman.

35. Sartori, G.; Savage, D. W., Sterically hindered amines for carbon dioxide removal from gases. *Industrial & Engineering Chemistry Fundamentals* **1983**, 22, (2), 239-249.

Article 5

The Influence of Nitrogen Dioxide Absorption on Sulfite Oxidation Rate in the Presence of Oxygen: On-Line Raman Measurements.

Jakob Johansson^{1*}, Jayangi D Wagaarachchige², Fredrik Normann¹, Zulkifli Idris², Eirik R
Haugen², Maths Halstensen², Wathsala Jinadasa², Klaus J Jens² and Klas Andersson¹

¹Department of Space, Earth and Environment, Chalmers University of Technology,
Gothenburg, Sweden

²Faculty of Technology, Natural Sciences and Maritime Sciences, University of South-Eastern
Norway, Kjolnes Ring 56, Porsgrunn,

Published in Industrial & Engineering Chemistry Research Journal, ACS Publications

<https://doi.org/10.1021/acs.iecr.3c01015>

Influence of Nitrogen Dioxide Absorption on the Sulfite Oxidation Rate in the Presence of Oxygen: Online Raman Measurements

Jakob Johansson,* Jayangi D. Wagaarachchige, Fredrik Normann, Zulkifli Idris, Eirik R. Haugen, Maths Halstensen, Wathsala Jinadasa, Klaus J. Jens, and Klas Andersson



Cite This: *Ind. Eng. Chem. Res.* 2023, 62, 21048–21056



Read Online

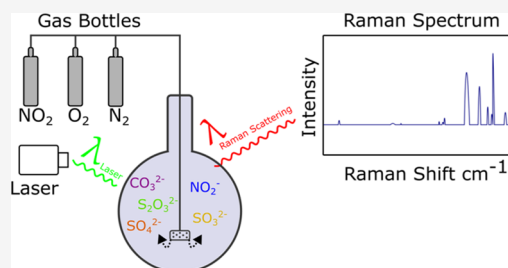
ACCESS |

Metrics & More

Article Recommendations

Supporting Information

ABSTRACT: The oxidation of sulfite(aq) is investigated by passing O₂, N₂, and NO₂ over a sulfite solution in a bubbling flask. The influence on sulfite oxidation of NO₂ absorption and the presence of thiosulfate (an oxidation inhibitor) is investigated. The experiment is focused on conditions relevant to a combined SO₂ and NO₂ industrial flue gas cleaning system. Liquid composition is measured in situ using Raman spectroscopy equipped with immersion probes. Regression models are developed to quantify SO₃²⁻, HSO₃⁻, S₂O₃²⁻, SO₄²⁻, NO₂⁻, NO₃⁻, and CO₃²⁻ also in mixtures of the mentioned chemicals. The results show that Raman spectroscopy is a possible method for liquid analysis of a NO_x/SO_x removal system. Speciation is successful within the limits of the experiment for most molecules. SO₄²⁻, CO₃²⁻, and S₂O₃²⁻ are quantified with high certainty; SO₃²⁻ and HSO₃⁻ are quantified with some uncertainty and should be above 10 mM for quantitative measurements. NO₃⁻ concentration is below the limit of detection in the continuous experiments. The measured reaction rates of sulfite (SO₃²⁻) and bisulfite (HSO₃⁻) oxidation with O₂ are in agreement with the reviewed literature. Absorption of NO₂(g) and the consequent formation of nitrite enhance sulfite oxidation. The addition of thiosulfate to the liquid reduces the rate of SO₃²⁻ oxidation by ~90% while maintaining NO₂ absorption. The influence of NO₂(g) and thiosulfate supports a previously proposed mechanism for sulfite oxidation via a radical chain mechanism.



1. INTRODUCTION

The simultaneous absorption of sulfur dioxide (SO₂) and nitrogen oxides (NO_x) has been identified as an emerging technology with a large potential in industries where conventional flue gas cleaning is impractical, for different reasons. Common to the approaches of combined removal is that the nitric oxide (NO) is oxidized to NO₂ to increase the solubility. After the oxidation of NO to NO₂, NO₂ can be absorbed, together with SO₂, in a wet scrubber, similar to conventional wet flue gas desulfurization (WFGD). S(IV) ions (SO₃²⁻ and HSO₃⁻) are crucial for the absorption of NO₂ to take place at a high rate.¹ S(IV) may be added as a salt or may be formed from absorbed SO₂(g). In the absorption of NO₂, the S(IV) is oxidized to S(VI), and the NO₂ is absorbed and hydrolyzed to NO₂⁻.² The oxidation of S(IV) can increase the absorption rate of SO₂ which has the benefit of removing SO₂ and NO_x in the same unit. However, sulfite has proven to oxidize at a much higher rate than can be explained by NO₂ absorption.¹ The addition of S(IV) salts to the liquid is conducted to maintain desirable NO₂ absorption levels. The S(IV) salt addition is associated with a cost, and the apparent kinetics of the sulfite oxidation is therefore of great interest to many researchers to better understand how the process can be controlled.

In Figure 1 a simplified schematic of the reaction paths possible when both SO₂(g) and NO_x(g) are present and in contact with an aqueous phase is shown. SO₂ absorption in

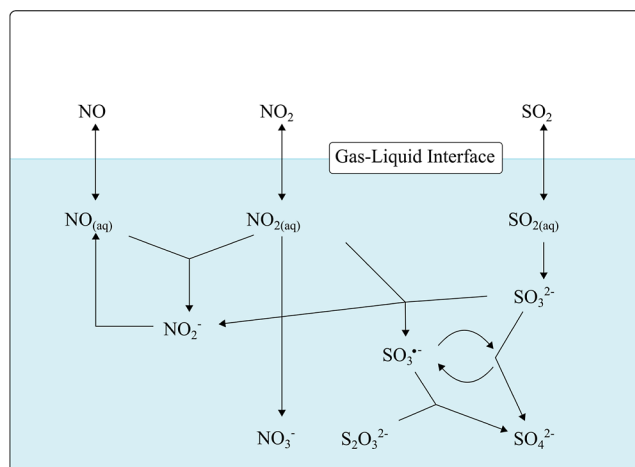


Figure 1. Schematic overview of the reaction paths used to describe the simultaneous absorption of NO_x and SO_x in an alkaline/neutral solution.

Received: March 29, 2023

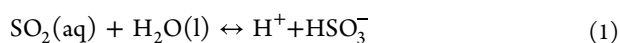
Revised: November 12, 2023

Accepted: November 15, 2023

Published: November 28, 2023



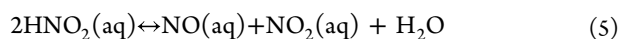
water is equilibrium-controlled and leads to the formation of bisulfite and sulfite according to reactions 1 and 2, respectively^{3–6}



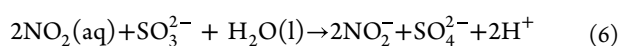
Absorption of NO_2 in water takes place according to either reactions 3 or 4, depending on the presence of NO and the pH level.^{7–9}



Nitrite, $\text{N}(\text{III})$, is inherently unstable, especially under acidic conditions, and it can decompose into NO and NO_2



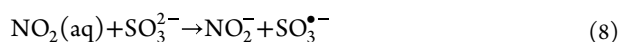
Several studies have shown that $\text{S}(\text{IV})$ is efficient at hydrolyzing $\text{NO}_2(\text{aq})$ at a high rate according to reaction 6.^{10–14}



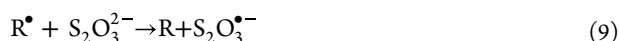
The SO_3^{2-} may also be oxidized by O_2 following reaction 7.



In experiments, it was found, as previously mentioned, that the oxidation of $\text{S}(\text{IV})$ progresses at a much higher rate than what is explained by reactions 6 and 7 alone. Nash² proposed that a radical-initiated chain of reactions was initiated by reaction 6 and rather progressed through reaction 8 where a sulfite radical was formed. This set of reactions enables depletion of SO_3^{2-} with only a single $\text{SO}_3^{\bullet-}$ radical formed if O_2 is present.



To break this chain of reactions a radical scavenger can be added to the liquid, which enables an alternative terminating step. One example of such a scavenger is $\text{S}_2\text{O}_3^{2-}$. Shen and Rochelle¹⁵ proposed that the formed radical species would react with $\text{S}_2\text{O}_3^{2-}$ and result in the production of $\text{S}_4\text{O}_6^{2-}$ through reactions 9 and 10. For a more detailed description of the proposed reaction chain and termination, see Littlejohn et al.¹¹



The motivation for research on sulfite oxidation has with time shifted from atmospheric chemistry motivated by the high emissions of SO_2 to WFGD systems employed to control SO_2 emissions and to combined removal systems of NO_x and SO_x . These systems have complex reaction patterns, and the previously applied analysis methods require ex situ measurements, titration, and ion chromatography, which have delivered results that vary by several orders of magnitude. Beilke, Lamb, and Müller¹⁶ studied the uncatalyzed SO_2 oxidation in a closed environment to investigate rate-determining steps in the formation of atmospheric sulfate. Results indicate a first-order reaction in regard to sulfite concentration and a zero-order reaction in regard to oxygen for a pH between 3 and 6. Only SO_2 and SO_4^{2-} were measured, and $\text{S}(\text{IV})$ oxidation was assumed to be the rate-limiting step. SO_3^{2-} was assumed to be the reacting species of $\text{S}(\text{IV})$, which was supported by a $[\text{H}^+]^{-2}$ trend. They

observed no significant dependence on temperature in the interval between 5 and 25 °C. Larson, Horike, and Harrison¹⁷ concur that the uncatalyzed oxidation of SO_2 by O_2 was first order in SO_3^{2-} but expressed the reaction in terms of additional H^+ dependencies of half order in the pH interval between 4 and 12. Unlike the previous study, they did observe a slight temperature dependence in the interval 5–25 °C. Connick et al.¹⁸ continued the study with a focus on the oxidation of bisulfite (pH 4) relevant to flue gas desulfurization (FGD) and atmospheric chemistry, where oxygen concentration and added NaOH was used to determine the reaction path and rate. They suggest that the reaction takes place via HSO_5^- formed from SO_3^{2-} . An expression was formulated for O_2 consumption as second order in HSO_3^- and H^+ and zero order in O_2 . Mo et al.¹⁹ investigated the sulfite oxidation rate by oxygen and the inhibiting effect on the oxidation by thiosulfate in a thermostatic reactor with continuous airflow. Continuous pH measurements and titration of the resulting liquid were used as a basis for analysis. They noted a decrease in oxidation rate from pH 6 to pH 3 and almost no effect of pH in the interval 7 to 8. The conclusion was the same as that in the previously mentioned studies where the low activity of HSO_3^- would decrease oxidation rate, and at a certain concentration of SO_3^{2-} the reaction was no longer limited by SO_3^{2-} concentration. The effect of $\text{S}_2\text{O}_3^{2-}$ as an inhibitor for the uncatalyzed oxidation of $\text{S}(\text{IV})$ was observed.

The research on $\text{S}(\text{IV})$ oxidation in the presence of NO_2 has been performed in parallel to oxidation by O_2 first due to the presence of NO_2 in the atmosphere and later coupled to flue gas treatment. NO_2 has, as mentioned, a large effect on $\text{S}(\text{IV})$ oxidation in the presence of O_2 , and the reaction is difficult to study as different approaches have been used and different rates have been proposed. Littlejohn, Wang, and Chang¹¹ and Rochelle & co-workers^{12,15} have performed several studies on sulfite and sulfide oxidation where the influence of NO_2 absorption was investigated. Gas analysis of NO_x was used for the determination of reaction rate, and the solution was analyzed with ion chromatography.

In this study, a similar setup to that used by Huang et al.²⁰ is used to provide additional information on the reaction of sulfite oxidation. In contrast to earlier studies, an online analysis method in Raman spectroscopy is used. The important advantage of this analysis method is that all reaction products will be possible to identify continuously, which is important in a complex system where both nitrogen and sulfur are present and reaction products include a great variety of species.²¹ The advantages of Raman spectroscopy also include that it is a quick, accurate, and nondestructive method that is seeing increased usage and rapid scientific development.^{22,23} This study aims to assess the suitability of Raman spectroscopy for liquid-phase analysis in a combined SO_x – NO_x removal system and thereafter investigate the rate of sulfite oxidation while bubbling O_2 through a bubble flask and to compare that rate when NO_2 is present in the gas phase and thiosulfate is present in the liquid phase. The hypothesis is that NO_2 will increase the oxidation rate of sulfite and that thiosulfate will lower the oxidation rate of sulfite, as has been seen in our research and in a study by Schmid et al.²⁴ The setup is not suitable to provide exact reaction rates, and the rates derived are used for comparison with the vast body of literature present.

Table 1. Summary of Continuous Experiments^a

Investigation	SO ₃ ²⁻ (mol/kg _{H₂O})	HSO ₃ ⁻ (mol/kg _{H₂O})	SO ₄ ²⁻ (mol/kg _{H₂O})	S ₂ O ₃ ²⁻ (mol/kg _{H₂O})	NO ₂ ⁻ (mol/kg _{H₂O})	CO ₃ ²⁻ (mol/kg _{H₂O})	NO ₂ (ppm)	O ₂ (%)
1	0.02	0.02						3
2				0.04				3
3	0.02	0.02		0.04				3
4	0.02	0.02					95	3
5				0.04			95	3
6	0.02	0.02		0.04			95	3
7	0.02	0.02	0.10	0.04	0.02	0.01	95	3

^aConcentrations correspond to the amount of salt added before equilibrium is reached.

2. MATERIALS AND METHODS

2.1. PLSR Model Preparation for Raman Spectrometer.

Chemicals used in this work were sodium salts of sulfite ($\geq 98\%$), bisulfite (99%), sulfate ($\geq 99\%$), thiosulfate ($\geq 99\%$), nitrite ($\geq 99\%$), nitrate ($\geq 99\%$), bicarbonate ($\geq 99\%$), and carbonate ($\geq 99\%$), all supplied by Sigma-Aldrich. In order to prepare the partial least-squares regression (PLS-R) models, known amount of these chemicals was mixed with known amount of Milli-Q water (resistivity 18.2 M Ω -cm). The methodology used in this study is a multivariate spectroscopic data evaluation approach in which Raman spectra of the seven species as mentioned earlier were carefully calibrated and validated. The procedure is explained below.

2.1.1. Sample Preparation for PLS-R Model Calibration and Validation. For each species studied in this work, a stock solution with a known amount of chemical components in Milli-Q water was prepared. A continuous set of samples with varying species concentrations was then made by diluting the stock with different weights of Milli-Q water in 10 mL sample vials. Typically, 40 samples are prepared for each species: one set of solutions was prepared for PLS-R model calibration, and a second independent set was used for validation. The upper concentration for species studied in this work was determined to include the relevant species concentrations for a combined SO₂ and NO₂ industrial flue gas cleaning system based on experiments and simulations.^{25,26} The samples were then analyzed using a Raman spectrometer as soon as they were prepared.

2.1.2. Raman Measurement. In this study, a RXN2 Raman spectrometer fitted with a Kaiser Raman short-focus immersion probe was used. Specifications of the spectrometer and the immersion probe are summarized in Table S1, Supporting Information. The instrument can be operated with a maximum laser power of 400 mW. In this study, the laser power was kept at its highest value of 400 mW to minimize exposure time because low laser power was shown to be insensitive to sulfite peaks. The signal-to-noise (S/N) ratio of the Raman measurements was optimized by changing the exposure time and number of scans. In this work, the optimized S/N ratio was obtained when the exposure time was 90 s with three scans.

Before starting a Raman measurement, the short-focus immersion optic was attached to the fiber optic probe head, and the probe area which would be in contact with the sample was cleaned with ethanol. The immersion probe was then positioned vertically using a stand, with the optical window facing downward. During measurement, it was ensured that the probe was immersed in the sample and the tip of the optic was positioned in the center of the glass vial. The sample and probe optic were protected from external light sources (such as fluorescent light) using aluminum foil. The Raman spectrum

was collected using a software called iC Raman (Kaiser Instruments). Before collecting the next spectrum, the Raman probe was cleaned with Milli-Q water and ethanol and wiped to avoid cross-contamination between samples.

2.1.3. Preprocessing of Raman Spectra and PLS-R Modeling. The Raman spectra obtained were exported to Matlab2018a (MathWorks Inc.) and PLS Toolbox 8.6.2 (eigenvector Research Inc.) software for data processing. Measurements were performed in diluted solutions, and in most cases, concentrations of species were very low, making result interpretation a challenge without a suitable preprocessing technique. In this work, the preprocessing method using Whittaker filter ($\lambda = 1$, $\rho = 0.001$) gives satisfactory baseline correction. These preprocessed spectra are then subjected to PLS-R. In all cases, normalization against an instrument peak was also applied. For raw and preprocessed spectra, see Figure S1, Supporting Information.

2.2. Sulfite Oxidation Experiments. Gases with known concentrations of NO₂ and/or O₂ in N₂ are led through a bubbling flask with a prepared batch solution of different salts. Each sample was prepared by weighing each salt and mixing it in a known amount of degassed Milli-Q water in an Erlenmeyer bottle. The sample was then sealed and stirred with a magnetic stirrer before it was weighed again to ensure correct preparation. The gases, 1% NO₂ in N₂, N₂, and O₂, were supplied by Linde gas. The Bronkhorst MFCs were calibrated for 0–0.1 NL/min (O₂), 0–0.019 NL/min (NO₂/N₂), and 0–5 NL/min (N₂). The gases were either led directly to the gas analyzer or through the bubble flask. Before each experiment, the setup was flushed with N₂ to evacuate O₂. The only O₂ present in the system before experiment initiation was that present in the bubble flask. The bubble flask was equipped with an aeration head, the Raman probe, and a pH electrode. Temperature and chemical composition were measured continuously. The pH electrode was connected to a Metrohm 905 Titrando, which was programmed to maintain pH at 7 for the samples by the addition of 0.1 M NaOH. The initial sample pH target of 7 is reached by the addition of an equimolar distribution of Na₂SO₃/NaHSO₃. The pH control during experiments was, however, unsuccessful during several experiments, with a resulting pH > 9 as too much NaOH was added. The gas analyzer (Testo 350, from Nordtec) measured the concentration of SO₂, O₂, NO, and NO₂ by electrochemical sensors on the basis of selectivity potentiometry. The amount of absorbed NO₂ was estimated by subtracting the measured exit concentration of NO₂ from the amount injected, which was quantified by a continuous log of supplied mV to the MFC. For a figure of the experimental setup, see Figure S2, Supporting Information.

The experimental matrix is specified in Table 1. The experiments were divided into seven sets, denoted “Inves-

Table 2. Characteristic Vibrational Modes for all Chemical Species Observed and Published in Literature^a

species	observed (cm ⁻¹)	published (cm ⁻¹)	refs
SO _{4(aq)} ²⁻	449, 613, 981*	449, 613, 981, 1111, 1125	28,29
SO _{3(aq)} ²⁻	474, 619, 965*	469, 620, 896, 933, 967	30
HSO _{3(aq)} ⁻	1022*, 1052*	235, 655, 730, 1052, 1023, 1052, 2350	31
NO _{3(aq)} ⁻	1048*, 1354	676, 713, 717, 719, 743, 770, 823, 830, 1045, 1048, 1050, 1052, 1075, 1342, 1358, 1384, 1413, 1450	32,33
NO _{2(aq)} ⁻	816*, 1329*	1323, 2640	34
CO _{3(aq)} ²⁻	1067*	680, 1065, 1380, 1436	35
S ₂ O _{3(aq)} ²⁻	336, 448*, 535, 668, 997*	336, 448, 535, 668, 997, 1122	36

^aThe observed peaks which were used for analysis are marked with an asterisk.

Table 3. Rate of Formation of Selected Species and NO₂ Absorption Rate from Gas to Liquid During the Continuous Experiments

Investigation	$\frac{d[S(IV)]}{dt}$ $\left(\frac{\text{mmol}}{\text{kg}_{\text{H}_2\text{O}} \cdot \text{min}}\right)$	$\frac{d[\text{SO}_4^{2-}]}{dt}$ $\left(\frac{\text{mmol}}{\text{kg}_{\text{H}_2\text{O}} \cdot \text{min}}\right)$	$\frac{d[\text{S}_2\text{O}_3^{2-}]}{dt}$ $\left(\frac{\text{mmol}}{\text{kg}_{\text{H}_2\text{O}} \cdot \text{min}}\right)$	NO ₂ absorption rate $\left(\frac{\text{mmol}}{\text{kg}_{\text{H}_2\text{O}} \cdot \text{min}}\right)$	[S(IV)] _{ox} /[NO ₂] _{abs} (mmol/mmol)
1	-0.07	0.06			
2	0.01	-0.00	0.02		
3	-0.00	0.00	0.00		
4	-0.84	0.54		0.028	-30.6
5	0.00	0.00	-0.00	0.020	0
6	-0.06	0.12	-0.04	0.030	-2.35
7	0.01	0.06	-0.04	0.032	0.88

tigations". Each investigation had a specific aim. Investigation 1 aimed to study the rate of sulfite oxidation from O₂ gas at a partial pressure of 3 kPa, 3%. Investigation 2 replicated Investigation 1 but with Na₂S₂O₃ instead of Na₂SO₃ to investigate the oxidation rate of thiosulfate by O₂. Investigation 3 aimed to establish the effect of thiosulfate on sulfite oxidation by O₂. Investigations 4 to 6 corresponded to Investigations 1 to 3 but with NO₂ present in the gas phase to establish the influence of NO₂ on the reaction chemistry. Investigation 7 had a liquid composition similar to what was expected for a combined NO_x and SO_x absorption system. The aim of Investigation 7 was to evaluate the suitability of the measurement technique used for process control in a combined NO_x and SO_x absorption system.

3. RESULTS AND DISCUSSION

3.1. Spectra Preprocessing and Peaks Assignment. For spectrum preprocessing, the Whittaker algorithm²⁷ was employed to reduce baseline noise and thereby provide an improved spectrum for further analytical purposes. Table 2 shows a list of Raman vibrational bands that were observed in this study in comparison to available data from the literature. Measurements in this work were performed on diluted and low-concentration species, and some signals were not significant. For example, the antisymmetric stretching SO₄²⁻ signal at 1111 cm⁻¹ observed by Irish, D., and Chen, H., was not visible in this work. Instead, the PLS-R model for sulfate is based on the peak at 981 cm⁻¹, which was distinct and, after preprocessing, clearly separated from other peaks. Of the seven chemical species studied in this work, at least one Raman peak could be used for PLS-R modeling, and the peak with the lowest associated error was used for analysis. The peaks used are marked with an asterisk in Table 2.

It is known that sulfite, bisulfite, and to some extent thiosulfate are oxidized to sulfate in the presence of air or O₂. During measurements, small increment to the sulfate peak at 981 cm⁻¹ could be seen as the concentration of sulfite increased. This oxidation, albeit small, will affect the accuracy of the PLS-R models. Therefore, in this work, initial concentrations of sulfite,

bisulfite, and thiosulfate were corrected to compensate the possible oxidation.

Based on the preprocessed Raman spectra, PLS-R models for sulfate, sulfite, bisulfite, thiosulfate, nitrite, nitrate, and carbonate were constructed. The final and optimized PLS-R models for the species studied in this work show low error of prediction (RMSEP) values, suggesting good reliability of these models: the highest RMSEP value is 0.00627 for CO₃²⁻, while the lowest RMSEP value is 0.00092 for SO₄²⁻. For a complete summary of the individual calibrations, see Figure S3 and Table S2, Supporting Information.

3.2. Continuous Liquid Composition Analysis Experiments. Table 3 compiles the rate of formation for the species of interest from each Investigation. Initial concentrations are given in Table 1. In addition, Table 3 presents the NO₂ absorption rate—estimated by comparing gas analyzer outlet concentrations of NO_x with MFC-voltage for the NO₂ inlet—as well as the ratio of oxidized moles of S(IV) to the NO₂ absorption rate. S(IV) includes both SO₃²⁻ and HSO₃⁻. When comparing the result of Investigations 1 and 4, it is obvious that NO₂ absorption increases the oxidation of S(IV), as the S(IV) oxidation rate is 10 times higher in the presence of NO₂ than when only O₂ is present. This is supported by the formation of a sulfite radical in reaction 8. Investigations 3 and 6 show that S₂O₃²⁻ is efficient at inhibiting S(IV) oxidation by eliminating the radical chain reaction as described by reactions 9 and 10, as there is no oxidation taking place without NO₂ presence and the oxidation of S(IV) is reduced by ~75% when NO₂ is present. The bubble flask has a baseline of absorption of NO_x at ~6% and NO₂ at ~17%.

3.2.1. Sulfite Oxidation without NO₂ Presence. Figure 2 shows the concentration profiles for Investigation 1. The initial flushing with N₂ is finished and O₂ injected 800 s after the log started. The initial concentrations of HSO₃⁻ (0.02 mol/kg_{H₂O}) and SO₃²⁻ (0.02 mol/kg_{H₂O}) are stable at the start of the experiment. The total amount of sulfur analyzed remains close to the starting concentration of 0.04 mol/kg_{H₂O}. The distribution

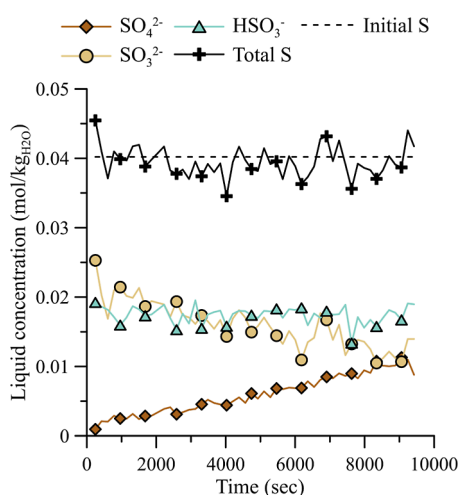


Figure 2. Concentration profile for Investigation 1: 20 °C, pH ~ 7, and 3% O₂. Total S is the total molar concentration of sulfur species analyzed by Raman spectroscopy. Initial S is the by weight estimated amount of moles of sulfur added to the sample.

between HSO₃⁻ and SO₃²⁻ changes with the pH, following the equilibrium from a pH of 7.1 at the start of the experiment to a pH of 6.7 at the end of the experiment (see Figure S4, Supporting Information). The rate of SO₄²⁻ formation observed can be compared to the rate expression obtained by Zhang and Millero³⁷ with second-order dependence on sulfite concentration and 0.5 order dependence on O₂ concentration. For O₂ concentration profile and Raman spectra profile, see Figures S5 and S6, Supporting Information.

Figure 3 shows the concentration profile for Investigation 2. The initial flushing with N₂ is finished and O₂ injection started at

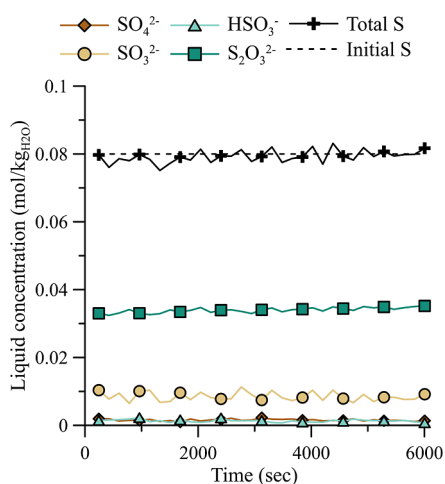


Figure 3. Concentration profile for Investigation 2, 20 °C, pH ~ 7.1, and 3% O₂. Total S is the total molar concentration of sulfur species analyzed by Raman spectroscopy. Initial S is the by weight estimated amount of moles of sulfur added to the sample.

1100 s. SO₃²⁻ and HSO₃⁻ are detected from the start of the measurements, formed from the introduced S₂O₃²⁻ (0.04 mol/kg_{H₂O}). The solution is bubbled with 3% O₂ in N₂. There is no clear oxidation of S₂O₃²⁻ taking place by O₂, which is in agreement with the previous work.³⁸ The pH increased from 7.1 at the start to 7.7 when the log ended (see Figure S7, Supporting

Information). For O₂ concentration profile and Raman spectra profile, see Figures S8 and S9, Supporting Information.

Figure 4 shows the concentration profile for Investigation 3. The initial flushing with N₂ is finished and O₂ injection started

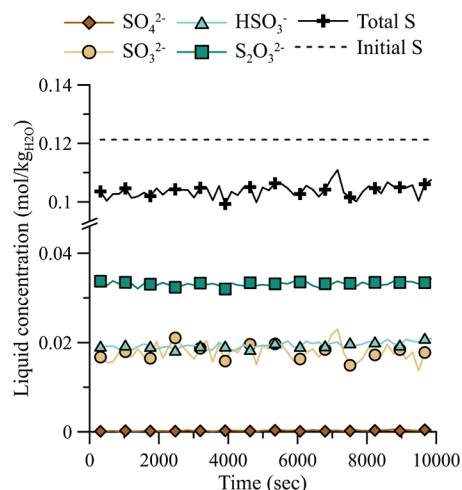


Figure 4. Concentration profile for Investigation 3, 20 °C, pH ~ 7.0, and 3% O₂. Total S is the total molar concentration of sulfur species analyzed by Raman spectroscopy. Initial S is the by weight estimated amount of moles of sulfur added to the sample.

1000 s after the log started. The initial concentrations of HSO₃⁻ (0.02 mol/kg_{H₂O}) and SO₃²⁻ (0.02 mol/kg_{H₂O}) remain stable throughout the experiment. The added amount of S₂O₃²⁻ (0.04 mol/kg_{H₂O}) is directly reduced to 0.03 mol/kg_{H₂O} and then constant throughout the experiment. It is evident that S₂O₃²⁻ inhibits the oxidation of SO₃²⁻ by O₂ and the formation of SO₄²⁻ when comparing the result with Investigation 1 in Figure 2. The pH remains constant at 7 throughout the experiment, see Figure S10, Supporting Information. For O₂ concentration profile and Raman spectra profile, see Figures S11 and S12, Supporting Information.

3.2.2. Sulfite Oxidation with NO₂ Presence. Figure 5 shows the concentration profile for Investigation 4. The initial flushing with N₂ is finished and O₂ and NO₂ injection started 1400 s after the log started. The total S concentration initially deviated from the starting concentration. The deviation corresponds to a low reading in SO₃²⁻ and HSO₃⁻ that could be attributed to noise in the Raman peak. SO₄²⁻ is rapidly increasing after 1400 s, and the rate of formation gradually decreases until reaching a stable concentration at 6000 s. The pH remains around 7 until the SO₃²⁻ and HSO₃⁻ concentrations are diminished at around 4000 s into the experiment. It then overshoots the addition of NaOH, and pH increases to 11 (see Figure S13, Supporting Information).

The combined rate of consumption of S(IV) in the initial time period 1000–3000 s is 0.85 mmol·kg_{H₂O}⁻¹ min⁻¹. The rate is comparable to, but lower than, the rate observed by Schmidt et al. of 2.5 mmol·kg_{H₂O}⁻¹ min⁻¹.³⁹ There is no nitrogen salt in the prepared sample, and according to the mass balance based on gas analysis, the nitrogen concentration in the liquid should be around 0.005 mol/kg_{H₂O} at the end of the experiments. The absorbed concentration is below the detection limit for NO₂⁻ and NO₃⁻.

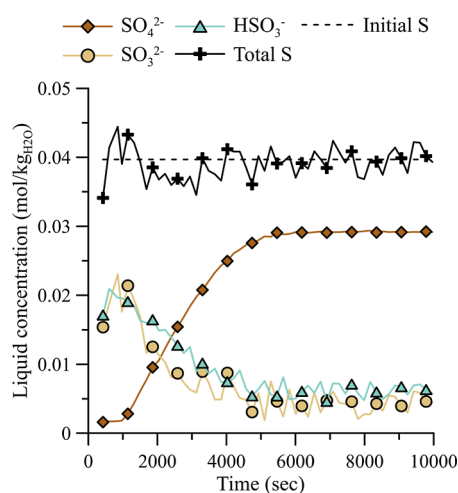


Figure 5. Concentration profile during Investigation 4: 20 °C, pH ~ 7.1, 95 ppm NO₂, and 3% O₂. Total S is the total molar concentration of sulfur species analyzed by Raman spectroscopy. Initial S is the by weight estimated amount of moles of sulfur added to the sample. The initial flushing with N₂ is finished at 1400 s on the y-axis. The pH is constant at 7 until 4000 s where it increases to 11.

When comparing the S(IV) oxidation rate between Investigations 4 and 1, it is clear that NO₂ absorption initiates a radical chain reaction where S(IV) is oxidized to S(VI) as shown by reaction 8. The molar ratio between oxidized S(IV) and absorbed NO₂ is ~31, which can be compared to the stoichiometry of 1 for the global reaction of NO₂ absorption in SO₃²⁻. See Figure S14, Supporting Information, for a gas concentration profile of NO_x and O₂ during the investigation and Figure S15 for a Raman spectra profile.

Figure 6 shows the concentration profile for Investigation 5 with an initial concentration of S₂O₃²⁻ (0.04 mol/kg_{H₂O}) and bubbled with 3% O₂ and 95 ppm NO₂ in N₂. The initial flushing with N₂ is finished and O₂ injection started at 1400 s after the log started. The concentration profile shows similar trends to

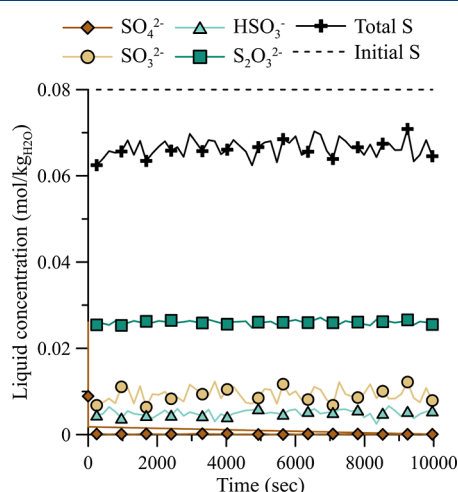


Figure 6. Concentration profile during Investigation 5, 20 °C, pH ~ 5.5, 95 ppm NO₂, and 3% O₂. Total S is the total molar concentration of sulfur species analyzed by Raman spectroscopy. Initial S is the by weight estimated amount of moles of sulfur added to the sample. The initial flushing with N₂ is finished at 900 s on the y-axis. The pH starts at 7, increases to 7.5 within 1000 s, and then decreases to 5.5 at 5000 s, where it remains stable for the rest of the experiment.

Investigation 2. Total S concentration remains slightly below that of the weight estimated in sample preparation throughout the experiment. The SO₃²⁻ formed together with S₂O₃²⁻ absorbs part of the NO₂ without clear consumption of the species. The pH increases from 7 to 7.5 initially and then decreases with the start of O₂/NO₂ injection until around 4000 s, when it stabilizes at pH 5.5 (see Figure S16, Supporting Information). For O₂ concentration profile and Raman spectra profile, see Figures S17 and S18, Supporting Information.

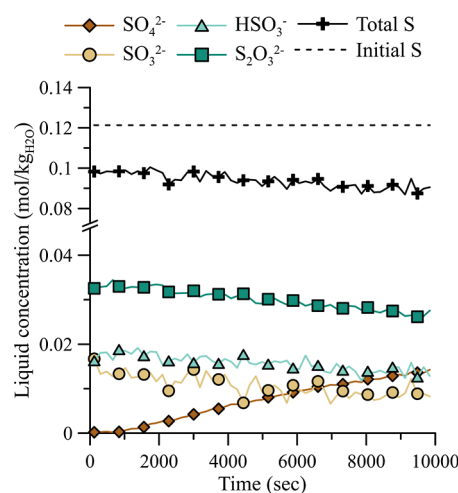


Figure 7. Concentration profile during Investigation 6, 20 °C, pH ~ 6.9, 95 ppm NO₂, and 3% O₂. Total S is the total molar concentration of sulfur species analyzed by Raman spectroscopy. Initial S is the by weight estimated amount of moles of sulfur added to the sample. The initial flushing with N₂ is finished at 1800 s on the y-axis.

Figure 7 shows the concentration profile for Investigation 6 with an initial concentration of HSO₃⁻ (0.02 mol/kg_{H₂O}), SO₃²⁻ (0.02 mol/kg_{H₂O}), and S₂O₃²⁻ (0.04 mol/kg_{H₂O}) and bubbled with 95 ppm NO₂, 3% O₂ in N₂. The initial flushing with N₂ is finished and O₂ and NO₂ injection started 1800 s after the log started. Initial concentration of total S is almost 20% off primarily due to the initial concentration of S₂O₃²⁻ (0.032 instead of 0.04). Both SO₃²⁻ and HSO₃⁻ are decreasing with time, and the SO₃²⁻ concentration remains below that of HSO₃⁻ throughout the experiment, following the pH. The combined rate of consumption of S(IV) after initial flushing is 0.07 mmol·kg_{H₂O}⁻¹ min⁻¹. The rate is comparable to but lower than that observed by Schmidt et al. of 0.23 mmol·kg_{H₂O}⁻¹ min⁻¹.³⁹

The total S concentration is diminishing with time, and an unidentified molecule is likely formed. In the Raman spectra, an unidentified peak at 259 cm⁻¹ is steadily increasing with time (see Figure S21, Supporting Information). A previously documented species formed from NO₂ absorption with S₂O₃²⁻ is S₂O₆²⁻; however, no Raman peaks have been reported for S₂O₆²⁻ at 259 cm⁻¹ in the reviewed literature. There are also studies that identify a number of nitrososulfonates (nitrogen-sulfur compounds) which can form in the bulk solution of a NO₂-S(IV) mixture; the formation is however more prevalent in acidic solutions. The only reference⁴⁰ to a peak in nearby regions for a species that has been documented as a product in NO₂ absorption with S₂O₃²⁻ is a peak at 260 cm⁻¹ of S₄O₆²⁻, tetrathionate, which is the product of reaction 10. The pH starts

at 6.9 and decreases to 6.7 at the end of the experiment (see Figure S19, Supporting Information). For O_2 concentration profile and Raman spectra profile, see Figures S20 and S21, Supporting Information.

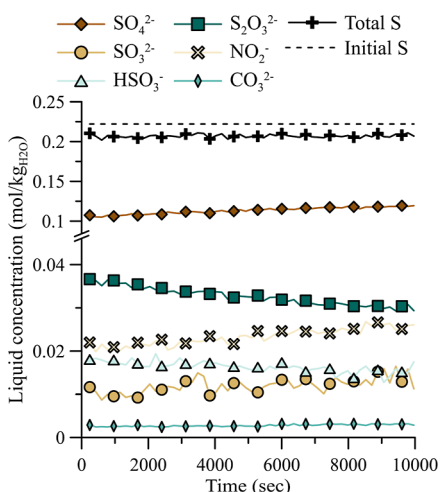


Figure 8. Concentration profile during Investigation 7, 20 °C, pH increasing from 7.1 to 8.5, 95 ppm NO_2 , and 3% O_2 . Total S is the total molar concentration of sulfur species analyzed by Raman spectroscopy. Initial S is the by weight estimated amount of moles of sulfur added to the sample.

Figure 8 shows the concentration profile for Investigation 7 with initial concentrations of HSO_3^- (0.02 mol/kg $_{H_2O}$), SO_3^{2-} (0.02 mol/kg $_{H_2O}$), $S_2O_3^{2-}$ (0.04 mol/kg $_{H_2O}$), SO_4^{2-} (0.1 mol/kg $_{H_2O}$), NO_2^- (0.02 mol/kg $_{H_2O}$), and HCO_3^- (0.01 mol/kg $_{H_2O}$) and bubbled with 95 ppm NO_2 , 3% O_2 in N_2 . The initial flushing with N_2 is finished and O_2 injection started 1100 s after the log started. Initial concentration of total S is around 10% off primarily due to the initial concentration of $S_2O_3^{2-}$ (0.036 instead of 0.04). The total S concentration is constant throughout the experiment, unlike that in Investigation 6. When comparing the results in Figure 8 of Investigation 7 with those in Investigation 6 and Figure 7, it is evident that the addition of either CO_3^{2-} or NO_2^- limits the S(IV) oxidation. When there is no $S_2O_3^{2-}$ present, SO_3^{2-} oxidation should increase with increasing concentrations of NO_2^- according to previous studies, something which is not observed in this experiment.^{20,41} The observed difference could also be due to the alkaline pH in this experiment compared to the acidic used in the mentioned references where NO_2^- is considerably less stable. Only 0.01 mmol·kg $_{H_2O}^{-1}$ min $^{-1}$ of HSO_3^- is consumed, but the total S(IV) concentration is more or less constant since SO_3^{2-} is increasing with 0.02 mmol·kg $_{H_2O}^{-1}$ min $^{-1}$. The analysis result of decreased S(IV) oxidation is supported by the lowered rate of formation of SO_4^{2-} which is only half of that in Investigation 6. The rate of consumption of $S_2O_3^{2-}$ is the same in both Investigations 6 and 7. The results for NO_2^- are included here since the high concentration from initial sample preparation makes quantification possible. There is a clear trend of increasing NO_2^- concentration over time from ~21 to ~26 mM, which corresponds to the absorbed amount of NO_2 estimated from the analysis of the gas to 4.7 mM.

Similar to Investigation 6, there is an unidentified peak at 259 cm^{-1} present, but only at half the intensity (see Figure S24, Supporting Information). The pH increases from 7 to 8.2 in the first 4500 s and then increases rapidly to pH 10 (see Figure S22, Supporting Information). For O_2 concentration profile and Raman spectra profile, see Figures S23 and S24, Supporting Information.

4. SUITABILITY AND APPLICATION OF RAMAN SPECTROSCOPY FOR ONLINE MEASUREMENTS IN A COMBINED SO_x – NO_x REMOVAL SYSTEM

The results obtained in this study show that Raman-spectroscopy can speciate and quantify SO_3^{2-} , HSO_3^- , SO_4^{2-} , and $S_2O_3^{2-}$ even in mixtures with NO_2^- , NO_3^- , and CO_3^{2-} . The sharp peak at 981 cm^{-1} gives a clear signal for SO_4^{2-} even at a concentration of 3 mM. The broad peak at 965 cm^{-1} is suitable for SO_3^{2-} quantification; however, the signal is less stable, and concentrations should be >10 mM to avoid interference with background noise. The same is true for HSO_3^- which has broad peaks at 1022 and 1052 cm^{-1} . $S_2O_3^{2-}$ is identified through a sharp peak at 997 and 448 cm^{-1} which gives a clear signal in the tested concentration range 20–40 mM.

Quantification of NO_2^- and NO_3^- is difficult in the present system with the chosen method. The low concentrations present in Investigations 1–6 are not possible to quantify. In Investigation 7 where NO_2^- is present at a higher concentration of 20 mM, it is quantifiable with some degree of uncertainty. However, the fact that the nitrogen balance is close to complete when accounting for the absorbed NO_2 indicates the success of the measurement.

The limit of detection for some species could be an issue for the use of Raman spectroscopy as a method for on line liquid analysis in a NO_x – SO_x removal system. The species include SO_3^{2-} , HSO_3^- , and NO_3^- . In this study, the concentrations of SO_3^{2-} and HSO_3^- are required to be ~20 mM each, together with ~30 mM $S_2O_3^{2-}$ to reach 80% NO_2 absorption. This is above the 10 mM minimum recommended limit of detection in this study. However, in our previous studies²⁵ where absorption units that are designed to maximize NO_2 absorption have been used, 80% NO_2 absorption was reached at only 1 g/L of Na_2SO_3 , corresponding to ~6 mM. In these studies, no $S_2O_3^{2-}$ was added to the liquid, and it was of interest to minimize the S(IV) added due to the rapid oxidation to SO_4^{2-} , which means higher Na_2SO_3 consumption and therefore an increased cost of operation. The results in Figure 8 indicate that $S_2O_3^{2-}$ is so efficient at limiting S(IV) oxidation that higher concentrations of S(IV) should be mainly beneficial due to increased NO_2 absorption. It is therefore likely that a NO_x – SO_x scrubber unit will be operating above 10 mM of SO_3^{2-} if $S_2O_3^{2-}$ is added. This result is in agreement with the findings of Sapkota et al.¹² NO_3^- is only present in concentrations below 10 mM and should therefore with the present model not be quantifiable by Raman spectroscopy, as it is not one of the main products in the reaction chain. If a strong oxidizer is present in the liquid phase, such as when O_3 is used for the oxidation and absorption of NO_2 , then NO_3^- will form from NO_2^- , resulting in higher concentrations, possibly above detection limits where usage of Raman spectroscopy could be suitable.

Raman spectroscopy is potentially a good analysis technique that in combination with standard gas analysis can be used for process control in a combined SO_2 and NO_2 flue gas cleaning system with large changes in concentration- and flow-profiles over time. The absorption rates of NO_2 and SO_2 would then

continuously be monitored through gas analysis while the concentrations of salts are quantified by the Raman instrument. This will enable exact control of liquid bleed amounts to minimize the loss of chemicals and addition of water while at the same time showing a precise need for addition of Na_2SO_3 and $\text{Na}_2\text{S}_2\text{O}_3$ needed for NO_2 absorption to maintain balance. For flue gas sources with stable concentration- and flow-profiles, simpler and less costly instruments, such as conductivity or redox meters, can be used after an initial testing period with Raman spectroscopy that characterize the scrubber and connect it to conductivity and / or redox potential.

5. FUTURE WORK

This initial study shows promising results both in interpreting the reaction mechanism of S(IV) oxidation with NO_2 absorption and monitoring the liquid phase composition. There are however several points that need further investigation. The unidentified peaks at 259, 665, 734, 1052, and 1384 cm^{-1} need to be further studied to enable speciation. If possible, new peaks for NO_2^- and NO_3^- should be identified and used for quantification; in the case of NO_2^- , much higher concentrations can be used since concentrations in an actual flue gas cleaning system preferably are as close to the precipitation limit as the system can handle.

After the questions in this study have been answered, more complex liquids can be studied. In a combined NO_2 and SO_2 flue gas cleaning system, a wide number of other impurities, depending on the flue gas source, will be present. Most of these will only be present in limited concentrations, but their spectra could still disrupt the Raman peaks used in this study. Some of the possible impurities like iron, manganese, and copper are also reported in the literature to have a catalytic effect on S(IV) oxidation,¹⁵ which is something that could be investigated with the method used in this study.

6. CONCLUSIONS

Seven PLS-R models for SO_3^{2-} , HSO_3^- , $\text{S}_2\text{O}_3^{2-}$, SO_4^{2-} , NO_2^- , NO_3^- , and CO_3^{2-} were developed using Raman spectroscopy. The models are applied to evaluate sulfite and bisulfite oxidation in a bubbling flask. Two oxidant compositions are investigated: O_2 at 3% and O_2 at 3% with NO_2 at 95 ppm. The oxidation of sulfite and bisulfite is also investigated with the addition of a free radical scavenger in $\text{Na}_2\text{S}_2\text{O}_3$. The key findings are summarized below.

- 1 Raman Vibrational bands of SO_3^{2-} , HSO_3^- , $\text{S}_2\text{O}_3^{2-}$, SO_4^{2-} , NO_2^- , CO_3^{2-} , and CO_3^{2-} are successfully identified and possible to separate from each other even in mixtures. Raman spectroscopy is a suitable method for liquid analysis of a combined NO_x/SO_x removal system.
- 2 S(IV) is oxidized at a rate of $\sim 0.07\text{ mmol}/(\text{kg}_{\text{H}_2\text{O}}\cdot\text{min})$ when the bubble flask is fed with 3% O_2 in N_2 . Total sulfur concentration remains constant, indicating that no other species than SO_4^{2-} is formed. When $\text{S}_2\text{O}_3^{2-}$ is added to the liquid, no S(IV) is oxidized by O_2 .
- 3 With NO_2 present in the gas phase, the S(IV) oxidation increases to $0.84\text{ mmol}/(\text{kg}_{\text{H}_2\text{O}}\cdot\text{min})$. The total S(IV) oxidation is increased by a factor of 10 compared to oxidation by the gas without NO_2 (i.e., only containing O_2). The ratio between absorbed NO_2 and oxidized S(IV) is ~ 31 , confirming the reaction scheme of S(IV) oxidation with a radical chain.

4 Addition of $\text{S}_2\text{O}_3^{2-}$ to the liquid inhibits or even eliminates the S(IV) oxidation even though NO_2 is absorbed. With a concentration of 35 mM $\text{S}_2\text{O}_3^{2-}$ and 20 mM SO_3^{2-} and HSO_3^- , 80% of the incoming NO_2 is absorbed, and no S(IV) oxidation takes place while $\text{S}_2\text{O}_3^{2-}$ is consumed at a rate of $0.04\text{ mmol}/(\text{kg}_{\text{H}_2\text{O}}\cdot\text{min})$ with a NO_2 absorption rate of $0.032\text{ mmol}/(\text{kg}_{\text{H}_2\text{O}}\cdot\text{min})$.

■ ASSOCIATED CONTENT

Supporting Information

The Supporting Information is available free of charge at <https://pubs.acs.org/doi/10.1021/acs.iecr.3c01015>.

Additional information about the spectrometer and additional experimental results, including Raman spectra profiles and gas concentrations (PDF)

■ AUTHOR INFORMATION

Corresponding Author

Jakob Johansson – Department of Space, Earth and Environment, Chalmers University of Technology, 41296 Gothenburg, Sweden; orcid.org/0000-0001-8011-7783; Phone: +46 31 7725248; Email: jakobjo@chalmers.se

Authors

Jayangi D. Wagaarachchige – Faculty of Technology, Natural Sciences and Maritime Sciences, University of South-Eastern Norway, 3918 Porsgrunn, Norway; orcid.org/0000-0002-1544-7169

Fredrik Normann – Department of Space, Earth and Environment, Chalmers University of Technology, 41296 Gothenburg, Sweden

Zulkifli Idris – Faculty of Technology, Natural Sciences and Maritime Sciences, University of South-Eastern Norway, 3918 Porsgrunn, Norway

Eirik R. Haugen – Faculty of Technology, Natural Sciences and Maritime Sciences, University of South-Eastern Norway, 3918 Porsgrunn, Norway

Maths Halstensen – Faculty of Technology, Natural Sciences and Maritime Sciences, University of South-Eastern Norway, 3918 Porsgrunn, Norway

Wathsala Jinadasa – Faculty of Technology, Natural Sciences and Maritime Sciences, University of South-Eastern Norway, 3918 Porsgrunn, Norway

Klaus J. Jens – Faculty of Technology, Natural Sciences and Maritime Sciences, University of South-Eastern Norway, 3918 Porsgrunn, Norway; orcid.org/0000-0002-9022-5603

Klas Andersson – Department of Space, Earth and Environment, Chalmers University of Technology, 41296 Gothenburg, Sweden; orcid.org/0000-0001-5968-9082

Complete contact information is available at <https://pubs.acs.org/doi/10.1021/acs.iecr.3c01015>

Notes

The authors declare no competing financial interest.

■ ACKNOWLEDGMENTS

This work was supported by the Swedish Energy Agency (grant number 50368-1) and Nouryon Pulp and Performance Chemicals AB (grant no 46438-1).

REFERENCES

- (1) Johansson, J.; Normann, F.; Sarajlic, N.; Andersson, K. Technical-Scale Evaluation of Scrubber-Based, Co-Removal of NO_x and SO_x Species from Flue Gases via Gas-Phase Oxidation. *Ind. Eng. Chem. Res.* **2019**, *58* (48), 21904–21912.
- (2) Nash, T. The Effect of Nitrogen Dioxide and of Some Transition Metals on the Oxidation of Dilute Bisulphite Solutions. *Atmos. Environ.* **1979**, *13* (8), 1149–1154.
- (3) Beyad, Y.; Burns, R.; Puxty, G.; Maeder, M. A Speciation Study of Sulfur(IV) in Aqueous Solution. *Dalton Trans.* **2014**, *43* (5), 2147–2152.
- (4) Siddiqi, M. A.; Krissmann, J.; PetersGerth, P.; Luckas, M.; Lucas, K. Spectrophotometric measurement of the vapour-liquid equilibria of (sulphur dioxide + water). *J. Chem. Thermodyn.* **1996**, *28* (7), 685–700.
- (5) Voegelé, A. F.; Tautermann, C. S.; Loerting, T.; Hallbrucker, A.; Mayer, E.; Liedl, K. R. About the Stability of Sulfurous Acid (H₂SO₃) and Its Dimer. *Chem.—Eur. J.* **2002**, *8* (24), 5644–5651.
- (6) Rhee, J. S.; Dasgupta, P. K. The Second Dissociation Constant of Sulfur Dioxide-Water. *J. Phys. Chem.* **1985**, *89* (9), 1799–1804.
- (7) Schwartz, S. E. Equilibria in the Nitrogen-Oxide Nitrogen Oxyacid-Water System. *Abstr. Pap. Am. Chem. Soc.* **1980**, *180* (Aug), 221-Phys.
- (8) Lee, Y. N.; Schwartz, S. E. Reaction-Kinetics of Nitrogen-Dioxide with Liquid Water at Low Partial-Pressure. *J. Phys. Chem.* **1981**, *85* (7), 840–848.
- (9) Park, J. Y.; Lee, Y. N. Solubility and Decomposition Kinetics of Nitrous-Acid in Aqueous-Solution. *J. Phys. Chem.* **1988**, *92* (22), 6294–6302.
- (10) Clifton, C. L.; Altstein, N.; Huie, R. E. Rate constant for the reaction of nitrogen dioxide with sulfur(IV) over the pH range 5.3–13. *Environ. Sci. Technol.* **1988**, *22* (5), 586–589.
- (11) Littlejohn, D.; Wang, Y.; Chang, S. G. Oxidation of Aqueous Sulfite Ion by Nitrogen Dioxide. *Environ. Sci. Technol.* **1993**, *27* (10), 2162–2167.
- (12) Sapkota, V. N. A.; Fine, N. A.; Rochelle, G. T. NO₂-Catalyzed Sulfite Oxidation. *Ind. Eng. Chem. Res.* **2015**, *54* (17), 4815–4822.
- (13) Sun, Y.; Hong, X. W.; Zhu, T. L.; Guo, X. Y.; Xie, D. Y. The Chemical Behaviors of Nitrogen Dioxide Absorption in Sulfite Solution. *Appl. Sci.* **2017**, *7* (4), 377.
- (14) Zhuang, Z.; Sun, C.; Zhao, N.; Wang, H.; Wu, Z. Numerical simulation of NO₂ absorption using sodium sulfite in a spray tower. *J. Chem. Technol. Biotechnol.* **2016**, *91* (4), 994–1003.
- (15) Shen, C. H.; Rochelle, G. T. Nitrogen Dioxide Absorption and Sulfite Oxidation in Aqueous Sulfite. *Environ. Sci. Technol.* **1998**, *32* (13), 1994–2003.
- (16) Beilke, S.; Lamb, D.; Müller, J. On the Uncatalyzed Oxidation of Atmospheric SO₂ by Oxygen in Aqueous Systems. *Atmos. Environ.* **1975**, *9* (12), 1083–1090.
- (17) Larson, T. V.; Horike, N. R.; Harrison, H. Oxidation of sulfur dioxide by oxygen and ozone in aqueous solution: A kinetic study with significance to atmospheric rate processes. *Atmos. Environ.* **1978**, *12* (8), 1597–1611.
- (18) Connick, R. E.; Zhang, Y. X.; Lee, S. Y.; Adamic, R.; Chieng, P. Kinetics and Mechanism of the Oxidation of HSO₃⁻ by O₂. The Uncatalyzed Reaction. *Inorg. Chem.* **1995**, *34* (18), 4543–4553.
- (19) Mo, J. S.; Wu, Z. B.; Cheng, C. J.; Guan, B. H.; Zhao, W. R. Oxidation Inhibition of Sulfite in Dual Alkali Flue Gas Desulfurization System. *J. Environ. Sci.* **2007**, *19* (2), 226–231.
- (20) Huang, X.; Ding, J.; Jia, Y.; Zhang, S.; Zhong, Q. Kinetics of Sulfite Oxidation in the Simultaneous Desulfurization and Denitrification of the Oxidation-Absorption Process. *Chem. Eng. Technol.* **2015**, *38* (5), 797–803.
- (21) Ajdari, S.; Normann, F.; Andersson, K.; Johansson, F. Reduced Mechanism for Nitrogen and Sulfur Chemistry in Pressurized Flue Gas Systems. *Ind. Eng. Chem. Res.* **2016**, *55* (19), 5514–5525.
- (22) Xu, J.; He, Q.; Xiong, Z.; Yu, Y.; Zhang, S.; Hu, X.; Jiang, L.; Su, S.; Hu, S.; Wang, Y.; Xiang, J. Raman Spectroscopy as a Versatile Tool for Investigating Thermochemical Processing of Coal, Biomass, and Wastes: Recent Advances and Future Perspectives. *Energy Fuels* **2021**, *35* (4), 2870–2913.
- (23) Henry, D. G.; Jarvis, I.; Gillmore, G.; Stephenson, M. Raman Spectroscopy as a Tool to Determine the Thermal Maturity of Organic Matter: Application to Sedimentary, Metamorphic and Structural Geology. *Earth Sci. Rev.* **2019**, *198*, 102936.
- (24) Schmid, D.; Hupa, M.; Paaola, M.; Vuorinen, I.; Lehtikoinen, A.; Karlström, O. Role of Thiosulfate in NO₂ Absorption in Aqueous Sulfite Solutions. *Ind. Eng. Chem. Res.* **2023**, *62* (1), 105–110.
- (25) Johansson, J.; Heijnesson Hultén, A.; Normann, F.; Andersson, K. Simultaneous Removal of NO_x and SO_x from Flue Gases Using ClO₂: Process Scaling and Modeling Simulations. *Ind. Eng. Chem. Res.* **2021**, *60* (4), 1774–1783.
- (26) Johansson, J.; Normann, F.; Andersson, K. Techno-Economic Evaluation of Co-Removal of NO_x and SO_x Species from Flue Gases via Enhanced Oxidation of NO by ClO₂-Case Studies of Implementation at a Pulp and Paper Mill, Waste-to-Heat Plant and a Cruise Ship. *Energies* **2021**, *14*, 8512.
- (27) Whittaker, E. T. On a New Method of Graduation. *Proc. Edinb. Math. Soc.* **1922**, *41*, 63–75.
- (28) Irish, D. E.; Chen, H. Raman Spectral Study of Bisulfate-Sulfate Systems. II. Constitution, Equilibria, and Ultrafast Proton Transfer in Sulfuric Acid. *J. Phys. Chem.* **1971**, *75* (17), 2672–2681.
- (29) Kruus, P.; Hayes, A. C.; Adams, W. A. Determination of Ratios of Sulfate to Bisulfate Ions in Aqueous Solutions by Raman Spectroscopy. *J. Solution Chem.* **1985**, *14* (2), 117–128.
- (30) Evans, J. C.; Bernstein, H. J. The Vibrational Spectrum of the Sulphite Ion in Sodium Sulphite. *Can. J. Chem.* **1955**, *33* (7), 1270–1272.
- (31) Littlejohn, D.; Walton, S. A.; Chang, S.-G. A Raman Study of the Isomers and Dimer of Hydrogen Sulfite Ion. *Appl. Spectrosc.* **1992**, *46* (5), 848–851.
- (32) Waterland, M. R.; Stockwell, D.; Kelley, A. M. Symmetry Breaking Effects in NO₃⁻: Raman Spectra of Nitrate Salts and Ab Initio Resonance Raman Spectra of Nitrate-Water Complexes. *J. Chem. Phys.* **2001**, *114* (14), 6249–6258.
- (33) Irish, D. E.; Walrafen, G. E. Raman and Infrared Spectral Studies of Aqueous Calcium Nitrate Solutions. *J. Chem. Phys.* **1967**, *46* (1), 378–384.
- (34) Reichenbacher, M.; Popp, J. *Challenges in Molecular Structure Determination*; Springer Science & Business Media, 2012; pp 63–143.
- (35) Wen, N.; Brooker, M. H. Ammonium Carbonate, Ammonium Bicarbonate, and Ammonium Carbamate Equilibria: A Raman Study. *J. Phys. Chem.* **1995**, *99* (1), 359–368.
- (36) Sun, S.; Cai, T.; Liu, Y.; Wang, J. Experimental and Theoretical Study of the Raman Spectra of Ammonium Thiosulfate Solution. *J. Appl. Spectrosc.* **2015**, *82* (2), 182–187.
- (37) Zhang, J.-Z.; Millero, F. J. The Rate of Sulfite Oxidation in Seawater. *Geochim. Cosmochim. Acta* **1991**, *55* (3), 677–685.
- (38) Rolia, E.; Chakrabarti, C. L. Kinetics of Decomposition of Tetrathionate, Trithionate, and Thiosulfate in Alkaline Media. *Environ. Sci. Technol.* **1982**, *16* (12), 852–857.
- (39) Schmid, D.; Karlström, O.; Kuvaja, V.; Vuorinen, I.; Paaola, M.; Hupa, M. Role of Sulfite Oxidation in NO₂ Absorption in a PH-Neutral Scrubber Solution. *Energy Fuels* **2022**, *36* (5), 2666–2672.
- (40) Gerding, H.; Eriks, K. The Raman Spectra of Di-Tri- and Tetrathionate Ions in Aqueous Solutions. *Recl. Trav. Chim. Pays-Bas.* **1950**, *69* (6), 724–728.
- (41) Shi, M.; Ding, J.; Liu, X.; Zhong, Q. Mechanisms of Sulfite Oxidation in Sulfite-Nitrite Mixed Solutions. *Atmos. Pollut. Res.* **2019**, *10* (2), 412–417.

Article 6

Fast water-lean solvent screening using FTIR spectroscopy: In-situ (in-line) monitoring using an ATR reaction cell integrated with on-line monitoring attached to a liquid-flow cell.

Jayangi D. Wagaarachchige¹, Zulkifli Idris², Klaus-J. Jens², and Maths Halstensen^{1*}

¹Department of Electrical, IT and Cybernetics, University of South-Eastern Norway,
Porsgrunn, Norway

²Department of Process, Energy and Environmental Technology, University of South-Eastern
Norway, Porsgrunn, Norway

Published in Proceedings of the TCCS-11 - Trondheim Conference on CO₂ Capture, Transport
and Storage, Trondheim (2021)

<https://hdl.handle.net/11250/2787331>

FAST WATER-LEAN SOLVENT SCREENING USING FTIR SPECTROSCOPY: IN-SITU (IN-LINE) MONITORING USING AN ATR REACTION CELL INTEGRATED WITH ON-LINE MONITORING ATTACHED TO A LIQUID-FLOWCELL

Jayangi D. Wagaarachchige¹, Zulkifli Idris², Maths Halstensen¹, Klaus-J. Jens^{2*}

¹ Department of Electrical, IT and Cybernetics, University of South – Eastern Norway, Kjølnes Ring 56, 3918 Porsgrunn, Norway

² Department of Process, Energy and Environmental Technology, University of South – Eastern Norway, Kjølnes Ring 56, 3918 Porsgrunn, Norway

* Corresponding author e-mail: Klaus.J.Jens@usn.no

Abstract

This study presents a fast and precise solvent characterizing method for the screening of novel CO₂ capture systems. In this method, time-base Attenuated Total Reflectance-Fourier Transform Infrared (ATR-FTIR) spectroscopy was used for in-situ monitoring of CO₂ absorption and desorption processes of non-aqueous amine systems. Different equal mole amines were used to qualify and quantify changes of the IR vibrations. The method enables identification of reaction mechanism along with full speciation. In order to confirm repeatability and representability of the screening test, a replication experiment using liquid-flow cell FTIR analysis is also presented.

Keywords: FTIR-ATR, fast solvent screening, representative sampling, non-aqueous solvents, speciation

1. Introduction

The annual increase in CO₂ emissions is the main contributor to the increase in the greenhouse gas (GHG) level causing climate changes and global warming [1]. Fossil-fuel combustion and industrial processes are the dominant triggers of anthropogenic CO₂ emissions [2]. Integration of the post-combustion CO₂ capture (PCC) to industrial point sources is an essential attempt to alleviate this phenomenon [3, 4].

Different processes are employed for CO₂ capture and separation such as distillation, absorption, adsorption, and advanced membrane filtration [5]. Aqueous amine based gas-liquid chemical absorption is the most common method currently being used in industrial plants [4, 6]. Aqueous 30% MEA solvent is the benchmark capture system and the first patented amine-based solvent system [7-9]. MEA-based solvents are most popular due to MEA's high reactivity and low cost.

However, main concerns of aqueous MEA systems are energy intensiveness, solvent corrosivity and degradation in addition to solvent emissions. Although amine based solvent development has been in focus for several decades to identify appropriate solvent systems, it is still challenging to overcome the aforementioned drawbacks. A method enabling fast screening of solvent systems is thus essential to identify promising CO₂ capture systems.

Amines are widely used for chemical absorption of CO₂. During this reaction, reversible carbonaceous products are formed. In this context, amines are an interesting group of chemical compounds which can be classified into three main groups of primary, secondary, or tertiary amines. Furthermore, amines may react differently due to

steric hindrance, cyclic structures or multiple amine functions present in one amine molecule. Aqueous, non-aqueous, water-lean, by-phasic, and ionic/eutectic amine based solvents systems are being investigated to identify the most promising capture systems.

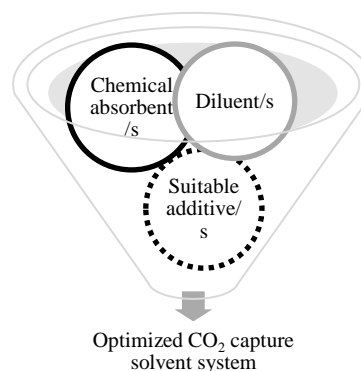


Figure 1: Amine based CO₂ capture system interpretation

Generally, an amine based CO₂ capture system is a blend of several components as shown in Figure 1. It may consist of an amine or a blend of amines to act as a chemical absorbent of CO₂. Moreover, this part is diluted with suitable diluents like water or organic solvents. Furthermore, this system may be optimized by addition of suitable additives to enhance the solvent's chemical and physical properties. Since all components may interact with each other, identifying a novel and promising CO₂ capture system is a challenging task. Therefore, combination of fast and precise chemical analytics with chemical mechanistic insight is paramount.

There are several methods currently being employed to characterize potential solvent. The wetted wall column (WWC) is a well-known apparatus for CO₂ absorption rate measurements also used in a modified version for solvent screening [10]. An atmospheric solvent screening apparatus has been developed to mimic the CO₂ absorption and desorption processes [11-13]. Solvent performance can be determined versus reference solvents by continuous monitoring of the CO₂ capture rate using non-dispersive infrared (ND-IR) CO₂ sensor [14]. The same method was used to screen strong bicarbonate-forming solvents gathering at the same time information on solvent foaming, solid precipitation, and discoloration [15]. Furthermore, Luo et.al. introduced a rapid screening apparatus for improved analysis of single and blended amine solvent systems [16]. Molecular simulations [17] or different modeling tools like soft SAFT[18], COSMO-RS [19, 20] are also used to predict reactive absorption properties of novel solvents without doing laborious experiments.

FT-IR spectroscopy is a versatile method for the analysis of chemical structures used in a wide range of applications. In FT-IR spectrum analysis, the bands of the functional groups and the molecular fingerprint of a chemical mixture are analyzed to give qualitative and quantitative chemical data. This is a fast and precise analysis method for efficient screening of chemicals at small sample volume. Furthermore, vibrational spectroscopy is well suited to application of multivariate calibration models to extract chemical data of species, especially for online monitoring of dynamic systems [21-23].

Chemical speciation of aqueous DEA [24] and heterocyclic amine [25] solvent systems has been performed by ATR-FTIR spectroscopic in situ monitoring. This method can be used for online monitoring of several chemical components simultaneously using Partial Least Regression (PLS-R) models [25-27].

We recently reported a novel sulfolane based non-aqueous solvent system for CO₂ capture [28]: a mixture of diisopropylamine (DIPA), sulfolane (SULF), and methanol (MeOH). Herein we report development and representativity[29]of a fast solvent screening method applied for analysis of the above-mentioned DIPA-MeOH-SULF study. The FTIR-based bulk liquid analysis was performed to confirm the fast-screening result are representative and reproducible.

2. Materials and Methods

All chemicals used in the experiments are tabulated in table 1.

Table 1 Chemical information: Name, CAS number, mole fraction purity, role, and supplier of chemicals.

Chemical name	CAS number	Mole fraction purity	Role	Supplier
Diisopropylamine (DIPA)	108-18-9	≥0.99	Amine	Sigma-Aldrich
Sulfolane (SULF)	126-33-0	≥0.99	Diluent	Sigma-Aldrich
Methanol (MeOH)	67-56-1	≥0.99	Diluent	VWR
Carbon dioxide (CO ₂)	124-38-9	0.9999	Gas	AGA Norge AS

2.1 Fast solvent screening method including solvent speciation

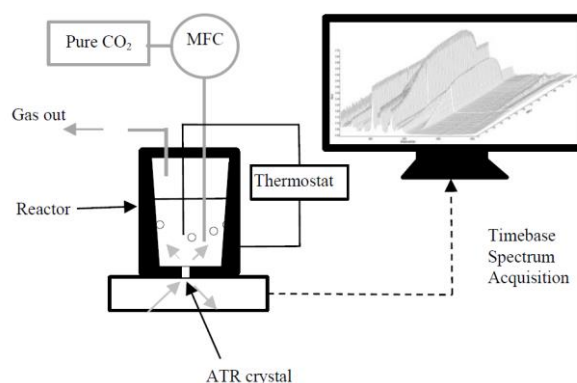


Figure 2: Schematic diagram of the experimental set-up used for the fast-screening of the non-aqueous DIPA system.

The schematic diagram of the fast-screening method is shown in Figure 2. A detailed description of the experimental procedure is given in an earlier publication [28]. The set-up1 (figure2) was used for screening a set of non-aqueous solvent systems as well as performance evaluation based on the spectroscopic information gathered by in-situ FTIR monitoring.

2.2 Bulk flow analysis for verifying the representativity of the screening results.

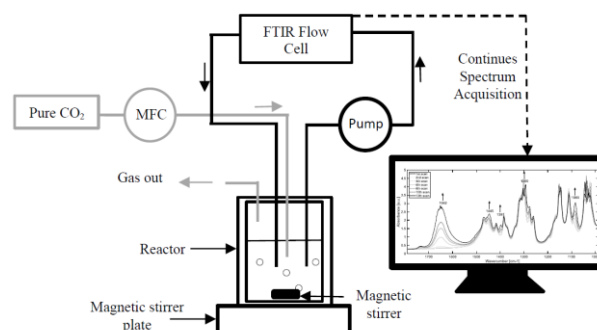


Figure 3: Schematic diagram of the experimental set-up2 for the acquisition of liquid flow cell FTIR spectra.

Since the FTIR-ATR method provides solvent composition on the surface of the ATR crystal, the representativeness of the fast-screening results for the

bulk solvent liquid needs to be assured. Hence, CO₂ absorption tests were performed using set-up2 i.e. bulk liquid-flow analysis. The schematic diagram of the set-up2 is shown in Figure 3. The reactor is a double-jacketed glass vessel with 4 inlet-outlet ports on the top. 50 ml of unloaded solution was placed inside the reactor and the solvent was mixed using a magnetic stirrer with a stirring rate of 250 rpm. Two ports were connected to the gas inlet and outlet while the other two ports were connected to the liquid flow cell inlet and outlet. To analyse the reaction liquid, the solvent was passed through a liquid-flow cell connected to a FTIR liquid sampling accessory. The liquid sampling accessory was attached to the Perkin Elmer Spectrum One FT-IR Spectrometer and the liquid passing through the sampling device was scanned at pre-determined set time. The sampling accessory is equipped with a programmable, variable-speed peristaltic pump to pass the liquid through the flow cell. The waste liquid end of the sampler was sent back to the reactor to recycle the liquid flow through the flow cell.

Prior to each experiment, a background scan of the empty flow cell was recorded. Then the sampler was turned on and unloaded CO₂ solvent started to flow through the cell. Several scans of unloaded liquid were recorded. Then, CO₂ gas was introduced into the glass reactor at a flow rate of 0.10 NL/min using a mass flow controller (MFC) from Sierra Instruments. Scans of the reaction liquid were performed timely during the CO₂ absorption reaction.

FTIR spectra were baseline corrected by Automatic Whittaker Filter method using a chemometrics software, PLS-toolbox with MATLAB® (R2019b).

3. Results and Discussion

3.1 In-situ monitoring and fast screening of a non-aqueous solvent system

In the experimental set-up1, in-situ monitoring was used to observe reaction changes during CO₂ absorption-desorption of the solvent system. The tests were performed in a reaction cell containing a diamond crystal top plate (P/N GS10507) with Golden Gate™ single reflection diamond ATR system. An inherent advantage of this system is that only small mass of solvent is needed (approx. 5g) for one screening experiment. An example of ATR-FTIR raw spectra obtained from time-based in-situ monitoring is shown in Figure 4 (a).

According to Figure 4(a), in-situ monitoring of the chemical changes in the reaction aliquot was performed in four stages. A time gap of each stage was decided during the experiment along with the appeared stack of spectra. The chemical reaction changes can be observed as ATR-FTIR spectra variations. This is a benefit of set-up1 since we can do the experiment without prior information about the time gaps of each step. It is possible to control the parameters accordingly during the experiment while observing the spectra.

Initially, a few FTIR scans were performed to check the unloaded solution. There was no evidence of premature CO₂ capture species formation or water contamination in the sample. Representative FTIR bands of mixture components were also identified.

Then CO₂ was introduced into the solvent. During this second stage, several peaks were seen to increase, decrease and shift. At the same time, several new peaks appeared according to the developing carbonaceous products. The second stage absorption step continues until the increasing band intensity is seen constant.

In the third step, the loaded solvent was observed after further CO₂ pumping. During this time all bands stayed stagnant, implying the capture products to be stable at this condition. This stage was completed after approximately 25 minutes.

In the fourth step, the temperature of the reaction cell was increased to observe the desorption reactions of the system. The reaction cell was heated up gradually and reduction of peaks were seen. Temperature for this step was kept at 58°C. At this stage, in-situ reaction monitoring is important to determine the proper desorption temperature of the new system through observation of spectra changes.

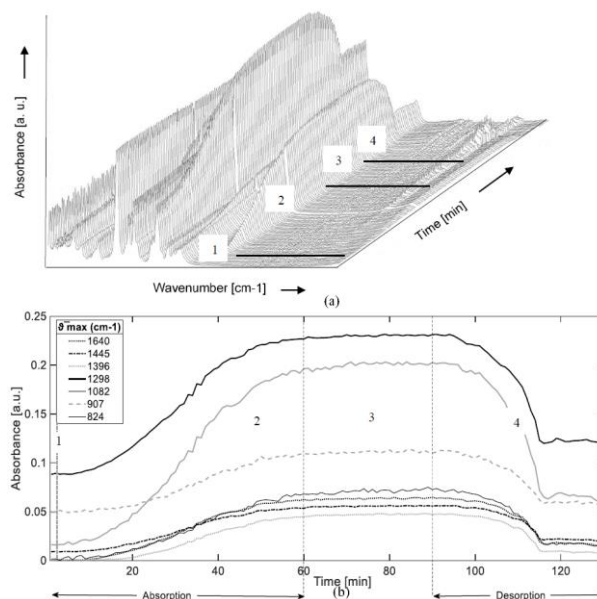


Figure 4: (a) Time-based ATR-FTIR scans (b) IR absorbance variation with time from changing IR vibrational bands; non-aqueous DIPA solvent system during the CO₂ absorption and desorption.

3.2 Full chemical speciation using time-based ATR-FTIR spectra of non-aqueous solvents

From in-situ monitoring of a reaction, plenty of chemical information about the reaction can be acquired. However, this information is available as the vibrational bands of the FTIR spectra. Vibrational band assignment of the

spectra was performed to identify the chemical species of the novel solvent system.

Spectroscopic spectra can be considered to be a multivariate output of a sample that consists of an abundance of hidden chemical information. Extracting the spectrum data would be an inexpensive method of chemical speciation. Data preprocessing tools are needed to extract qualitative and quantitative information from a specific spectrum. In this contribution, qualitative information extraction will be discussed.

Vibrational peak assignment was carried out for the changing peaks of the baseline-corrected spectra. The baseline corrected fingerprint region of the IR spectra of unloaded, loaded, and desorbed solvent are shown in Figure 5. Wavenumbers of all the increasing peaks were recognized and assigned to the relevant vibrational groups according to literature. Tabulated peak assignment information is given in Table 2. According to the peak assignment for increasing peaks, we identified the CO₂ capture product of the non-aqueous solvent system to be monomethyl carbonate (MMC) species. A proposed reaction mechanism according to the vibrational assignments has been published [28].

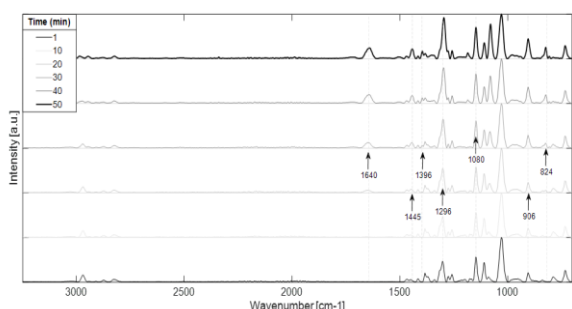


Figure 5: Increasing of the specific peak's intensities with the time during the CO₂ absorption reaction of the non-aqueous DIPA solvent system.

Therefore, in-situ monitoring by ATR-FTIR spectroscopy is a fast-screening method which is able to observe the CO₂ absorption-desorption reaction with full speciation.

Table 3. Monomethyl carbonate (MMC) peak identification of the non-aqueous DIPA system

Characteristic IR vibrational bands ν_{max} (cm ⁻¹)	MMC Peak Assignment	Reference
1640	C=O Stretching vibration	[30] [31]
1443	CH ₃ asymmetric deformation	[30] [31]
1396	CH ₃ symmetric deformation	[30] [31]
1296	O-C-O asymmetric stretching vibration	[30] [31]

1080	O-C-O symmetric stretching vibration	[30] [31]
906	CH ₃ -O stretching	[31]
824	CO ₃ deformation	[31]

However, concluding full chemical reaction speciation by in-situ monitoring in a closed system might have some uncertainties. The concerns on the non-aqueous systems could be two-fold.

1. If the system becomes heterogeneous during the absorption (e.g. phase change) the spectroscopic results will not be accurate
2. If precipitation happens on the ATR crystal the observed spectra may not represent the liquid CO₂ capture solvent.

To address the above-mentioned concerns, bulk analysis of the reaction system was conducted by using the same FTIR instrument with a different reactor set-up.

3.3 On-line bulk liquid flow monitoring of the non-aqueous solvent system to verify the fast-screening results

This experiment was conducted to check the representability of the results of the fast-screening method.

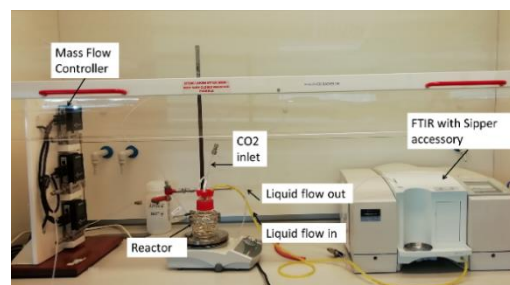


Figure 6: Laboratory arrangement of Set-up2 with a glass reactor

Precipitation on the ATR crystal may lead to analysis error, since the solvent penetration depth of the ATR measurement is very narrow, and the analysis happens at the bottom of the reaction volume. In set-up2 (shown in Figure 6), a glass reactor without an ATR crystal was used to perform the CO₂ absorption reaction. The solvent was continuously circulated through a FTIR flow cell. Therefore, the solvent system bulk was identified thus enabling verification that not solidification or precipitation occurred during the CO₂ absorption reactions.

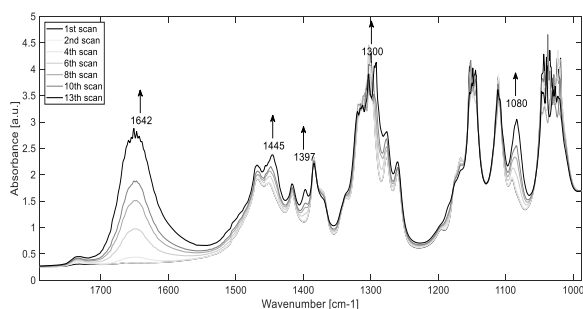


Figure 7: IR spectra obtained from liquid-flow cell measurements during CO₂ absorption experiments

All relevant MMC bands from 1000 cm⁻¹ to 1800 cm⁻¹ were identified by the liquid stream analysis using the liquid-flow cell. However, the band at 824 cm⁻¹ (MMC O-CO₂ deformation) was invisible due to the CaF₂ window material cut-off of the liquid-flow-cell. The obtained results confirmed the fast-screening speciation and showed the representativeness of the fast-screening results of the non-aqueous DIPA CO₂ absorption system.

Conclusion

From in-situ reaction monitoring using set-up1, it is shown that it was possible to obtain a fast and easy chemical characterization of non-aqueous CO₂ capture solvents. The instant observability of the reaction changes at running conditions and the possibility of inexpensive reaction mechanism identification are the main benefits of the set-up1. Furthermore, it is connected to qualitative and quantitative comparability of several solvent systems according to the IR vibrational changes.

The replication experiments using set-up2 confirm the results by addressing some concerns of set-up1. The qualitative results from set-up1 are repeatable and independent of the way of performing the FTIR analysis and the level of solvent mixing. This confirms the capture products are not a solid, gel, or high viscous liquid since the same results were obtained from liquid-flow cell measurements.

Therefore, screening set-up1 is a fast, reliable approach for identification of unknown solvent systems requiring less volume, less time, and less money as compared to traditional solvent analysis methods. Furthermore, representativeness and repeatability of the results was ensured. For non-aqueous amine systems use of an enhanced method like set-up2 is recommended.

Acknowledgements

This work was supported by the Ministry of Education and Research of the Norwegian Government.

References

[1] IPCC, IPCC Special Report on Carbon Dioxide Capture and Storage, Prepared by Working Group III of the

Intergovernmental Panel on Climate Change, in, Cambridge, 2005.

[2] IPCC, Based on Global Emissions From 2010. Details About the Sources Included in These Estimates Can Be Found in the Contribution of Working Group III to the Fifth Assessment Report (AR5) of the Intergovernmental Panel on Climate Change, in, 2014.

[3] IEA, World energy outlook special report on energy and climate change. International Energy Agency (IEA), in, 2015.

[4] G.T. Rochelle, Amine Scrubbing for CO₂ Capture, Science, 325 (2009) 1652-1654.

[5] N. MacDowell, N. Florin, A. Buchard, J. Hallett, A. Galindo, G. Jackson, C.S. Adjiman, C.K. Williams, N. Shah, P. Fennell, An overview of CO₂ capture technologies, Energy & Environmental Science, 3 (2010) 1645-1669.

[6] Y. Wang, L. Zhao, A. Otto, M. Robinius, D. Stolten, A Review of Post-combustion CO₂ Capture Technologies from Coal-fired Power Plants, Energy Procedia, 114 (2017) 650-665.

[7] P. Luis, Use of monoethanolamine (MEA) for CO₂ capture in a global scenario: Consequences and alternatives, Desalination, 380 (2016) 93-99.

[8] R.B. Roberts, U. S. Patent No. 1,783,901, in: D. Washington (Ed.) U. S. Patent and Trademark Office, 1930.

[9] H. Lepaumier, E.F. da Silva, A. Einbu, A. Grimstvedt, J.N. Knudsen, K. Zahlén, H.F. Svendsen, Comparison of MEA degradation in pilot-scale with lab-scale experiments, Energy Procedia, 4 (2011) 1652-1659.

[10] J. Kim, H. Kim, J. Kim, S.J. Hwang, K.S. Lee, Experimental method for simultaneous and continuous measurement of absorption rate, viscosity and heat of reaction of carbon dioxide capture solvents, Journal of Industrial and Engineering Chemistry, 61 (2018) 152-160.

[11] U.E. Aronu, H.F. Svendsen, K.A. Hoff, Investigation of amine amino acid salts for carbon dioxide absorption, International Journal of Greenhouse Gas Control, 4 (2010) 771-775.

[12] P. Brüder, A. Grimstvedt, T. Mejdell, H.F. Svendsen, CO₂ capture into aqueous solutions of piperazine activated 2-amino-2-methyl-1-propanol, Chemical Engineering Science, 66 (2011) 6193-6198.

[13] A. Hartono, A.F. Ciftja, P. Brüder, H.F. Svendsen, Characterization of Amine-impregnated Adsorbent for CCS Post Combustion, Energy Procedia, 63 (2014) 2138-2143.

[14] F.A. Chowdhury, K. Goto, H. Yamada, Y. Matsuzaki, A screening study of alcohol solvents for alkanolamine-based CO₂ capture, International Journal of Greenhouse Gas Control, 99 (2020) 103081.

[15] A. Hartono, S.J. Vevelstad, A. Ciftja, H.K. Knuutila, Screening of strong bicarbonate forming solvents for CO₂ capture, International Journal of Greenhouse Gas Control, 58 (2017) 201-211.

[16] X. Luo, S. Liu, H. Gao, H. Liao, P. Tontiwachwuthikul, Z. Liang, An improved fast screening method for single and blended amine-based solvents for post-combustion CO₂ capture, Separation and Purification Technology, 169 (2016) 279-288.

[17] J. Noroozi, W.R. Smith, Accurately Predicting CO₂ Reactive Absorption Properties in Aqueous Alkanolamine Solutions by Molecular Simulation Requiring No Solvent Experimental Data, Industrial & Engineering Chemistry Research, 59 (2020) 18254-18268.

[18] I.I.I. Alkhatib, M.L. Ferreira, C.G. Alba, D. Bahamon, F. Llovel, A.B. Pereiro, J.M.M. Araújo, M.R.M. Abu-Zahra, L.F. Vega, Screening of Ionic Liquids and Deep Eutectic Solvents for Physical CO₂ Absorption by Soft-SAFT Using Key Performance Indicators, Journal of Chemical & Engineering Data, 65 (2020) 5844-5861.

- [19] Z. Song, X. Hu, H. Wu, M. Mei, S. Linke, T. Zhou, Z. Qi, K. Sundmacher, Systematic Screening of Deep Eutectic Solvents as Sustainable Separation Media Exemplified by the CO₂ Capture Process, *ACS Sustainable Chemistry & Engineering*, 8 (2020) 8741-8751.
- [20] M. Nakaoka, K.V.B. Tran, K. Yanase, H. Machida, K. Norinaga, Prediction of Phase Behavior of CO₂ Absorbents Using Conductor-like Screening Model for Real Solvents (COSMO-RS): An Approach to Identify Phase Separation Solvents of Amine/Ether/Water Systems upon CO₂ Absorption, *Industrial & Engineering Chemistry Research*, 59 (2020) 19020-19029.
- [21] M.H.W.N. Jinadasa, K.-J. Jens, L.E. Øi, M. Halstensen, Raman Spectroscopy as an Online Monitoring Tool for CO₂ Capture Process: Demonstration Using a Laboratory Rig, *Energy Procedia*, 114 (2017) 1179-1194.
- [22] M. Akram, M.H.W.N. Jinadasa, P. Tait, M. Lucquiaud, K. Milkowski, J. Szuhanski, K.-J. Jens, M. Halstensen, M. Pourkashanian, Application of Raman spectroscopy to real-time monitoring of CO₂ capture at PACT pilot plant; Part 1: Plant operational data, *International Journal of Greenhouse Gas Control*, 95 (2020) 102969.
- [23] M. Halstensen, H. Jilvero, W.N. Jinadasa, K.-J. Jens, Equilibrium Measurements of the NH₃-CO₂-H₂O System: Speciation Based on Raman Spectroscopy and Multivariate Modeling, *Journal of Chemistry*, 2017 (2017) 7590506.
- [24] F. Diab, E. Provost, N. Laloué, P. Alix, V. Souchon, O. Delpoux, W. Fürst, Quantitative analysis of the liquid phase by FT-IR spectroscopy in the system CO₂/diethanolamine (DEA)/H₂O, *Fluid Phase Equilibria*, 325 (2012) 90-99.
- [25] A. Einbu, A.F. Ciftja, A. Grimstvedt, A. Zakeri, H.F. Svendsen, Online Analysis of Amine Concentration and CO₂ Loading in MEA Solutions by ATR-FTIR Spectroscopy, *Energy Procedia*, 23 (2012) 55-63.
- [26] A. Grimstvedt, M. Wiig, A. Einbu, S.J. Vevelstad, Multi-component analysis of monethanolamine solvent samples by FTIR, *International Journal of Greenhouse Gas Control*, 83 (2019) 293-307.
- [27] G. Richner, G. Puxty, Assessing the Chemical Speciation during CO₂ Absorption by Aqueous Amines Using in Situ FTIR, *Industrial & Engineering Chemistry Research*, 51 (2012) 14317-14324.
- [28] J.D. Wagaarachchige, Z. Idris, N.B. Kummamuru, K.A.S. Sætre, M. Halstensen, K.-J. Jens, A new sulfolane based solvent for CO₂ capture, in: 15th International Conference on Greenhouse Gas Control Technologies, GHGT-15, 15th 18th March 2021 Abu Dhabi, UAE, 2021.
- [29] C. Wagner, K.H. Esbensen, Theory of Sampling: Four Critical Success Factors Before Analysis, *Journal of AOAC INTERNATIONAL*, 98 (2019) 275-281.
- [30] G. Socrates, *Infrared and Raman Characteristic Group Frequencies: Tables and Charts*, 3rd ed., Wiley, 2004.
- [31] W. Behrendt, G. Gattow, M. Dräger, Über Chalkogenolate. LXI. Untersuchungen über Halbester der Kohlensäure. 1. Darstellung und Eigenschaften von Monomethyl- und Monoäthylcarbonaten, *Zeitschrift für anorganische und allgemeine Chemie*, 397 (1973) 237-246.

Article 7

Application of Multivariate Data Analysis of Raman Spectroscopy Spectra of 2-oxazolidinone

Federico Mereu^{1,3} Jayangi D. Wagaarachchige² Klaus-J. Jens³ Zulkifli Idris³

¹Department of Civil and Environmental Engineering, Politecnico di Milano, Piazza Leonardo
da Vinci 32, Milano, Italy

²Department of Electrical, IT and Cybernetics, University of South-Eastern Norway,
Porsgrunn, Norway

³Department of Process, Energy and Environmental Technology, University of South-Eastern
Norway, Porsgrunn, Norway

Published in Proceedings of SIMS EUROSIM 2021

<https://doi.org/10.3384/ecp2118516>

Application of multivariate data analysis of Raman Spectroscopy spectra of 2-oxazolidinone

Federico Mereu^{1,2} Jayangi D. Wagaarachchige³ Klaus-J. Jens² Zulkifli Idris^{2,*}

¹Department of Civil and Environmental Engineering, Politecnico di Milano, Piazza Leonardo da Vinci 32, 20133 Milano, Italy

²Department of Process, Energy and Environmental Technology, University of South-Eastern Norway, Kjølnes Ring 56, 3918 Porsgrunn, Norway

³Department of Electrical, IT and Cybernetics, University of South-Eastern Norway, Kjølnes Ring 56, 3918 Porsgrunn, Norway

*corresponding author: zulkifli.idris@usn.no

Abstract

Chemical absorption of carbon dioxide (CO₂) using amine solution is considered as the readiest technology available for capturing CO₂ gas from industrial processes. The well-known amine for this process is 2-aminoethanol (MEA) which is normally mixed with water to a typical concentration of 30 wt%. MEA degrades over time producing non-reactive chemicals such as 2-oxazolidinone (OZD) due to exposure to impurities and high process temperature. It is thus important to find a suitable method for OZD qualification and quantification. In this work, we approach this challenge by means of Raman spectroscopy and multivariate data analysis. We started by collecting Raman spectra of 40 OZD samples and applying Principal Component Analysis to study these samples.

Keywords: multivariate data analysis, MEA, Raman spectroscopy, CO₂ capture, degradation

1 Introduction

Due to the economic development and the subsequent increase in world population, the global demand for energy will continue to rise in the following decades. The dependence on fossil fuels, the primary source of energy, emitting copious amount of CO₂, is the main cause of global warming. Even if large investments are underway to decarbonise the world energy production, renewable electricity may not be suitable for certain applications, such as the cement, iron and steel, and chemical sectors.

Carbon capture and storage (CCS) and its ability to avoid CO₂ emissions at their source, represents a solution in the fight against climate change. Among all the different alternatives, post-combustion capture by using amine-based solvent is considered to be the most advanced technology (Sexton and Rochelle, 2011). This process relies on the ability of the amine solution to chemically react with CO₂ in the flue gas. The best absorbents are the ones with high net cyclic capacity, fast reaction with CO₂, low heat of reaction, high chemical stability, low vapor pressure and minimally corrosive (Hartono et al., 2017). Of

the many solvents tested, 2-aminoethanol (MEA) is the most used due to its good operational properties and relatively low price. The solvent used in operating plants simply consists of water and amines, whose concentration is usually made based on operating experience (typical concentration range values goes from 12% wt to a maximum of 32% wt (Kohl and Nielsen, 1997)).

A typical chemical absorption process for CO₂ capture plant is shown in Figure 1.

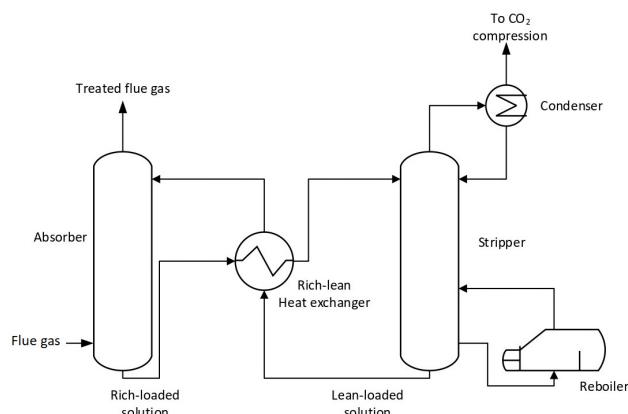
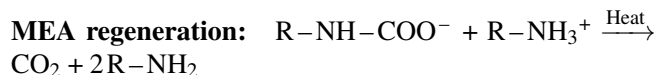
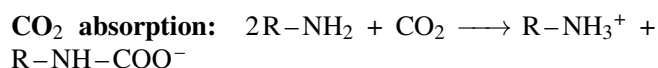


Figure 1. Schematic of a chemical absorption process for CO₂ capture.

After a preliminary purification from NO_x, SO_x, and particulate matter, the flue gas enters the absorber. Through contact with MEA solvent, part of CO₂ in the flue gas is absorbed into amine solution, forming a weakly bonded and quite stable compound, carbamate. The scrubbed gas is then washed with water to remove the solvent and discharged into the atmosphere. Then, the rich-loading solvent (with absorbed CO₂) passed through a cross-heat exchanger and pumped up to the head of the stripper. In the stripper, the high temperature and pressure generated by a reboiler cause the carbamate to dissociate back to MEA and CO₂. The obtained product stream with high CO₂ purity is conveyed to compression for trans-

portation to storage sites. At the bottom of the stripper, the high temperature lean-loading is conveyed to a heat exchanger to decrease the temperature of the lean-loading solution before entering the absorber again.

The entire process chemistry is complex, and the two main reactions taking place in the absorber and the stripper are:



For simplicity, MEA is expressed by R-NH₂, where R stands for OH-CH₂-CH₂. The first reaction shows that only half a mole of CO₂ is absorbed per mole of MEA, leading to the formation of carbamate. In the second equation, under the application of heat, the carbamate dissociates to give back CO₂ and amine sorbent.

However, there is a main problem associated with this process, which is degradation of the solvent caused by heat exposure and impurities in the exhaust gas. This leads to foaming, fouling, increased viscosity, corrosion and formation of different degradation compounds that are unreactive towards CO₂. In the case of MEA, one of the main degradation products is 2-oxazolidinone (OZD), a heterocyclic five-membered ring organic compound, which formation pathway is shown in Figure 2.

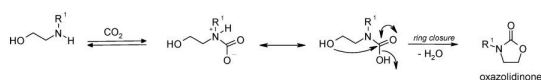


Figure 2. Oxazolidinones formation (R¹, R²: H, alkyle) (Lepaumier et al., 2009).

The formation of OZD starts with a reaction between MEA and CO₂, which leads to the formation of carbamate complex, as shown in the first equation above. Elimination of a water molecule from the carbamate complex during a ring closure reaction yields an OZD molecule. The formation of OZD is a problem because it is unstable and will react giving other degradation products (namely HEEDA, HEIA, AEHEIA, BHEI (Gouedard et al., 2012)) that must be purged from the system to prevent their build-up.

For this purpose, it is essential to find a procedure for the conversion of the molecule to its precursor amine. This requires a preliminary identification and quantification step.

Raman spectroscopy is a valuable technique for qualitative and quantitative analyses, since there is a relationship between intensity of the Raman band, chemical information and the concentration of a sample being analyzed (Larkin, 2011). Raman spectrums are generally plotted as intensity against Raman Shift (or wavenumber). Vibrations of functional groups of a molecule appear in a Raman spectrum at characteristic Raman shift, which is similar for all molecules containing the same functional group.

Chemometric multivariate analysis is an advanced statistical method that can be used to extract this huge information by building specific model for specific chemical species.

The approach in this paper started with the analysis of OZD samples at different concentrations using Raman spectrometer. Principal component analysis (PCA) was then performed on these samples to check for any outliers, relevant peaks for OZD, and monitor changes in the OZD at different concentrations.

2 Materials & Methods

2.1 Sample preparation and Raman analysis

The first big part of this work consisted of sample preparation. Stock solution of OZD was prepared dissolving 2-Oxazolidinone (Sigma-Aldrich, purity 98%) in Milli-Q® water (18.2 MΩ ·cm at 25°C). Samples of increasing concentration from 5 to 815 mM were then prepared by diluting the stock solution in distilled water.

The amount of OZD and water needed were weighted using a Mettler-Toledo MS 105 balance.

The Raman scans were taken using a Kaiser Raman Rxn2 analyzer of 785 nm laser wavelength, 400 mW laser power and 150-3425 cm⁻¹ spectral range. In a typical experiment, a vial containing OZD solution was placed inside a black sample holder to avoid light disturbance and the top part of the sample holder was also covered with aluminum foil to further reduce any possible disturbance from fluorescence of external light sources. A fiber-optic immersion probe (optic of ¼ inch) from Kaiser Optical Systems Inc. was used for the measurement. To avoid contamination, the probe was first washed with deionized water followed by acetone before each measurement to remove any possible impurities/leftovers on the probe tip. The Raman probe was kept at the same depth and same temperature (20 °C) for all the measurements to ensure consistency and to avoid changes of acquisition background. In order to improve sample sensitivity for off-line analysis of each measurement, maximum laser power (400 W) was used with exposure time of 30 seconds and an average of six scans. iC Raman software from Kaiser Optical Systems Inc. was used for the acquisition of the spectra.

2.2 Principal Component Analysis (PCA)

PCA is a data simplification technique used in multivariate statistics. The aim of the technique is to reduce the high number of variables describing a set of data to a smaller number of compressed variables, called Principal Components, PCs, which describe the variation and structure of the data. The PCs can then be plotted to visualize the relationship between samples and variables through the use of scores (which describe the relationship between observations) and loading plots (which show the relationship of the variables) (Wold et al., 1987).

The data is seen as a matrix, called data matrix or X

matrix, composed by n objects (samples) and p variables (the measurement for each object) (Esbensen, 2012). This data matrix can be represented in a Cartesian co-ordinate system of dimension p . Considering the first variable, X_1 , its entries can be plotted along a 1-dimensional axis. This approach can be extended considering the next variable, X_2 , resulting in a 2-dimensional plot and so on, until all p variables are covered. This p -dimensional co-ordinate system is the variable space.

To better understand, it is assumed an X matrix with n objects and 3 variables. Its variable space will be composed by 3 axes: one for each variable. And for each object in the variable space, its x -value will be plotted, meaning that all the objects can be as a point in the variable space. When all the points are plotted, the result is a swarm of points. It is then possible to recognize a linear behaviour, which can be described by a line that lies along the direction of maximum variance in the data set, called the first Principal Component, PC1. Further PCs can be plotted; the second principal component will lie along the direction of the second largest variance, and it will be orthogonal to the first PC. The third PC will be orthogonal to both PC1 and PC2, lying along the direction of the third largest variance and so on for the subsequent PCs. This PCs system will constitute a new coordinate system, where each PC will represent successively smaller and smaller variances. The PCs are uncorrelated with each other since they are mutually orthogonal.

There are two main parameters used in PCA: loadings and scores. The loadings are coefficient of linear combination for each PC, namely p_{ka} , where k is the index for p variables and a is the index for principal component direction coefficients. All the loadings constitute a matrix, P , which expresses the transformation between the initial variable space and the new space formed by the PCs. These loading vectors, namely the columns in P , are orthogonal. In synthesis, loadings describe the relationship between the initial p variables and the PCs.

The score is the distance between the object and its projection into the PC, and it is called score for object i , t_{i1} , if it refers to PC1. The projection of object i onto PC2 will give the score t_{i2} , and so on. The projected object i will correspond to a point in the new co-ordinate system, an A -dimensional surface. Each object will thus have its own set of scores in this dimensionality-reduced subspace. The NIPALS (Nonlinear Iterative Partial Least Squares) algorithm (Wold, 1966) is one of the several methods used to find the score and loading vectors. In this study, NIPALS algorithm was applied when using PLS toolbox with MATLAB® software.

3 Results & Discussion

3.1 Pre-processing of raw spectra

Raw spectra from 40 different OZD samples in water at different concentration are shown in Figure 3.

The raw spectra contain important information on

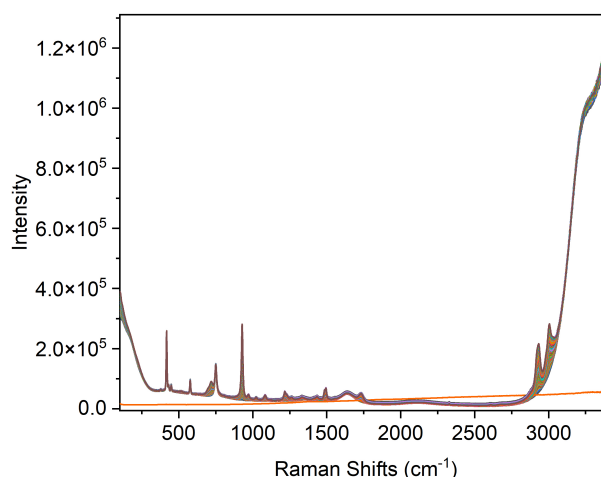


Figure 3. Raman raw data of the 40 analysed samples.

chemical fingerprints of the samples but also noise from background and instrument. Pre-processing of the raw spectra can be applied to extract useful information and to remove offset and irrelevant signals.

The raw spectra were subjected to a baseline correction technique by applying Automatic Whittaker filter with lambda equals to 100 and P equals to 0.001. The Whittaker filter used is an extended version of Eilers, 2003, available in the PLS toolbox in MATLAB, where a weighted least square method was applied to remove baseline variations and background noise. The factor lambda controls the curvature allowed for the baseline, while the P factor governs the extent of asymmetry required of the fit (Eilers, 2003).

Baseline corrected spectra of OZD samples are shown in Figure 4. As can be seen, as the concentration of OZD increases, the intensity values of some peaks also increase, suggesting that OZD concentration is proportional to the peak intensity, according to the Beer-Lambert law.

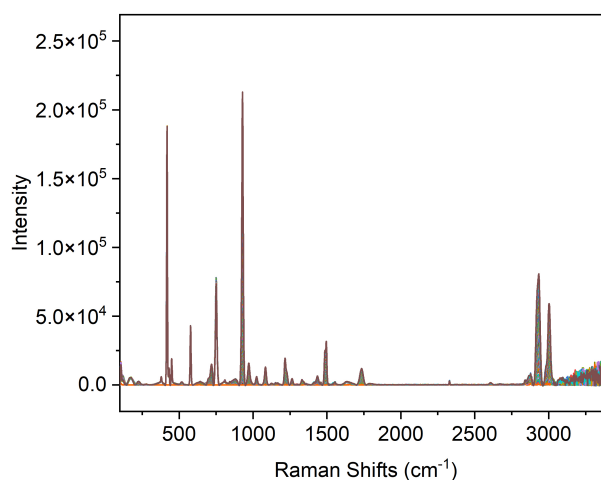


Figure 4. Baseline corrected Raman spectra of the 40 analysed samples.

The peaks that change according to changes in the OZD

concentration are now easily identified and their signals and band assignments are listed in Table 1.

Observed frequency [cm^{-1}]	Vibrational mode
719	C-C stretch
928	C-C stretch
1083	C-H ₂ rock
1216	C-H ₂ twist
1333, 1261	C-H ₂ wag
1436	C-H ₂ scissor
1495	C'-N stretch; C=O stretch
1733	C=O stretch
2932	C-H ₂ symmetric stretch
3003	C-H ₂ asymmetric stretch

Table 1. Vibrational assignments of OZD (McDermott, 1986) (C' = carbonyl carbon).

All the band assignments were referenced to earlier work from McDermott (1986) from the spectra of γ -butyrolactone and 2-pyrrolidinones, which are cyclic esters, like 2-oxazolidinone.

There are also strong peaks at wavelengths 418, 577, and 750 cm^{-1} that do not change according to the changes in OZD concentration and these peaks can be assigned to the noise from the Raman instrument. These peaks were also seen previously in earlier publication from Jinadasa (2019).

Concerning water, its characteristic peaks are cut off from the range of interest, since it usually shows bands below 300 cm^{-1} corresponding to the hydrogen bond bending and stretching motions and strong bands above 3000 cm^{-1} typical of the O-H stretching region; the low intensity peak at 1650 cm^{-1} arises from the intramolecular bending motion (Franks, 1972).

3.2 Initial PCA Analysis

Using the whole spectra as a starting point, the pre-processed OZD spectra were then subjected to initial PCA analysis. Figure 5 illustrates the cumulative variance of the PCA model. PC1 is defined as the first principal component which relates to the maximum variance of the data, while PC2 is the second principal component which corresponds to the second largest variance. The number of PCs corresponds to the number of orthogonal variables in the spectral data set. As can be seen, PC1 explains 92.58% of the total variance, while PC2 describes an additional 6.88%. These two PCs make up 99.46% of the variation in the model, suggesting that they are probably sufficient to determine the most important variables for the description of OZD samples.

In Figure 6, a score plot of PC1 versus PC2 for the pre-processed OZD spectra is shown. The dotted circle represents a 95% confidence level. As can be seen, one of the samples is outside the area of interest meaning that this sample is most likely an outlier. By checking the raw spectra of OZD samples, this sample is confirmed to be an

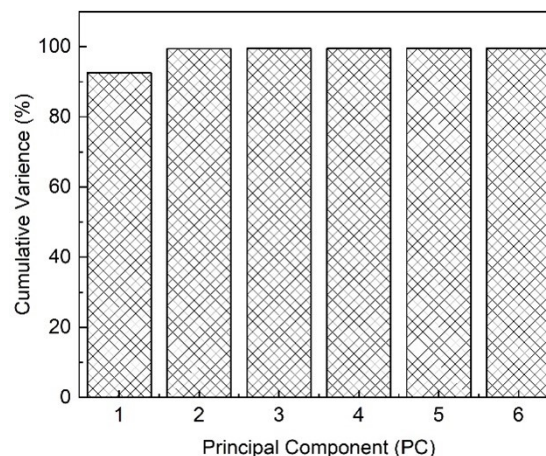


Figure 5. Cumulated percentage variation explained.

outlier and it is probably coming from an error when using the Raman instrument. The outlier was thus removed.

The pre-processed OZD spectra as shown in Figure 4 also show some noise in the region of $>3000 \text{ cm}^{-1}$ Raman shift and this region was also removed in the next PCA analysis.

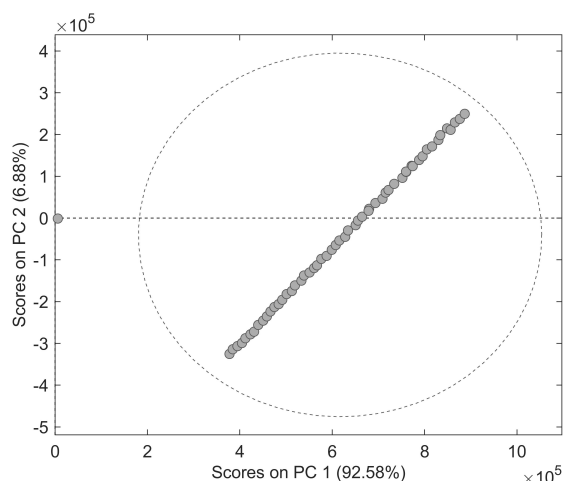


Figure 6. PCA analysis for preprocessed Raman data, first score plot of PC1 vs PC2.

The loading plot for PC 1 for the PCA model is shown in Figure 7. As mentioned by Wold et al. (1987), loading plots define what a principal component represents. The higher the loading value, the higher the contribution of the variable to the PC. In the case of this work, these plots will represent OZD concentrations in the samples. Figure 7 indicates that significant contribution comes from peaks at 418, 577, and 750 cm^{-1} . These peaks however do not correspond to OZD or water, and thus most likely coming from the instrument. The fact that these peaks have higher loading values even though they do not really represent the actual components in the samples necessitates further correction to the PCA model. These peaks were therefore excluded from the model.

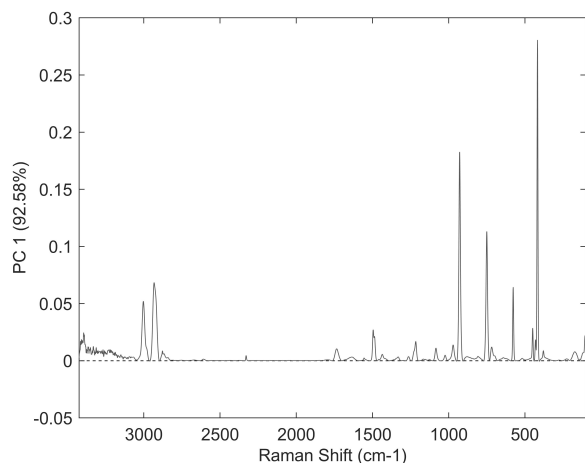


Figure 7. Loading plot for PC1.

3.3 Optimized PCA with Variable Selection

Based on earlier considerations, the PCA model was recalibrated, and Figure 8 displays the new cumulative variance of the model. PCA model was recalibrated by selecting the variable range of OZD to optimize the PC1, which mainly describes the OZD concentration variation.

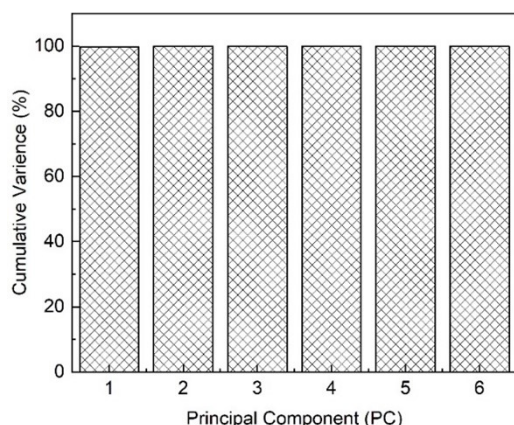


Figure 8. Cumulated percentage variation for different principal components.

The new score plot is shown in Figure 9. Based on the figure, PC1 and PC2 account for 99.78 and 0.17% of the model variance, respectively. These two principal components already make up 99.95% of the cumulative variance for the model suggesting that it is very likely that the OZD changes are sufficiently described by PC1.

With the elimination of outliers, all samples are now at 95% confidence level. Values of PC1 are always positive, whilst values of PC2 change from positive to negative for all the samples. The samples also show a linear trend suggesting that there is a linear trend between Raman intensity and OZD concentration and that the PCA model can be used to classify OZD.

The loading plot for PC1 is illustrated in Figure 10. According to the plot, the sharp OZD peak at 928 cm^{-1}

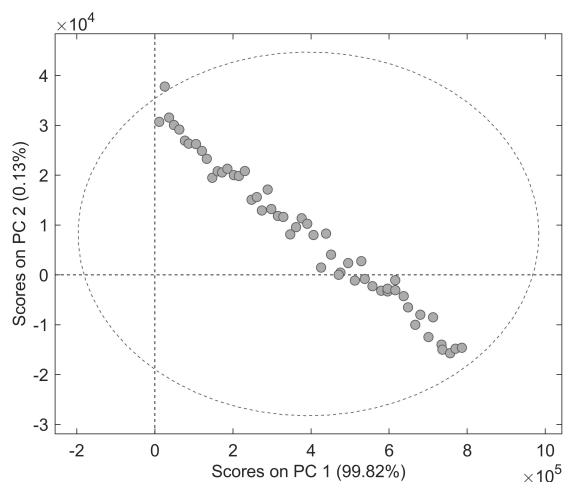


Figure 9. PCA analysis for preprocessed Raman data, score plot of PC1 vs PC2 after removal of variables below 650 cm^{-1} .

gives the highest contribution to PC1. This indicates that this peak can be used as an indicator for the presence or changes in OZD concentration in a sample. Other peaks that positively contribute to PC1 loading plot include $3003, 2933, 1736, 1496,$ and 720 cm^{-1} and these peaks are observed as relevant functional group peaks for OZD, as shown in Table 1.

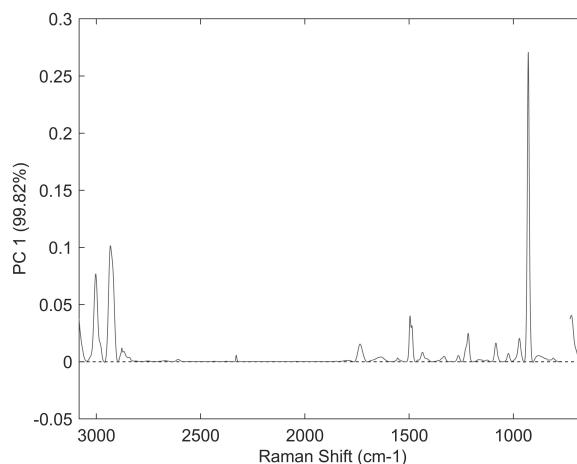


Figure 10. Loading plot for PC1 with variable selection.

4 Conclusion

This paper aims to analyze Raman spectra of 2-oxazolidinone samples by using Principal Component Analysis to detect relevant peaks, monitor changes in the samples at different concentrations and remove outliers.

After spectra acquisition and a preliminary baseline correction, the data were subjected to PCA analysis. The first two PCs, which made up 99.46% of the variation in the model, were considered for the analysis. After that, outlier removal was performed and the PCA model was recalibrated by selecting relevant variable range of OZD

to optimize PC1, which describes the OZD concentration variation. With these considerations, the two PCs made up 99.95% of the cumulative variance, an increase of 0.49 percentage point.

Finally, according to the loading plot for PC1, it was found out that the sharp OZD peak at 928 cm^{-1} gave the highest contribution to PC1, indicating that this peak can be used as an indicator for the presence or changes in OZD concentration in a sample.

By using PCA, we have shown in this work that we can systematically identify with precision any outliers, relevant peaks for OZD, and monitor changes in the OZD at different concentrations.

References

- Paul H. C. Eilers. A perfect smoother. *Analytical Chemistry*, 75(14):3631–3636, 2003. doi:10.1021/ac034173t. PMID: 14570219.
- K. H. Esbensen. *Multivariate data analysis in practice: an introduction to multivariate data analysis and experimental design*. 5th ed. edition, 2012. ISBN 978-8299333030.
- Felix Franks. *The Physics and Physical Chemistry of Water*. Springer New York, 1972. ISBN 978-1-4684-8336-9 978-1-4684-8334-5. doi:10.1007/978-1-4684-8334-5.
- C. Gouedard, D. Picq, F. Launay, and P.L. Carrette. Amine degradation in CO₂ capture. i. a review. *International Journal of Greenhouse Gas Control*, 10:244–270, 2012. doi:https://doi.org/10.1016/j.ijggc.2012.06.015.
- Ardi Hartono, Solrun Vevelstad, Arlinda Ciftja, and Hanna Knuutila. Screening of strong bicarbonate forming solvents for CO₂ capture. *International Journal of Greenhouse Gas Control*, 58:201–211, 2017. doi:https://doi.org/10.1016/j.ijggc.2016.12.018.
- M.H. Wathsala N. Jinadasa. *Process analytical technology for real-time quantitative speciation of aqueous phase CO₂ capture solvents*. PhD thesis, University of South-Eastern Norway, 2019.
- Arthur L. Kohl and Richard B. Nielsen. *Gas Purification*. Gulf Professional Publishing, fifth edition, 1997. ISBN 978-0-88415-220-0. doi:https://doi.org/10.1016/B978-088415220-0/50002-1.
- Peter Larkin. *Infrared and Raman Spectroscopy*. Elsevier, 2011. ISBN 978-0-12-386984-5. doi:10.1016/B978-0-12-386984-5.10001-1.
- Helene Lepaumier, Dominique Picq, and Pierre-Louis Carrette. New amines for CO₂ capture. i. mechanisms of amine degradation in the presence of CO₂. *Industrial & Engineering Chemistry Research*, 48(20):9061–9067, 2009. doi:10.1021/ie900472x.
- Dana P. McDermott. Vibrational assignments and normal-coordinate analyses of γ -butyrolactone and 2-pyrrolidinones. *The Journal of Physical Chemistry*, 90(12):2569–2574, 1986. doi:10.1021/j100403a006.
- Andrew J. Sexton and Gary T. Rochelle. Reaction products from the oxidative degradation of monoethanolamine. *Industrial & Engineering Chemistry Research*, 50(2):667–673, 2011. doi:10.1021/ie901053s.
- H. Wold. Estimation of principal components and related models by iterative least squares. *Multivariate analysis*, pages 391–420, 1966.
- Svante Wold, Kim Esbensen, and Paul Geladi. Principal component analysis. *Chemometrics and Intelligent Laboratory Systems*, 2:37–52, 1987. doi:https://doi.org/10.1016/0169-7439(87)80084-9.

Article 8

Response Surface Modelling to Reduce CO₂ Capture Solvent Cost by Conversion of OZD to MEA.

Federico Mereu¹, Jayangi D. Wagaarachchige¹, Maths Halstensen¹, Zulkifli Idris¹, Klaus-J.
Jens¹

¹University of South-Eastern Norway, Porsgrunn, Norway

Published in Proceedings of SIMS 2023

<https://ecp.ep.liu.se/sims>

Response Surface Modelling to Reduce CO₂ Capture Solvent Cost by Conversion of OZD to MEA

Federico Mereu ^a, Jayangi D. Wagaarachchige ^a, Maths Halstensen ^a, Zulkifli Idris ^a, Klaus-J. Jens ^{a, *}

^a University of South – Eastern Norway, Kjølnes ring 56, 3918 Porsgrunn, Norway
Klaus.J.Jens@usn.no

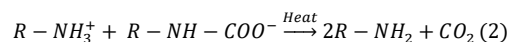
Abstract

The increasing CO₂ concentration in the atmosphere is the most urgent global challenge. The most mature CO₂ abatement option is post-combustion CO₂ capture employing Monoethanolamine (MEA) solvent. One challenge of using MEA is its in-service degradation to 2-oxazolidinone (OZD), a heterocyclic five-membered organic ring compound. Furthermore, OZD degrades more MEA leading to CO₂ capture solvent loss and hence increased operational cost. It is therefore of interest to investigate methods to convert OZD back to MEA. This work reports the conversion of 2-oxazolidinone to MEA by heat treatment at an alkaline condition. Raman spectroscopy and Ion-Exchange chromatography were applied to qualify and quantify the reaction. The optimal reaction parameters were identified by an experimental design model using the Response Surface Methodology (RSM). A second-order model with three variables and five levels of focus was employed, with the OZD conversion percentage as the response. This methodology was chosen because such a model could estimate the main effects, interactions and quadratic terms by relying on a relatively small number of experiments. 17 experimental runs were designed by the software using this method. At a reaction time of 35 minutes, reaction temperature of 100°C, and 2.5 mole of hydroxide per mole of OZD resulted in a complete conversion of OZD to MEA.

1. Introduction

Carbon dioxide capture and storage (CCS) is so far considered the most promising technology to sequester CO₂ from large emission point sources (Rochelle, 2009). Post-combustion carbon capture (PCC) gas-liquid chemical adsorption is the predominant CCS technology today because of the development status (*US Department of Energy*, 2017) and that it can be retrofitted to existing CO₂ emitting plants.

Aqueous 30 wt% Monoethanolamine (MEA) is one of the most investigated CO₂ absorption solvents due to its good operational properties and relatively low price (Kohl & Nielsen, 1997; Buvik, 2021). Figure 1 shows the typical CO₂ absorption-desorption process scheme. The flue gas enters the absorber bottom after pre-treatment and flows upwards while the solvent solution e.g., aqueous 30 wt% MEA moves downwards in counter flow. Through a contact of these two streams, the CO₂ flue gas content is absorbed into the amine solution, forming mainly amine carbamate (equation (1)) which can release CO₂ upon heating to 120-140°C in the process stripping section according to equation (2) (Eimer, 2014). For simplicity, MEA is expressed by R-NH₂, where R stands for a -CH₂-CH₂OH group.



However, aqueous MEA solvent has a high energy need in the solvent regeneration section and it is degrading in service due to contact with air in the absorption section and high temperature in the stripping section of the process (Fredriksen & Jens, 2013). These degradation reactions reduce solvent absorption capacity. Furthermore, these degradation products have to be removed and replaced with fresh MEA solvent which adds to operational cost. This degradation (reclaimer waste) varies in the range of 0.1-14.9 kg waste /ton CO₂ captured (IEAGHG, 2014).

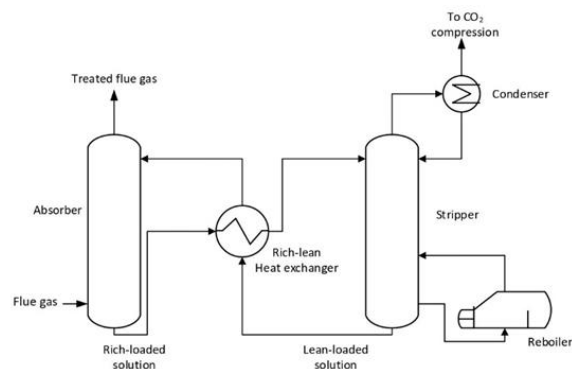


Figure 1: Basic schematic diagram of the chemical absorption-desorption CO₂ capture process.

The first step of thermal MEA degradation is the formation of oxazolidone (Davis & Rochelle, 2009; Dyen & Swern, 1967; Poldermann et al., 1955) from the reaction of MEA with CO₂. Several patents (Miller, 1985; Pottiez & Verbeest, 1972; Snoble, 1981; Turoff et al., 2008) claim hydrolytic alkaline splitting of the alkanolamine derived oxazolidone back to the original alkanolamine and carbonate anion as shown in Figure 2.

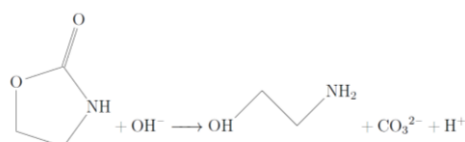


Figure 2: Reaction for Splitting of oxazolidone by alkali to MEA and a carbonate anion.

It is therefore desirable to understand the optimum reaction conditions for splitting of oxazolidone type thermal degradation products back to the original CO₂ capturing alkanolamine. Hence, this work determines optimal reaction conditions for splitting of oxazolidone by Design of Experiment utilizing the Response Surface Methodology (RSM) (Myers et al., 2016). Furthermore, a process integration concept into a CO₂ capture plant is proposed.

2. Methodology

2.1 Design of Experiments

A screening design (Eriksson et al., 2008; Esbensen & Swarbrick, 2017) was used to identify the most important parameters, thus reducing the number of experiments needed. For the optimization experiments, a Central Composite Design (Eriksson et al., 2008; Esbensen & Swarbrick, 2017) was used to vary the parameters at 5 levels as indicated in Figure 3.

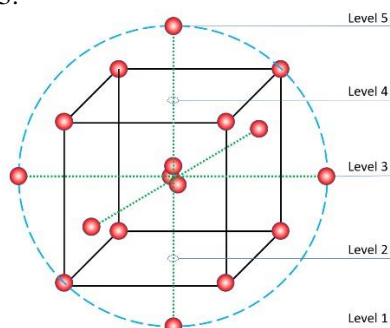


Figure 3. Central composite design with three center samples resulting in 17 experiments. The 5 different levels of the vertical variable are indicated.

The optimal reaction parameters were identified by an experimental design model using the RSM provided by the JMP software.

2.2 Chemicals

Chemicals were used as received and are summarized in Table 1. All aqueous solutions were prepared with Milli-Q® water (18.2 MΩ·cm at 25°C).

Table 1. Chemicals used in the experiments.

Chemical name	CAS number	Supplier	Mole Fraction purity (%)
Ethanolamine	141-43-5	EMSURE	≥ 99.5
2-Oxazolidinone	497-25-6	Sigma-Aldrich	98
Sodium carbonate	497-19-8	Sigma-Aldrich	99.9

2.3. Chemical Analysis

Cation chromatography and Raman spectroscopy were used to determine the reference concentrations.

2.3.1 Cation chromatography

The samples were analyzed by a Dionex 5000 Cation chromatograph controlled by Chromeleon® software and equipped with a Dionex IonPac CS16 2 mm column. The eluent was methanesulfonic acid run at a gradient method (Table 2) and a constant flow rate of 0.5 mL/min at 60°C temperature. Samples were diluted with 0.3 ppm Li⁺ containing Milli-Q water (internal standard) to a factor of 900 and filtered before injection using a 0.2 mm syringe filter.

Table 2. Eluent gradient concentrations

Time [min]	Concentration [mM]
0	6
13	8
25	55
30	60
32	60
34	6
40	0

2.3.2 Raman spectroscopy.

The spectra were acquired with a RXN2 Raman spectrometer fitted with a 785nm laser delivered by Kaiser Optical Systems Inc. The samples were placed inside a black sample holder covered with an aluminium foil to suppress background light and were measured using a fiber optic immersion probe. The probe was washed with deionized water

followed by acetone before each measurement. The analysis exposure time was 30 seconds with 6 scans for each sample. A blank water sample preceded each analysis run. All Raman spectra were baseline corrected using the Whittaker filter (Eilers, 2003; Whittaker, 1922) (available in PLS toolbox in the MATLAB @software suite) before further processing.

2.4 Oxazolidone (or 2-Oxazolidinone) splitting experiment.

The experimental set-up is shown in Figure 4. A sample of aqueous 3M oxazolidone stock solution and NaOH pellets or 0.1M NaOH solution was placed in a flask connected to a reflux condenser and heated under stirring to a pre-determined temperature and time. The pH of the reaction mixture was monitored by a pH electrode.

In a typical experiment, 25g 3M aqueous oxazolidone solution was titrated with 0,1 M NaOH solution using a Mettler Toledo T50 titrator pH 14 or a total solution volume of 80 ml whatever happened first. The latter produced a pH value of 12.4 at 80 ml solution. The solution was heated to 110°C for a few minutes, cooled to room temperature and analyzed for oxazolidone conversion by Raman spectroscopy. An alternative typical experiment of the above procedure substituted the 0.1 M NaOH solution by anhydrous NaOH pellets followed by water dilution to pH14. The aqueous dissolution of NaOH pellets is an exothermic process. Hence, the reaction solution was cooled to room temperature before Raman spectroscopic analysis.

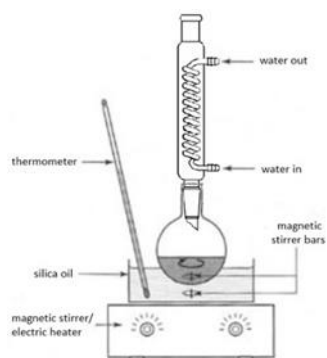


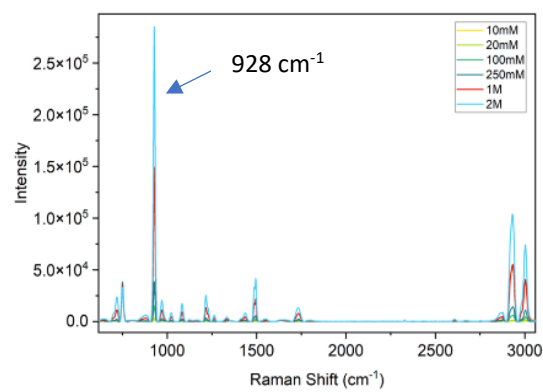
Figure 4: Experimental set-up

3. Results and Discussions

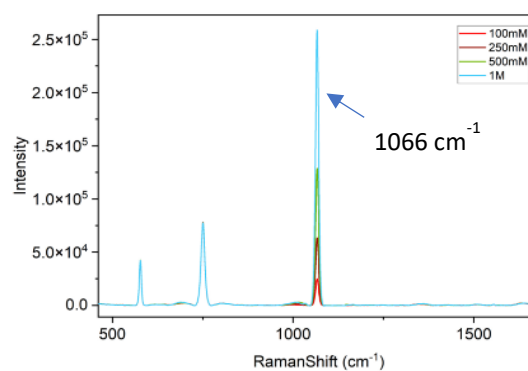
3.1. Chemical Calibration for MEA and OZD Quantification

Concentrations of OZD were quantified using Raman Spectroscopic analysis. The spectral peaks of oxazolidone at 928 cm^{-1} (Figure 5 (a)) (ref: McDermott (1986)) and of Na_2CO_3 at 1066 cm^{-1}

(Figure 5 (b)) were chosen for subsequent qualitative and quantitative analysis.



(a)



(b)

Figure 5: (a) Raman spectra of oxazolidone (b) sodium carbonate at various concentrations

Cation chromatography was then used for the quantification of MEA. The MEA peak was identified in the chromatogram (Figure 6) by spiking it with an authentic MEA sample. Quantitative analysis was based on a calibration curve in the appropriate concentration range.

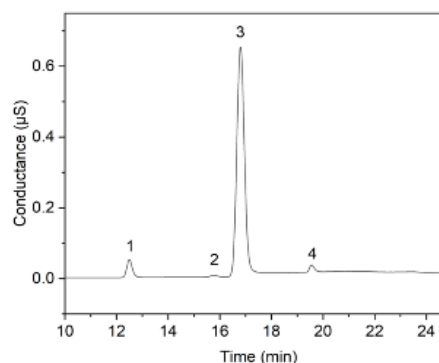


Figure 6: MEA chromatogram: MEA (3); Na⁺ (1); NH₄⁺ (2); K⁺ (4).

3.2 Optimization of conversion of OZD to MEA

3.2.1 Phase 1

screening investigations. The initial experiments in this phase verified oxazolidone splitting to MEA. As a preliminary study to verify the conversion of OZD to MEA, four tests were carried out using the alternative typical experiment procedure with solution reflux at 120°C and 2 hour duration (Table 3).

Table 3: Parameters for the oxazolidone (OZD) splitting experiment

Experiment	OZD conc. [mM]	OH ⁻ /OZD	Temp. [°C]	Time [min]
3	200	28	90	100
4	400	14	140	60
5	600	12	100	120
6	80	73	130	30

Three parameters were identified based on the initial screening experiments. The parameters were varied at two levels and three parameters were identified. Reaction time, reaction temperature, and the relationship between mole of hydroxide per mole of OZD were all found as the most significant contributors to the conversion of OZD to MEA.

3.2.1 Phase 2

Optimization model for OZD conversion percentage. In phase 1, 3 three variables were chosen for the second phase: temperature (°C), time (min), and OH⁻/OZD molar ratio. The Response Surface Methodology was chosen because it can fit a second-order polynomial model that estimates main effects, interactions, and quadratic terms relying on a relatively small number of runs. The quadratic terms are useful because they can capture a possible curvature in the relationship between the response and the experimental factors. The three main variables are represented by the coefficients A, B, and C; the three two-way interactive terms are described by AB, AC, and BC; the three quadratic terms by A², B², and C².

With these considerations, the number of central points (cp) was set to 3, the number of factorial points (Cube) was 8, and the number of axial points was 6. Three additional runs (No NaOH (3a), 1a and 2a) were added to the design resulting in a total of 20 experimental runs. Experimental plan details and the

responses (OZD conversion %) are given in Table 4. Figure 7 (a) and (b) show the response surface contour plots of OZD conversion for 100°C (temperature) and 35 min (time), respectively.

Table 4: Optimization model data and results

Exp. No.	Data			Results
	Temp. [°C]	Time [min]	OH ⁻ /OZD	OZD conversion [%]
1	100	38	4	100
2	118	51	3.2095	99.88
3	118	24	3.2095	99.94
4	82	24	3.2095	99.83
5	82	51	3.2095	99.93
6	70	38	2.05	89.2
7	130	38	2.05	99.53
8	100	38	2.05	98.83
9	100	60	2.05	99.58
10	100	38	2.05	98.92
11	100	15	2.05	94.52
12	100	38	2.05	98.69
13	82	51	0.8905	53.34
14	82	24	0.8905	48.17
15	118	24	0.8905	59.52
16	118	51	0.8905	74.63
17	100	38	0.1	10.48
1a	130	60	0.8905	72.21
2a	130	60	0.1	13.54
3a	130	60	0	0

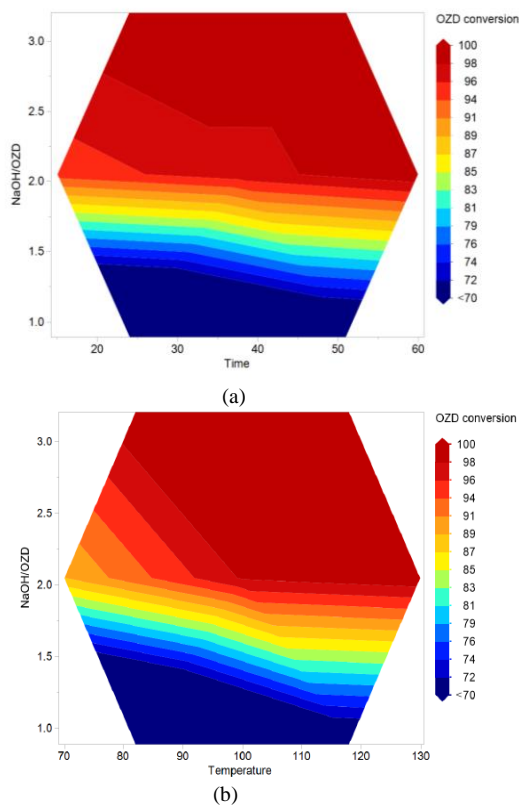


Figure 7: OZD conversion in function of OH-/OZD mole ratio (a) and time at 100°C (fixed temperature) (b) and temperature at 35 min (fixed time)

The summarizing prediction performance (Table 5) and the coefficient values of the optimization model (Table 6) indicate it to be satisfactory.

Table 5: Optimization model: prediction performance

RMSE	P-value	R ²	Adj. R ²
2.1958	<0.0001	0.99727	0.993167

Table 6: F-ratios and P-values of coefficients values (A: temperature, B: time, C: OH-/OZD)

Coefficient	F-ratio	P-value
A	37.7291	0.00085
B	12.5534	0.01217
C	803.7899	0.00000
AB	2.4178	0.17096
AC	27.5179	0.00193
BC	10.5144	0.01763
A ²	3.4492	0.11266
B ²	0.1520	0.71013
C ²	507.2047	0.00000

The model shows several sets of possible variable combinations (Table 7) depending on desired reaction condition application.

Table 7: Model responses for selected variable sets

OH-/OZD	Temp. [°C]	Time [min]	OZD conversion achieved [%]
1	130	60	83.46
1.5	130	60	98.59
1.8	100	60	96.97
1.8	120	45	99.01
2	100	47	99.12
2	110	36	99.11
2.2	100	24	98.96
2.5	76	15	98.99

Analytic chemical evidence of reaction response for selected variable combinations is given in Figure 8.

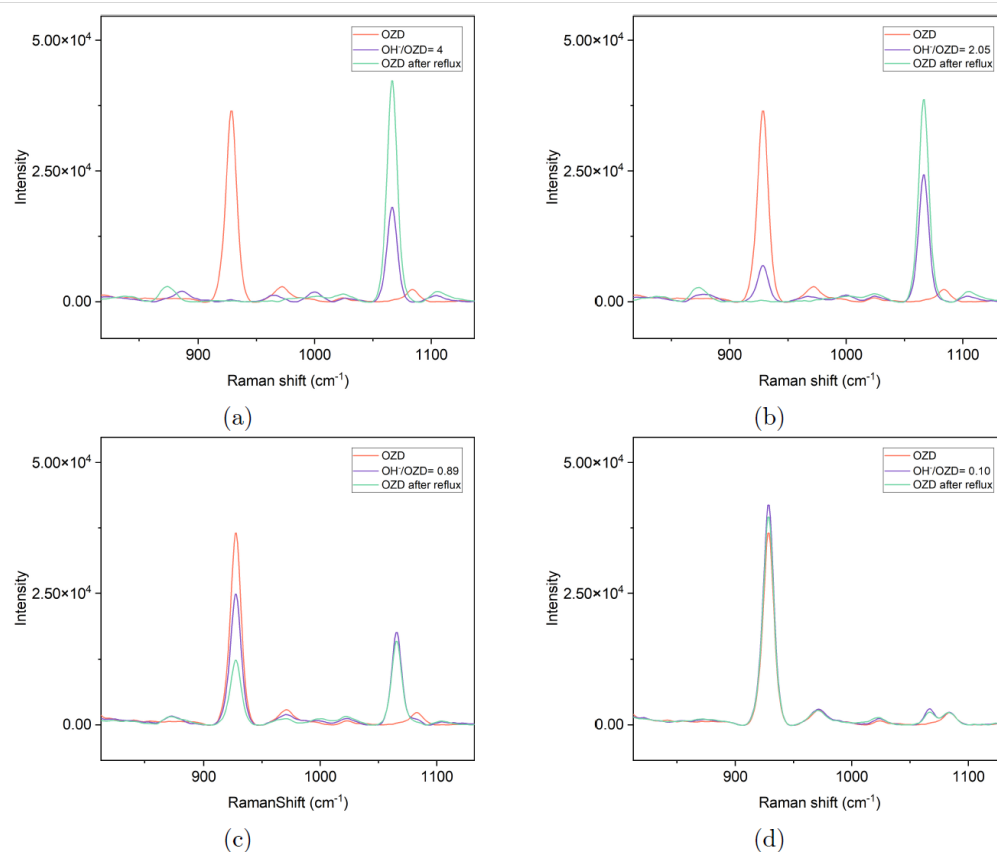


Figure 8. Raman spectra of selected experiments: Axial C (high) (a); Axial B (high) (b) and Axial C (low) (d).

3.3 Potential integration of the oxazolidone splitting reaction into a carbon dioxide capture unit.

The optimal reaction conditions for oxazolidone (OZD) splitting (Table 7) depend mostly on the OH-/OZD mole ratio. The reaction itself could be run in the reboiler of the CO₂ stripper or in a separate reactor connected to it (Figure 1). This would provide a temperature of the reaction vessel in excess of 100°C (Poldermann et al., 1955). As suggested by a US patent (Turoff et al., 2008), a slipstream of the stripper bottoms could be sent to a separate reactor where NaOH is added, the reaction is conducted and the recovered alkanolamine is separated from the caustic by phase splitting. Some caustic could be recycled to the reaction vessel while the rest is treated as solvent reclaiming waste. The US patent (Turoff et al., 2008) teaches this proposal for splitting of the oxazolidone hydroxypropyloxazolidone (HPOZD) to diisopropanolamine (DIPA) and CO₂. Our optimal reaction conditions for OZD splitting would fit well with the above process integration proposal.

4. Conclusion

- Society needs to stabilize and reduce CO₂ emissions. Large-scale post-combustion

carbon capture is expected to be necessary in the near future. Our contribution puts focus on the cost reduction of aqueous alkanolamine carbon capture solvent.

- Alkanolamine recovery by splitting of oxazolidone (OZD) to the original MEA alkanolamine solvent and CO₂ can be satisfactorily modeled and optimized by the RSM method.
- The model variables are in order of importance OH-/OZD ratio, reaction temperature and reaction time.
- A CO₂ capture process integration concept for splitting of OZD to MEA is proposed.

References

- Buvik, V. Høisæter, K. Vevelstad, S. & Knuutila, H. (2021). A review of degradation and emissions in post-combustion CO₂ capture pilot plants. *International Journal of Greenhouse Gas Control* 106 (2021) 103246.
- Davis, J., & Rochelle, G. (2009). Thermal degradation of monoethanolamine at stripper conditions. *Energy Procedia*, 1(1), 327-333. <https://doi.org/https://doi.org/10.1016/j.egypro.2009.01.045>
- Dyen, M. E., & Swern, D. (1967). 2-oxazolidones. *Chem Rev*, 67(2), 197-246. <https://doi.org/10.1021/cr60246a003>

- Eilers, P. H. C. (2003). A Perfect Smoother. *Analytical Chemistry*, 75(14), 3631-3636. <https://doi.org/10.1021/ac034173t>
- Eimer, D. (2014). *Gas treating : absorption theory and practice*. John Wiley & Sons, Inc.
- Eriksson, L., Johansson, E., Kettaneh-Wold, N., Wikström, C., & Wold, S. (2008). *Design of experiments : principles and applications* (3 ed.). Umetrics, Umeå.
- Esbensen, K. H., & Swarbrick, B. (2017). *Multivariate Data Analysis: An introduction to Multivariate Analysis, Process Analytical Technology and Quality by Design* (6th ed.). CAMO software AS.
- Fredriksen, S. B., & Jens, K.-J. (2013). Oxidative Degradation of Aqueous Amine Solutions of MEA, AMP, MDEA, Pz: A Review. *Energy Procedia*, 37, 1770-1777. <https://doi.org/https://doi.org/10.1016/j.egypro.2013.06.053>
- IEAGHG, (2014). Evaluation of Reclaimer Sludge Disposal from Post-Combustion CO₂ Capture. (March 2014).
- Kohl, A., Nielsen, R. (1997). *Gas Purification*. Gulf Prof. Publ.
- Miller, A. E. (1985). *Catalytic process for converting 2-oxazolidinones to their corresponding alkanolamines*.
- Myers, R. H., Montgomery, D. C., & Anderson-Cook, C. M. (2016). *Response surface methodology: process and product optimization using designed experiments*. John Wiley & Sons.
- Poldermann, L. D., Dillon, C. P., & Steele, A. B. (1955). Why MEA Solution Breaks Down in Gas Treating Service. *Oil and Gas Journal*, 4.
- Pottiez, F., & Verbeest, R. (1972). Process for the regeneration of alkanolamines by distillation, alkali hydroxide treatment, heat, phase separation and distillation. In: Google Patents.
- Rochelle, G. T. (2009). Amine Scrubbing for CO₂ Capture. *Science*, 325(5948), 1652-1654. <https://doi.org/10.1126/science.1176731>
- Snoble, K. A. J. (1981). Catalytic process for converting oxazolidinones to their corresponding aminoalcohols. In: Google Patents.
- Turoff, M. L. H., Cummings, A. L., Waite, S. W., & Horan, R. L. (2008). Process for improving the conversion of oxazolidones to alkanolamines. In: Google Patents.
- US Department of Energy (2017) Accelerating Breakthrough Innovation in Carbon Capture, Utilization and Storage.
- Whittaker, E. T. (1922). On a new method of graduation. *Proceedings of the Edinburgh Mathematical Society*, 41, 63-75.

Proceeding 1

(Extended Abstract)

New Sulfolane based Solvent for CO₂ Capture

Jayangi D. Wagaarachchige¹, Zulkifli Idris², Bjørnar Arstad³, Nithin B. Kummamuru², Kai A. S. Sætre², Klaus-J. Jens², and Maths Halstensen^{1*}

¹Department of Electrical, IT and Cybernetics, University of South-Eastern Norway,
Porsgrunn, Norway

²Department of Process, Energy and Environmental Technology, University of South-Eastern
Norway, Porsgrunn, Norway

³SINTEF Materials and Chemistry, 0314 Oslo, Norway

Published in Proceedings of the 15th Greenhouse Gas Control Technologies Conference 15-
18 March 2021, Available at SSRN

<https://ssrn.com/abstract=3817192>

or

<http://dx.doi.org/10.2139/ssrn.3817192>



15th International Conference on Greenhouse Gas Control Technologies GHGT-15

5th -8th October 2020, Abu Dhabi, UAE

A new sulfolane based solvent for CO₂ capture

Jayangi D. Wagaarachchige¹, Zulkifli Idris², Nithin B. Kummamuru², Kai A. S. Sætre², Maths Halstensen¹, Klaus-J. Jens^{2*}

¹Department of Electrical, IT and Cybernetics and ²Department of Process, Energy and Environmental Technology, University of South – Eastern Norway, Kjølnes ring 56, 3918 Porsgrunn, Norway

Abstract

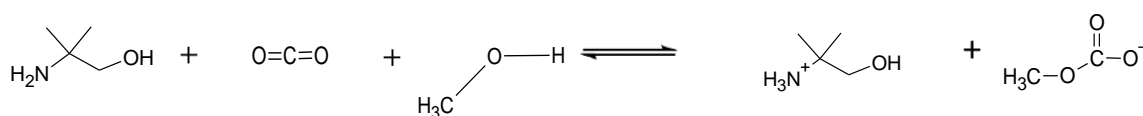
Chemical absorption using aqueous amine is considered as the established technique for post combustion CO₂ capture [1]. The most studied amine for this purpose is the aqueous monoethanolamine (MEA) and 30wt% MEA is the benchmark system and standard first-generation mixture for CO₂ capture. MEA is preferred as the solvent due to it being least expensive, highly reactive, water soluble and has a high absorption capacity with acid gases in gas mixtures [1, 2]. However, MEA is a highly corrosive chemical and has been shown to react with construction materials such as pipes and column walls [3]. Therefore, concentrated MEA solution should be avoided to minimize corrosion. Absorbing CO₂ using aqueous MEA also has other drawbacks such as high energy requirement and solvent degradation at high temperature [4].

Other amine-based solutions have also been investigated to optimize the process, and these solvents are usually classified as the second-generation CO₂ capture solvents. Aqueous piperazine is one of the these solutions, which can reduce operational expenditure (OPEX) by providing higher capture capacity and lower regeneration energy [5].

The regeneration energy can be reduced further by replacing aqueous amine systems with water-lean solvent systems [6]. For example, the K₂Sol solvent system is claimed to reduce the regeneration energy by 35% in comparison to MEA [7]. These organic solvents can also be good physical absorbents of CO₂ [4, 5, 8]. Furthermore, these solvents can be regenerated at low temperature since the absorption reaction leads to formation of less stable alkyl carbonate species [9]. Over the years, a number of water-lean systems utilizing different amines such as 2-amino-2-methyl-1-propanol (AMP), MEA, diethanolamine (DEA), 2-(2-aminoethoxy)ethanol (DGA) and methyl diethanolamine (MDEA) with different alcohols, polyethylene glycol (PEG), ethylene glycol (EG) or glycol ethers have been proposed [3, 9-16].

In this work, we evaluate five different amines in a new water-lean system containing sulfolane and methanol. Sulfolane and methanol are commercially available chemicals and sulfolane has been used as one of the components in the sulfinol process. Solutions were prepared by mixing a known amount of amine with sulfolane and methanol at a mole ratio of 1:0.3:1.1. In order to evaluate the effectiveness of the new solvent system, we have performed CO₂ absorption and desorption tests. The absorption was conducted at 20 °C whilst the desorption at 58 °C. Both of these reactions were monitored in-situ using a time-based ATR-FTIR spectrometer.

Figure 1 shows typical time-based ATR-FTIR spectra for AMP system during experiments. Upon introduction of CO₂, it can be seen that some chemical reactions took place as indicated by the formation of new peaks. These peaks were then reduced during desorption. In figure 2, selected ATR-FTIR scans of AMP system are shown. During experiments, changes in peak height were seen at wavenumbers of 1640, 1445, 1396, 1298, 1082, and so on. The peak at 1640 cm⁻¹ can be assigned to the C=O stretching bond of monomethyl carbonate species (MMC). The peak at 1290 cm⁻¹ is associated with the asymmetric stretching bond of O-C-O of MMC. No peak at 1575 cm⁻¹, which may indicate formation of carbamate, is observed during experiments suggesting that the reaction in the amine system proceeds through alkyl carbonate formation. Earlier investigation by Barzagli et. al. [8] also suggested the formation of alkyl carbonate, as shown in scheme 1. This may also explain the ability of our amine system to be regenerated at mild temperature of 58 °C.



Scheme 1. Suggested reaction for the formation of monomethyl carbonate by sulfolane based non-aqueous AMP solvent system.

We present further characterization of our new solvents in the full paper [17], and how they are compared to the existing solvents available. Details on the reaction mechanism will also be discussed.

Keywords: FTIR-ATR; Non-aqueous; Organic solvents; Sulfolane; Carbon dioxide capture

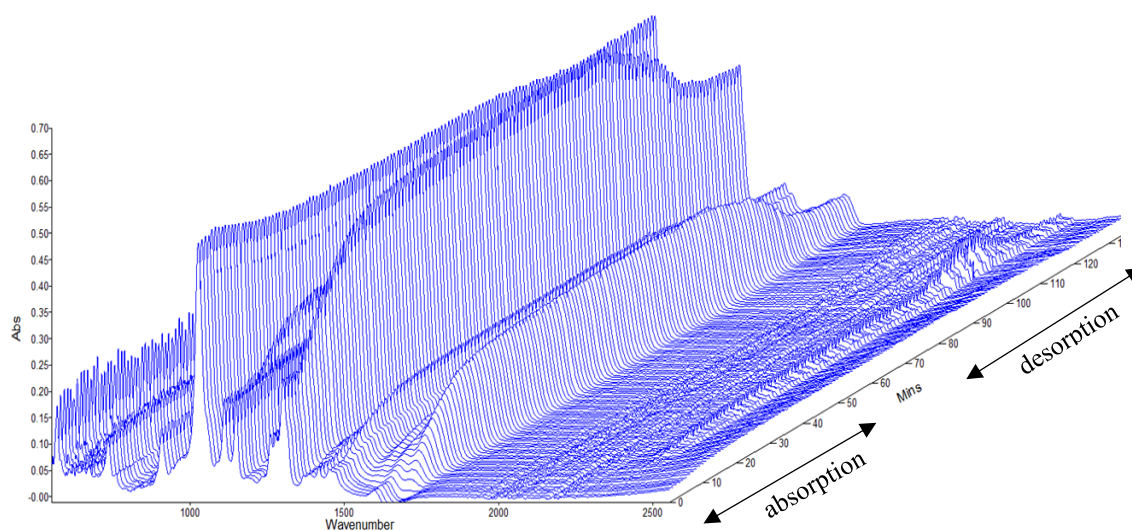


Figure1: Time-based ATR-FTIR scans of for the sulfolane based AMP non-aqueous solvent during CO₂ absorption and desorption

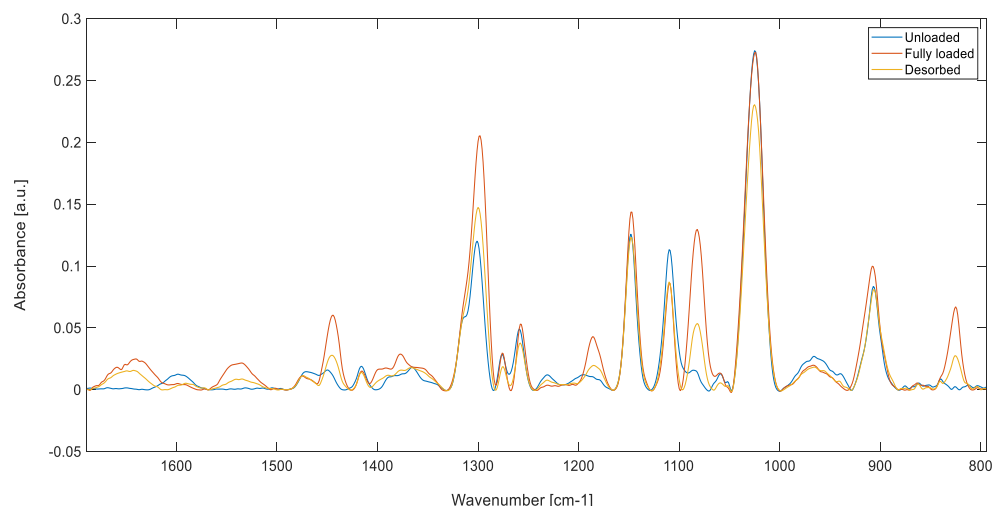


Figure 2: Spectra obtained by FTIR analysis for sulfolane based AMP non-aqueous solvent

References

1. Rochelle, G.T., Amine Scrubbing for CO₂ Capture. *Science*, 2009. **325**(5948): p. 1652-1654.
2. Lepaumier, H., D. Picq, and P.-L. Carrette, New Amines for CO₂ Capture. I. Mechanisms of Amine Degradation in the Presence of CO₂. *Industrial & Engineering Chemistry Research*, 2009. **48**(20): p. 9061-9067.
3. Song, J.-H., et al., Solubility of Carbon Dioxide in Monoethanolamine + Ethylene Glycol + Water and Monoethanolamine + Poly(ethylene glycol) + Water. *Journal of Chemical & Engineering Data*, 1996. **41**(3): p. 497-499.
4. Dezhong Yang, M.L., Jie Chena Efficient non-aqueous solvent formed by 2-piperidineethanol and ethylene glycol for CO₂ absorption. *Chemical Communications*, 2019. **55**(83): p. 12483-12486.
5. Wanderley, R.R., et al., CO₂ solubility and mass transfer in water-lean solvents. *Chemical Engineering Science*, 2019. **202**: p. 403-416.
6. Rochelle, G., et al., Aqueous piperazine as the new standard for CO₂ capture technology. *Chemical Engineering Journal*, 2011. **171**(3): p. 725-733.
7. Hwang, J., et al., An experimental based optimization of a novel water lean amine solvent for post combustion CO₂ capture process. *Applied Energy*, 2019. **248**: p. 174-184.
8. Barzagli, F., F. Mani, and M. Peruzzini, Efficient CO₂ absorption and low temperature desorption with non-aqueous solvents based on 2-amino-2-methyl-1-propanol (AMP). *International Journal of Greenhouse Gas Control*, 2013. **16**: p. 217-223.
9. Barzagli, F., S. Lai, and F. Mani, Novel non-aqueous amine solvents for reversible CO₂ capture. *Energy Procedia*, 2014. **63**: p. 1795-1804.
10. Guo, H., et al., Nonaqueous amine-based absorbents for energy efficient CO₂ capture. *Applied Energy*, 2019. **239**: p. 725-734.
11. Sada, E., et al., Chemical kinetics of the reaction of carbon dioxide with ethanolamines in nonaqueous solvents. *AIChE Journal*, 1985. **31**(8): p. 1297-1303.
12. Henni, A. and A.E. Mather, Solubility of Carbon Dioxide in Methyl-diethanolamine + Methanol + Water. *Journal of Chemical & Engineering Data*, 1995. **40**(2): p. 493-495.
13. Oyevaar, M.H., H.J. Fontein, and K.R. Westerterp, Equilibria of carbon dioxide in solutions of diethanolamine in aqueous ethylene glycol at 298 K. *Journal of Chemical & Engineering Data*, 1989. **34**(4): p. 405-408.
14. Barzagli, F., et al., Reversible carbon dioxide capture by aqueous and non-aqueous amine-based absorbents: A comparative analysis carried out by ¹³C NMR spectroscopy. *Applied Energy*, 2018. **220**: p. 208-219.
15. Tan, J., et al., Mixture Absorption System of Monoethanolamine–Triethylene Glycol for CO₂ Capture. *Industrial & Engineering Chemistry Research*, 2011. **50**(7): p. 3966-3976.
16. Park, S.-W., B.-S. Choi, and J.-W. Lee, Chemical absorption of carbon dioxide with triethanolamine in non-aqueous solutions. *Korean Journal of Chemical Engineering*, 2006. **23**(1): p. 138-143.
17. Wagaarachchige, J.D., et al., A new sulfolane based solvent for CO₂ capture. *International Journal of Greenhouse Gas Control*, 2021. **submitted**.

Proceeding 2

(Extended Abstract)

Demonstration of CO₂ Capture Process Monitoring and Solvent Degradation Detection by Chemometrics – CO₂ Technology Centre Mongstad.

Jayangi D. Wagaarachchige¹, Zulkifli Idris², Ayandeh Khatibzadeh¹, Audun Drageset³, Klaus-J.
Jens², and Maths Halstensen^{1*}

¹Department of Electrical, IT and Cybernetics, University of South-Eastern Norway,
Porsgrunn, Norway

²Department of Process, Energy and Environmental Technology, University of South-Eastern
Norway, Porsgrunn, Norway

³Technology Center Mongstad (TCM-DA), Mongstad, Norway

Presented in TCCS-12 - Trondheim Conference on CO₂ Capture, Transport and Storage,
Trondheim, Norway, June 19-21, 2023



DEMONSTRATION OF CO₂ CAPTURE PROCESS MONITORING AND SOLVENT DEGRADATION DETECTION BY CHEMOMETRICS—CO₂ TECHNOLOGY CENTRE MONGSTAD

Jayangi D. Wagaarachchige¹, Zulkifli Idris², Ayandeh Khatibzadeh¹, Audun Drageset³, Klaus-J. Jens², Maths Halstensen^{1*}

¹Department of Electrical, IT and Cybernetics, University of South – Eastern Norway, Kjølnes ring 56, 3918 Porsgrunn, Norway

²Department of Process, Energy and Environmental Technology, University of South – Eastern Norway, Kjølnes ring 56, 3918 Porsgrunn, Norway

³Technology Center Mongstad (TCM-DA), 5954 Mongstad, Norway
Corresponding author's e-mail address: Maths.Halstensen@usn.no

Keywords: Post-combustion capture, Solvent absorption, Solvent degradation

ABSTRACT

The 30 wt% aqueous monoethanolamine (MEA) solution is considered as the benchmark solvent for CO₂ capture.¹ High energy penalty for solvent regeneration corrosivity of the solvent, high solvent losses due to oxidative and thermal degradations and environmental concerns due to possible emissions are major concerns that need to be addressed for an effective operation of the process. In order to maintain the optimal performance of the CO₂ capture, the process needs to be monitored and controlled. The application of Process Analytical Technology (PAT)² using spectroscopy is an important approach for an optimal control of CO₂ capture operations. Partial least squares regression (PLS-R) is a valuable statistical method to extract the quantitative chemical information from the spectroscopic data.

Heat stable salts (HSS) are oxidative degradation products of amines and identified as an early stage solvent degradation species which participates subsequently in solvent degradation³ and plant corrosion.⁴ Hence, early stage detection of HSS is important with respect to control of other associated process issues such as solvent degradation and corrosion. Grimstvedt et. al. indicated that the CO₂ model residuals might be useful to determine the concentration of HSS in a degraded aqueous solution of MEA.⁵

The Technology Centre Mongstad (TCM) operated several test campaigns using aqueous 30 wt% MEA solvent and the outcomes from these campaigns have been published by giving insight into the base-case testing, degradation, corrosion, solvent reclaiming and atmospheric emission, etc.⁶⁻⁸

This study demonstrates the application of multivariate methods (i.e., PLS-R, MSPC) to monitor and control the process performances based on process analytical tools (i.e., FTIR) using TCM real campaign data. In long term solvent monitoring, PLS-R model prediction errors (RMSEP) is increasing due to solvent changes (i.e., solvent degradation, corrosion). Model maintenance along with the model diagnostics measures is important in achieving stable model predictions. Solvent degradation is one of the main challenges of amine-based CO₂ capture plant operations and it can

be easily detected using the PLS-R model based Multivariate Statistical Process Control (MSPC). Furthermore, residual (FTIR) spectra obtained from the 1st Generation model's (CO₂ and amine) prediction were further examined with multivariate calibration. Heat stable salts (HSS) and Total amine degradation products (TADP) were calibrated using residual FTIR spectra and offline sample measures of TCM campaign to predict formation of these species by on-line monitoring.

ACKNOWLEDGMENT

The authors gratefully acknowledge the staff of TCM DA, Gassnova, Equinor, Shell and TotalEnergies for their interest in this work and particularly for access to data from the TCM DA facility. The authors also gratefully acknowledge Gassnova, Equinor, Shell, and TotalEnergies as the owners of TCM DA for their financial support and contributions.

REFERENCES

1. Rochelle, G. T., Amine Scrubbing for CO₂ Capture. *Science* **2009**, 325, (5948), 1652-1654.
2. Kim H. Esbensen, B. S., *Multivariate Data Analysis: An introduction to Multivariate Analysis, Process Analytical Technology and Quality by Design* 6th ed.; CAMO software AS: 2017; p 452.
3. Supap, T.; Idem, R.; Tontiwachwuthikul, P., Mechanism of formation of heat stable salts (HSSs) and their roles in further degradation of monoethanolamine during CO₂ capture from flue gas streams. *Energy Procedia* **2011**, 4, 591-598.
4. Tanthapanichakoon, W.; Veawab, A.; McGarvey, B., Electrochemical Investigation on the Effect of Heat-stable Salts on Corrosion in CO₂ Capture Plants Using Aqueous Solution of MEA. *Ind. Eng. Chem. Res.* **2006**, 45, (8), 2586-2593.
5. Grimstvedt, A.; Wiig, M.; Einbu, A.; Vevelstad, S. J., Multi-component analysis of monoethanolamine solvent samples by FTIR. *Int. J. Greenhouse Gas Control* **2019**, 83, 293-307.
6. Flø, N. E.; Faramarzi, L.; de Cazenove, T.; Hvidsten, O. A.; Morken, A. K.; Hamborg, E. S.; Vernstad, K.; Watson, G.; Pedersen, S.; Cents, T.; Fostås, B. F.; Shah, M. I.; Lombardo, G.; Gjernes, E., Results from MEA Degradation and Reclaiming Processes at the CO₂ Technology Centre Mongstad. *Energy Procedia* **2017**, 114, 1307-1324.
7. Morken, A. K.; Pedersen, S.; Kleppe, E. R.; Wisthaler, A.; Vernstad, K.; Ullestad, Ø.; Flø, N. E.; Faramarzi, L.; Hamborg, E. S., Degradation and Emission Results of Amine Plant Operations from MEA Testing at the CO₂ Technology Centre Mongstad. *Energy Procedia* **2017**, 114, 1245-1262.
8. Hjelmaas, S.; Storheim, E.; Flø, N. E.; Thorjussen, E. S.; Morken, A. K.; Faramarzi, L.; de Cazenove, T.; Hamborg, E. S., Results from MEA Amine Plant Corrosion Processes at the CO₂ Technology Centre Mongstad. *Energy Procedia* **2017**, 114, 1166-1178.

Appendix A: Supplementary Information of Article 2

Supporting Information of Article 2

Manuscript title: Demonstration of CO₂ Capture Process Monitoring and Solvent Degradation Detection by Chemometrics at the Technology Centre Mongstad CO₂ Capture Plant: Part II

Authors: *Jayangi D. Wagaarachchige¹, Zulkifli Idris², Ayandeh Khatibzadeh¹, Audun Drageset³, Klaus-J. Jens², Maths Halstensen^{1*}*

Affiliations:

¹*Department of Electrical, IT and Cybernetics, University of South – Eastern Norway, Kjølnes ring 56, 3918 Porsgrunn, Norway*

²*Department of Process, Energy and Environmental Technology, University of South – Eastern Norway, Kjølnes ring 56, 3918 Porsgrunn, Norway*

³*Technology Center Mongstad (TCM-DA), 5954 Mongstad, Norway*

Corresponding Author: Maths.Halstensen Tel: +4735575187

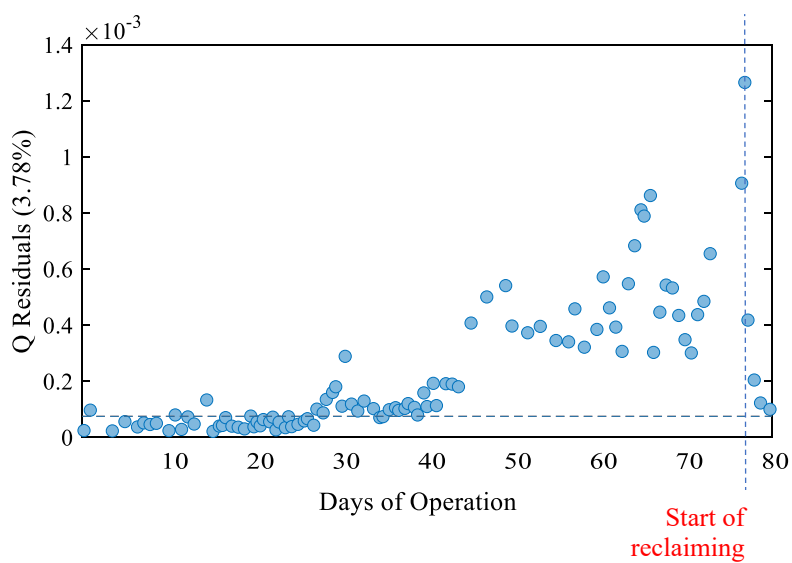


Figure S1: Initial TA model's prediction Qs with Days of operation of MEA2 campaign.

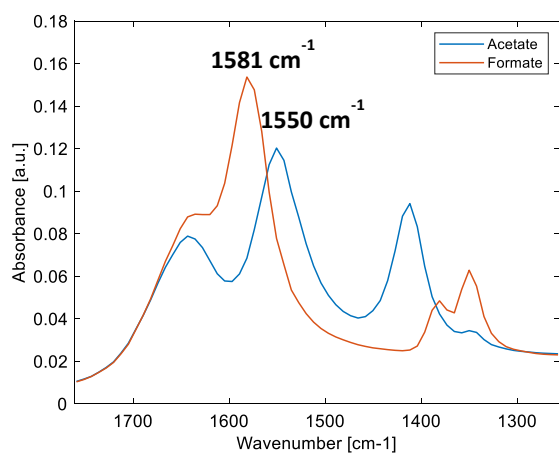


Figure S2: ATR-FTIR lab analysis spectra of formate and acetate anions

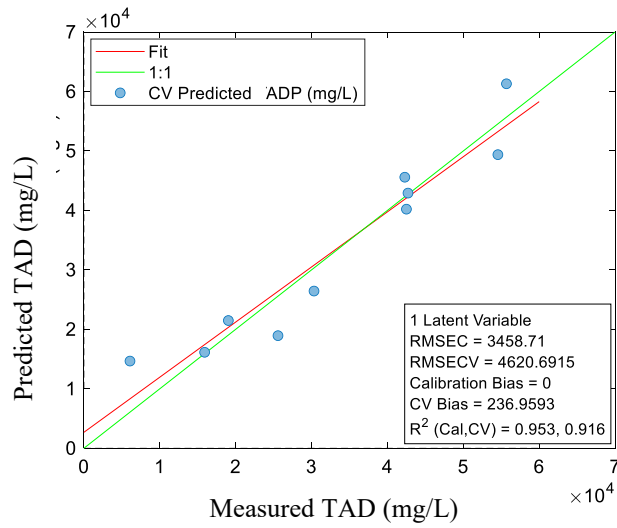


Figure S3: PLS-R model calibration for Amine Degradation Products (ADP) using residual spectra of TA model.

Appendix B: Supplementary Information of Article 4

Supporting Information of Article 4

Manuscript title: Low-Viscosity Non-aqueous Sulfolane-Amine-Methanol Solvent Blend for Reversible CO₂ Capture: Part II. Blend Optimization, Water Effect, and Speciation.

Authors: *Jayangi D. Wagaarachchige*¹, *Zulkifli Idris*², *Bjørnar Arstad*³, *Maths Halstensen*¹, *Klaus-J. Jens*^{2*}

Affiliations:

¹*Department of Electrical, IT and Cybernetics*

²*Department of Process, Energy and Environmental Technology, University of South – Eastern Norway, Kjølnes ring 56, 3918 Porsgrunn, Norway*

³*SINTEF Materials and Chemistry, Forskningsveien 1, 0314 Oslo, Norway*

Corresponding Author: Klaus.J.Jens@usn.no Tel: +4735575193

Table S1: D-optimal design experimental plan

Sample no	DPA wt%	Methanol wt%	Sulfolane wt%	T _{ab} °C
1	10	60	30	45
2	40	10	50	25
3	45	45	10	25
4	80	10	10	35
5	22.5	57.5	20	30
6	40	10	50	45
7	10	40	50	25
8	80	10	10	25
9	10	60	30	35
10	60	10	30	45
11	10	80	10	35
12	10	40	50	45
13	10	40	50	45
14	10	60	30	25
15	10	80	10	35
16	35	35	30	35
17	10	40	50	25
18	35	35	30	35
19	80	10	10	45
20	40	10	50	35

21	35	35	30	25
22	35	35	30	25
23	40	10	50	25
24	60	10	30	25
25	10	80	10	45
26	40	10	50	35
27	10	80	10	25
28	10	60	30	35
29	60	10	30	25
30	45	45	10	35
31	10	80	10	25
32	80	10	10	35
33	22.5	57.5	20	30
34	80	10	10	45
35	45	45	10	45
36	10	60	30	25
37	35	35	30	35
38	45	45	10	45
39	60	10	30	45
40	80	10	10	25
41	10	80	10	45
42	10	60	30	45
43	40	10	50	45
44	45	45	10	35
45	45	45	10	25

Table S2: Mixture designs plan

Designs	Sample no	DPA wt%	Methanol wt%	Sulfolane wt%
Simplex-shaped mixture design 1 CP: 45:45:10	1	47.5	47.5	5
	2	40	40	20
	3	55	40	5
	4	45	45	10
	5	40	47.5	12.5
	6	45	45	10
	7	45	45	10
	8	47.5	40	12.5
	9	40	55	5
Simplex-shaped mixture design 2 CP: 35:35:30	10	30	45	25
	11	37.5	30	32.5
	12	37.5	37.5	25
	13	35	35	30
	14	30	30	40
	15	35	35	30
	16	45	30	25
	17	30	37.5	32.5
Simplex-shaped mixture design 3 CP: 25:25:50 (only three mixtures used)	18	20	35	45
	19	27.5	27.5	45
	20	35	20	45
Random samples	21	50	50	0
	22	45	55	0
	23	40	60	0

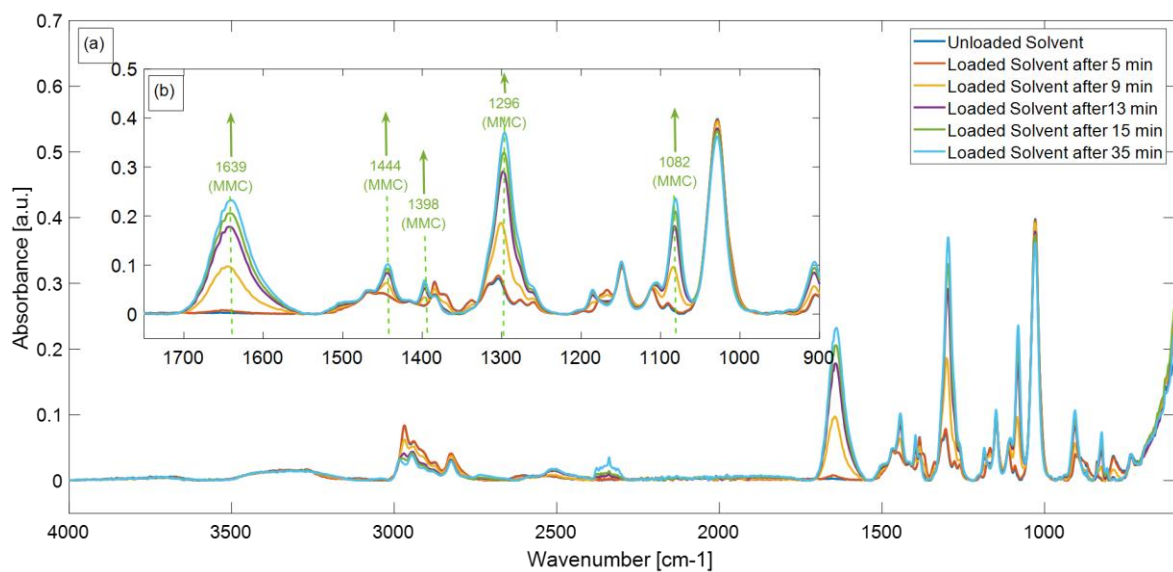


Figure S1 : ATR-FTIR spectra; CO₂ absorption of the DPA solvent with no water (a) Raw spectra (variable range: 4000-600 cm⁻¹) (b) baseline corrected spectra (variable range: 1750-950 cm⁻¹)

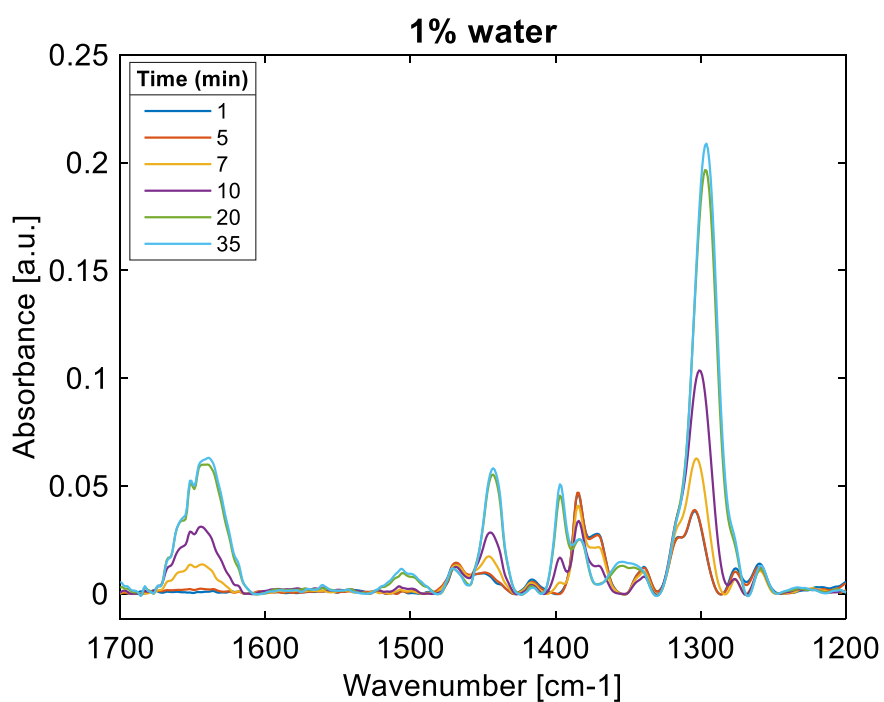


Figure S2: ATR-FTIR spectra; CO₂ absorption of the DPA solvent with 1 wt% water

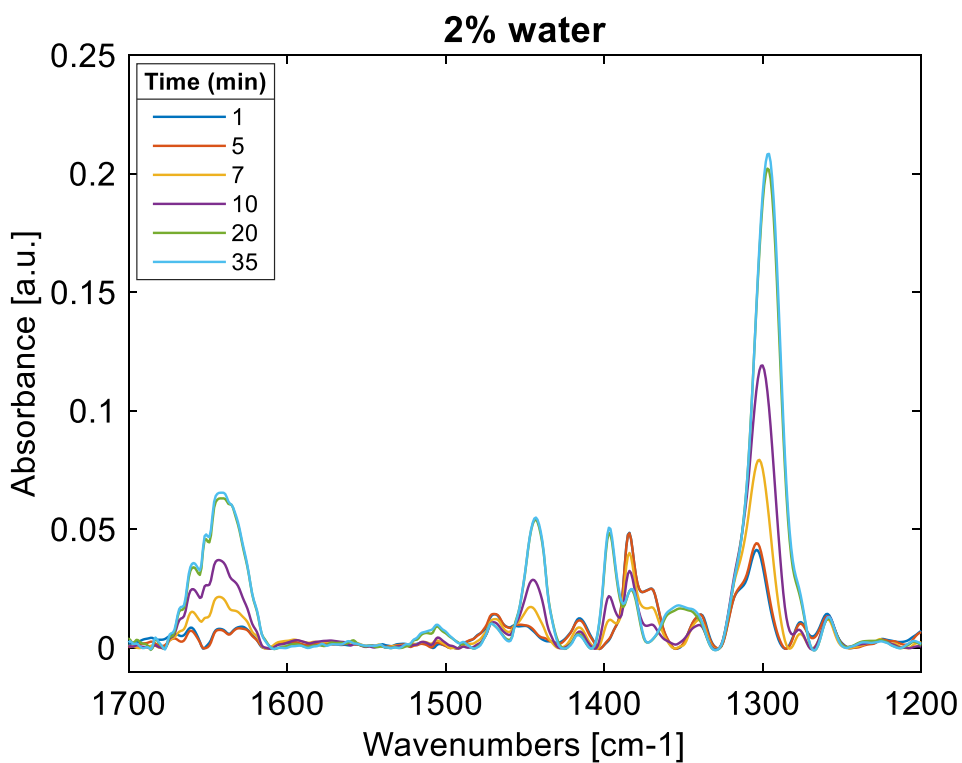
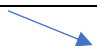



Figure S3: ATR-FTIR spectra; CO₂ absorption of the DPA solvent with 2 wt% water

Table 3: CO₂ loading calculations of water lean solvents (D and E)

CO ₂ loading calculations					
Solvent D Experiment	↘	85%	Sovent D	+	15% water
D (DPA-30, methanol -60, sulfolane -10)wt%					
Mass of sample used =	100	g			
Mass of CO ₂ loaded until TTOS	10.51	g			
Molar weight of DPA	101.19	g/mol			
Moles of amine in the sample =	0.252001186	mol	↙	$((30/100)*85)/101.19$	
Molar weight of CO ₂	44	g/mol			
Moles of CO ₂ absorbed	0.238863636	mol			

CO₂ loading (mol CO₂/mol amine)	0.947867112	mol/mol DPA			
CO₂ loading (mol CO₂/Kg of solvent)	2.388636364	mol/kg sol			
Solvent E Experiment		85%	Sovent E	+	15% water
E (DPA-40, methanol-50, sulfolane-10) wt%					
Mass of sample used =	100	g			
Mass of CO ₂ loaded until TTOS	11.6	g			
Molar weight of DPA	101.19	g/mol			
Moles of amine in the sample =	0.336001581	mol		$((40/100)*85)/101.19$	
Molar weight of CO ₂	44	g/mol			
Moles of CO ₂ absorbed	0.263636364	mol			
CO₂ loading (mol CO₂/mol amine)	0.784628342	mol/mol DPA			
CO₂ loading (mol CO₂/Kg of solvent)	2.636363636	mol/kg sol			

**Pushing Technology
Boundaries:
Monitoring and Optimization
of Carbon Capture Solvents**
Jayangi Dinesha
Wagaarachchige

**Doctoral dissertations at the
University of South-Eastern
Norway no. 196**

ISBN 978-82-7206-862-1 (print)
ISBN 978-82-7206-863-8 (online)

usn.no